

AFCRL-70-0097
FEBRUARY 1970
TRANSLATIONS, NO. 49

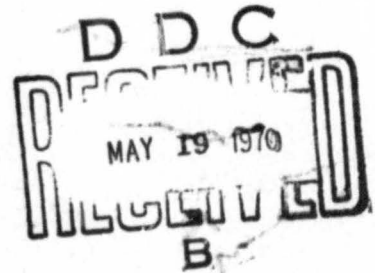


AIR FORCE CAMBRIDGE RESEARCH LABORATORIES

L. G. HANSCOM FIELD, BEDFORD, MASSACHUSETTS

**On the Investigation of Instrumental Errors
of Universal and Transit Instruments by
Means of Autocollimation**

REINER SCHWEBEL



**OFFICE OF AEROSPACE RESEARCH
United States Air Force**



Reproduced by the
CLEARINGHOUSE
for Federal Scientific & Technical
Information Springfield Va. 22151

197

AD705537

AFCRL-70-0097
FEBRUARY 1970
TRANSLATIONS, NO. 49



AFCRL RESEARCH LIBRARY
AIR FORCE CAMBRIDGE RESEARCH LABORATORIES
L. G. HANSCOM FIELD, BEDFORD, MASSACHUSETTS

On the Investigation of Instrumental Errors of Universal and Transit Instruments by Means of Autocollimation

REINER SCHWEBEL

Translated from German Geodetic Commission at the Bavarian
Acad. of Sciences-Ser. C: Dissertations - Vol. 117, 1968

Translated by The Legal Translating Service, 1278 Massachusetts
Avenue, Cambridge, Massachusetts 02138

Translated and Printed by Permission of Deutsche Geodatische
Kommission, Marstallplatz 8, West Germany

This document has been approved for public
release and sale; its distribution is unlimited.

OFFICE OF AEROSPACE RESEARCH
United States Air Force



Abstract

Geodetic astronomy depends to a certain degree on the precision of available instruments. This investigation covers the instrument errors that effect the determination of a horizontal direction and the effect of these errors on position accuracy determination by horizontal angle measurements and vertical transits. The following errors were investigated:

- 1) axis errors; that is, horizontal, tilt and target axis
- 2) instrument errors; that is, divided circle, micrometer, and level bubble
- 3) instrument stability errors; that is, substructure rotation, roll error, and heat deflection of the telescope.

These errors seldom exceed +1". Three common first order instruments, the Wild T-4, Kern DKM-3, and the Askania AP70 were investigated. The direct investigation of the instrumental errors was conducted utilizing very precise auto-collimation methods, and statistical methods for defining the type and magnitude of the errors. Instrument errors cannot be ignored but they can be significantly reduced through the use of an adequate observation program.

Contents

1. INTRODUCTION	1
2. ANGLE MEASUREMENT WITH AUTOCOLLIMATION	4
2.1 Principle of Angle Measurement With Reciprocal Collimation and Autocollimation	4
2.2 Technical Realization of Autocollimators	8
2.2.1 Optical Autocollimators	8
2.2.2 Electro-optical Autocollimators	10
2.3 Autocollimation Systems and Their Properties	12
2.3.1 Image Migration Under Three-Dimensional Rotations of Plane Optical Surfaces	12
2.3.2 Simple Autocollimation	14
2.3.3 Multiple Reflection	16
2.3.3.1 Principle of Multiple Reflection	16
2.3.3.2 Image Migration Under Three-Dimensional Rotations of a Mirror Pair	19
2.3.4 Multiple Autocollimation	21
2.3.4.1 Principle and Technical Realization of Multiple Autocollimation	21
2.3.4.2 Image Migration Under Three-Dimensional Rotations of Fully and Partially Reflecting Mirrors	23
2.3.5 2.3.4.3 Reduction of Images of Higher Order Because of Unstable Positioning of Mirrors	25
2.3.5 Evaluation of Multiple Reflection and Multiple Autocollimation	27
2.4 Construction, Adjustment, and Calibration of a 1500mm Autocollimation System	28
2.4.1 Construction of the 1500mm Autocollimation System	28
2.4.2 Calibration of the AC System	32
2.4.2.1 Determination of the Focal Length of the Objective	32
2.4.2.2 Investigation and Calibration of the Micrometer	36
2.4.2.3 Interferometric Testing of the Flatness of the Autocollimation Mirror	36

Contents

2.5	Focusing an Autocollimation System on Infinity	37
2.5.1	Focusing With Flat Autocollimation Mirrors	38
2.5.2	Focusing With Curved Autocollimation Mirrors	40
2.5.2.1	The Dependence of Axial Image Position on Residual Curvature of the AC Mirror	40
2.5.2.2	Dependence of Axial Image Position on Wavelength	43
2.5.2.3	Object and Image Position in Parallax-free Focusing	43
2.5.3	Execution and Results of Focusing	44
2.5.3.1	Focusing by Image Sharpness	44
2.5.3.2	Focusing by Illumination Parallax	45
2.6	Determination of the Scale Factor of an Autocollimation System	46
2.6.1	Autocollimation With Nonparallel Beams	46
2.6.2	Direct Determination of the Scale Factor on an AC System	49
2.6.3	Determination of the Scale Factor From Focus Differences	52
2.7	On the Accuracy of Angle Measurement by Means of Autocollimation	53
2.7.1	Internal Accuracies	53
2.7.1.1	Coincidence Accuracy	53
2.7.1.2	Accuracy of the Measurement System	55
2.7.2	Influence of External Factors on the Precision of an AC System	57
2.7.2.1	Refraction	57
2.7.2.2	Temperature Sensitivity of the Positioning of the Autocollimator and the Mirror System	58
2.7.2.3	Stability of an AC System Under Normal Thermal Conditions	61
3.	INSTRUMENTAL ERRORS OF UNIVERSAL AND TRANSIT INSTRUMENTS: DEFINITION AND EFFECT	63
3.1	Primary and Secondary Axis Errors	63
3.1.1	General Definition of Primary and Secondary Axis Errors	63
3.1.2	Primary Axis Errors of Universal and Transit Instruments	66
3.1.3	Secondary Axis Errors of Universal and Transit Instruments	68
3.2	Definition of Measurement Device Errors	69
3.3	Stability Errors	73
3.4	Influence of Instrumental Errors on Direction Observations	75
4.	PROCEDURES FOR THE DETERMINATION OF INSTRUMENTAL ERRORS	80
4.1	Measurement Procedures With Autocollimation	81
4.2	Evaluation of Measurements With Autocollimation	84
4.3	Measurement Methods Without Autocollimation	89
4.4	Analysis of Instrumental Error	90
4.4.1	Evidence of Systematic Error	90
4.4.2	Analysis of Systematic Errors	93
5.	EXPERIMENTAL RESULTS FOR THE UNIVERSAL INSTRUMENTS WILD T4, KERN DKM3, AND THE TRANSIT INSTRUMENT ASKANIA AP70	95
5.1	Azimuthal and Vertical Substructure Rotation	96
5.2	Azimuthal and Vertical Roll Effect	101
5.3	Thermal Deflection of the Telescope	106
5.4	Secondary Tilt Axis Error	108
5.4.1	Measurement Program for Determining Secondary Tilt Axis Errors; Results	108
5.4.2	Analysis of Error Causes	109

Contents

5.5	Secondary Vertical Axis Error	115
5.5.1	Measurement Program	115
5.5.2	Theoretical Considerations of Error Causes in Semi-kinematic and Fully Kinematic Vertical Axis Systems	115
5.5.3	Results and Analysis of Error Causes	123
5.6	Horizontal Circle Reading Precision	127
5.7	Level Error	131
5.8	Inclination Components and Level Components of the Wobble Error in the Tilt Axis	132
5.9	Summary of Results and Conclusions	134
6.	THE INFLUENCE OF INSTRUMENTAL ERRORS ON THE ACCURACY OF HORIZONTAL ANGLE MEASUREMENTS AND DETERMINATIONS OF ASTRONOMICAL POSITIONS	137
6.1	Simultaneous Propagation of Random and Systematic Errors	138
6.2	Accuracy of the Measurement of a Horizontal Angle	141
6.2.1	Horizontal Angle Measurements by Horizontal Aiming	141
6.2.2	Horizontal Angle Measurements With Inclined Aiming	143
6.3	The Influence of Instrumental Errors on the Accuracy of Determinations of Astronomical Positions	145
6.3.1	Position Determination From Vertical Passages With A Transit Instrument	145
6.3.2	Position Determination From Measurements of Azimuthal Difference With a Universal Instrument	151
6.3.3	Numerical Values for the Accuracy and Consequences for Astronomical Position Determinations	152
7.	SUMMARY	157
	REFERENCES	161
	CURRICULUM VITAE	165
	APPENDIX A	A1
	APPENDIX B	B1
	APPENDIX C	C1
	APPENDIX D	D1
	APPENDIX E	E1
	APPENDIX F	F1
	APPENDIX G	G1
	APPENDIX H	H1
	APPENDIX I	I1
	APPENDIX J	J1
	APPENDIX K	K1
	APPENDIX L	L1

Contents

APPENDIX M	M1
APPENDIX N	N1
APPENDIX O	O1
APPENDIX P	P1
APPENDIX Q	Q1
APPENDIX R	R1
APPENDIX S	S1
APPENDIX T	T1
APPENDIX U	U1

Illustrations

1. Angle Measurement with Reciprocal Collimation	4
2. Measurement of Mirror Rotations with Reciprocal Collimation	7
3. Optical System of the Leitz Autocollimation Telescope	9
4. Leitz Autocollimation Telescope	9
5. Optical System of the Micro-optic Autocollimator of Hilger & Watts	10
6. Principle of the Electro-Optical Autocollimator TA58 of Hilger & Watts	11
7. Vectorial Formulation of Reflection and Refraction Laws	13
8. Vector Components on 90° Deflection with Deflection Mirror	14
9. Principle of Multiple Reflection with a Mirror Pair	16
10. Principle of Multiple Autocollimation	21
11. Multiple Autocollimation: Image Orders 0 to IV	22
12. Definition of the Prism Elements of the Semitransparent Mirror	23
13. Construction of the 1500mm Autocollimator	29
14. Total View of the 1500mm Autocollimation System	29
15. Principle and Systematic Errors in Focal Length Determination of an Objective	33
16. Beam Path Upon Focusing at Infinity	38
17. Focusing on Infinity by Means of Displacement of the Micrometer Head	39
18. Ray Path with a Curved Autocollimation Mirror	40
19. Combination of the Image-forming System O_a of the Autocollimator with the Mirror System O_g into the Equivalent System O_e	42
20. Focusing Procedure with Curved Autocollimator Mirrors	44
21. Scale Determination with Nonparallel Rays	47

Illustrations

22. Distribution of Measurement Settings in the Testing of the System of Measurement	56
23. Refraction Between Objective and AC Mirror	59
24. Image Migration with Thermal Changes	60
25. General Definition of Axis Errors	65
26. Primary Theodolite Axis Errors in Vectorial Representation	65
27. Mounting the Azimuth Component Measurement Mirror on Tilt Axis Investigation (Wild T4)	81
28. Measuring Substructure Rotation with Multiple Autocollimation (Wild T4)	84
29. Vertical Axis Investigation - Fitted Ellipse	85
30. Measurement of Level Error (Level in operation)	90
31. Azimuthal Substructure Rotation During a Large Number of Revolutions	97
32. Vertical Substructure Rotation During a Full Revolution (Wild T4)	100
33. Addition of the Residual Roll Defect During a Tilt Axis Experiment	104
34. Theoretical Motion of the Mean Axis During a Tilt Axis Experiment	104
35. Effect of Heat Deflection of the Telescope in Telescope Seats I and II (Transit instrument)	106
36. Effect of Heat Deflection of the Telescope on the Basis of Manual Heat Distribution	107
37. Practical Solutions for Tilt Axis Seating(scale 1:1)	111
38. Motion Run-off in a Spherical Seat	112
39. Azimuth Secondary Tilt Axis Error of the Wild T4. Analysis a, b, c of Error Causes	114
40a. Semikinematic Axis System of the Wild T4 (front sketch)	116
40b. Motion of a Sphere Opposite Axis and Case (cross section)	116
41. Motion of the Alidade and the Spherical System Opposite the Case (Wild T4)	117
42. Error Causes in Semikinematic Axis Systems	119
43a. Radial Component v_r of the Secondary Vertical Axis Error (Wild T4)	124
43b. Remaining Error According to Fourier Analysis	124
44. Wobble Error of the Vertical Axis (x-component) Because of the Inequality of Spherical Diameter (Wild T4)	125
45. Error of Sliding Adjustment (360° period) After Reducing Residual Error (six revolutions)	126
46a. Radial Component of the Secondary Vertical Axis Error of the Kern DKM3	124
46b. Residual Error According to Fourier Analysis	124
47. Secondary Micrometer Error for Wild T4 and Kern DKM3	130
48. Diameter Corrections (Wild T4)	130
49. Level Error According to Reduced Cast Lines (Wild T4)	133

Illustrations

50. Mean Error of an Angle α at Very Different Zenith-Distances of the Aims	144
51. Determination of Position with Vertical Base Lines	145
52. Possibilities of Arranging the Pairs of Stars	150
53. Mean Error m_e of the Base Line Distance e Dependent on the Zenith Distance of Star 1	155

Tables

1. Variants of Angle Measurement with Reciprocal Collimation	6
2. Multiple Reflections with a Mirror Pair	18
3. Image Migration of K th-order Images in Multiple Autocollimation	25
4. Results of the Direct Scale Determinations for the 1500mm AC System	51
5. Dependence of Coincidence Accuracy on Reading Optics, Mirror Size and Number of Reflections	54
6. Dependence of Refraction on Mirror Separation	58
7. Image Migration at Normal Temperature Variation	62
8. Measurement of Instrumental Errors - Procedures with Autocollimation	82
9. Azimuthal Substructure Rotation per Alidade Revolution or Shift	99
10. Azimuthal Substructure Rotation Over a Long Observation Time	99
11. Test Data for Roll Effect	103
12. Results of the Tilt Axis Experiments	110
13. Error Causes and Results of Error Analysis (Wild T4)	121
14. Summary of Results of Vertical Axis Investigations for the Wild T4 and the Kern DKM3	125
15. Results of the Micrometer Experiments	128
16. Results of the Divided Circle Experiments (Wild T4)	128
17. Results of the Level Experiments According to Wanach	128
18. Summary of the Results of the Instrument Investigations	135

On the Investigation of Instrumental Errors of Universal and Transit Instruments by Means of Autocollimation

1. INTRODUCTION

The performance of geodetic astronomy depends, to a special degree, on the precision of available instruments. Although there exist today excellent special instruments for fixed observations, as, for example, the impersonal astrolabe of Danjon or the photographic zenith telescope, whose accuracy hardly leaves anything to be desired; nevertheless, one is constrained to use portable instruments for the truly geodetic-astronomic measurements, namely position and azimuth determination at field stations. These are necessarily somewhat less accurate than the stationary special instruments.

In making precise position and azimuth determinations at field stations, the question arises whether instruments and methods with or without scale readings should be used. T. Nathammer (1932) defends the opinion that "only those methods are to be designated accurate, which do not include the measurement of a vertical or horizontal angle, so that the result may not be distorted by the influence of scale division errors." The development of modern high-performance universal instruments, especially the improvement in precision of scale division, has indicated that this view is not shared today by various authors, as for example, A. Gougenheim and F. Mugica-Buhigas, even as concerns methods of horizontal angle measurement. In contrast with some processes of vertical angle measurement, however; for example, the

(Received for publication 1 December 1969)

astronomic angle method for determination of latitude, the methods of horizontal angle measurement have till this day had but little application. Since for a definite stellar arrangement the methods of horizontal angle measurement are just as accurate, with respect to errors of transit time and stellar coordinates, as the methods with a transit instrument; the supposed or the actual differences in the attainable accuracy can only be determined experimentally. The present work will therefore investigate how great the instrumental errors are in universal and transit instruments that affect the determination of a horizontal direction, and what influence these errors have on the accuracy of position determination by horizontal angle measurement and vertical transits.

The treatment of this question by means of astronomic observation seemed unpromising, since the influence of instrumental errors is overlapped by the influence of errors in star coordinates, time duration, refraction, etc. The direct investigation of individual instrumental errors not only gives dependable results, but also yields information about the origin of the errors and their elimination by procedural precautions. Aside from the investigation of scale division and level errors, there are available few dependable statements about individual instrumental errors in modern precision instruments. Up to now, there has been no comprehensive investigation of all instrumental errors. It is therefore not remarkable that, for example, in Mugica-Buhigas (1960) methods for position and azimuth determination are developed, which partly depend on wildly inappropriate assumptions about the magnitude and effect of separate instrumental errors. For these reasons it proves advantageous and necessary to investigate systematically the separate instrumental errors one by one, and exclusively by means of laboratory measurements.

The class of errors having to do with targeting (target errors, entrance errors, personal factor and secondary target axis errors) were excluded from the investigation. These errors must be considered in conjunction with the performance of the telescope tube (Michalcak, 1966) and with the methods of targeting (Steinert, 1961) in astronomic observations, so that their treatment exceeds the scope of a single work. It may be assumed that in this respect the investigated instruments differ less widely. In Section 6, the precision considerations were taken from corresponding quotations in the literature.

The universal instruments Wild T4 and Kern DKM3* and the transit instrument Askania AP70 were chosen for the investigation. The Wild T4 and the transit instrument AP70 are more or less equivalent in size and handiness. The Kern DKM3 is especially suitable for field use because of its compact build and light weight. Since

*The universal instrument Kern DKM3 A of the Geodetic Institute was required for investigations of stellar motion. Since the DKM3 and the DKM3 A have fundamentally the same construction, the results may be considered as applicable also to the Kern DKM3 A.

it differs essentially from the Wild T4 also in principle, that is, in a different system of axes, the comparison between these two instruments is of special interest. The investigation of both these universal instruments must also be seen in the light of the appearance of the universal instrument Theo 002 of the JENA optical works. In the Theo 002, determination of inclination by means of a level is replaced by stabilization of the target axis against inclination errors by means of a compensator (Jochmann, 1964). The expected improvement in accuracy depends on the contribution of the error of inclination determination and on the contribution of the azimuthal effective error of the tilt axis to the total accuracy of the instrument, and it will be possible to estimate this on the basis of the present results.

The instrumental errors to be investigated will, as a rule, not significantly exceed a magnitude of $1''$. Since measurements have to be reported with an accuracy such that their magnitudes are, wherever possible, greater by an order of magnitude than these error quantities, the development of suitable measurement methods becomes decisively important. In the present investigations, a maximum mean error of $\pm 0.05''$ in a single measurement of an individual instrumental error is strived for. It is further to be noted that the measurement procedures sought are to be universally applicable, since the instrumental errors to be measured are of very different nature and three different instrument types must be investigated. The measurement methods considered are fundamentally only interference and autocollimation methods. Interference methods are satisfactory with regard to accuracy, but demand high instrumental expense and are useful for goniometry only in several special cases at the present time (Duhmke, 1964). The autocollimation method, on the otherhand, is universally applicable, but the available autocollimators, according to specifications of manufacturers and the investigations of the author, yield no better accuracy than $\pm 0.2''$. Since specifications for the accuracy of angle measurement with collimators of long focal distance of Ochsenhirt (1962) promised a corresponding improvement in accuracy of autocollimation methods, these methods were chosen over the interference methods, and it was decided to construct an autocollimator of long focal distance. Optical angle measurements with a mean error of only a few hundredths of a second of arc are of substantial general technological interest since in principle no apparatus is available more accurate than the accuracy to which its errors can be measured. Furthermore, methods which apply to highest demands of precision can be applied to less demanding objects; for example, in the geodetic field, and to the investigation of second theodolites.

The author knows of no research on the accuracy of autocollimation measurements that goes beyond the determination of accuracy of coincidence (Ochsenhirt, 1962). Accordingly, the necessary investigation is to be undertaken. A separate section (Section 2) is devoted to the results and to the essential theoretical considerations. It may be read independently of the rest of the work. The arguments of Section 2.1

are intended only for those readers who are unfamiliar with the principle of autocollimation. The following Section 2.2 on the technical realization of optical and electro-optical autocollimators is included for the sake of completeness. Those readers who are interested exclusively in autocollimators are referred also to Sections 4.1 and 4.2, where methods for the investigation of instrumental errors are described.

At this point, I would like to express my sincere thanks to Professor Dr. K. Ramsayer, Director of the Geodetic Institute of TH Stuttgart, for his stimulation in this work and for his valuable support. My colleagues at the Geodetic Institute and at the Institute for Technical Optics of TH Stuttgart, as well as Dr. Ochsenhirt of Staatliche Ingenieurschule für Bauwesen in Essen stood by me in counsel and in deed. In special degree, I thank master mechanic E. Krause and engineer K. Rosch for their valuable collaboration on the construction of the autocollimation system. Likewise, I thank Messrs. E. Schmidt, H. Waimer, M. Stephani, and P. Vogel. Under guidance of the author, they have worked on subordinate projects in the framework of their own theses (Schmidt, 1963), (Waimer, 1965), (Stephani, 1965) (Vogel, 1966) and have contributed a substantial amount to the success of this investigation.

2. ANGLE MEASUREMENT WITH AUTOCOLLIMATION

2.1 Principle of Angle Measurement With Reciprocal Collimation and Autocollimation

Collimators are used in many ways in the investigation and adjustment of geodetic instruments in the laboratory (Ochsenhirt, 1962). Most often they serve to supply artificial distant targets, and excel in target definition and insensitivity against centering errors, and in other respects. In this case, the collimator consists essentially of an objective O_K and an illuminated mark M_1 located in the focal plane of the objective (Fig. 1). The rays from M_1 leave the objective parallel and

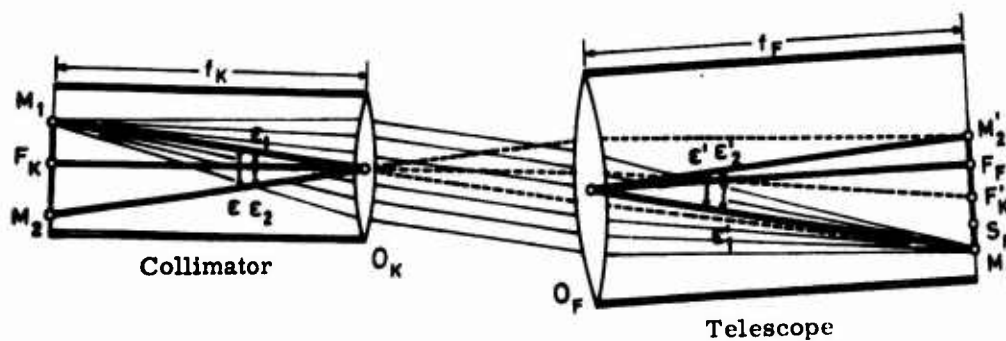


Figure 1. Angle Measurement with Reciprocal Collimation

form an image of the mark at infinity. Thus the collimator fixes a direction in space. The objective O_F of a telescope focused at infinity, that is, of a focal system with parallel incident and emitted rays, forms an image of the mark, apparently at infinity, as M_1' in the focal plane. The collimator and telescope are arranged in reciprocal collimation, that is, both systems are so arranged with respect to each other that the focal plane of one system is formed at the image in the focal plane of the other. The collimator is targeted by bringing the cross-hair S_F of the telescope into coincidence with the image M_1' . The target axes of collimator and telescope are thereby made three-dimensionally parallel.

Collimators are furthermore set up for the precise measurement of small angles. In Figure 1, the main rays through marks M_1 and M_2 and their images M_1' and M_2' form angles ϵ_1 and ϵ_2 , ϵ_1' and ϵ_2' , respectively, with the main rays through the focal points F_K and F_F , respectively. The following relations may be established in connection with the focal distances f_K and f_F :

$$\tan \epsilon_1 = \frac{\overline{M_1 F_K}}{f_K}; \tan \epsilon_2 = \frac{\overline{F_K M_2}}{f_K}; \tan \epsilon_1' = \frac{\overline{M_1' F_F}}{f_F}; \tan \epsilon_2' = \frac{\overline{F_F M_2'}}{f_F}$$

Because of the parallelism of the depicted main rays,

$$\epsilon = \epsilon' \quad (1)$$

For $\epsilon < 1^\circ$ the approximation

$$\tan \epsilon_1 = \epsilon_1,$$

holds with an error $< 0.1\%$ so that

$$\tan \epsilon_1 + \tan \epsilon_2 = \epsilon_1 + \epsilon_2 = \epsilon = \frac{\overline{M_1 M_2}}{f_K}; \tan \epsilon_1' + \tan \epsilon_2' = \epsilon_1' + \epsilon_2' = \epsilon' = \frac{\overline{M_1' M_2'}}{f_F}. \quad (2a, b)$$

Equations (1) and (2a, b) may be used to make angle measurements with reciprocal collimation. Measuring the separation of the marks or the mark images, one can compute the angles ϵ and ϵ' formed by the main rays, knowing the focal distances f_K and f_F . If, for example, the collimator is equipped with an illuminated cross-hair and the telescope with an ocular and scale, the tilt $\Delta\epsilon$ of the collimator can be determined by scale measurement of the displacement Δs of the crosshair image in the telescope focal plane. The tilt $\Delta\epsilon$, according to Eq. (2b), is given by

$$\Delta\epsilon = \frac{\Delta s}{f_F}.$$

The common variants of angle measurement by means of reciprocal collimation are summarized in Table 1. The collimator is equipped with an illumination device and the telescope with a reading device. The collimator and telescope may each be further equipped with crosshairs, scale or micrometer. Direction changes can be effected by tilting the collimator, tilting the telescope, displacing the crosshairs, or resetting the micrometer. It is to be noted that parallel displacements of collimator or telescope do not influence the image position or the angle measurement. The possibilities enumerated in Table 1 may be doubled by interchange of illumination and reading devices.

Table 1. Variants of Angle Measurement with Reciprocal Collimation

Collimator equipped with	Telescope equipped with	Means of Direction Alteration	Method of Angle Measurement
Illumination, Crosshairs	Ocular-Scale	Tilting the Collimator Displacement of Coll. Crosshairs Tilting the Telescope	Reading the Image Displacement on the Scale (f_F)*
Illumination, Crosshairs	Ocular-Micrometer	Tilting the Collimator Displacement of Coll. Crosshairs Tilting the Telescope	Micrometer Meas. of Image Displacement (f_F)
Illumination, Crosshairs	Ocular Crosshairs -Divided Circle	Tilting the Collimator Displacement of Coll. Crosshairs	Coincidence of Crosshairs Reading on Divided Circle
Illumination, Scale	Ocular-Crosshairs	Tilting the Collimator Tilting the Telescope Displacement of Coll.	Reading the Crosshair Displacement on the scale (f_K)
Illumination, Micrometer (Artificial Star)	Ocular-Crosshairs Ocular-Micrometer	Displacement of Coll. Micrometer	Coincidence of Crosshairs and Reading on the Micrometer (f_K, f_F)

*Focal length for conversion of Image Displacement to angle measurement.

A direction change of the collimator can be measured, according to Table 1, also by means of readings from the divided circle of a theodolite. Rotating the alidade as required in the measurement procedure causes a three-dimensional turning of the theodolite telescope. In angle measurement with a scale or micrometer, on the other hand, the position of the telescope is preserved. Such a telescope

that is equipped with a measuring device, and which does not change its direction in space during the measurement process, will be designated a measuring telescope to separate it from a target telescope.

The condition, imposed until now, that the target axes of the collimator and telescope be parallel, may be dropped if the beam of parallel rays is appropriately directed by a flat mirror (Fig. 2). Here the above statements on angle measurement by means of reciprocal collimation apply unqualified. But if the collimator and telescope are held fixed, and the flat mirror tilted through α , the reflected rays are

turned through 2α ; the mark image M' goes to the position M'' . The image displacement $M'M'' = s$ and the mirror tilt α are related by the expression

$$\alpha = \frac{s}{2f} \quad (3)$$

where f means the focal length of the system in whose focal plane the image displacement is measured.

The reciprocal stability of collimator and telescope is best guaranteed when the telescope is identical with the collimator, as is the case in autocollimators. An autocollimator is a measuring telescope which projects to infinity a mark in the focal plane of the objective and reforms the image in the focal plane from rays reflected from a plane mirror. The separation of projected and reflected ray bundles is accomplished by an optical separation surface in the vicinity of the focal point. The autocollimation mirror (AC^{*}-mirror) must be set up perpendicular to the target axis according to the measurement range. The autocollimator and the AC-mirror form together an autocollimation system (AC-system). Specifics are given in the following section on the technical realization of autocollimators, but

*The designation AC here and later refers to "autocollimation."

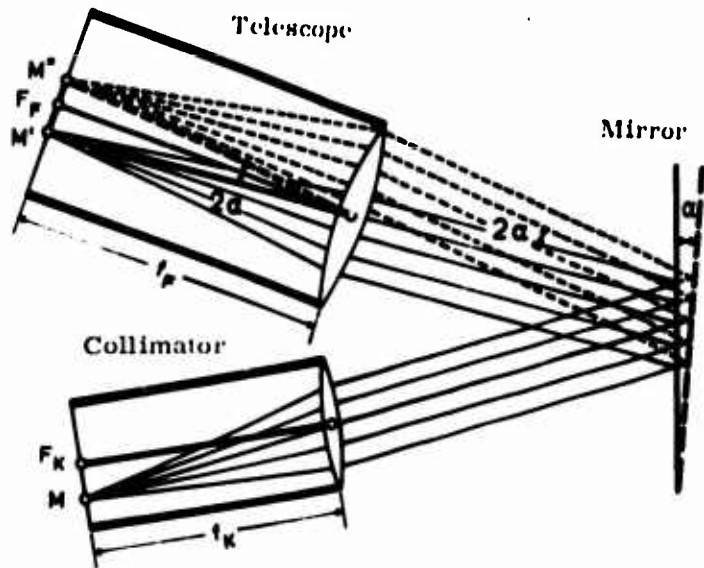


Figure 2. Measurement of Mirror Rotations with Reciprocal Collimation

only autocollimators with micrometers are considered.

2.2 Technical Realization of Autocollimators

There are today numerous possibilities for the technical realization of the autocollimation principle (Hume, 1964). The two main groups of autocollimators differ fundamentally in the method by which image displacement is measured. In optical autocollimators with visual reading, the measurement devices consist essentially of optical and mechanical elements, while in electro-optical autocollimators the image displacement is measured by photo-electric techniques.

2.2.1 OPTICAL AUTOCOLLIMATORS

According to Eq. (3) the tilt of the AC-mirror α is determined, with knowledge of the focal length f_K of the autocollimator, from measurement of image displacement s . If s is in error by ds and f_K by df_K , then

$$d\alpha = \frac{1}{2f_K} ds - \frac{s}{2f_K^2} df_K. \quad (4)$$

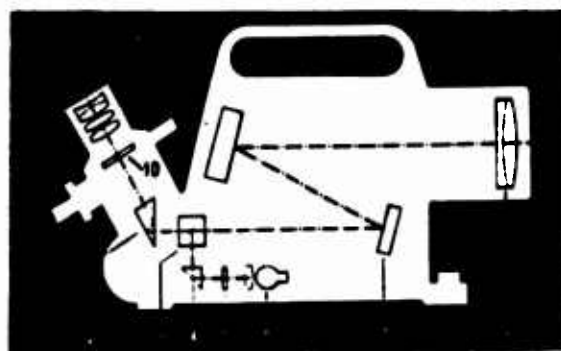
Thus, for example,

$$f_K = 500\text{mm}, df_K = -0.25\text{mm}, s = 5\text{m}, ds = 1\mu\text{m}; d\alpha = 0.4'' + 0.5'' = 0.9''.$$

An error ds enters directly into the angle measurement with a factor $1/2f_K$; the error df_K , which is constant for an AC-system, is manifested as a scale error $df_K/2f_K^2$. Accordingly, the largest possible focal lengths are strived for in the construction of autocollimators; simultaneously, the length of the instrument should be as small as possible for the sake of handiness. According to Eq. (4), the accuracy of angle measurement depends directly on the accuracy of the micrometer measurement, so that special attention should be devoted to the design of the micrometer. Besides the objective and the micrometer, the incorporation of the AC graduated dial and the choice of the optical separation surface are other essential aspects to the construction of the autocollimator. Before the introduction of different production line instruments, the technical construction of an optical autocollimator, by way of example, will be explained in detail.

As an example, the Leitz autocollimation telescope of $f = 500$ is introduced (Figs. 3, 4) because of the use of the Leitz coordinate measurement ocular. In Figure 3, the rays go out from the collimator graduated dial 5, meet by way of the deflection prism 4 on the separation cube 3 and are then directed by its optical separation surfaces to the mirrors 7 and 8. The crosshair plate 5 is located in the focal plane of the objective 9, so that the rays are parallel upon leaving the objective. The rays reflected from a plane mirror form an image through the objective by way of mirrors 8 and 7, separation cube 3 and deflection prism 2 in the micrometer measurement

plane 10 corresponding to the focal plane of the fine measurement ocular 1. A separation cube consists of two equal-sided right-angle prisms; the hypotenuse surface of one prism is semitransparent. The displacement of the crosshair image is measured with a fine measurement ocular (App. A). The fine measurement ocular is available in two forms for the direct measurement of one coordinate and for the direct measurement of two coordinates (coordinate ocular). It carries in the measurement plane a fixed crosshair plate with a 0.5 minute interval; the crosshair image is displaced and measured by means of an optical micrometer with a plane plate. In the coordinate ocular, the plane plate is tipped about a diagonal, so that the crosshair image is movable diagonally in the right angled coordinate system (App. B) After the description of the Leitz autocollimation telescope, specifications will be given in the following about the construction and technical data of different production line autocollimators (App. C). The optical system, the measurement devices, and the arrangement of crosshairs and micrometer with respect to the optical axis, will be treated in detail.



1. Fine Measurement Ocular
2. Deflection Prism
3. Separation Cube
4. Deflection Prism
5. Crosshair Plate
6. Light Source
7. Deflection Mirror
8. Deflection Mirror
9. Objective
10. Micrometer Measurement Plane

Figure 3. Optical System of the Leitz Autocollimation Telescope

The optical system consists, in the simplest case, of objective and ocular (App. C, Nos. 3, 7). The average focal length of 500mm requires elongated construction, which can be reduced almost in half by means of folding the ray path with plane mirrors (Nos. 1, 6, 8). A shortening of the body length is likewise possible if, in place of an ocular, a microscope is used (Nos. 2, 4, 5); telescopic objective and microscope objective form a tele-system, whose equivalent focal length enters into Eq. (3) as the effective focal length (Fig. 5).



Figure 4. Leitz Autocollimation Telescope

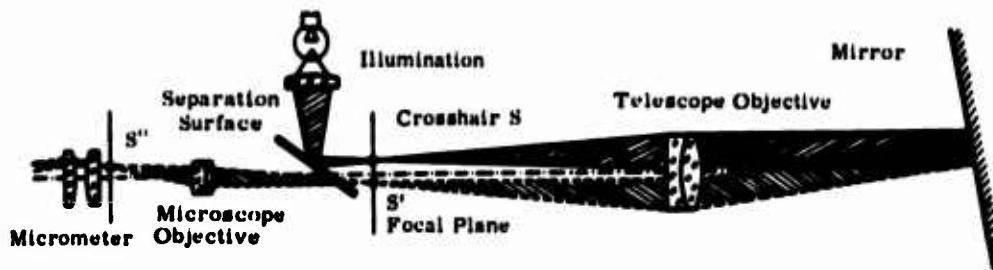


Figure 5. Optical System of the Micro-optic Autocollimator of Hilger & Watts

As a rule, a screw micrometer serves as the measuring device; optical micrometers are used in connection with the fixed division of a crosshair plate because of the required measurement range of several millimeters (No. 3, 6). For many practical tasks it is important to know if the displacement of the crosshair image can be directly measured in one or two coordinate directions (App. C, column "coordinate directions"). In instruments with which only one coordinate direction can be measured directly, the micrometer or the telescope may be turned by 90° , so that in this manner also measurements in another coordinate direction are possible.

The arrangement of crosshair and micrometer with respect to the optical axis of the objective depends, among other things, on the choice of the optical system. In systems without tele-objective, the crosshair can be situated laterally, that is, perpendicular to the optical axis of the objective, and the micrometer can be situated centrally, that is, on the optical axis (No. 2, 3, 6). Conversely, the crosshair can be situated centrally and the micrometer laterally (No. 8). In systems with tele-objectives, the crosshair and the micrometer are situated, as a rule, centrally (No. 4, 5, 7), so that crosshairs and crosshair image appear simultaneously in the field of vision (Fig. 5).

2.2.2 ELECTRO-OPTICAL AUTOCOLLIMATORS

The principle of autocollimation presents itself to automation very conveniently, since in contrast with other image measurement procedures, the shape and manner of the object to be projected can be broadly determined by the designer. In electro-optical autocollimators, photo-electric measurements replace visual observation and optical-mechanical measurement of image displacement. The measurement principle will be demonstrated by way of an example, the "servo operated autocollimator" TA58 of Hilger & Watts (Hume, 1964) (Fig. 6). The model TA58 represents further development of the TA3, which was adopted by the author in his investigations for comparison measurements. The laterally situated crosshair S

forms the image S' by way of separation cube 1, objective, mirror, objective, and separation cube 2. A moveable slit, whose width corresponds roughly to the crosshair image, and which oscillates with a frequency of 50 Hz and an amplitude of twice the slitwidth, has then the exit arrangement depicted in Figure 6. The incident rays pass the oscillating slit, according to its instantaneous position, in variable cross sections, and meet at a photocell. The photocell has a modulated alternating voltage, which is demodulated in a discriminator, retaining the phases. The smoothed and amplified direct current, whose sign and magnitude depend on allocation by the slit, drives a servomotor, which in turn moves the oscillating slit on a spindle. In the case of coincidence of slit and crosshair image, the photocell generates a sinusoidally alternating voltage of 100 Hz, so that after the demodulation there is no current fed to the servomotor. At this setting of the oscillating slit, the potentiometer, which is likewise driven by the servomotor, gives an output voltage that is proportional to the position of the oscillating slit, that is, to the displacement of the crosshair image. The output voltage of the potentiometer can be further manipulated in analog or digital form.

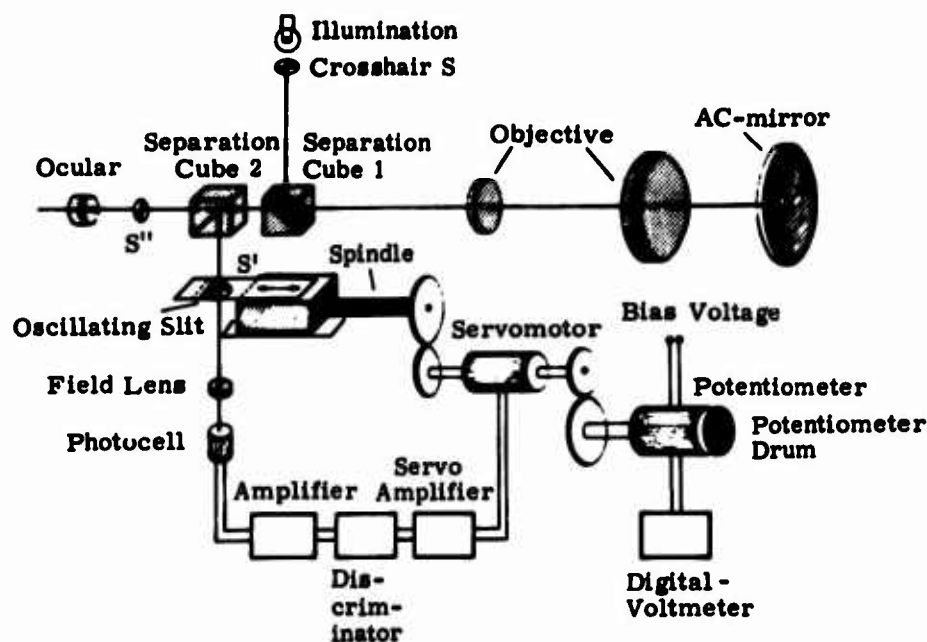


Figure 6. Principle of the Electro-Optical Autocollimator TA58 of Hilger & Watts

As a consequence of the growing demands of machine construction in aerospace and space technology, the development and demand for electro-optical autocollimators has been strongly catalyzed, so that today a number of electro-optical autocollimators

are available, which can also be employed advantageously for investigations of geodetic instruments. In Appendix D are presented the production line electro-optical autocollimators known to the author. The specifications were partially taken from prospectuses and in part conveyed by users. There are two groups to differentiate as regards measurement devices:

1. Measurement devices with motor-driven parts (Nos. 1-4, 6, 7): The moveable part of a micrometer is turned by a servomotor in a measurement, until a photocell determines coincidence of object mark and image mark by means of modulated or polarized light.
2. Measurement devices without motor driven parts (Nos. 5, 8): the ray bundle reflected from the mirror is split and falls on two photocells; by measurement of the difference of the two light currents, the position of the image mark is determined directly with respect to a relative value.

The measurement output may be realized in analog form by means of drum readings, scale readings, or a recorder; the digital output from a digital voltmeter can be displayed numerically or taken up by a printer or a data register. Aside from the wide choice of output possibilities, the following are further advantages of automatic measurement: High measurement speed, arbitrarily long measurement duration, remote control and elimination of crude errors. Different electro-optical autocollimators have the capacity to take continuous measurements of slow mirror rotations up to $200''/\text{sec}$ (App. D, column "retrieval speed") and, for example, of steering rotations of the AC mirror by way of feedback according to prescribed rules. The relative accuracy of the autocollimators lies as a rule between 1% and 5% of the measurement magnitude. Different models offer the possibility of reducing the measurement magnitude by one or two powers of ten, whereby the tolerance brackets are reduced correspondingly. As a certain disadvantage of the electro-optical devices it may be mentioned that the reference point of the measurements does not remain constant (App. D, column "Zero constancy"). The changes in setup due to external influences can nevertheless, according to Section 2.7.2.2, reach similar values. Further, the high procurement costs must be mentioned, which makes the installment of electro-optical autocollimators justifiable only for sequential investigations or for important projects.

2.3 Autocollimation Systems and Their Properties

2.3.1 IMAGE MIGRATION UNDER THREE-DIMENSIONAL ROTATIONS OF PLANE OPTICAL SURFACES

In the AC systems treated up to now, it was demanded that the AC measuring mirror be set up perpendicularly on the target line of the autocollimator in accordance with the measurement range of the autocollimator. This condition is eliminated if plane optical surfaces (plane mirrors, prisms) are introduced between the

autocollimator and measuring mirror, to deflect the ray path as required. Since three-dimensional rotations of a deflection element produce a migration of the AC-crosshair image, it is necessary to derive the relation between vertical and azimuthal components of image migration and the three-dimensional rotations of the different optical surfaces. In derivation of the formulas, it is best to resort to the vectorial formulation of the reflection and refraction laws (Flugge, 1956, 1962).

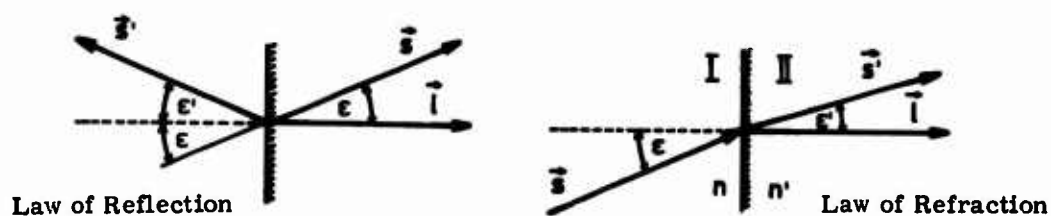


Figure 7. Vectorial Formulation of Reflection and Refraction Laws

If \vec{s} is the vector of an incident ray, \vec{I} the normal vector of the optical surface and n and n' the refraction indices of media I and II (Fig. 7), then for the vector \vec{s}' of the reflected or refracted ray:

$$\vec{s}' = \vec{s} - 2(\vec{s} \cdot \vec{I}) \vec{I}, \quad (\text{Reflection law}) \quad (5)$$

$$\vec{s}' = \frac{n}{n'} \vec{s} - \frac{n}{n'} (\vec{s} \cdot \vec{I}) \vec{I} + \sqrt{1 - \left(\frac{n}{n'}\right)^2 + \left(\frac{n}{n'}\right)^2 (\vec{s} \cdot \vec{I})^2} \vec{I}. \quad (\text{Refraction law}) \quad (6)$$

The vectors can be analyzed in a three-dimensional right-handed coordinate system whose $+y$ axis coincides with the zenith, and whose $+x$ axis coincides with a horizontal reference direction, for example, the meridian, into their x, y, z components. Since AC systems are insensitive to parallel displacements of their elements, the vectors may be translated to the origin of the coordinate system. At the origin, the vectors coincide with the coordinate axis or with other reference directions, as, for example, the vector \vec{s} of the incident ray (target axis of the autocollimator) with the $+x$ axis. Turning the vectors \vec{s} and \vec{I} each in turn through the angle α about the $+x$ axis, through the angle β about the $+y$ axis and through the angle γ about the $+z$ axis, the components of the rotated vectors can be given as functions of rotation angle. The rotation angles may be qualified as small ($< 1^\circ$), and are positive if a rotation is made from the reference direction clockwise to the instantaneous position. The vectorial calculation proceeds by taking the deflected beam \vec{s}' as the incident beam \vec{s} for the next optical deflection. After the last deflection, the $+y$ component of the vector \vec{s}' gives the inclination of the beam entering the

autocollimator with respect to the horizontal and $-z$ component gives the azimuthal rotation from the reference direction.

2.3.2 SIMPLE AUTOCOLLIMATION

There often arise, in practical applications, aside from direct autocollimation with a vertical AC measuring mirror (App. E, top), measurement arrangements with a 90° deflection of the beam path. For a horizontal AC measuring mirror, the deflection can be executed with a deflection mirror inclined at 45° or, for instance, with a pentagonal prism. Thereby it is of special interest to what degree three-dimensional rotations of the deflection mirror and the pentagonal prism affect the azimuthal components of image migration. The investigation follows in the formulation, described in Section 2.3.1, of the reflection and refraction laws, and the deflection by means of a deflection mirror (App. E, middle) is treated in detail. The vectors \vec{s} , \vec{T}_u , and \vec{T}_a are depicted in Figure 8 together with their components, and are presented in Appendix E.

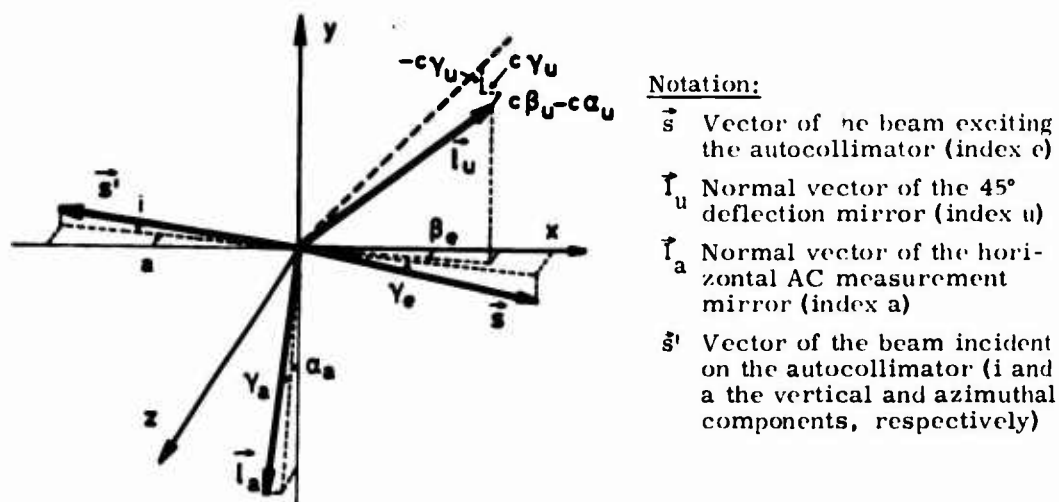


Figure 8. Vector Components on 90° Deflection with Deflection Mirror

The reflection (1) of the incident beam at the deflection mirror, the reflection (2) at the AC measuring mirror and the reflection (3) at the deflection mirror lead to the following intermediate results.

Vector	x	y	z
$\vec{s}_1 = \vec{s}$	+ 1	- γ_e	+ β_e
\vec{s}_1'	- $2\gamma_u + \gamma_e$	- 1	- $\beta_u + \beta_e + \alpha_u$
\vec{s}_2'	- $2\gamma_u + \gamma_e + 2\gamma_a$	+ 1	- $\beta_u + \alpha_u + \beta_e - 2\alpha_a$
$\vec{s}_3' = \vec{s}'$	- 1	+ $4\gamma_u - \gamma_e - 2\gamma_a$	- $2\beta_u + 2\alpha_u + \beta_e - 2\alpha_a$

The components of the vector \vec{s}' after the last reflection are taken up in Appendix E. The analogous calculation of the beam path for a pentagonal prism gives the results presented in Appendix E (bottom). According to that, the inclination i of the beam entering the autocollimator with respect to the horizontal is

$$\text{with deflection mirror: } i_u = 4\gamma_u - \gamma_e - 2\gamma_a, \quad (7a)$$

$$\text{with pentagonal prism: } i_p = -\gamma_e + 2\gamma_a. \quad (7b)$$

A tilt γ_u of the deflection mirror about the z axis enters with a four-fold magnitude while -- as is already known -- small three-dimensional rotations of the pentagonal prism have no influence on the vertical components of the image position. The azimuthal rotation α of the beam entering into the autocollimator with respect to a reference direction is, according to Appendix E, independent of deflection method:

$$\text{Deflection mirror: } a_u = +2\beta_u - 2\alpha_u - \beta_e + 2\alpha_a, \quad (8a)$$

$$\text{Pentagonal prism: } a_p = +2\beta_p - 2\alpha_p - \beta_e + 2\alpha_a. \quad (8b)$$

If, accordingly, the azimuthal rotation α_a of the AC-measuring mirror is necessary, then the pentagonal prism (or Wollaston prism) offers no advantage over a 45° deflection mirror. The rotations α_u and β_u of the deflection mirror and α_p and β_p of the pentagonal prism can, however, according to Section 2.3.4.3, be controlled by means of multiple autocollimation, where the control with a pentagonal prism is to be considered the more practical. A prism combination which deflects the beam path by 90° and whose three-dimensional rotations also have no influence on the azimuthal component a of the image position, would be advantageous for numerous applications in technical optics. In view of Eqs. (8a, b) and of greater applicability, as, for instance for multiple reflection described in the following section, deflection mirrors were chosen over deflection prisms in the present work.

2.3.3 MULTIPLE REFLECTION

2.3.3.1 Principle of Multiple Reflection.

Multiple reflection represents an extension of simple autocollimation with deflection mirrors. A mirror pair, for example, deflection mirror and AC measuring mirror, forms the angle δ ($\delta < 45^\circ$) (Fig. 9). Incident light rays are each multiply-reflected on the two mirror surfaces, then, after a certain number of reflections, change the direction of their path and, after further reflections, leave the mirror pair. This phenomenon is also called optical multiplication and is employed, in part, in measurement apparatuses (Flugge, 1956; Janich, 1954). The 90° deflection with a deflection mirror represents a limiting case of multiple reflection. For quantitative description, angles are defined by the notation of Figure 9.

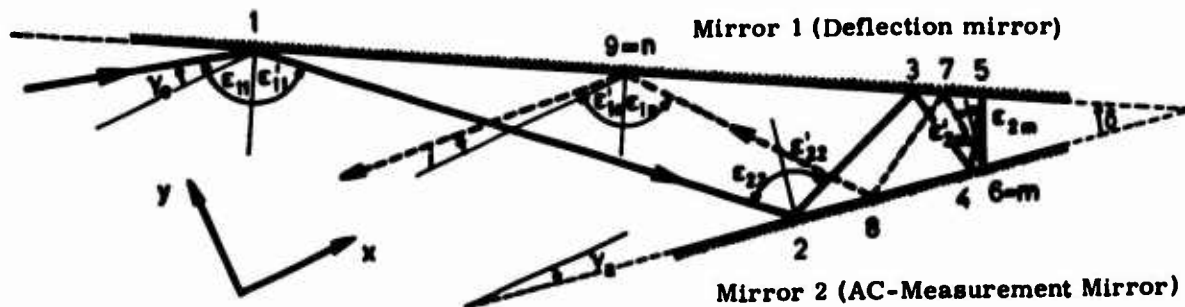


Figure 9. Principle of Multiple Reflection with a Mirror Pair

If γ_e is the vertical angle between the x axis of the coordinate system defined in Section 2.3.1 and the incident beam, and γ_a is the vertical angle between the x axis and mirror 2, (the AC measuring mirror), and the first reflection occurs on mirror 1 (the deflection mirror), then according to Janich (1954), the incident and outgoing angles ϵ_{1k} and ϵ_{1k}' , and $\epsilon_{2,k+1}$ and $\epsilon_{2,k+1}'$ are related to the reflection k of mirror 1 and $k+1$ of mirror 2 as follows:

$$\begin{aligned}
 \epsilon_{11} &= (90^\circ + \gamma_e - \gamma_a) - \delta, & \epsilon_{11}' &= -(90^\circ + \gamma_e - \gamma_a) + \delta, \\
 \epsilon_{22} &= (90^\circ + \gamma_e - \gamma_a) - 2\delta, & \epsilon_{22}' &= -(90^\circ + \gamma_e - \gamma_a) + 2\delta, \\
 &\vdots & &\vdots \\
 \epsilon_{1k} &= (90^\circ + \gamma_e - \gamma_a) - k\delta, & \epsilon_{1k}' &= -(90^\circ + \gamma_e - \gamma_a) + k\delta, \\
 \epsilon_{2,k+1} &= (90^\circ + \gamma_e - \gamma_a) - (k+1)\delta, & \epsilon_{2,k+1}' &= -(90^\circ + \gamma_e - \gamma_a) + (k+1)\delta.
 \end{aligned} \tag{9}$$

For the given δ , γ_e and γ_a there occurs, at a certain number of reflections m , a sign change of the incidence angle at mirror 1 or 2.

from

$$90^\circ + \gamma_e - \gamma_a - m'\delta = 0$$

can be obtained

$$m' = \frac{90^\circ + \gamma_e - \gamma_a}{\delta}. \quad (10)$$

Rounding m' off to the nearest whole number m gives the number of reflections upon which the incidence angle changes sign. The quantity δ is determined by Eq. (17) in Section 2.3.3.2. Depending on whether m is odd or even, the sign change occurs on mirror 1 or mirror 2. For the AC system it is only of interest to determine the measurement arrangement for which the first and last reflection takes place on the same mirror (mirror 1). In this case, the number of reflections at mirror 1 is $n_1 = m-1$ and at mirror 2, $n_2 = m-2$, and the total number of reflections is $n = 2m-3$. The angle $(\gamma_e - i)$, formed by the incident rays and the outgoing rays, is

$$\gamma_e - i = \gamma_e - (\epsilon_{1n} - (90^\circ - \gamma_a - \delta)) = 180^\circ + 2\gamma_e - 2\gamma_a - (n+1)\delta. \quad (11)$$

$(\gamma_e - i)$, in autocollimation, may not exceed the measurement range of the autocollimator, that is,

$$\gamma_e - i = 180^\circ + 2\gamma_e - 2\gamma_a - (n+1)\delta \approx 0. \quad (12)$$

Given a definite number of reflections n , the corresponding angle is, according to Eqs. (11) and (12)

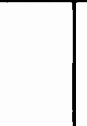
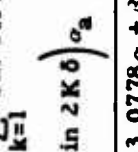
$$\delta = \frac{180^\circ + 2\gamma_e - 2\gamma_a}{n+1} \quad (13)$$

If the incident ray and mirror 2 both lie exactly on the x axis, then

$$\delta_0 = \frac{180^\circ}{n+1}. \quad (13a)$$

Equation (13a) checks with the specifications in Janich (1954). In Table 2 the useful cases of multiple reflection with a mirror pair in autocollimation are displayed. The detailed discussions are given in the following section.

Table 2. Multiple Reflections with a Mirror Pair

Defl. Angle δ_0	No. of Refl. n	Refl. in sign change	Representation	Image Migrations under 3D Rotations		Magn. Comp. V_0	Measure. range (%)			Mirror ϕ const. (de+d)
				Vertical Compon.	Azimuthal Components		Vert. Az.	Mir.	Ak-Mir.	
1	2	3	4	5	6	7	8	9	10	11
45°	3	2 or 3		$4\gamma_u - \gamma_e - 2\gamma_a$	$-2\beta_u + 2(\sin 2\theta)\alpha_u + \beta_e$ $-2(\sin 2\theta)\alpha_a$	1	100	100	1, 41	1, 00
30°	5	3 or 4		$6\gamma_u - \gamma_e - 4\gamma_a$	$-2\beta_u + 2(\sin 2\theta + \sin 4\theta)\alpha_u$ $+ \beta_e - 2(\sin 2\theta + \sin 4\theta)\alpha_a$ $-2\beta_u + 2\sqrt{3}\alpha_u + \beta_e - 2\sqrt{3}\alpha_a$	$\frac{2}{\sqrt{3}}$	50	58	2, 00	1, 15
22, 5°	7	4 or 5		$8\gamma_u - \gamma_e - 6\gamma_a$	$-2\beta_u + 2\left(\sum_{k=1}^3 \sin k \cdot 2\theta\right)\alpha_u + \beta_e$ $-2\left(\sum_{k=1}^3 \sin 2k\theta\right)\alpha_a$	$\frac{3}{1+\sqrt{2}}$	33	41	2, 61	1, 41
18°	9	5 or 6		$10\gamma_u - \gamma_e - 8\gamma_a$	$-2\beta_u + 2(1+\sqrt{2})\alpha_u + \beta_e - 2(1+\sqrt{2})\alpha_a$ $-2\beta_u + 2\left(\sum_{k=1}^4 \sin 2k\theta\right)\alpha_u + \beta_e$ $-2\left(\sum_{k=1}^4 \sin 2k\theta\right)\alpha_a$ $-2\beta_u + 2 \cdot 3.0778\alpha_u + \beta_e - 2 \cdot 3.0778\alpha_a$	$\frac{4}{3.078}$	25	32	3, 24	1, 70
$\frac{180}{n+1}$	n	$\frac{(n+1)/2}{\text{or}} \frac{(n+2)/2}$	See Figure 9	$2\left(\frac{n+1}{2}\right)\gamma_u - \gamma_e - 2\left(\frac{n-1}{2}\right)\gamma_a$	$-2\beta_u + 2\left(\sum_{k=1}^{\frac{n-1}{2}} \sin 2k\theta\right)\alpha_u$ $+ \beta_e - 2\left(\sum_{k=1}^{\frac{n-1}{2}} \sin 2k\theta\right)\alpha_a$	$\frac{n-1}{2 \cdot c_0}$	$\frac{200}{n-1}$	$\frac{100}{c}$	$\frac{1}{\sin \delta_0}$	$\frac{1}{\sin 2\delta_0}$

2.3.3.2 Image Migration Under Three-Dimensional Rotations of a Mirror Pair

The three-dimensional rotation of the beam entering the autocollimator can be represented, according to Section 2.3.1, in analog form as a function of the three-dimensional rotations of the beam leaving the autocollimator, \vec{s} , and the normal, \vec{T}_a , of mirror 2 (AC measuring mirror). The components of the vectors are as follows:

Vector	x	y	z	
\vec{s}	+1	$-\gamma_e$	$+\beta_e$	
\vec{T}_u	$v+u\gamma_u$	$u-v\gamma_u$	$v\beta_u-u\alpha_u$	$u = \cos \delta$
\vec{T}_a	$-\gamma_a$	-1	$+\alpha_a$	$v = \sin \delta$

γ_u is the vertical angle between the normal \vec{T}_u of the deflection mirror and the vector \vec{T}_0 , which gives the deficit direction of \vec{T}_u and is inclined to the xz plane by $90^\circ - \delta_0$ ($\delta_0 = 45^\circ, 30^\circ, 22.5^\circ \dots$). The vector calculation for the general case with n reflections gives:

Vertical components i of image migration:

$$i = 2 \left(\frac{n+1}{2} \right) \gamma_u - \gamma_e - 2 \left(\frac{n-1}{2} \right) \gamma_a \quad n = 3, 5, 7, \dots \quad (14)$$

Azimuthal components a of image migration:

$$a = -2\beta_u + 2c \alpha_u + \beta_e - 2c \alpha_a \quad n = 3, 5, 7, \dots \quad (15)$$

where c is defined by

$$c = \sum_{k=1}^{(n-1)/2} \sin(2k\delta) \quad (16)$$

δ is the instantaneous angle between the deflection and AC measuring mirrors:

$$\delta = \delta_0 + \gamma_u - \gamma_a \quad (17)$$

Equations (14) and (15) check with the corresponding specifications in Janich (1954). In the case

$$\delta = \delta_0 = 100^\circ / (n+1)$$

the identity holds:

$$c_0 = \sum_{k=1}^{(n-1)/2} \sin \left(2k \frac{180^\circ}{n+1} \right) = \cotan \frac{180^\circ}{n+1} \quad n = 3, 5, 7, \dots \quad (16a)$$

With Eq. (16a), Eq. (15) becomes

$$a = -2\beta_u + 2 \cotan \frac{180^\circ}{n+1} \alpha_u + \beta_c - 2 \cotan \frac{180^\circ}{n+1} \alpha_a \quad n = 3, 5, 7, \dots \quad (15a)$$

Since the actual angle δ is not a priori accurately known, one must be satisfied, for many applications, with Eq. (15a) instead of Eq. (15). Further, it is to be noted that according to Eqs. (16) and (17) the factor c is not constant if there is a longitudinal tilt (γ_a) in addition to the transverse tilt (α_a) of the AC measuring mirror. The following table shows the affect of a change Δc in the factor c on the measurement of the transverse tilt α_a , based on a measurement range of 5' and 15' in simple autocollimation.

δ_0	Measurement Range 5' with Simple AC				Measurement Range 15' with Simple AC			
	45°	30°	22.5°	18°	45°	30°	22.5°	18°
γ_a max ["]	300	150	100	75	900	450	300	225
c_0	1.0000	1.7321	2.4142	3.0777	1.0000	1.7321	2.4142	3.0777
c	1.0000	1.7313	2.4133	3.0757	0.99996	1.7298	2.4092	3.0717
Δc [‰]	0.00	0.46	0.58	0.65	0.04	1.13	2.07	1.95
α_a max ["]	300	173	124	97	900	520	373	292
$\Delta \alpha_a$ [‰]	0.00	0.08	0.07	0.06	0.04	0.59	0.77	0.57

The error in c can be eliminated either by limiting the measurement range or by simultaneous measurement in both coordinate directions and taking into account, in the computation, of the measured change in γ_a , according to Eqs. (17) and (16).

According to Eqs. (14) and (15), the relation between image migration w and α_a with longitudinal tilt α_a and transverse tilt is:

$$w = \frac{n-1}{2c} \alpha_a \quad (18)$$

In Table 2, column 7, is entered the scale relation w_0 for $\delta = \delta_0$. According to Eq. (18), it should be noted that the scale criteria for longitudinal and transverse tilt are different even at 90° deflection, since the deviation γ_u of the mirror normal \vec{I}_u from the reference direction \vec{I}_0 ($\delta_0 = 45^\circ$) can assume greater values with each alignment of the mirror and autocollimator.

Besides the reduction of the measurement range of the vertical and azimuthal image migration by a factor $2/(n-1)$, or $1/c$ (col. 8, 9), the required size of the mirror (col. 10, 11) is also of interest. If the diameter of the image-forming ray bundle is not to fall under a definite value d_a , the diameters of the reflection mirror and the

AC measurement mirror are constrained to the following values:

$$\phi_u = (d_0 + d) / \sin \delta, \quad \phi_a = (d_0 + d) / \sin 2\delta,$$

where d refers to the minimum separation of the two mirrors. From experience in practice, it is known that d_0 should, where possible, be greater than 45mm. Then, for example, for $\delta_0 = 22.5^\circ$ and $d = 20\text{mm}$,

$$\phi_u = 170 \text{ mm}, \quad \phi_a = 90 \text{ mm}.$$

The advantages and disadvantages of multiple reflection are treated in Section 2.3.5.

2.3.4 MULTIPLE AUTOCOLLIMATION

2.3.4.1 Principle and Technical Realization of Multiple Autocollimation

Multiple autocollimation, like multiple reflection, is a process for the multiplication of the measurement accuracy attainable by simple autocollimation. Multiple autocollimation offers additional advantages in that the region of applicability is wider in comparison to multiple reflection. The method was first applied by Graul (1952) to the improvement in measurement accuracy in dispersion measurements with a spectrometer, and was subsequently not applied to the general AC measurement technique. Bringing into the beam path between autocollimator and AC mirror a semitransparent mirror (T mirror), that is, a plane parallel plate where one surface is coated with a layer of definite reflectivity, the rays between the AC mirror and the semitransparent mirror, according to Figure 10, are partially multiply-reflected and enter the autocollimator through the semitransparent mirror.

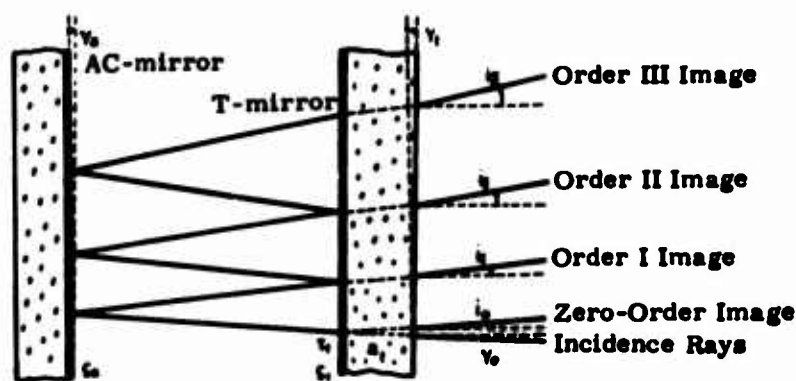


Figure 10. Principle of Multiple Autocollimation

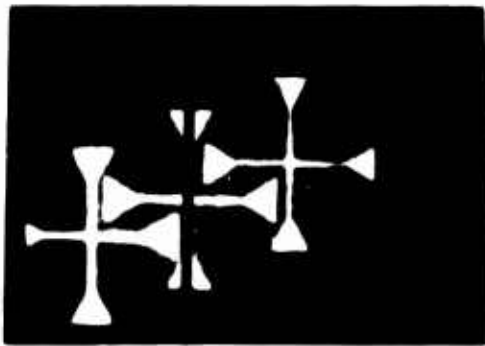


Figure 11. Multiple Autocollimation: Image Orders 0 to IV

The resulting image of zero order (directly reflected on the T mirror), and I., II., ...K. orders appear upon the corresponding inclination of the mirror in the field of view of the autocollimator and can be separated according to their decreasing brightness (Fig. 11). If desired, the semitransparent mirror can be set up so that its semitransparent layer is either facing toward or facing away from the AC measurement mirror; the former arrangement is optically more advantageous. Upon turning the AC mirror

through γ_a , the image of order I migrates by $2\gamma_a$, order II by $4\gamma_a$, order III by $6\gamma_a$, and so forth. In the present investigations, images could be observed up to sixth order, and micrometrically measured up to third order. The realization of multiple autocollimation essentially depends on the solution of the optical problem. From previous experience, multiple autocollimation can be achieved only if a slit is used in place of the collimator crosshair. The intensity of the slit image of the Kth order depends on the order K, the light source intensity, the geometrical arrangement of the path of the illumination beam, and on the reflectivity of the semitransparent mirror.

Letting

- ϕ_0 be the light current leaving the autocollimator,
- ϕ_K the light current entering from the image of Kth order,
- s_a the reflectivity of the AC measurement mirror,
- s_t the reflectivity, a_t the absorptivity, and τ_t the transmission factor of the semitransparent mirror, then, with the semitransparent surface facing the AC measurement mirror,

$$\phi_K = \tau_t^2 \cdot s_t^{K-1} \cdot s_a^K \cdot \phi_0.$$

Here it is taken into account that $s_t + a_t + \tau_t = 1$. The optimum brightness of the image of Kth order, that is, the maximum light current ϕ_K as a function of the reflectivity, is determined by:

$$\frac{d\phi_K}{ds_t} = \text{const} \left((K-1) (1-2a_t + a_t^2) s_t^{K-2} + K (2a_t-2) s_t^{K-1} + (K+1) s_t^K \right) = 0. \quad (19)$$

For $K = 2$, that is, for the image of second order, which in the present work was

most often used,

$$(1-2a_t + a_t^3) + 2(2a_t-2)s_t + (2+1)s_t^3 = 0. \quad (19a)$$

From Eq. (19a) it follows that:

$$s_t = \frac{1-a_t}{3}.$$

The following table shows that the second order image is roughly at 30% optimal brightness for reflectivity s_t .

a_t	0.05	0.10	0.15	0.20
s_t	0.32	0.30	0.28	0.27
τ_t	0.63	0.60	0.57	0.53
ϕ_{II}/ϕ_0	0.10	0.09	0.07	0.06

The strong diminution of light intensity may be compensated for by a corresponding increase in the illumination intensity. Aside from the optical problem, the quality of the optical surfaces plays an essential role - as in the realization of the simple autocollimator. The influence of irregularities in the mirror on the image position and image quality are treated in Sections 2.4.3.3, 2.5.2, and 2.6.1.

2.3.4.2. Image Migration Under Three-Dimensional Rotations of Fully and Partially Reflecting Mirrors

As in the previously treated AC systems, the areas of interest are the relation between image migration of an image or order K and the three-dimensional rotations α , β , and γ of the AC measurement mirror (Index a), of the semitransparent mirror (Index t), and of a possible deflection mirror (Index u). The semitransparent mirror is in actuality not a plane surface, but rather a prism with a wedge angle κ_0 . The breaking edge of the prism forms, in the vertical T mirror, the angle φ with the y axis and with the x axis in the horizontal mirror (Fig. 12). For the derivation of formulas, it is recommended that the breaking and reflecting surfaces of the T mirror be introduced separately with the vectors \vec{I}_D and \vec{I}_R . The symmetry surface of the prism is denoted by the vector \vec{I}_t . The components of the vectors \vec{I}_D , \vec{I}_R , and \vec{I}_t are related to the operative



Figure 12. Definition of the Prism Elements of the Semitransparent Mirror

prism angle, for example for case a) below, as follows:

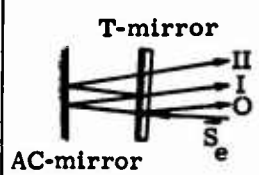
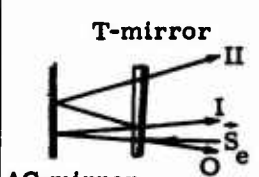
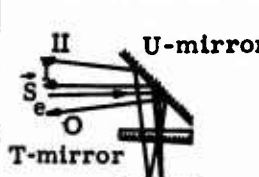
$$\begin{aligned} \gamma_b &= \gamma_t + \frac{\kappa_0}{2} \sin \varphi, & \beta_b &= \beta_t + \frac{\kappa_0}{2} \cos \varphi, \\ \gamma_r &= \gamma_t - \frac{\kappa_0}{2} \sin \varphi, & \beta_r &= \beta_t - \frac{\kappa_0}{2} \cos \varphi, \end{aligned} \quad (20)$$

The vector calculation with the vector \vec{T}_a of the AC-measurement mirror, the vectors \vec{T}_b and \vec{T}_r and the vector \vec{s} of the beam entering the autocollimator, gives the results for image migration of the Kth order image entered in Table 3 under i_K' and a_K' . Converting i_K' and a_K' to the image migrations i_K and a_K by means of Eqs. (20), there results, for example in case a), that is, for a vertical mirror whose semitransparent side is toward the AC mirror, the following separation into vertical components:

$$\begin{aligned} \text{Zero-order image} & \quad i_0 = -\gamma_e + (1-2n) \cdot \kappa_0 \cdot \sin \varphi + 2\gamma_t, \\ \text{Ist-order image} & \quad i_I = -\gamma_e + (2-2n) \cdot \kappa_0 \sin \varphi + 2\gamma_a, \\ \text{IInd-order image} & \quad i_{II} = -\gamma_e + (3-2n) \cdot \kappa_0 \sin \varphi - 2\gamma_t + 4\gamma_a, \\ \text{Kth-order image} & \quad i_K = -\gamma_e + (1+K-2n) \cdot \kappa_0 \sin \varphi + 2(1-K)\gamma_t + 2K\gamma_a. \end{aligned} \quad (21a)$$

Equations (21a) show the following: A tilt γ_a of the AC measuring mirror enters the vertical image displacement with a factor $2K$. A tilt γ_t of the semitransparent mirror has no influence on the Ist-order image and equally affects the zero- and IInd-order images in magnitude and with different signs. The wedge angle $\kappa_0 \sin \varphi$, which is constant for a single setup, causes a constant displacement. A change of inclination γ_e of the incident rays, for example, a tilt of the autocollimator or a change of refraction, causes a constant displacement of all images. Formula (21b) for the azimuthal image migration is entered in Table 3 and can be interpreted analogously. In case b), that is, with a vertical T mirror whose semitransparent surface is turned away from the AC mirror, there arise further intensity losses from multiple absorption. With regard to image migration (for formulas, see Table 3), only the operative wedge angle $\kappa_0 \sin \varphi$ or $\kappa_0 \cos \varphi$ has a different effect than in case a). Image migration with a 45° deflection mirror (u), a semitransparent mirror, and AC measurement mirror is given under (c). Again the mirror tilt γ_u goes into the vertical components i_K with a factor of 4. The mirror tilts α_u and β_u enter the azimuthal components a_K with a double magnitude, whence observations on c in Eq. (16) are to be noted. In Table 3 only these mirror arrangements are tabulated, which are employed in the present work. Should the need arise, the formulas for further combinations of deflection mirrors, semitransparent mirrors, and AC measurement mirrors may be derived by means of the above methods.

Table 3. Image Migration of Kth-order Images in Multiple Autocollimation

Case a: Multiple AC T-layer facing	$i_K^i = 2(1-n)\gamma_b + 2(n-K)\gamma_r - \gamma_e + 2K\gamma_a$ $a_K^i = 2(1-n)\beta_b + 2(n-K)\beta_r - \beta_e + 2K\beta_a$	
	$i_O = 2\gamma_t + (1-2n)\alpha_o \sin\varphi - \gamma_e$ $i_I = \quad + (2-2n)\alpha_o \sin\varphi - \gamma_e + 2\gamma_a$ $i_{II} = -2\gamma_t + (3-2n)\alpha_o \sin\varphi - \gamma_e + 4\gamma_a$	
	$i_K = 2(1-K)\gamma_t + (1+K-2n)\alpha_o \sin\varphi - \gamma_e + 2K\gamma_a$	(21a)
	$a_K = 2(1-K)\beta_t + (1+K-2n)\alpha_o \cos\varphi - \beta_e + 2K\beta_a$	(21b)
Case b: Multiple AC T-layer turned away	$i_K^i = 2K(n-1)\gamma_b + 2(1-Kn)\gamma_r - \gamma_e + 2K\gamma_a$ $a_K^i = 2K(n-1)\beta_b + 2(1-Kn)\beta_r - \beta_e + 2K\beta_a$	
	$i_O = 2\gamma_t + \alpha_o \sin\varphi - \gamma_e$ $i_I = \quad + (2-2n)\alpha_o \sin\varphi - \gamma_e + 2\gamma_a$ $i_{II} = -2\gamma_t + (3-4n)\alpha_o \sin\varphi - \gamma_e + 4\gamma_a$	
	$i_K = 2(1-K)\gamma_t + (K+1-2Kn)\alpha_o \sin\varphi - \gamma_e + 2K\gamma_a$	(22a)
	$a_K = 2(1-K)\beta_t + (K+1-2Kn)\alpha_o \cos\varphi - \beta_e + 2K\beta_a$	(22b)
Case c: Multiple AC with 45° deflection mirror	$i_K^i = 2(n-1)\gamma_b + 2(K-n)\gamma_r + 4\gamma_u - \gamma_e - 2K\gamma_a$ $a_K^i = 2(n-1)\beta_b + 2(K-n)\beta_r - 2\beta_u + 2\alpha_u + \alpha_e - 2K\alpha_a$	
	$i_O = -2\gamma_t + (1-2n)\alpha_o \sin\varphi + 4\gamma_u - \gamma_e$ $i_I = \quad + (2-2n)\alpha_o \sin\varphi + 4\gamma_u - \gamma_e - 2\gamma_a$ $i_{II} = \quad + 2\gamma_t + (3-2n)\alpha_o \sin\varphi + 4\gamma_u - \gamma_e - 4\gamma_a$	
	$i_K = 2(K-1)\gamma_t + (1+K-2n)\alpha_o \sin\varphi + 4\gamma_u - \gamma_e - 2K\gamma_a$	(23a)
	$a_K = 2(K-1)\alpha_t + (1+K-2n)\alpha_o \cos\varphi - 2\beta_u + 2\alpha_u + \beta_e - 2K\alpha_a$	(23b)

2. 3. 4. 3 Reduction of Images of Higher Order Because of Unstable Positioning of Mirrors

The supplementary optical elements - deflection mirrors in multiple reflection and semitransparent mirrors in multiple autocollimation - cannot, as a rule, be positioned so stable that they will not experience displacements over long periods of time. Multiple autocollimation makes it possible, by simultaneous observation of images of zero and IInd order, to control and, if necessary, to eliminate rotations γ_t or α_t of the semitransparent mirror. Taking as constant the setting of the autocollimator and the operative prism angle $\alpha_o \sin\varphi$, and letting $i_o(t_1)$ and

$i_{II}(t_1)$ be the vertical components of images of order zero and II at time t_1 and $i_0(t_2)$ and $i_{II}(t_2)$ the vertical components at time t_2 , then according to Eq. (21a) the following relations hold:

Time t_1 :

measured components	$i_0(t_1) = -\gamma_e + (1-2n) \kappa_0 \sin\varphi + 2\gamma_t(1)$
measured components	$i_{II}(t_1) = -\gamma_e + (3-2n) \kappa_0 \sin\varphi - 2\gamma_t(1) + 4\gamma_a(1)$
reduced components	$i_1' = i_0(t_1) + i_{II}(t_1) = -2\gamma_e + (4-4n) \kappa_0 \sin\varphi + 4\gamma_a(1).$

Time t_2 :

measured components	$i_0(t_2) = -\gamma_e + (1-2n) \kappa_0 \sin\varphi + 2\gamma_t(2)$
measured components	$i_{II}(t_2) = -\gamma_e + (3-2n) \kappa_0 \sin\varphi - 2\gamma_t(2) + 4\gamma_a(2)$
reduced components	$i_2' = i_0(t_2) + i_{II}(t_2) = -2\gamma_e + (4-4n) \kappa_0 \sin\varphi + 4\gamma_a(2).$
error-free inclination difference	$i_2' - i_1' = \Delta i_{II}' = 4(\gamma_a(2) - \gamma_a(1)).$

By addition of the components of zero and IInd order images, the inclination differences $\Delta i_{II} = i_{II}(t_2) - i_{II}(t_1)$ are reduced by the amount of the undesired mirror rotations γ_t . Nevertheless it suffices in many cases to hold the semitransparent mirror under control with the zero order image and to use reduction only when changes of γ_t reach larger values. The zero order image should be measured only at such time intervals when the tendency of the inclination changes of the T mirror can be determined with sufficient accuracy (see Section 2.7.2.3).

Besides the elimination of vertical and azimuthal rotations of a semitransparent mirror, plane semitransparent surfaces can be used in connection with the necessary deflection elements to control the stability of these deflection elements, that is, to eliminate the instability. Coupling, for example, according to Table 3c, a 45° deflection mirror with a semitransparent mirror, and assuming that both mirrors execute a common rotation $\Delta\gamma_u$, the following equations obtain according to Eq. (23a) (Table 3c):

Zero order image

time t_1	$i_0(t_1) = -\gamma_e - (2n-1) \kappa_0 \sin\varphi - 2\gamma_t(1) + 4\gamma_u(1)$
time t_2	$i_0(t_2) = -\gamma_e - (2n-1) \kappa_0 \sin\varphi - 2\gamma_t(1) + 4\gamma_u(1) + 2\Delta\gamma_u$
reduced components	$i_0'' = i_0(t_2) - i_0(t_1) = 2\Delta\gamma_u$

IInd order image

time t_1	$i_{II}(t_1) = -\gamma_e - (2n-3) \kappa_0 \sin\varphi + 2\gamma_t(1) + 4\gamma_u(1) - 4\gamma_a(1)$
time t_2	$i_{II}(t_2) = -\gamma_e - (2n-3) \kappa_0 \sin\varphi + 2\gamma_t(1) + 4\gamma_u(1) + 6\Delta\gamma_u - 4\gamma_a(2)$
reduced components	$i_{II}'' = i_{II}(t_2) - i_{II}(t_1) = 6\Delta\gamma_u - 4(\gamma_a(2) - \gamma_a(1))$
error-free inclination change	$\Delta i_{II}'' = i_{II}'' - 3i_0'' = -4(\gamma_a(2) - \gamma_a(1))$

Azimuthal rotations α and β of a 90° deflection element can, according to Eqs. (8a, b), only then be fully defined, when the deflection element is equipped with two semitransparent surfaces. The fixed coupling of the semitransparent surfaces with the deflection surfaces is best realized by means of a prism. If, for example, in a pentagonal prism (App. E) the surfaces F_1 and F_4 are semitransparently mirrored, then the azimuthal rotations of the prism can be controlled by means of the two resulting zero-order images.

Another application of the simultaneous observation of zero- and IInd-order images is discussed in Section 5.1. A rotation of the intermediate plate P (Fig. 28) affects the semitransparent and AC measurement mirror equivalently; the rotation can then be measured with a zero-order image and, if necessary, used as a correction of the IInd-order image.

2.3.5 EVALUATION OF MULTIPLE REFLECTION AND MULTIPLE AUTOCOLLIMATION

Multiple reflection and multiple autocollimation are methods by means of which the deviation of a light ray falling on a rotated AC measurement mirror is multiplied with respect to simple autocollimation. According to Section 2.7.2.3 the multiplication of the angle deflection cancels only indirectly in the measurement precision of the AC system. Both methods require an additional optical element. The measurement range, on the other hand, is proportional to angle multiplication.

Multiple reflection can be realized with two fully reflecting AC mirrors without further precautions in any autocollimator. The following facts can be considered to be disadvantages of multiple reflection:

- 1) No control over rotations of the deflection mirror,
- 2) Different scale factors for vertical and azimuthal rotations of the measurement mirror,
- 3) The deflection mirror and measurement mirror must be arranged as in Figure 9.
- 4) Reduction of the image-forming ray-bundle diameter with increasing angle multiplication,
- 5) Change of scale factor for azimuthal rotations on simultaneously occurring vertical rotations.

Multiple autocollimation offers a series of advantages, which permit a considerable extension in the field of applicability in comparison with the original target determination described by Graul (1952), that is, in the enhancement of measurement precision:

- 1) Control and elimination of the rotations of the semitransparent mirror,
- 2) Control and elimination of rotations of optical deflection elements,
- 3) Simultaneous measurement of several, serially-arranged measurement objects, on each of which may be attached a semitransparent mirror,

- 4) Investigation of the accuracy autocollimators by means of simultaneous observation of 1st- and 2nd-order image displacements (see Section 2.7.1.2).

The disadvantages of multiple autocollimation are:

- 1) The technical realization necessitates a special illumination device, a collimator slit and a micrometer device fitted to the slit,
- 2) Limitation of angle multiplication to $K \geq 3$,
- 3) Differing brightnesses and eventual overlapping of images of different order,
- 4) Focus differences in images of different order because of residual curvature of the mirrors (see Section 2.5.2).

If one is able to make the necessary arrangements for multiple autocollimation, one can, from previous experience, take these disadvantages in stride. May it be noted in closing that it is possible to combine multiple autocollimation with multiple reflection directly. In the investigations of Section 2.7.2.3, such a measurement setup was employed in which the rotations of the measurement mirror were multiplied 12-times.

2.4 Construction, Adjustment, and Calibration of a 1500mm Autocollimation System

2.4.1 CONSTRUCTION OF THE 1500mm AUTOCOLLIMATION SYSTEM

According to Section 1, a mean error of $\pm 0.05''$ was set as a maximum for the single measurement of an instrumental error, that is, with use of autocollimation for the single measurement of the direction of the mirror normals. This precision, which must apply to the entire measurement range ($3' - 5'$), lies considerably above the customary tolerances of machine construction (Hume, 1964; Janich, 1954) and above the values given in investigations of the precision of geodetic instruments up to the present time (Hoffmann, 1965; Janich, 1954). In production-line optical autocollimators (App. C) one must rely on a mean error of $\pm 0.2'' - 0.5''$. Of the electro-optical autocollimators, according to Appendix D, only the Midarm System of the Razdow Laboratories, USA, satisfies the highest expectations. The high procurement costs of this system, however, are not justified by the intended investigations. Therefore a stationary 1500mm autocollimation system was constructed in Measurement Basement II of the Geodetic Institute of the TH Stuttgart according to the specifications of the author (Figs. 13, 14). All the mechanical parts of the system were obtained at the machine shop of the Geodetic Institute. The AC system was submitted to exhaustive testing. The results are presented in Sections 2.5 to 2.7 (Waimer, 1965). In the following sections details will be given on the design and construction of the autocollimation system and on the adjustment of the autocollimator.

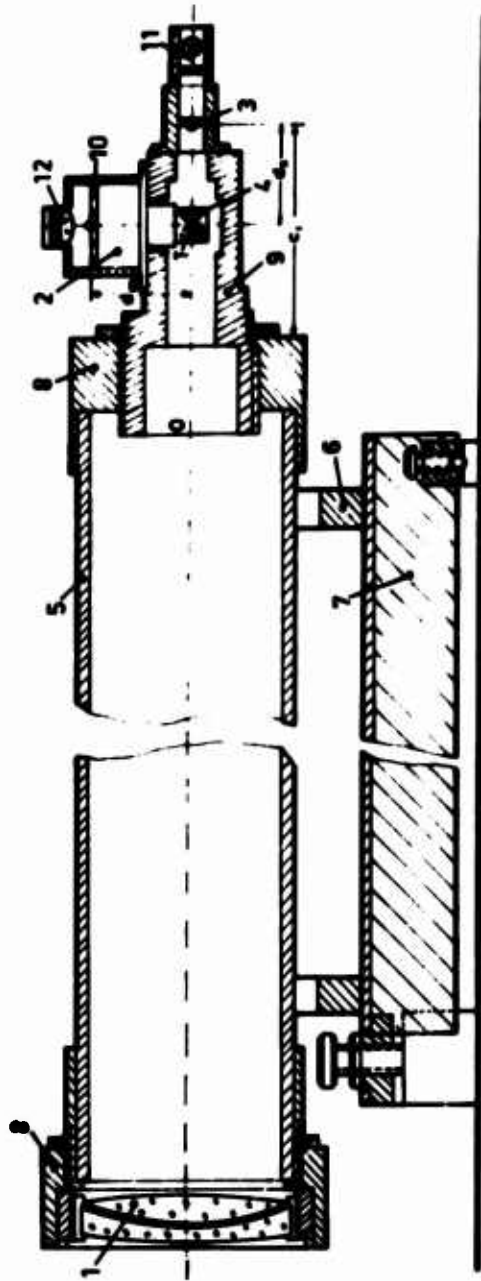


Figure 13. Construction of the 1500mm Autocollimator

1. Objective
2. Micrometer
3. Crosshair
4. Separation cube
5. Collimator tube
6. U-bed
7. Connection piece
8. Micrometer head
9. Micrometer surface
10. Illumination source normal
11. Ocular
12. Observation microscope
13. Special illumination device
14. Stage pillar
15. Deflection mirror
16. Mirror carriage
17. Horizontal carrier
18. Wild T4 in vertical axis investigation



Figure 14. Total View of the 1500mm Autocollimation System

a) Autocollimator

The construction of the autocollimator is shown in Figure 13. The objective (1) is a double lensed apochromate with a focal length $f = 1503,3\text{mm}$ and a clear objective diameter of 100mm. Micrometer (2), can be a screw micrometer of the Wild plane surface testing apparatus, or the coordinate measurement ocular of the Leitz autocollimation telescope. Each micrometer has its own crosshair (3) and its own separation cube (4). The measurement magnitude of the autocollimator amounts to about $5'$. The collimator tube (5) rests in two V-beds (6) on a U-track (7) that can be set vertically and horizontally. The objective is connected to the collimator tube by means of the connection piece (8) and may be displaced by small amounts in the plane perpendicular to the tube axis for adjustment of the autocollimator. Since, as a rule, both vertical and azimuthal mirror rotations are to be measured, the image plane, that is, the micrometer plane (10), must be adaptable for vertical or horizontal setting. The crosshair image was observed, normally, in a separate microscope (13), since ocular observation proved unsuitable. Besides the normal crosshair illumination (11), there is also a special turnable illumination device (14) for focusing by illumination parallax (Section 2.5.3) and for multiple autocollimation. All parts of the autocollimator are so designed and arranged, to insure the greatest possible stability of the telescope and its carriage under the necessary observation of adjustment and setup precautions.

In micrometric measurement of image displacement, a mean error of $\pm 0,5\mu\text{m}$ cannot in principle be improved upon. Leaving other errors out of consideration Eq. (4) would lead to a mean error in a direction measurement of $\pm 0,035''$ with a focal length of 1500 mm. The mechanical precision of the micrometer must correspond to the precision of the visual setting up of the micrometer mark on the crosshair image. With the eye's symmetrizing precision of about $6''$, which is the controlling factor in the micrometer employed, there results a setup precision of $0,3\mu\text{m} \approx 0,02''$ for 20-times ocular magnification.

It is further to be noted that the autocollimator with the Leitz measurement device may be directly applied as a collimator with a crosshair scale, if the crosshair of the micrometer scale is illuminated. Likewise, the autocollimator can be used as a telescope with a scale or a micrometer, so that, for example, the target line of a theodolite can be observed directly. The Wild measurement device is less suitable for such tasks because of the slit-type crosshair.

b) Pillar and Mirror Suspension

The body length of the autocollimator, the heavy weight of the instruments to be investigated, as well as the large number of different observation arrangements have necessitated the incorporation of a special pillar (15) in the design (Fig. 14). The autocollimator and object of investigation are situated on one and the same pillar, so that unavoidable motions of the surroundings have the least possible

influence on the reciprocal position of measurement instrument and object of measurement. The objects to be investigated must be positioned vertically (horizontally, in case of 90° deflection) so that the target line of the autocollimator strikes the AC measurement mirror roughly in the middle. For this reason, the pillar was graduated step-wise so that, in conjunction with a transportable set plate of $50 \times 50 \times 10$ cm, all required pillar heights could easily be attained. The graduated pillar is covered with heavy bore plates which can be levelled. Since the separation between the autocollimator and AC measurement mirror must be kept as small as possible because of the influence of refraction (Section 2.7.2.1), the autocollimator is mountable at different places along the length of the pillar axis. For 90° deflection of the beam path, and for the investigation of multiple reflection, the deflection mirror (16) must be arranged perpendicular to the AC mirror at the level of the target axis and with corresponding inclination. The deflection mirror is suspended from a mirror carriage which can be moved on the horizontal carrier (18) and which is removed from the carrier in the measurement setting. The deflection mirror may be inclined between 10° and 50° to the horizontal. The greatest possible stability is demanded in the whole facility for mirror suspension. Because of the strong temperature sensitivity of the AC system (see Section 2.7.2), the carriers are equipped with thermal insulation.

c) Adjustment of the autocollimator

In the adjustment of the autocollimator, the following conditions must be fulfilled:

- 1) The crosshair (3) must lie in the focal plane of the objective (1) (Fig. 13);
- 2) The separation d_m of the micrometer plane (10) from the point T and the separation d_g of the crosshair from T must be equal. T is the point of intersection of the target axis through the separation surfaces;
- 3) The target axis of the autocollimator must be approximately parallel to the mechanical axis;
- 4) The optical axes of objective and ocular must be perpendicular to each other and must run through the point T.

The realization of the first adjustment condition is described exhaustively in Section 2.5 (Focusing an AC System on Infinity). The second adjustment condition may be fulfilled in the following fashion: crosshair and micrometer scale are simultaneously observed with a microscope from the opening O in the micrometer head (Fig. 13). After displacing the crosshair in the direction of the axis until the crosshair and scale coincide parallax-free, the separations d_m and d_g are equal; this condition is satisfied in the present autocollimator with a precision of ± 0.1 mm.

In the adjustment of the target axis, it is observed through a telescope whether the crosshair of the autocollimator remains stationary during a rotation of the micrometer head and the tube, that is, whether the crosshair and objective are aligned

on the mechanical axis. The adjustment is executed by means of the displacement of the crosshair or objective in the plane perpendicular to the mechanical axis, and was determined with a precision of $\pm 5''$. The adjustment of the optical axis and the associated investigation of image errors of the system by Foucault's method of deflection images of stars (König, Köhler, 1959; Straubel, 1894) could not be applied. The quality of the AC images, however, permits a satisfactory mechanical arrangement of the optical axis.

In practical applications, it can be further demanded that

- 1) The AC mirror and target axis of the autocollimator be arranged perpendicular to each other, and that
- 2) The target axis of the autocollimator be horizontal.

The first demand is fulfilled if the so-called autocollimation point $P_a(x_a, y_a)$ is known (see App. B). P_a gives the position x_a, y_a of the crosshair image when the mirror and target axis are perpendicular to each other. The coordinates of P_a are obtained upon deflection of the parallel ray bundle at exactly 180° by, for example, a triple prism, and reading the coordinates of the crosshair. The horizontalization of the target axis can then be obtained in the well-known way with a mercury level, where the beam path is deflected by a pentagonal prism by 90° to the mercury mirror and the autocollimator is tilted until the crosshair image gives the vertical components of P_a . In the use of the transparent pentagonal prism of Leitz, the full objective opening for further observations with reciprocal collimation or autocollimation is available.

2.4.2 CALIBRATION OF THE AC SYSTEM

2.4.2.1 Determination of the Focal Length of the Objective

The focal length of the objective is needed, as for the principle of autocollimation, for the expression of image displacement s in terms of the angle rotation α of the AC mirror [Eq. (3)]. For the investigations of focusing and of the calibration of an AC system (Sections 2.5 and 2.6) it must, however, be noted that Eq. (3), that is, the focal length, can be used only approximately for the expression of image displacement, since the actual conversion factor - denoted the scale factor in Section 2.6 - depends additionally on the residual curvature of the mirror, of the separation cube, and of the state of adjustment of the autocollimator. Because of the dependence of focal length on scale factor, the focal length must be determined with the greatest possible accuracy.

Of the methods for the accurate measurement of mean objective focal lengths, the determination of object size and image angle are to be considered particularly suited to the geodeticist (Flugge, 1954; Ochsenhirt, 1962). Scale A_1B_1 with the known length p is situated, as in Figure 15, in the focal plane of the objective and

is set up at right angles and symmetric to the optic axis. The focal length may be computed from p and the measured image angle ϵ' of the main rays through A_1 and B_1 :

$$f = \frac{p}{2 \tan \frac{\epsilon'}{2}} \quad (24)$$

The scale length p was determined by a Leitz Universal-Comparator 200 of the Institute for Technical Optics of the TH Stuttgart; the image angle ϵ' was measured by means of green light ($\lambda = 0.55\mu\text{m}$) with a Wild T4 theodolite where the vertical axis D of the theodolite must intersect the optical axis of the objective O . In Figure 15, a) denoted the position of the theodolite on aiming at mark A_1 ; b) the position on aiming at B_1 .

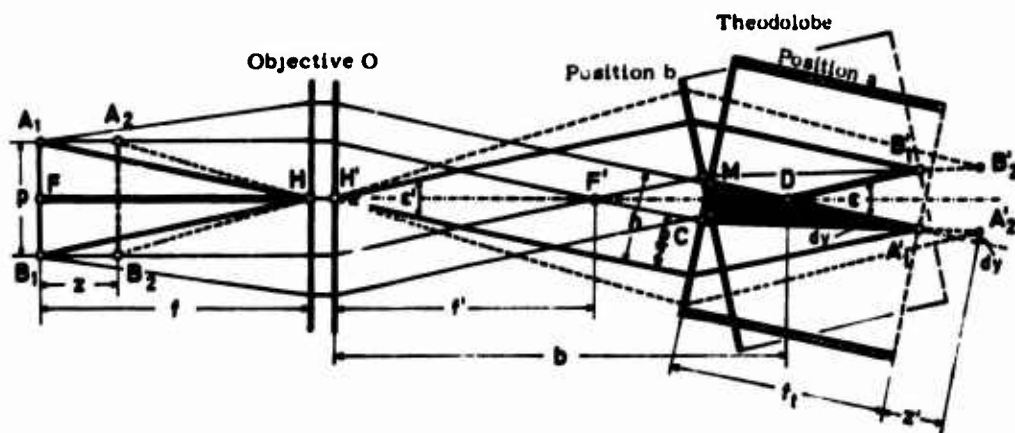


Figure 15. Principle and Systematic Errors in Focal Length Determination of an Objective

- Notation: F = focal point on object side
 H = main point on object side
 f = object focal length
 z = focal point separation from the object
 M = optical middle point
 F' = image-side focal point
 H' = image-side main point
 f' = image focal length
 z' = focal point separation from the image

Before going into the accuracy of the focal length determination, the above summary of the notation of the fundamental optical quantities is pointed out, since it will be relevant also to the discussions in Sections 2.5 and 2.6. The separate optical systems will, as a rule, be separated by separate indices. In this section, the quantities of the system O, whose focal length is to be determined, will be unindexed, and the quantities of the theodolite system will be denoted by the index t.

The precision of focal length determination depends on the precision of the quantities to be measured, on the scale length, and on the influence of the objective (Fig. 15, scale setting $A_2 B_2$). The mean coincidental error m_f is, from the error propagation law applied to Eq. (24):

$$m_f = \pm \sqrt{\left(\frac{f}{p}\right)^2 m_p^2 + \left(\frac{f}{\epsilon'}\right)^2 m_{\epsilon'}^2}. \quad (25)$$

m_p = the mean scale uncertainty; $m_{\epsilon'}$ = mean error in the angle

According to Eq. (25), the scale length is to be maximized. Because of the distortion, it is, however, recommended that the focal length determination be executed also for small scale lengths. For a given focus error z , the marks A_2 and B_2 form images A_2' and B_2' . A_2' and B_2' are each a distance dy from the target axis, so that the angle ϵ' is in error by

$$d\epsilon' = \frac{-2dy}{f_t}$$

dy is defined by the triangle $MA_1'C$

$$dy = \frac{MC}{f_t} z' = \frac{h-p}{f_t} z'.$$

where

C = intersection point of the axis-parallel beam from A_1 through the theodolite objective

h = height of incidence of the main beams on the theodolite objective

z' = focus error of the mark images.

According to Ochsenhirt (1962), z' is obtained from

$$z' = \frac{f_t^2}{f \cdot f'} z,$$

so that

$$d\epsilon' = \frac{p-2h}{f \cdot f'} z = \frac{(f' - b)\epsilon'}{f \cdot f'} z. \quad (26)$$

According to Eqs. (24) and (26), the focal length change df is related to angle change $d\epsilon'$ by

$$df = -\frac{f}{\epsilon'} d\epsilon' = -\left(1 - \frac{b}{f'}\right) z. \quad (27)$$

According to Eq. (26), the focusing error z does not affect the angle measurement if the incidence height h is equal to half the scale length p . This favorable case occurs when the rotation axis D of the theodolite is located on the image-side focal point F' of the objective, that is, when $b = f'$. In this case, for telecentric beam path, that is, for main rays parallel to the axis in the object space, it is to be noted that the focusing error causes no angle error, only a decrease in sharpness. Since for a large opening of the collimator objective the capacity of the telescope objective acts as an aperture blind of the collective system, two different eccentric zones of the collimator objective are used for the determination of focal length in readings from telecentric beam paths. It is therefore recommended that different scale lengths be used and that the strict fulfillment of Eq. (27) be abandoned for the sake of an axial focal-length value. Nevertheless it should here be taken into consideration that the focusing error z may assume larger values, depending on focusing method and the behavior of the focal lengths f and f_t .

The focal length was determined with scale lengths of 20mm. The special conditions of the investigation design have necessitated a separation of 650mm between objective and rotation axis of the theodolite. For this reason, the focal length determination was executed for three different scale settings. In the middle setting, the scale is assumed to lie in the focal plane for the minimization of parallax. The results are summarized in the following table:

Scale-length	$p \pm m_p$	20 mm \pm 0.5 μ m				60 mm \pm 1.0 μ m			
Cross-section	z [mm]	ϵ'	$m_{\epsilon'}$ ["]	f [mm]	m_f [mm]	ϵ'	$m_{\epsilon'}$ ["]	f [mm]	m_f [mm]
1485.3	-0.4					2°17'10.48"	± 0.18	1503.48	± 0.04
1484.9	0.0	45' 44.07"	± 0.21	1503.35	± 0.12	2°17'11.13"	± 0.15	1503.36	± 0.04
1484.2	+0.7	45' 44.27"	± 0.16	1503.24	± 0.09	2°17'13.14"	± 0.20	1502.99	± 0.04

The changes arising in the focal length in dependence on the focus setting z correspond roughly to the values calculated from Eq. (27). As the result of the focal length determination, the value $f = 1503.3\text{mm} \pm 0.15\text{mm}$ is retained for further investigations.

2.4.2.2 Investigation and Calibration of the Micrometer

The accuracy of $\pm 0.5\mu\text{m}$, set as a condition on the micrometric measurement of image migration, must be manifested also in measurement ranges of several millimeters in precision micrometers, and, in need, must be attainable by calibration

a) The Wild Screw Micrometer

In the screw micrometer of the Wild firm, in turning the micrometer spindle (0.4mm per turn), the female piece is displaced with micrometer threads. The setting of the micrometer thread must correspond exactly to the readings on the micrometer drum. The investigation is carried out on the Leitz Universal-Comparator 200, and the micrometer drum is turned through definite intervals and the actual resulting displacement of the micrometer thread is measured with the comparator (mean error in the comparator measurement is $\pm 0.3\mu\text{m}$). The micrometer has a periodical error and one that is progressive with the range setting. The progressive error reaches a maximum of 2.0 micrometers and can be calculated by a power series of second order with a mean approximation of $\pm 0.3\mu\text{m}$ [defined in Section 4.4.2, (Eq. 89)]. The periodic error, that is, that which recurs with each turn of the drum, has an amplitude of $1.8\mu\text{m}$ and is represented by a sine function with a mean approximation of $\pm 0.3\mu\text{m}$. The values of the coefficients in the equation are solved for and given in Appendix F. The individual correction values are bracketed in a mean error of $\pm 0.4\mu\text{m}$. According to the investigations of Section 2.7.1.2, the precision of the micrometric measurements with the Wild micrometer is improved by a factor 2.5 by application of the correction.

b) The Leitz Coordinate Ocular

The Leitz coordinate ocular, according to Appendixes A and B, is a micrometer in which the setting of the crosshair is determined by the main division of a fixed crosshair plate and the micrometric measurement is executed within the interval of the main division. The equal separation of the main division can be ascertained directly by a comparator measurement. The standard deviation of an interval from the mean value of all intervals amounts to $\pm 0.4\mu\text{m}$ for the x and y axes. The errors of the micrometric measurement cannot be directly investigated by a comparator, since the crosshair image and not the main division is displaced by tilting the plane plate. The working precision of the optical micrometer was therefore checked by a comparison measurement with a precision level tester, where the corresponding changes of an AC mirror are set on the level tester and measured. The good agreement (mean error from differences $\pm 0.02^{\text{m}} = 0.3\mu\text{m}$) permits the unconditional application of the optical micrometer. The Leitz coordinate measurement ocular thereby yields a satisfactory precision.

2.4.2.3 Interferometric Testing of the Flatness of the Autocollimation Mirror

According to the principle of autocollimation, the parallel rays emitted from the autocollimator are reflected from a plane mirror again as parallel rays. Very

high demands must be made on the flatness of the mirror surfaces, since residual curvature of the mirrors affects the autocollimation images and, according to Section 2.5 introduce focus errors and changes in the scale factor. Good optical plane surfaces are tested, as a rule, by interferometric methods, since these offer the highest precision required, in contrast to a relatively more simple treatment. The mirrors employed were tested with the Zeiss Michelson Interferometer of the Institute for Technical Optics of TH Stuttgart. The interference mirror and tested mirror form an air wedge plate so that the interference fringes give curves of equal thickness. The deviation from linearity of the parallel fringes, measured in fringe widths $\lambda/2 = 0.27\mu\text{m}$, gives the deviation from planeness in the tested mirror: the unevenness is thereby topographically displayed with an accuracy of about $0.05\mu\text{m}$. The results of the testing are given in the following table:

Mirror	Deflection mirror U	Autocoll. mirror Am	Prism astrolab. mirror PA	Semitransp. T mirror	Autocoll. mirror As
Firm	Moller	Moller	Opt. et Precis. de Levallois	Moller	Askania
Diameter	180mm	100mm	100mm	110mm	55mm
Total error	$0.25\mu\text{m}$	$0.2\mu\text{m}$	$0.1\mu\text{m}$	$0.15\mu\text{m}$	$0.1\mu\text{m}$
Error in surface use	$0.1\mu\text{m}$	$0.15\mu\text{m}$	$0.1\mu\text{m}$	$0.15\mu\text{m}$	$0.1\mu\text{m}$
Residual curvature radius	25 km	8 km	18 km	10 km	4 km

The deflection mirror, AC measurement mirror Am, and the semitransparent mirror manifest within a border zone of about 10mm a border reduction of 0.1 to $0.15\mu\text{m}$ and an additional deformation of $0.1\mu\text{m}$ at the fastening points of the mounting. The interference pictures show that the general surface curvature is relatively constant, that is, that the mirror surfaces can be approximated as spheres. The radius R of the sphere can be calculated from the well-known formula from the diameter d and the average unevenness Δ of the mirrors:

$$R = \frac{d^2}{\Delta} .$$

2.5 Focusing an Autocollimation System on Infinity

In the preceding considerations it was assumed that the autocollimator is focused on infinity, that is, that the collimator crosshair lies in the focal plane of the objective. If the focusing is to be done in a laboratory, one can, according to Ochsenhirt (1962), favorably apply the principle of autocollimation. In the following paragraphs the error influences arising in focusing with autocollimation and how the focusing can be practically realized will be explained.

2.5.1 FOCUSING WITH FLAT AUTOCOLLIMATION MIRRORS

Focusing may be approached in a simple way if the autocollimator is equipped with a Gauss ocular (App. G), in which crosshair S and crosshair S' can be observed simultaneously. The crosshair is displaced until S and S' coincide parallax-free. Focusing with a Gauss ocular is described in detail in Ochsenhirt (1962), where the absolute flatness of the surfaces of the separation element and the AC mirror is assumed. In the following quantitative observations, the projecting system O_p and the image-forming system O_a are separated. O_p and O_a are separated by twice the mirror separation $2a$ (Fig. 16). The notation of Figure 15 for fundamental optical quantities applies to O_a and O_p ; indices p and a denote the quantities associated with the projecting and image-forming systems, respectively. The crosshair S is projected into the image space to S_1 by O_p . The assumed absolutely flat AC mirror causes only a reflection of the light direction, so that, after the reflection, S_1 is formed in image space as S' through O_a . Since the separation surfaces likewise can be assumed absolutely flat, and the same medium lies on both sides of systems O_p and O_a , it holds that:

$$f_p = f_p' = f_a = f_a' = f. \quad (28)$$

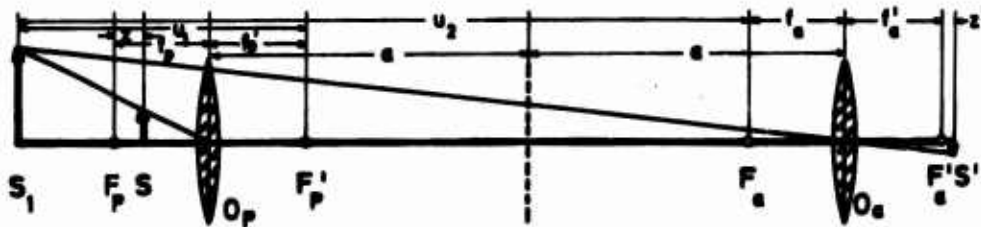


Figure 16. Beam Path Upon Focusing at Infinity

If the crosshair S is outside the focal plane of O_p by z , then according to Newton's law, Eq. (28) and Figure 16, the following relations hold:

$$z \cdot u_1 = -f^2; \quad u_2 \cdot z' = -f^2; \quad u_1 - u_2 + 2f - 2a = 0. \quad (29a, b, c)$$

From (29a, b, c) is derived the separation z' of the crosshair image from the focal point F_a' :

$$z' = \frac{z}{1 - \frac{2z}{f} + \frac{2az}{f^2}}. \quad (30)$$

With $a < 2m$ and $z < f$, Eq. (30) becomes

$$z' = z. \quad (30a)$$

For $z = 0$, the crosshair image lies in the focal plane of the objective. In auto-collimators with micrometric angle measurement devices, the crosshair or the micrometer is laterally arranged as a rule, according to Appendix C, so that the crosshair and crosshair image may not be simultaneously observed. An adjustment of the micrometer is required in the focusing procedure as it is altered by this. According to Section 2.4.1 and Figure 13, the separation of the intersection point of the target axis with the separation surface, from the micrometer surface, is equal to d_m , and from the crosshair, equal to d_s , where, on the basis of the adjustment, $d_m - d_s = d \leq 0.2\text{mm}$. Focusing on infinity is now achieved by displacing the entire micrometer head along the target axis until the micrometer scale MS and the crosshair image S' coincide parallax-free.

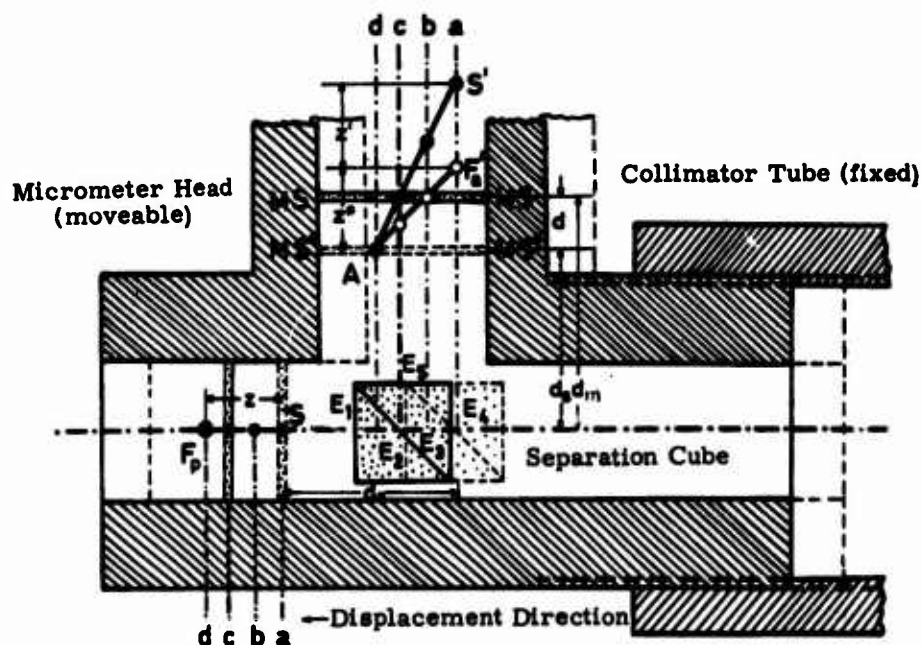


Figure 17. Focusing on Infinity by Means of Displacement of the Micrometer Head

In the initial setting a) the crosshair S is formed as image S' . S' is at a distance from the focal point F_a' of the image-forming system. Because of the adjustment error d , the micrometer scale does not have position MS^* , but rather the position

MS. MS^* is separated from F_a' by the distance z^* , where $z^* = z'$. S' is separated from MS by the distance $z' + z^* - d = 2z - d$. For focusing, the micrometer head, that is, the crosshair S, is displaced in a direction toward the focal point F_p . S' and F_a' migrate thereupon to point A. In the focused position, setting c, that is, on parallax-free observation of crosshair image and micrometer scale,

$$2z - d = 0,$$

that is, the crosshair is a distance $z = d/2$ from the focal point F_p . Thus the rays between objective and mirror are slightly divergent because of an adjustment error d.

2.5.2 FOCUSING WITH CURVED AUTOCOLLIMATION MIRRORS

2.5.2.1 The Dependence of Axial Image Position on Residual Curvature of the AC Mirror

According to Section 2.4.2.3, the AC mirrors employed have a curvature $1/R$ with the radius R between 4 km and 25 km. Similarly, the surfaces of the optical separation elements will have similar residual curvature magnitudes for reasons of mounting errors. What influence the residual curvature has on the axial position of the crosshair image will be investigated in the following paragraphs.

The distinctions, introduced in Section 2.5.1, between the projecting system O_p and the image-forming system O_a , correspond to physical reality. In the present case, the surfaces E_1 , E_2 , E_3 , and E_4 of the separation cube form, with the objective, the projecting equivalent system O_p with focal length f_p , and the surfaces E_4 , E_3 , and E_5 form the equivalent image-forming system O_a of focal length f_a (Fig. 17). Because of the residual curvature of the AC mirror, the rays are reflected with different angles, which can be represented in the virtual lens system O_a of focal length $f_g = R/2$ (Fig. 18).

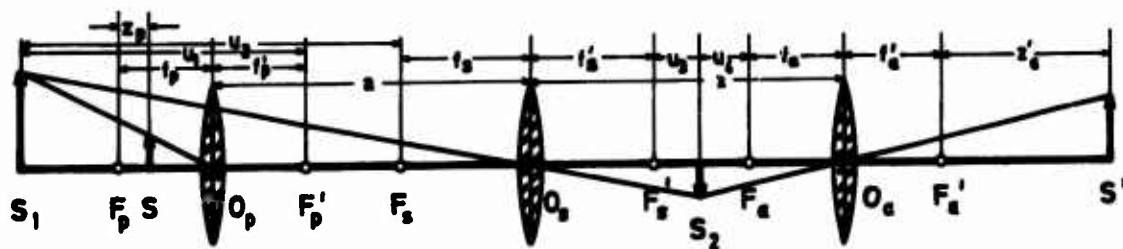


Figure 18. Ray Path with a Curved Autocollimation Mirror

The crosshair S , at a distance z_p from the focal point F_p of the projecting system O_p , is projected by O_p to S_1 . The intermediate image S_2 is cast by reflection on the AC mirror through the mirror system O_s from S_1 . This is in turn cast by the image-forming system O_a of the autocollimator to S_1 . S' is the crosshair image formed by autocollimation; it lies at distance z_a' from the focal point F_a' . According to Newton's law for image formation, in the notation of Figure 18, the following relations hold:

$$z_p \cdot u_1 = -f_p^2; \quad u_2 \cdot u_3 = -f_s^2; \quad u_4 \cdot z_a' = -f_a'^2. \quad (31a, b, c)$$

Furthermore, with a mirror distance a and with proper accounting for signs:

$$u_1 - u_2 + f_p + f_s - a = 0; \quad u_3 - u_4 + f_a + f_s - a = 0. \quad (32a, b)$$

Combining the equations, starting with Eq. (31c), one obtains

$$z_a' = \frac{f_p^2 \cdot f_a'^2 + a \cdot f_a'^2 \cdot z_p - f_p \cdot f_a'^2 \cdot z_p - f_a'^2 \cdot f_s \cdot z_p}{-f_p^2 \cdot f_a' + a \cdot f_p^2 - f_p^2 \cdot f_s - a \cdot (f_a' + f_p) \cdot z_p - 2a \cdot f_s \cdot z_p + (f_a' + f_p) \cdot f_s \cdot z_p + f_a' \cdot f_p \cdot z_p}. \quad (33)$$

For $f_s \rightarrow \infty$, that is, for an absolutely plane AC mirror, and for $f_a' = f_p = f$, Eq. (33) reduces to Eq. (30). With $f_s > z_p$, f_p , f_a' , and a , Eq. (33), after several manipulations, becomes

$$z_a' = \frac{z_p}{\frac{f_p^2}{f_a'^2} - 2 \frac{f_p}{f_a'^2} z_p + 2 \frac{a}{f_a'^2} z_p} - \frac{f_a'^2}{f_s - 2 \frac{z_p}{f_p} f_s + 2 \frac{a z_p}{f_p^2} f_s} = I + II. \quad (33a)$$

I corresponds to Eq. (30), while II gives the influence of residual mirror curvature $1/2f_s$ on the axial position of the crosshair image. With $z < f_p$, f_a' is obtained from Eq. (33a)

$$z_a' = z_p - \frac{f_a'^2}{f_s} = z_p - g. \quad (33b)$$

According to Eq. (33b), the image position is independent of the distance of the mirror; the residual curvature $1/2f_s$ affects the image position with the factor $f_a'^2$; thus autocollimators with large focal length are sensitive to residual curvature of the AC mirror. The following table gives some numerical values for $g = f_a'^2/f_s$. With a large focal length, focusing differences of 1-2mm can arise, as proved in Appendix H. Autocollimators with large focal length must therefore provide the facility for focusing if different AC mirrors are used. In the present case, focussing is accomplished by displacing the micrometer head, similar to a sliding eye piece.

Residual curvature radius R [km]	Focal length f_s [km]	Focal length autocollimator		
		$f=0.5\text{m}$	$f=1.0\text{m}$	$f=1.5\text{m}$
20	10	0.03	0.10mm	0.22mm
10	5	0.05	0.20mm	0.45mm
5	2.5	0.10	0.40mm	0.90mm
2	1	0.25	1.00mm	2.25mm

Since, in some measurement procedures, for example, using mirror polygons, a refocusing by interchanging mirrors is not possible, given poor mirror quality, a large focal length can have a decidedly detrimental effect.

In the further treatment of the focusing process, it is convenient to combine mirror system O_s and the image forming system O_a into the equivalent system O_e (Fig. 19). The mirror system O_s may consist of several mirrors.

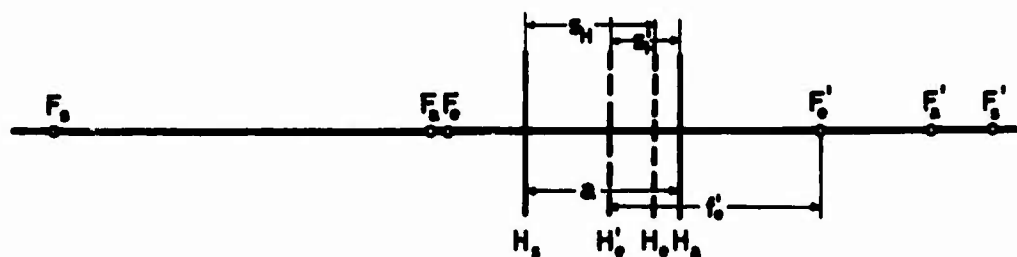


Figure 19. Combination of the Image-forming System O_a of the Autocollimator with the Mirror System O_s into the Equivalent System O_e

In Figure 19, the image-forming system O_a is given by the main plane H_a and the focal points F_a and F_s' . From Konig (1959), the focal length f_e' of the equivalent system O_e is given by:

$$f_e' = \frac{f_s' f_a'}{f_s' + f_a' - a} \quad (34)$$

The separations s_H and $s_{H'}$ of the main planes H_e and H_e' of the equivalent system, from given main planes H_s and H_a , are given by:

$$s_H = \frac{a \cdot f_s'}{f_a' + f_s' - a}; \quad s_{H'} = \frac{-a \cdot f_e'}{f_s'} \quad (35a, b)$$

s_H and $s_{H'}$ are positive in the beam direction from H_s and H_a , respectively.

With $f_s' > f_a'$, Eq. (34) becomes:

$$f_e' = f_a' \left(1 - \frac{f_a'}{f_s'} + \frac{a}{f_s'} \right). \quad (34a)$$

The separation $\overline{F_a' F_e'}$ of the image side equivalent focal point F_e' from the object-side focal point of the image-forming system F_a' is expressed, according to Figure 19:

$$\overline{F_a' F_e'} = f_a' - s_{H'} - f_e' = f_a' + \frac{a \cdot f_e'}{f_s'} - f_a' + \frac{f_a'^2}{f_s'} - \frac{a \cdot f_a'}{f_s'} = \frac{a}{f_s'} (f_e' - f_a') + \frac{f_a'^2}{f_s'}. \quad (36)$$

With $f_e' \approx f_a'$, the first term of Eq. (36) vanishes, so that

$$\overline{F_a' F_e'} = -\frac{f_a'^2}{f_s'} = -g. \quad (36a)$$

For $z = 0$, Eq. (33b) is equivalent to Eq. (36a), that is, an object at the focal point F_p of the projecting system O_p is imaged in the focal point F_e' of the equivalent system O_s . Expressing the image width z_a' in Eq. (33b) in terms of the focal point F_e' , Eqs. (33b) and (30a) become equivalent.

2.5.2.2 Dependence of Axial Image Position on Wavelength

The achromatics and apochromatics used customarily as collimator objectives are completely corrected chromatically only for two wavelengths. The residual secondary spectrum causes the dependence of axial image position on wavelength. For the apochromatics used here, $f = 1500\text{mm}$ gives, according to Konig and Kohler (1959), an image displacement of 0.5mm with red light ($\lambda = 0.656\mu\text{m}$) and green light ($\lambda = 0.546\mu\text{m}$). The value obtained by measurement amounts to 0.7mm . It is therefore recommended that focal length determination, focusing, and scale determination be referred to the same wavelength.

2.5.2.3 Object and Image Position in Parallax-free Focusing

Focusing at infinity follows in a fashion analogous to Section 2.5.1: The micrometer head is displaced until the micrometer scale MS coincides with the crosshair image S' without parallax. In Figure 20, the focusing procedure is represented in steps a, b, c, and d. In the initial setting a), the crosshair S is a distance z_p from the focal point F_p and is imaged at S' . S' has distance z_a' from F_a' and z_e' from F_e' . With $b = f_p - f_a$ and the adjustment error, described in Section 2.5.1, $d = d_m - d_s$, the separation e between the crosshair image and the micrometer plane MS is

$$e = z_a' - b + z_p' - d = z_a' - b + z_p' - d. \quad (37)$$

for a single focus setting in the Wild and Leitz micrometer, each measured 10×10 times:

Micrometer	Manner of Determination	Mean Error in a Focusing	
		on micrometer scale	on crosshair image
Wild	Repeated meas. of microm. head displ.	$\pm 0.06\text{mm}$	$\pm 0.15\text{mm}$ $\pm 0.24\text{mm}$
Leitz	Repeated meas. of microm. head displ.	$\pm 0.08\text{mm}$	$\pm 0.14\text{mm}$ $\pm 0.26\text{mm}$

Besides its determination through repeated measurements, the mean error of focusing may be determined from the crosshair image by a method involving moving the micrometer head through definite error-free measurable values and comparing these values with the measured focusing difference. The results show that focusing on the micrometer scale is more accurate and that with repeated measurements the focusing by image sharpness can be assumed to have a mean error of about $\pm 0.1\text{mm}$.

2.5.3.2 Focusing by Illumination Parallax

The accuracy of focusing by image brightness may be increased, in general, by focusing on parallax. The precision of focusing on vision parallax is given, according to König (1959) and Ochsenhirt (1962), by

$$z_r = \frac{f_{ok}}{d \cdot \delta} \delta. \quad (40)$$

- z_r = residual focus error
- d = diameter of exit aperture
- f_{ok} = ocular focal length
- δ = minimum sight angle

According to Eq. (40), the focusing precision can be enhanced by increasing ocular magnification. The diameter of the exit aperture is reduced thereby and must not be permitted to go below 1 mm in focusing applications (König and Köhler, 1959).

In the Wild coincidence setup, in which a dark hair is set over the bright slit image (see Fig. 11), primarily the photometric properties of the eye are satisfied; parallax is recognized by motion of the eye pupil only very unsatisfactorily. In placing a blind over the slit, on the other hand, or turning the illumination lamp about an axis perpendicular to the micrometer plane, the mutual brightness variations can be observed with full coincidence precision with a stationary eye, and the focusing can be measured with high precision. To differentiate normal parallax

reading by eye motion, the focusing method applied here will be called focusing by illumination parallax. With good illumination of the AC image the error of focusing was determined to be $\pm 0.03\text{mm}$ from 10×10 repetition measurements. Also in less favorable conditions, a mean focus error of less than $\pm 0.1\text{mm}$ can be counted on.

Appendix H gives the results of the focusings of all mirror combinations arising in the present work. Each focus setting c_i , that is, the setting of the crosshair against a fixed reference point on the collimator tube (Fig. 13) obtained in each focusing case, was obtained by means of the Wild micrometer in illumination parallax four times and reduced in focusing setting c_o by the Askania mirror (As). The results confirm that focusing differences of up to 2mm can arise; this can become disturbingly noticeable in multiple autocollimation. It is furthermore empirically asserted that the focusing settings are independent of mirror separations. It should be noted that focusing can be assumed as unambiguously satisfied only when the external conditions (see Section 2.7.2.1) are as ideal as possible. A partial repetition of the focusing after one year can reveal changes up to 0.3mm, which can result from alterations in mirror curvature.

2.6 Determination of the Scale Factor of an Autocollimation System

In conversion of image displacement s into mirror rotation α according to Eq. (3), it is required that image displacement and focal length be given in the same units. If this condition is not met, then it is advisable to write Eq. (3) in the general form

$$\alpha = m \cdot s . \quad (41)$$

Here m is to be called the scale factor of the AC system; it differs from the quantity $1/2f$ by a constant factor.

2.6.1 AUTOCOLLIMATION WITH NONPARALLEL BEAMS

For highest demands of precision, it must be considered that the crosshair is a distance z_p from the focal point F_p of the projecting system, according to Eq. (38), and that the image displacement s is to be converted into the angle measure with the equivalent focal length f_e of the system mirror-objective-separation cube. The focusing error z_p and the mirror curvature $1/2f_s$ cause the rays between objective and AC mirror not to run parallel. The influence of the convergence of the rays on angle measurement by means of autocollimation will be investigated in the following paragraphs.

Figure 21 depicts an autocollimation system with parallax-free focusing. The AC mirror is at a distance a from the objective of the autocollimator and is set in the exit setting (0) perpendicular to its target axis. The crosshair S is projected

by the projecting system O_p to S_o^* . The rays leaving the objective are reflected at the AC mirror and form the image S_o'' of S by means of the equivalent system O_e in the micrometer plane MS. The rays reflected from the AC mirror seem to emanate from point S_o' , which lies at a distance $2(a-f_p)$ from point S_o'' . Turning the mirror through the angle α (setting 1), the rays appear to come from point S_1' and form an image S_1'' of S . According to an insertion of Waimer (1965), the relationship between the rotation α of the mirror and the resulting image displacement $s = S_o''S_1''$ is as given in the following figure:

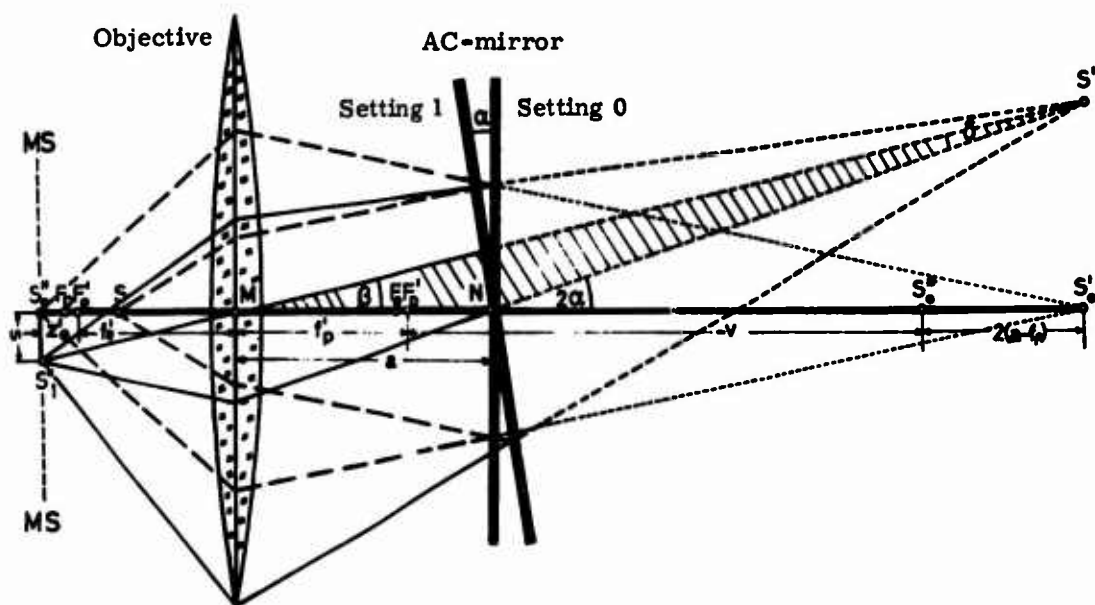


Figure 21. Scale Determination with Nonparallel Rays

In triangle MNS_1' , according to the sine law:

$$\frac{f_p' - v + 2(a-f_p)}{\alpha \cos \beta} = \frac{\sin(180-2\alpha)}{\sin \delta} \quad (42)$$

for small angles α , β , and γ , Eq. (42) becomes

$$\delta = 2\alpha \frac{a}{-v + 2a - f_p'}$$

v is computed from Newton's image formation equation $v = -f_p^2/z_p$, so that

$$\delta = \frac{2a \cdot \alpha}{\frac{z_p}{f_p} + 2a - f_p'}$$

according to Figure 21,

$$\beta = 2\alpha - \delta = 2\alpha - \frac{2a \cdot \alpha \cdot z_p}{f_p^2 + 2a \cdot z_p - z_p \cdot f_p'}$$

and

$$s = (f_e' + z_e') \beta = (f_e' + z_e') \cdot 2\alpha \left(1 - \frac{a \cdot z_p}{f_p^2 + 2a \cdot z_p - z_p \cdot f_p'} \right). \quad (43)$$

With $f_1 = f_p' \approx f_e'$ for terms of higher order, after some manipulation of Eq. (43)

$$s = 2f_e' \cdot \alpha + 2z_e' \cdot \alpha - \frac{2a \cdot z_p}{f_p} \alpha - \frac{2a \cdot z_p \cdot z_e'}{f_p^2} \alpha + \frac{2a \cdot z_p^2}{f_p^2} \alpha - \frac{4a^2 \cdot z_p^2}{f_p^3} \alpha.$$

For $z_p, z_e < f_p$, a the last three terms can be neglected, so that

$$s = 2\alpha \left(f_e' + z_e' - \frac{a \cdot z_p}{f_e'} \right). \quad (43a)$$

The scale factor m is obtained in conjunction with Eqs. (41) and (43a) as

$$m = \frac{1}{2 \left(f_e' + z_e' - \frac{a \cdot z_p}{f_e'} \right)} = \frac{1}{2f_e'} \left(1 - \frac{z_e'}{f_e'} \left(1 - \frac{a}{f_e'} \right) \right) = \frac{1}{2f_e'} \left(1 - \frac{z_p}{f_e'} \left(1 - \frac{a}{f_e'} \right) \right) \quad (44)$$

and with Eq. (38)

$$m = \frac{1}{2f_e'} \left(1 - \frac{1}{2f_e'} (g + b + d) \left(1 - \frac{a}{f_e'} \right) \right). \quad (44a)$$

For $a = f_e'$, that is, for the setup of the mirror at the focal point F_e' of the equivalent system, a focusing error z_p of the projection or a focusing error z_e' of the image does not affect the scale. From Appendix I it is seen that in this case the mirror mount acts as an aperture blind, and the observation is performed in both cases on telecentric beam path.

In multiple autocollimation with the image of K th order, the angle $(S_1' N S_0')$ in Figure 21 is equal to $2K\alpha$. It can be shown that the scale factor m_K for the image of K th order can be computed from the following formula:

$$m_K = \frac{1}{2K \cdot f_{ek}} \left(1 - \frac{z_{ek}'}{f_{ek}} + \frac{a \cdot z_{pk}}{f_{ek}^2} \right). \quad (44b)$$

z_{pk} and z'_{ek} are separations of the crosshair and crosshair image, respectively, from focal points F'_p and F'_e , respectively, which arise in the focusing case. Setting in Eq. (44) the values for f'_e and z'_e from Eqs. (34a) and (39a), one obtains, upon several manipulations, the scale factor as a function of the focal length f'_a of the image-forming system:

$$m = \frac{1}{2f'_a} \left(1 - \frac{z'_a}{f'_a} \left(1 - \frac{a}{f'_a} \right) \right) = \frac{1}{2f'_a} \left(1 - \frac{1}{2f'_a} (-g+b+d) \left(1 - \frac{a}{f'_a} \right) \right). \quad (44c)$$

For $a = f'_a$, the observation is again on telecentric beam path; for this case, according to Eq. (34a), the focal length of the image-forming system corresponds to that of the equivalent system. Equations (44) and (44b) show that a focusing change in consequence of residual mirror curvature affects only the scale factor to change it from its value in the case of error-free optical plane surfaces. This statement agrees with the specifications on the effect of a focusing error in reciprocal collimation (Ochsenhirt, 1962), since in autocollimation a change of the incidence height h of the main beam is only proportional to the change of the measurement range. The following table gives several numerical values of the change Δm ["/mm image displacement] of the scale factor and its effect $\Delta \alpha$ on the angle measurement for a range of 300" ($a = 500\text{mm}$, $f'_e = 1503\text{mm}$).

z_p [mm]	0	0.1	0.5	1.0	2.0	3.0
Δm ["/mm]		-0.003	-0.015	-0.030	-0.061	-0.091
m ["/mm]	68.604	68.601	68.589	68.574	68.543	68.513
α ["]	300.00	299.99	299.93	299.87	299.73	299.60
$\Delta \alpha$ ["]	0.00	-0.01	-0.07	-0.13	-0.27	-0.40

Accordingly, for investigations which require great accuracy with a large measurement range, for example, the testing of optical micrometers, the knowledge of the precise scale factor is required. Since the quantities f'_e and z'_e in Eq. (44) or the quantities g , b , and d in Eq. (44a) are not directly obtainable, it must be investigated how a direct determination of the scale factor is assumed.

2.6.2 DIRECT DETERMINATION OF THE SCALE FACTOR ON AN AC SYSTEM

a) Principle

The scale factor m_0 of an AC system, that is, of an autocollimator with a definite mirror system and mirror separation, can be directly determined from Eq. (41) in the following way: One fastens the relevant AC measurement mirror on the alidade of a theodolite and arranges the mirror for observation with the autocollimator.

A rotation α of the alidade can be read off on the divided circle of the theodolite; the image displacement s is measured with the autocollimator in units of the micrometer. The scale factor m_0 is obtained from Eq. (41)

$$m_0 = \frac{\alpha}{s}. \quad (41a)$$

The direct determination of the scale factor according to Eq. (41a) is superior to the determination from the focal length of the objective for the following reasons:

1. The direct determination gives the actual scale factor of the corresponding AC system, accounting for the curvatures of the mirrors and of the separation cube and for the misalignment of the micrometer head.
2. The units of the micrometer [MU] are not necessarily units of length.
3. The direct determination is made with the autocollimator in its deployment state and simultaneously gives information about its function readiness.
4. The determination of the scale factor can be executed with greater accuracy for the same cost as a focal length determination.

The accuracy of the procedure depends on the accuracy of the theodolite measurement and on the accuracy of the AC measurement. The accuracy of the theodolite measurement is essentially dependent on the precision of the divided circle, the micrometer, and the coincidence. The long- and short-period divided circle errors are not manifested in a measurement range of 5'; the incidental divided circle errors are determined each according to the kind of circle, or they can be eliminated by shifting the circle. The systematic micrometer errors are eliminated in taking both readings at the same micrometer setting for corresponding choice of angle magnitudes. The coincidence accuracy can then be enhanced in multiple coincidence. In the AC measurement, error in the determination of the scale factor due to incidental or systematic micrometer errors is avoided by varying the angle.

It should be mentioned that other angle measurement apparatuses besides the theodolite, for example optical tables, can be used, insofar as accuracy conditions are fulfilled. In the investigations of the author, production line autocollimators have considerable scale factor errors; these can easily be determined by the user with the given methods and could be used in scale improvements.

b) Practical Realization and Results

The determination of the scale factor was executed with simple autocollimation for the theodolite Wild T4 No. 48978. The AC mirror Askania with the focal length f_s was mounted on the horizontal telescope tube of the theodolite. The mirror separation amounted to 500mm; the wavelength of the light used was $\lambda = 0.55\mu\text{m}$. To be free from the determination of the micrometer units in units of length (Section 2.4.2.2), and from the residual curvature of the surfaces of the separation cube,

the scale factor was determined for the Wild micrometer as well as for the Leitz micrometer. For the control of possible changes, the scale factor determination for the Wild micrometer was repeated after a prolonged time. For the Leitz micrometer the scale factor was determined separately for the x and y directions. Care must be taken in the measurements that the separate parts of the AC system be so horizontalized that a full mirror rotation is measured. Because of the desired high accuracy, each relevant scale factor was obtained by a minimum of thirty independent determinations. The results are displayed in Table 4 and show that the scale factor can be fixed with a mean error of ± 0.2 percent.

Table 4. Results of the Direct Scale Determinations for the 1500mm AC System

Micrometer	Wild-Micrometer		Leitz-Coord. micr.	
	1. 3. 65	17. 5. 66	x	y
Measurement range [mm]	4. 8000	4. 8000	4. 6384	4. 6400
1 Micrometer unit [μm]	4. 0000	4. 0000	4. 8315	4. 8335
Focus setting [mm]	36. 88	37. 11	29. 00	29. 00
No. of scale determinations	33	35	31	30
Minimum angle [$^{\circ}$]	258. 66	239. 10	239. 23	239. 02
Maximum angle [$^{\circ}$]	317. 64	301. 20	301. 28	301. 60
Scale m [$''/\text{MU}$]	0. 27430	0. 27445	0. 33188	0. 33194
Scale m_0^o [$''/\text{mm}$] image displ.	68. 575	68. 612	68. 691	68. 675
Measurement range [$^{\circ}$]	329. 16	329. 34	318. 60	318. 74
Measurement error, 1 det. [$''/\text{MU}$]	$\pm 0. 00015$	$\pm 0. 00033$	$\pm 0. 00032$	$0. 00035$
M.E. 1 det [%]	$\pm 0. 57$	$\pm 1. 25$	$\pm 0. 97$	$\pm 1. 06$
M.E. 1 det [$''/\text{mm}$]	$\pm 0. 04$	$\pm 0. 08$	$\pm 0. 07$	$\pm 0. 07$
M.E. 1 det [$^{\circ}$] with 300 $^{\circ}$ range	$\pm 0. 17$	$\pm 0. 37$	$\pm 0. 29$	$\pm 0. 32$
M.E. median [$''/\text{MU}$]	$\pm 0. 00003$	$\pm 0. 00006$	$\pm 0. 00006$	$\pm 0. 00006$
M.E. median [%]	$\pm 0. 10$	$\pm 0. 21$	$\pm 0. 17$	$\pm 0. 19$
M.E. median [$''/\text{mm}$]	$\pm 0. 01$	$\pm 0. 01$	$\pm 0. 01$	$\pm 0. 01$
M.E. median [$^{\circ}$] with 300 $^{\circ}$ range	$\pm 0. 03$	$\pm 0. 06$	$\pm 0. 06$	$\pm 0. 06$

Using the lengths discussed in Section 2. 4. 2. 2 and given in Table 4 for the micrometer units, the scale factor can be referred to 1mm image displacement in both micrometers. There is evidence of a difference between the Wild micrometer and Leitz micrometer of $0. 09''/\text{mm}$ in the image displacement, or 1. 3 percent, which is caused by the different residual curvatures of the Wild and Leitz separation cubes. For the value, determined in Section 2. 4. 2. 1, of the focal length of the objective, $f = 1503. 3\text{mm}$, there results a scale factor $m = 68. 604''/\text{mm}$ image displacement.

2.6.3 DETERMINATION OF THE SCALE FACTOR FROM FOCUS DIFFERENCES

According to Section 2.6.1, the scale factor of an AC system depends on the residual curvature of the mirror system and its separation from the autocollimator. A direct determination of the scale factor for each mirror system and each mirror setting is, however, so laborious that it seems desirable to determine the changes in scale factor in terms of the measurable mirror separations and the measurable focus differences. For the mirror separations a_0 and a'_0 , according to Eq. (44c), it holds that:

$$m_0 = \frac{1}{2f_a} \left(1 - \frac{z'_{a0}}{f_a} \left(1 - \frac{a_0}{f_a} \right) \right) = \frac{1}{2f_a} \left(1 - \frac{1}{2f_a} (-g_0 + b + d) \left(1 - \frac{a_0}{f_a} \right) \right)$$

$$m'_0 = \frac{1}{2f_a} \left(1 - \frac{z'_{a0}}{f_a} \left(1 - \frac{a'_0}{f_a} \right) \right) = \frac{1}{2f_a} \left(1 - \frac{1}{2f_a} (-g_0 + b + d) \left(1 - \frac{a'_0}{f_a} \right) \right)$$

Assuming the scale factor determinations m_0 and m'_0 for the mirror separations a_0 and a'_0 for one and the same mirror system (g_0), f_a , and z'_{a0} can be obtained from the above equations. For a third mirror separation a_i , the scale factor is solvable from Eq. (44c) for given f_a and z'_{a0} .

If another mirror system is employed (g_i), the focus setting z'_{ai} of the autocollimator is altered. For the appropriate scale factor m_i it holds that:

$$m_i = \frac{1}{2f_a} \left(1 - \frac{z'_{ai}}{f_a} \left(1 - \frac{a_i}{f_a} \right) \right) = \frac{1}{2f_a} \left(1 - \frac{1}{2f_a} (-g_i + b + d) \left(1 - \frac{a_i}{f_a} \right) \right)$$

Setting $m_i = m_0 + \Delta m$, $a_i = a_0 + \Delta a$, $z'_{ai} = z'_{a0} + \Delta z'_a = z'_{a0} + \Delta g$, change Δm of the scale factor m_i relative to the directly determined value m_0 is:

$$\Delta m = \frac{1}{2f_a} \left(1 - \frac{(z'_{a0} + \Delta z'_a)}{f_a} \left(1 - \frac{a_0 + \Delta a}{f_a} \right) \right) - m_0.$$

Some manipulation gives

$$\Delta m = -\frac{1}{2f_a} \left(\frac{z'_{a0}}{f_a} \Delta a + \Delta z'_a \left(1 - \frac{a_0 + \Delta a}{f_a} \right) \right) = c_1 \Delta a + c_2 \Delta z'_a + c_3 \Delta a \Delta z'_a.$$

c_1 , c_2 , and c_3 are constant factors which are ascertained from the two given scale determinations. Δa and $\Delta z'_a$ are directly measurable. On micrometer interchange not only the focal lengths f_p and f_a but also the adjustment error of the micrometer head are changed, so that the direct determination of the new scale factor is advisable.

2.7 On the Accuracy of Angle Measurement by Means of Autocollimation

The preceding investigations of the accuracy of autocollimation measurements have been referred to separate parts of the AC system, aside from the determination of the scale factor. The internal accuracy that can be attained in the interaction of the separate parts and the degree to which external factors affect the measurement system, will be investigated in the following paragraphs.

2.7.1 INTERNAL ACCURACIES

The internal precision of the measurement system is denoted by the mean error m_o of a single measurement, that is, by the mean error in a single measurement of the direction of the mirror normals. m_o is calculated from the distribution of the measured values under fixed external conditions. On the basis of the investigations of Section 2.7.2, the influence of the external factors can be broadly excluded by appropriate experimental arrangement within a small time interval. The group of measurements available thereby is used for the determination of internal accuracy. Since for extremely small mirror rotations (for example, see Section 5.1) the internal accuracy is practically identical with the coincidence accuracy, the coincidence accuracy will be investigated next for different measurement arrangements.

2.7.1.1 Coincidence Accuracy

Coincidence accuracy is characterized by the mean error m_K of a double coincidence; m_K may be computed from the distribution of the mean values of any coincidence from the right and left. Next, the relationship between coincidence accuracy and the type and magnification of the observation optics will be investigated. Table 5, top, shows that the coincidence accuracy is essentially independent of the observation optics. In the measurements of the present work, the readings were taken, as a rule, with simple autocollimation with 20-times microscope magnification, and with multiple autocollimation with 12-times magnification. For the Wild measurement facility there results a mean error between ± 0.2 and $\pm 0.3 \mu\text{m}$ corresponding to $\pm 0.02''$. For the Leitz measurement facility the mean error lies somewhat higher at $\pm 0.4 \mu\text{m} \cong \pm 0.03''$. Further, it is of interest to determine what size to choose for optimum and minimum mirror diameter. Table 5, middle, shows that coincidence accuracy is very slightly diminished with decreasing mirror diameter. This is explained in terms of the blinding out of the mirror border zones which, according to the interferometric investigation, have extra unevennesses. Although the m_K values for mirror diameters of 50 and 40mm are small, it must be remembered that the crosshair image is of significantly poorer quality and that coincidence can be ascertained only with effort. As a rule, one can say that the diameter of

of the exit aperture, that is, of the mirror mounting, which acts as an aperture blind on the ocular-side image, must not go below the value of 0.5mm.

Table 5. Dependence of Coincidence Accuracy on Reading Optics, Mirror Size, and Number of Reflections

Coincidence Accuracy and Reading Optics					
Reading Optics	Magnification	No. of series a' 10 dbl co	Mean co-incidence error [μm]	Corresp. Tilt of AC mir.	Observations
Micrometer-ocular	15x	6	± 0.24	$\pm 0.017''$	Vert. angle simple AC mirror 90mm Wild Microsc.
Microscope	12x	18	± 0.22	$\pm 0.015''$	
Microscope	20x	36	± 0.25	$\pm 0.017''$	
Microscope	28x	18	± 0.30	$\pm 0.021''$	
Binocular-microscope	20x	12	± 0.17	$\pm 0.012''$	
Microscope	20x	6	± 0.36	$\pm 0.024''$	Leitz micr.H.W.
Microscope	20x	6	± 0.44	$\pm 0.031''$	Leitz micr.V.W.
Coincidence Accuracy and Mirror Size					
Mirror ϕ mm	Exit Aperture ϕ [mm]	No. of series a' 10 dbl co	Mean co-incidence error [μm]	Corresp. Tilt of AC mir.	Observations
90	0.75	33	± 0.28	$\pm 0.019''$	Vert. angle simple AC Microscope 20X Wild microm.
80	0.67	6	± 0.23	$\pm 0.016''$	
70	0.58	21	± 0.27	$\pm 0.018''$	
60	0.50	6	± 0.19	$\pm 0.013''$	
50	0.42	6	± 0.22	$\pm 0.015''$	
40	0.33	6	± 0.21	$\pm 0.014''$	
Coincidence Accuracy and Number of Reflections					
AC Principle	No. of reflections	No. of series a' 10 dbl co	Mean co-incidence error [μm]	Corresp. Tilt of AC mir.	Observations
Simp. AC. AM Mir. *	1	66	± 0.24	$\pm 0.016''$	Wild microm. Vert. angle
Simp. AC. T-Mir.	1	26	± 0.23	$\pm 0.016''$	
Simp. AC. As-Mir.	1	6	± 0.26	$\pm 0.018''$	
Simp. AC. U-Mir.	3	29	± 0.21	$\pm 0.015''$	Horiz. angle
Simp. AC. m. U-Mir.	3	10	± 0.28	$\pm 0.019''$	
Mult. AC. 2. Ord.	8	35	± 0.33	$\pm 0.011''$	Vert. angle
Mult. Reflex. 22.5°	7	15	± 0.34	$\pm 0.008''$	

*For abbreviations, see Appendix H

For multiple reflection and multiple autocollimation, it is important to know if the coincidence accuracy decreases as a result of the greater number of reflections (Table 5). The noticeable decrease in image quality affects coincidence accuracy only very slightly, so that the theoretical multiplication order of the accuracy is manifested almost completely. For multiple autocollimation with the IInd order image, a mean error of coincidence of $\pm 0.01''$ is attained. The mirror diameter should not go below a value of 60-70mm.

2.7.1.2 Accuracy of the Measurement System

As was already mentioned in Section 2.3.5, multiple autocollimation offers the possibility to thoroughly ascertain the accuracy of the measurement system by means of using images of higher order. If, for example, the AC mirror is tilted through a definite angle $\Delta\gamma_a$, then according to Eq. (21a) the displacement Δi_{II} of the image of IInd order (observation l_2) must be twice as great as the displacement Δi_I of the image of Ist order (observation l_1). The condition equation relating observations l_1 and l_2 is:

$$2(l_1 + v_1) - (l_2 + v_2) = 0.$$

For the discrepancy $w_a = 2l_1 - l_2$, one obtains the correlate k_a by way of the normalized equation:

$$k_a = -\frac{w_a}{5}.$$

The mean error m_1' of an observed quantity, that is, of an angle difference, is obtained from:

$$m_1' = \sqrt{\frac{[vv]}{n-u}} = \sqrt{\frac{-w_a \cdot k_a}{1}} = \frac{w_a}{\sqrt{5}} = 0,447 w_a.$$

The mean error m_1 in the direction of the mirror normal is

$$m_1 = \frac{m_1'}{\sqrt{2}} = \frac{w_a}{\sqrt{10}} = 0,316 w_a. \quad (45)$$

According to Eq. (45), each discrepancy w_a gives a value for the accuracy of the measurement system. For a thorough-going testing, the measurement settings are distributed as equally as possible over the whole range of the micrometer. The distribution for the 110 determinations of w_a are shown in Figure 22. The angle changes $\Delta\gamma_a$ can be set, for example, with the help of a bubble level tester on whose tilting table is fastened the AC measurement mirror. The present investigations were carried out in two experimental arrangements: 30 determinations of w_a were made

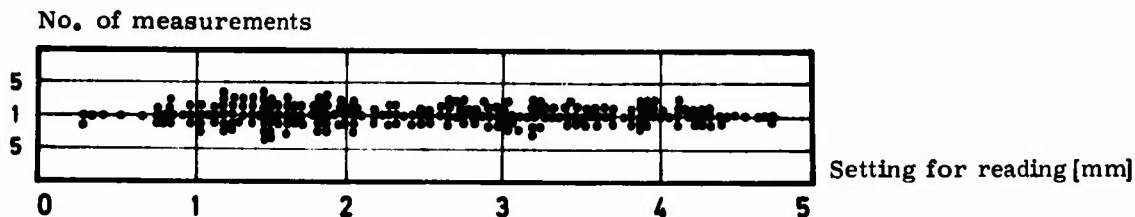


Figure 22. Distribution of Measurement Settings in the Testing of the System of Measurement, \circ without deflection, \bullet with deflection

with a deflection mirror (Table 3c) and 80 determinations were made without a deflection mirror (Table 3a). In the observations with the deflection mirror, reductions are occasioned in part due to readings of the zero-order image, (Section 2.3.4.2 the set angle changes lie between $5''$ and $15''$. The measurements were made with the Wild micrometer, so that micrometer improvements are to be made according to Appendix F. The root mean square value of the 110 determinations of m_1 amounts to:

$$m_1 = \pm \sqrt{\frac{w_a \cdot w_a}{10 \cdot 110}} = \pm 0.56 \mu\text{m} \hat{=} \pm 0.038'' .$$

If no micrometer improvements are brought about, m_1 is given by $\pm 0.10''$; taking into account the micrometer error enhances the accuracy by a factor of 2.5. The value for m_1 agrees well with the micrometer accuracy given in Section 2.4.2.2 at $0.4 \mu\text{m}$, if the coincidence accuracy of $0.25 \mu\text{m}$ is taken into account.

The described investigation methods yield:

Errors of the micrometer,

extra-axial image errors of the projection and image-forming systems,

scale errors due to focus differences of the images of Ist and IInd orders and

stability error in the measurement system during the determination of w_a .

The errors in the determination of the scale factors, which affect the images of Ist and IInd order equally remain unaccounted for. The obtained value m_1 must therefore be combined with the mean error m_2 in the determination of the scale factor to a mean error m_0 in the direction of the mirror normals:

$$m_0 = \pm \sqrt{\frac{1}{2} \left(2m_1^2 + \left(\frac{\alpha}{\alpha_{\max}} \right) m_2^2 \right)} = \pm \sqrt{0.038''^2 + \frac{\alpha''}{2 \cdot 300''} 0.05''^2} . \quad (46)$$

Here α means the value of the angle in $''$, whose one edge is formed by the direction. The internal accuracy for simple autocollimation is, corresponding to (46), dependent on the range as follows:

α ["]	10"	30"	60"	120"	180"	300"
m_o ["]	$\pm 0.038''$	$\pm 0.040''$	$\pm 0.042''$	$\pm 0.044''$	$\pm 0.047''$	$\pm 0.052''$
m_o [‰]	± 3.8 ‰	± 1.3 ‰	± 0.7 ‰	± 0.4 ‰	± 0.3 ‰	± 0.2 ‰

Since in most of the present investigations a measurement range of less than 1' is required, the mean error in a direction of the mirror normals can be given with $\pm 0,04''$.

2.7.2 INFLUENCE OF EXTERNAL FACTORS ON THE PRECISION OF AN AC SYSTEM

Generally it is necessary, in fine measurements, to approximate as much as possible, the internal precision of the measurement system with the external accuracy of the measurements, that is, the accuracy under changing experimental conditions. To this end, the different external factors are now submitted to extreme changes, so that the influence of each on the measurement system can be recognized. The obtained risk factors must be compensated by corresponding countermeasures, and the measurement procedure must be dictated thereby. Preliminary investigations showed that normal mechanical shocks, for example, a person walking into the experiment room, could only be observed when working with deflection mirrors and that these shocks could be suppressed by damping devices. Temperature changes have a considerably larger influence, which affects the refraction, mirror surfaces, and positioning of the mirrors and the autocollimator.

2.7.2.1 Refraction

The ray between the objective and mirror undergoes a direction change which depends, according to Wiemerslage (1962), on vertical temperature gradients and depends on the lengths of the path traversed. The temperature gradient changes even with relatively constant temperature conditions up to $(0.5^\circ/\text{m})/\text{h}$, so that measurement accuracy is disturbed by changes in index of refraction. The direction fluctuation manifests itself as a flickering of the crosshair image, and may be determined by means of the coincidence procedure for mirror separations of under 1m without special measures. The observed oscillations of period 1-5 min. are dangerous; without suitable precautions (ventilators) these considerably affect the measurement results. The results of the investigations of this effect are displayed in Table 6. For different mirror arrangements and mirror separations the mean error is computed from repeated measurements (measurement duration 4-8 min.) for each ten double coincidences. These mean errors serve as a measure for the magnitude of the oscillations.

Table 6. Dependence of Refraction on Mirror Separation

AC Principle and mirror	Mirror separ.	No. of meas. rep. per 10 double coinc.	Mean sq. of error [μm]	Direction change due to refraction γ_e	Corresp. mirror tilt m_{γ_a}	Observations
1	2	3	4	5	6	7
Simp. -AC with Am*	0.3m	132	± 0.64	$\pm 0.09''$	$\pm 0.04''$	without ventil.
Simp. -AC with As	0.3m	9	± 0.96	$\pm 0.13''$	$\pm 0.07''$	without ventil.
Simp. -AC with Am	0.3m	66	± 0.24	$\pm 0.03''$	$\pm 0.02''$	with ventil.
Simp. AC with U mir.	1.1m	16	± 1.6	$\pm 0.22''$	$\pm 0.11''$	without ventil.
Simp. AC with U mir.	3.0m	8	± 2.8	$\pm 0.38''$	$\pm 0.19''$	without ventil.
Simp. AC with U mir.	3.0m	8	± 0.9	$\pm 0.12''$	$\pm 0.06''$	with ventil.
Mult. Ref. 22.5°	0.7m	8	± 1.4	$\pm 0.20''$	$\pm 0.03''$	without ventil.

*For abbreviations, see Appendix H.

Assuming refraction changes to be the only cause for image migration, there obtain the values γ_e of column 5 for the mean square of the direction changes of the ray. If the oscillations which occur are not recognized as such, but rather interpreted as mirror tilts, the AC measurements are limited by the uncertainty m_{γ_a} given in column 6. The table shows a substantial increase in direction changes with distance. Thus γ_e at a mirror separation of 0.3m is equal to $\pm 0.1''$, and at a mirror separation of 3m, $\pm 0.4''$. The increase obtained does not, however, correspond to the value calculated by Wiemerslage (1962). The reduction influence is diminished according to Table 6, by about a third through the inclusion of ventilators. The AC measurements of the present work were therefore made exclusively with the use of ventilators. A graphic representation of the dependence of refraction changes on mirror separation and of the reduction by ventilation is given in Figure 23. For the cases presented there, the measurement values are displayed for each 3 measurement series per 10 double coincidences as a function of time. The ventilators must be set up so as to avoid turbulence between objective and mirror, and so that mirror surfaces are bathed by air currents. The latter is recommended because of the temperature sensitivity of the mirror surfaces which was ascertained in the investigation on focusing.

2.7.2.2 Temperature Sensitivity of the Positioning of the Autocollimator and the Mirror System

The strong temperature sensitivity of the AC system as was observed in the investigations was more closely investigated by means of several special temperature investigations. Because of the different length expansions of the separate

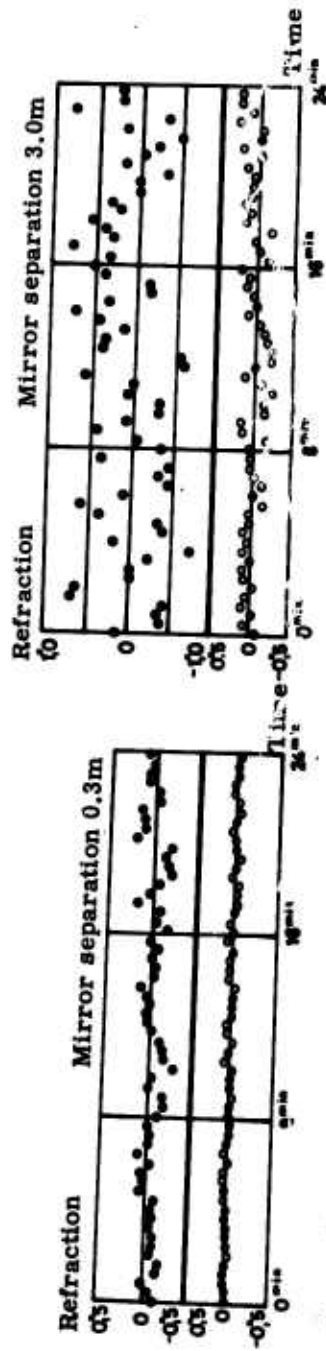


Figure 23. Refraction between Objective and AC Mirror. ● without ventilator, ○ with ventilator

parts, temperature changes cause angle changes in the autocollimator and in the different mirrors, which in turn cause image migration. The temperature changes are artificially imposed, and the resulting observed image migrations are recorded. Since, in the AC system with deflection mirrors, the greatest temperature sensitivity is observed, and the simultaneous observation of several images can give conclusions on the origins of tilt, the investigations were carried out with multiple autocollimation with deflection mirrors.

The first thermal investigation over 12 hours is described in detail in the following. After a 6°C heating over 12 hours by means of 5 distributed heaters, the system was cooled in the ambient by 5°C in the first hour and by 1.5°C in the next 7 hours. The observed image migrations are shown in Figure 24.

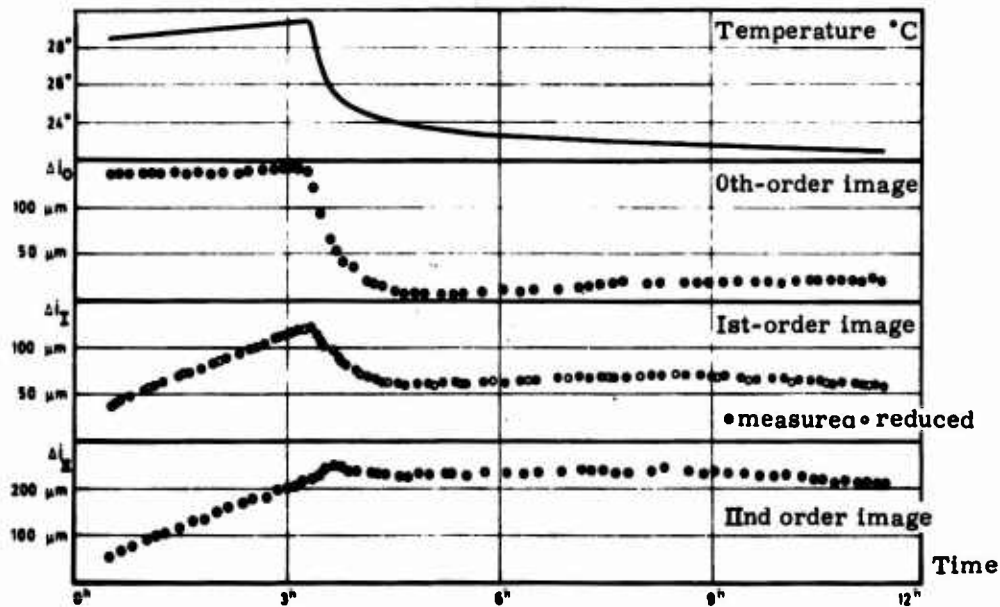


Figure 24. Image Migration with Thermal Changes

There is manifested a greatly similar behavior of the temperature curve and the migrations of images of 0th and 1st order. The 2nd order image was measured as a control, and was reduced to the 1st order image together with the 0th order image by means of Eq. (23a):

$$i_{\text{Ired.}} = (i_0 + i_{\text{II}}) / 2.$$

Since the observed quantities are correlated, it is in general not possible to express the individual rotations $\Delta\gamma_e$, $\Delta\gamma_t$, $\Delta\gamma_u$, and $\Delta\gamma_a$ in terms of the image migrations Δi_o , Δi_I , and Δi_{II} . With the requisite experimental precautions, thermal insulation, separate heating of the individual parts, etc., the separate unknowns can, nevertheless, be obtained individually. The analysis of such an investigation yields the following angle changes:

$$\Delta\gamma_e = 0.08''/0.1^\circ\text{C}; \Delta\gamma_t = 0.16''/0.1^\circ\text{C}; \Delta\gamma_u = 0.16''/0.1^\circ\text{C}; \Delta\gamma_a = 0.11''/0.1^\circ\text{C}.$$

A further experiment for the investigation of thermal sensitivity of the mirror surfaces gave no unambiguous results.

For the three above-mentioned experiments, the image migrations are reported per 0.1° temperature change in the following table according to sign and magnitude.

Means of Thermal Change	Temp. chng. per unit time [$^\circ\text{C}/\text{h}$]	Image Migration [$\mu\text{m}/0.1^\circ\text{C}$]			Corres. Mirror tilt [$''/0.1^\circ\text{C}$]		
		0.	I.	II. Ord.	0.	I.	II. Ord.
Small temp. increase	0.1 - 0.3 $^\circ$	2.6	5.5	10.0	0.18 $''$	0.38 $''$	0.35 $''$
Small temp. decrease	0.1 - 0.2 $^\circ$	0.6	2.4	5.3	0.04 $''$	0.17 $''$	0.18 $''$
Large temp. increase	5 $^\circ$ - 10 $^\circ$	0.7	1.1	1.2	0.05 $''$	0.07 $''$	0.04 $''$
Large temp. decrease	4 $^\circ$ - 6 $^\circ$	1.5	1.0	1.4	0.10 $''$	0.07 $''$	0.05 $''$

The rotations γ_a of the AC mirror, corresponding to the image migrations are very different, and reach, in part, significantly higher values than the mirror rotations which occur for normal thermal conditions (Section 2.7.2.3). A steady heating over several hours proves to be especially dangerous.

2.7.2.3 Stability of an AC System Under Normal Thermal Conditions

The temperature changes which occur under normal conditions are between $0.2^\circ/\text{h}$ and $0.5^\circ/\text{h}$. Their effect is not unilateral in the same way as for the artificially-imposed temperature changes. Therefore, the following observed image migrations, observed under normal conditions were much more relevant to the determination of the stability of the AC system.

The data from Section 2.7.1.1, on the determination of coincidence accuracy, is utilized in part for the investigation of stability. The changes in the mean values from each 10 double coincidences are here observed over longer time periods. The curve for the relationship between image migration and time is approximated, for a given time interval, by fitting a linear or quadratic curve. The image migrations obtained are referred to a time interval of 30 min. and displayed in Table 7 for the entire time interval. The mean approximation (for definition, see Section 4.4.2) of the linear or parabolic curve is a measure of the steady behavior of

the stability changes. The use of polynomials of higher order gives no essentially different results. The following values are obtained for the individual AC systems:

Table 7. Image Migration at Normal Temperature Variation

AC System	Mult. of Mirror tilt	Mirror Separation	Duration of Measurements	Total No. of Double Coincidences	Image Migration μm per 30 min	Corres. Tilt of Meas. Mirror per 30 min	Mean Approx. \pm Linear Fit	Mean Approx. \pm Parabolic Fit
Simple AC	2	0.3m	17.4h	1050	0.7	0.046"	$\pm 0.044''$	$\pm 0.039''$
Simple AC with defl.	2	0.9m	6.3h	500	2.3	0.156"	$\pm 0.051''$	$\pm 0.033''$
Mult. AC with defl. IInd order image	4	0.9m	9.1h	480	3.7	0.127"	$\pm 0.108''$	$\pm 0.066''$
Mult. Reflec. + mult. AC arr. IInd order image	12	0.9m	2.8h	230	3.4	0.038"	$\pm 0.013''$	$\pm 0.007''$

The data in Table 7 are corroborated by the results of the instrumental investigations described in Section 5. In determining the stability of this report (Section 5.1) the stability of the AC-System can be derived from the migration of the image of zeroth order. In determining the tilt and vertical axes, (Sections 5.4 and 5.5) the stability of the AC-System can be deduced from the displacement of the mean of the continuously measured several series of observations. The mean image migrations (referred to the time unit of 30 minutes) are presented in the following table:

Instrumental Investigation	AC-System	Mirror Separation	Duration of Meas.	Image Migration per 30 min (μm)		Corresponding Tilt of the Measuring Mirror per 30 min	
				Horiz.	Vertical	Horiz.	Vertical
Azimuthal Rotation of the Support	Multiple AC-of 2nd order	0.5m	21.6h	0.8	-	0.04"	-
Tilt Axes	Single AC	0.3m	3.0h	1.9	1.3	0.13"	0.09"
Vertical Axes	Single AC with De-flecting mirror	1.3m	12.9h	1.2	2.0	0.08"	0.14"

The results of the investigations on the stability of AC systems may be summarized as follows:

1. In simple autocollimation, the errors due to instability of an AC measurement are smaller than $0.1''/30$ min.
2. In use of the deflection mirrors, the mirror arrangement of Table 3c, and if necessary, a reduction according to Section 2.3.4.3, are recommended since inclination changes of up to $0.2''/30$ min. may arise.
3. Enhancement of accuracy by multiple reflection or multiple autocollimation is increasingly difficult to realize as the measurement duration is increased.
4. The duration of a single measurement series should not exceed 30 min. Because of the largely linear character of the changes, it suffices to take control measurements in time intervals of 10-15 min., in long measurement series or in working with deflection mirrors.

Upon observation of these rules, internal and external accuracy coincide.

3. INSTRUMENTAL ERRORS OF UNIVERSAL AND TRANSIT INSTRUMENTS: DEFINITION AND EFFECT

The goal of the present work is the derivation of the accuracy of astronomic position determination attainable in universal and transit instruments from the collective effect of their separate errors. This is possible only when the individual errors are known as to origin, magnitude, random or systematic character, and effect. It is also necessary to define the instrumental errors unambiguously. To this end, axis errors, setup errors, and stability errors are differentiated in the present section. In the definition of axis errors, Mathias (1961) is referred to, in part. The definitions are made as general as possible. The treatment of the effects of individual errors on direction readings by means of a universal instrument or on the determination of a vertical by means of a transit instrument depends on the definitions of these errors.

3.1 Primary and Secondary Axis Errors

3.1.1 GENERAL DEFINITION OF PRIMARY AND SECONDARY AXIS ERRORS

Axes in the physical sense are bodies that execute a rotation about a rotation axis.* In the ideal case, the direction of the rotation axis remains fixed during a rotation in three-dimensional space. In actuality, the following deviations occur:

*"Axis" denotes the actual physical rotating part of an axis system, while "rotation axis" is a mathematical concept.

- a) Axis and guide* are deformed under the influence of external effects (for example, heat);
- b) the axis and guide are spatially displaced under external influences (for example, force);
- c) the axis changes its spatial position with respect to the guide, because of mechanical shortcomings in the axis or the guide.

The repositionings of the rotation axis named in c) are the genuine errors of the axis system, and are in the future denoted as "secondary axis errors." The changes in axis and guide named in a) and b) are denoted stability errors, and are handled in Section 3.3.

In the following definitions of axis errors, stability errors are assumed non-existent; in the measurement of axis errors (Section 4), the stability errors must accordingly be kept sufficiently small.

Under the above-mentioned condition that no deformations arise, the rotation axis is the straight line relative to which all points of the axis have the same angular velocity. The rotation axis is mathematically described by the vector \vec{w} for the angular velocity. \vec{w} is to be considered a unity vector in the following, since the magnitude of an angular velocity is without meaning. Of further relevance to the problem at hand are only the angular components of the spatial displacements of the rotation axis. The direction of the "instantaneous axis" \vec{w}_i , that is, of the rotation axis during the incremental rotation $d\alpha$, is defined (Fig. 25) in a spatially fixed cartesian coordinate system (x, y, z) by the angles φ_i and ψ_i . φ_i gives the inclination of \vec{w}_i to the (xy) plane, and ψ_i the orientation of the (w_i, z) plane with respect to the x axis. The coordinate system is fixed to the guide of the axis.

Assuming the direction of instantaneous axis $\vec{w}_i (\varphi_i, \psi_i)$ during a rotation α as given, the direction of the "mean axis" $\vec{w}_m (\varphi_m, \psi_m)$ is determined in the following fashion:

The vectors \vec{w}_i and \vec{w}_m form the angle τ_i , which can be computed from the rule of vector addition (Rothe, 1956):

$$\cos \tau_i = \cos \varphi_i \cos \varphi_m \cos (\psi_i - \psi_m) + \sin \varphi_i \sin \varphi_m. \quad (47)$$

The direction of the mean axis is defined according to Janich (1954) and Mathias (1961) by those vectors $\vec{w}_m (\varphi_m, \psi_m)$ for which

$$[\tau\tau] = \text{Minimum}. \quad (48)$$

The direction of the mean axis must, as a rule, match the direction of a given vector $\vec{w}_0 (\varphi_0, \psi_0)$. A deviation of the mean axis from the required direction gives

*By "guide" of an axis is meant the stationary part of an axis system.

For secondary axis errors \vec{w}_{si} is defined as the difference of the vector \vec{w}_i and the vector \vec{w}_m of the mean axis.

$$\vec{w}_{si} = \vec{w}_i - \vec{w}_m. \quad (52)$$

The values of \vec{w}_{si} are obtained from Eqs. (50a,b,c) and (51a,b,c), respectively, if the indices p, m, o are replaced by s, i, and m. Index s denotes the secondary axis error. Giving the (x,y,z) system the orientation described in Section 3.1.2 (+z axis in plumb direction and azimuthal direction of +y axis in the direction of the mean tilt axis), the following special cases for the definition of the theodolite axis errors can be given:

Case a) (Target axis): $\psi_o = 0^\circ$; $\psi_m \approx \psi_i \approx 0^\circ$; $\phi_i \approx \phi_m \approx \phi_o$.

The required direction falls in the (x, z) plane and the instantaneous and mean axes deviate only slightly from the required direction. The vector of the axis error lies in a plane perpendicular to the required direction.

Case b) (Tilt axis): $\phi_o = 0^\circ$; $\psi_m = \psi_o = 90^\circ$; $\phi_i \approx \phi_m \approx 0^\circ$; $\psi_i \approx 90^\circ$.

The required direction falls in the +y axis; the instantaneous and mean axes deviate only slightly from the required direction. The vector of the axis error is parallel to the (x, z) plane, so that Eq. (50b) and Eq. (51c) drop out.

Case c) (Vertical axis): $\phi_o = 90^\circ$; $\phi_m \approx \phi_i \approx 90^\circ$.

The required direction falls on the +z axis and the instantaneous and mean axes deviate only slightly from the required direction; the vector of the axis error is parallel to the (x,y) plane, so that Eq. (50c) and Eq. (51b) drop out.

3.1.2 PRIMARY AXIS ERRORS OF UNIVERSAL AND TRANSIT INSTRUMENTS

The axis system of a universal or transit instrument consists of target axis, tilt axis, and vertical axis, or of target axis and tilt axis, respectively. The "mean vertical axis" is the mean rotation axis of the vertical axis system resulting from a rotation of the alidade, according to Eq.(48). The "mean tilt axis" is the mean rotation axis of the tilt axis system resulting from a rotation of the telescope.

The target axis is an optical-mechanical axis in contrast to the vertical and tilt axes. For this reason one must proceed differently from Section 3.1.1 in the definition of mean and instantaneous target axes. The mean target axis, according to Mathias (1961), is given by the line defined by the image of the center point of the crosshair S upon focusing on infinity, and the point M_m . M_m is the intersection point of the mean tilt axis and the plane defined by the mean vertical axis and S. In an analogous way, the instantaneous target axis is given by the image of S, on focusing at a definite distance, and the point M_i ; M_i is the intersection

point of the instantaneous tilt axis and the plane determined by the instantaneous vertical axis and S.

In a theodolite adjusted without errors, the mean target axis is at right angles to the mean tilt axis, and the mean tilt axis is at right angles to the mean vertical axis, as is known. Furthermore, the instrument should be set up so that the mean vertical axis falls on the plumb direction. This axis system can be represented, according to Figure 26, by an (x, y, z) coordinate system, whose z axis is identical to the plumb direction. The mean vertical axis falls on the +z axis, the mean tilt axis on the +y axis, and the mean target axis lies in the (x, z) plane.

The following primary axis errors are enumerated as in Mathias (1961) for the universal instrument:

- 1) Primary target axis error c (Section 3.1.1, case a):

$$c = \gamma - 90^\circ \quad (49a)$$

γ is the angle between the mean target axis pointing in the target direction and the left side of the mean tilt axis - as seen in the target direction. In Section 3.1.1, γ corresponds to the angle $90^\circ + \psi_m / \cos \phi_m$ if ψ_m and ψ_o in Section 3.1.1 are measured clockwise.

- 2) Primary tilt axis error i (Section 3.1.1, case b):

$$i = 90^\circ - j. \quad (49b)$$

Here j is the angle formed by the left side of the mean tilt axis with the mean vertical axis pointing in the zenith. j corresponds, in Section 3.1.1 to $90^\circ - \tau_p$, where according to Eq. (51a) $\tau_p = \phi_m$.

- 3) Primary vertical axis inclination $\vec{v}(\nu, a_v)$ (Section 3.1.1, case c):

$$\vec{v} = \vec{St}_m - \vec{Z}_o. \quad (49c)$$

\vec{v} is the difference of the vector \vec{St}_m for the mean vertical axis and the vector \vec{Z}_o for the plumb direction, and is given by the magnitude ν and the direction a_v . ν is the angle between the mean vertical axis and the zenith and a_v corresponds to τ_p , which according to Eq. (51a) is equal to $90^\circ - \phi_m$. a_v is the horizontal angle formed by the plane through zenith and mean vertical axis with a starting direction. a_v corresponds to ψ_p , which, according to Eq. (51c), is equal to ψ_m .

The relationship between the magnitudes of the parameters of the general case, and those of the theodolite axis system, is given in Appendix J. Since, in the axis errors, as defined, one deals with small angles, $|\vec{x}_p|$, $|\vec{y}_p|$, $|\vec{z}_p|$ may be replaced

by the sectors of the corresponding angles in Eqs. (50a, b, c). Because of the introduced axis errors c , i , and (ν, a_ν) , the mean target axis goes from position P to position P_c , $P_{c,i}$, and $P_{c,i,\nu}$ (Fig. 26; see p. 65). $P_{c,i,\nu}$ must be turned about the mean vertical axis St_m by the angle $\Delta a_{c,i,\nu}$, whereby the mean target axis again lies in the (x, z) plane. $\Delta a_{c,i,\nu}$ can, according to Mathias (1961), be computed as follows:

$$\Delta a_{c,i,\nu} = c/\sin z_I + i \cotan z_I + \nu \sin(a - a_\nu) \cotan z_I. \quad (53a)$$

Here z_I is the zenith distance in telescope position I and a is the horizontal angle with respect to the exit direction for a_ν in telescope position I. The signs of the primary axis errors as well as the secondary axis errors defined in Section 3.1.3 are chosen so that for positive axis errors the circle reading is improved by the positive amount Δa .

Equation (49a) holds for the transit instrument in regard to its target axis errors. In place of the primary tilt axis error and the primary vertical axis inclination there is the primary tilt axis inclination i_p (Section 3.1.1, case b).

$$i_p = 90^\circ - j. \quad (49d)$$

Here j is the angle formed by the left side of the mean tilt axis with the zenith. Target axis error and tilt axis inclination cause an azimuthal rotation $\Delta a_{c,ip}$ of the instrument vertical determined by the mean target axis.

$$\Delta a_{c,ip} = c/\sin z_I + i_p \cotan z_I. \quad (53b)$$

The primary axis errors can be eliminated, as is known, by way of measurement in two telescope positions and measurement of inclination.

3.1.3 SECONDARY AXIS ERRORS OF UNIVERSAL AND TRANSIT INSTRUMENTS

The precision of a universal and transit instrument depends, in a large degree, on the kind and magnitude of the secondary axis errors which arise. The secondary theodolite axis errors are defined as follows, in accordance with Eq. (52):

- 1) The secondary axis error is equal to the difference \vec{v}_{si} of the vector $\vec{St}_i(\nu_i, a_{\nu_i})$ of the instantaneous vertical axis and the vector $\vec{St}_m(\nu, a_\nu)$ of the mean vertical axis.

$$\vec{v}_{si} = \vec{St}_i - \vec{St}_m. \quad (52a)$$

\vec{v}_g is given by the magnitude v_g and its direction a_{v_g} . v_g is equal to the angle between the instantaneous and mean vertical axes and is denoted the total stagger error of the vertical axis. a_{v_g} is the horizontal angle formed by the plane of the instantaneous and mean vertical axes with a horizontal direction (+x axis), and is denoted the direction of the secondary vertical axis error. v_g and a_{v_g} correspond to the quantities τ and ψ , respectively, in Eqs. (51a) and (51c).

- 2) The secondary tilt axis error is equal to the difference \vec{r}_{si} of the vector \vec{R}_i of the instantaneous tilt axis from the vector \vec{R}_m of the mean tilt axis.

$$\vec{r}_{si} = \vec{R}_i - \vec{R}_m. \quad (52b)$$

Here \vec{r}_{si} is given by the vertical components i_v (vertical stagger errors of the tilt axis) and the azimuthal components i_a (azimuthal stagger errors of the tilt axis). i_v is equal to the vertical and i_a the horizontal angle between the instantaneous and the mean tilt axes.

- 3) Secondary target axis error is equal to the difference \vec{c}_{si} of the vector \vec{Z}_i for the instantaneous target axis from the vector \vec{Z}_m for the mean tilt axis.

$$\vec{c}_{si} = \vec{Z}_i - \vec{Z}_m. \quad (52c)$$

Only the azimuthal component c_a of the secondary target axis error is here of interest; inasmuch as it is constant for a constant target, it can be completely eliminated by taking readings in two telescope positions. Direction changes in the target axis caused by external thermal fluctuations may not, because of the above definition, be denoted secondary axis errors (for discussion, see Section 3.3).

The total axis error is equal to the sum of primary and secondary axis errors. The definition of the secondary tilt axis and target axis errors holds also for the transit instrument. The relationship between individual theodolite axis errors and axis errors, as defined in general in Section 3.1.1, is given in Appendix J. Primary and secondary axis errors are given in cartesian and spherical coordinates, which can be derived by Eqs. (50a) to (51c) for the individual special cases. The effect of the primary and secondary axis errors on the direction measurements is treated in detail in Section 3.4.

3.2 Definition of Measurement Device Errors

Universal and transit instruments are provided with measurement devices by means of which rotations of separate instrument body parts, occasioned by the observation procedure, are measured. Between a rotation of a body part (alidade, telescope, and tilt axis) and the readings of the measurement devices (divided circle,

micrometer, and bubble level), there should be a linear relationship. Denoting an angle setting of a body part by α_1 and corresponding reading of the measurement device by β_1 , the following relationships are obtained:

$$\alpha_1 = a \beta_1 + o \quad (54)$$

or

$$\beta_1 = \alpha_1/a - o/a. \quad (54a)$$

Here a is a conversion factor and o an unknown of the orientation. The measurement devices are, as a rule, associated with errors v_e which cause that the reading value β must be improved by v_{β} in order for the rotation α of the body part to be read without error. Equation (54a) must therefore be modified by the inclusion of $v_{\beta 1}$:

$$\beta_1 + v_{\beta 1} = \alpha_1/a - o/a \quad (55)$$

or

$$v_{\beta 1} = \alpha_1/a - o/a - \beta_1. \quad (55a)$$

Equation (55a) is to be taken as the improvement equation, in which α_1 is given error-free. β_1 is measured and a and o are obtained from the minimization of $[v_{\beta} v_{\beta}]$. o can also be directly eliminated in the observation or evaluation procedure.

The error v_{ei} in the measurement device is obtained from:

$$v_{ei} = a \cdot v_{\beta 1} = \alpha_1 - o - a \beta_1. \quad (55b)$$

If the conversion factor a is qualified by a deficit value a_o , then the total error u_e in the measurement device resulting with a_o is:

$$u_e = \alpha_1 - a_o \beta_1 - o. \quad (55c)$$

The deviation $a-a_o$ and the factor v_e , by the definition of axis errors (Section 3.1.1), can be denoted, respectively, primary and secondary axis errors of the measuring device. The general formulation of errors of the measurement device is now applied to the errors of divided circle, micrometer, and bubble level.

a) Divided Circle Errors

In a divided circle the position of each individual divided circle line is given geometrically. The deviation of a divided circle line from its position is denoted the divided circle line error. In automatic reading, the reading is in error by the

mean of the divided circle line errors of circle settings employed. The mean divided circle line errors of circle settings on a diameter are called diameter errors, and are denoted t . t is, as a rule, not obtained directly, but rather by comparison of a known rotation of the alidade with the rotation read off on the divided circle. If β is the circle reading, that is, the angle between an external reference direction and a reference direction associated with the alidade, and α the angle between an external reference distance and a reference direction referred to the alidade, then according to the sketch below:

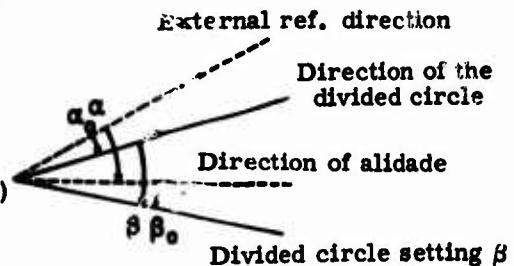
$$\alpha = \beta + (\alpha_0 - \beta_0) = \beta + o.$$

If there occurs a diameter error $t = t(\beta)$ at position β , then

$$\alpha = \beta + t + o. \quad (56)$$

From Eq. (56), which corresponds to Eq. (55c) with $a_0 = 1$, the diameter error t can be computed if o is determined by computation or eliminated in the procedure. The latter occurs, for example in the Heuvelink procedure, in which the externally determined angle $\alpha_2 - \alpha_1$ is compared with the angle $\beta_2 - \beta_1$ read off on the circle:

$$\alpha_2 - \alpha_1 = \beta_2 + t_2 - (\beta_1 + t_1). \quad (56a)$$



b) Micrometer Errors

In the circle reading, the micrometer serves to measure the setting of an index mark - in the present cases the setting of diametric circle division - between the divided circle lines of the main divisions. In using the micrometer, the values β read off on the micrometer scale should be equal to the angular separation α of the index mark from the corresponding divided circle line. In a micrometer functioning with errors, the micrometer reading must be corrected by the total micrometer error m :

$$\alpha = \beta + m. \quad (57)$$

Taking into account that the normalization value a_0 of the conversion factor is equal to 1, and drops out of the orientation unknown, Eq. (57) is equivalent to Eq. (55c). The deviation $a-1$ of the actual conversion factor a from the normalization value 1 is termed a run. Separating the linearly growing error $(a-1) \cdot \beta$ from the total

micrometer error m , one obtains, in accordance with Eq. (55b), the secondary micrometer error m_s

$$m_s = m - (a-1) \cdot \beta = \alpha - a \cdot \beta. \quad (57a)$$

As a rule, the angle setting α of the alidade is compared to the micrometer reading instead of α' , which is not directly measurable. α' is the angle between an external reference direction and a reference direction fixed to the alidade. Since an orientation unknown is included in α' , the secondary micrometer error m_s is obtained from:

$$m_s = \alpha' - a \beta + o. \quad (57b)$$

where a and o are to be obtained by equalization.

c) Bubble Level Errors

In an error-free bubble level there is a linear relationship between the displacement of the bubble and an inclination change of the set line. If α is the inclination of the set line, that is, the angle between the plumb and the effective direction of the set line, and p is the pars value, β the setting of the bubble middle with respect to the bubble level zero point, then:

$$\alpha = p(\beta - \beta_0). \quad (58)$$

The linear relation Eq. (58), which corresponds to Eq. (54), is in actuality not disturbed by curvature errors of the mirrors and thermal effects. Because of the curvature errors, the effective pars value $p_{\beta B} = p(\beta, B)$ depends on the position β of the bubble middle and on the bubble length B . The dependence on β and B can be accounted for by means of a calibration of the level division for different bubble lengths (Tarczy-Hornoch, 1961; Ramsayer, 1967). The read-off value β of the bubble middle is corrected by the factor l_β , which depends on bubble length and position, so that Eq. (58) becomes:

$$\alpha = p_B(\beta + l_\beta - \beta_0). \quad (58a)$$

Equation (58a) is the basis for bubble level investigations according to Wanach (1926), where α and β are measured, p_B determined by equalization and β_0 as well as the additional orientation unknown α_0 are eliminated by reduction. With p_0 as the normalization value of the pars quantity, $p_B - p_0$ is the primary level error; the secondary bubble level error $l_s = p_B \cdot l_\beta$ can be introduced, to supplement Wanach (1926), as a calibration correction of the bubble level readings $p_B \cdot \beta$.

In this case it is, however, more advantageous to relate the calibration corrections to the generally rounded normalization value p_0 of the par quantity, so that Eq. (58a) goes to the formula corresponding to Eq. (55c):

$$l = \alpha - \alpha_0 - p_0 (\beta - \beta_0) = \alpha - p_0 \beta + (p_0 \beta_0 - \alpha_0) = \alpha - p_0 \beta + C. \quad (58b)$$

Here l is the total bubble level error. Equation (58b) is the basis for the evaluation according to "reduced sum lines" (Ramsayer, to be published). An inclination change $\alpha_2 - \alpha_1$ is given, together with Eq. (58b) by:

$$\alpha_2 - \alpha_1 = p_0 \beta_2 + l_2 - (p_0 \beta_1 + l_1). \quad (59)$$

3.3 Stability Errors

Besides the described errors in the axis systems and measurement devices, there arise, in the instruments under discussion, so-called stability errors. They describe the deformations and misalignments of the axes and their guides, defined in Section 3.1.1 under a) and b), which occur through handling the instrument. In the operations requiring manual manipulation (for example, turning the alidade, the tilt axis and telescope), forces are exerted on individual body parts (substructure, tilt axis, telescope) which, because of a certain amount of free play in positioning,* lead to displacements of the body parts. Basically, each operation influences the freely positioned body parts. In practice, however, one can confine oneself to the following cases according to Steinert (1964) and on the basis of the author's own investigations.

a) Substructure Rotation

Let α_{u0} be the horizontal angle between an external reference direction fixed in space (for example, a meridian or the target axis of a collimator) and a reference direction fixed to the substructure (for example, the zero of the divided circle) before a rotation of the alidade; let α_{u1} be the corresponding horizontal angle after the rotation of the alidade. The azimuthal substructure rotation u_a of a universal is determined from:

$$u_a = \alpha_{u1} - \alpha_{u0}. \quad (60)$$

In a transit instrument, "rotation of the alidade" must be replaced by "turning the tilt axis" in the above definition. A vertical substructure tilt u_v is referred to the corresponding vertical directions and is to be defined similarly as Eq. (60).

*In the free equilibrium position, the length changes effected externally in moveable parts are retained.

b) Stability Errors of the Tilt Axis

In a zenith distance change of the telescope, it is required that the mean tilt axis retain its direction in space. However, the forces involved in turning the telescope lead to a displacement of the mean tilt axis, which is termed a wobble error. If α_{w0} is the horizontal angle between the mean tilt axis and an external reference direction fixed in space, before a rotation of the telescope, and α_{wi} the corresponding angle after the rotation, then the azimuthal wobble error w_a is defined as follows:

$$w_a = \alpha_{wi} - \alpha_{w0}. \quad (61)$$

The vertical wobble error w_i is to be determined in accordance with Eq. (61) from vertical reference directions.

According to Section 3.1, the instantaneous tilt axis is directly accessible to observation. Since the direction of the instantaneous axis is furthermore influenced by secondary axis errors for different zenith distances, Eq. (61) cannot be realized by observational techniques. Therefore, the wobble error is characterized by the so-called wobble effect w_e , which is defined as follows: α_{wz} is the horizontal angle between an external reference direction and an arbitrary reference direction fixed on the tilt axis after setting the zenith distance clockwise; α_{wg} is the corresponding angle on setting the same zenith distance counterclockwise. The azimuthal wobble effect w_e is then determined from

$$w_e = \frac{1}{2} (\alpha_{wz} - \alpha_{wg}). \quad (61a)$$

The rotation sense is always viewed from the ocular in instruments with lateral sighting. The definition of vertical wobble effect cannot be made in analogy with Eq. (61a) and is therefore given in a different way in Section 5.2.

Aside from the wobble effect, other operations can affect the stability of the mean tilt axis, for example, clamping and turning the tilt axis. These stability errors can be referred to an arbitrary direction fixed on the tilt axis.

c) Thermal Expansion Bending of the Telescope

Aside from the substructure rotation and wobble error, there was manifested in the instruments under investigation a further important error of the nature of a stability error, arising from the handling of the instrument. In the setting of the telescope, it is nonuniformly heated, so that the direction of the mean target axis changes with time. In instruments with lens telescopes, the direction change is caused essentially by a deflection of the telescope tube. If α_{b0} is the horizontal angle between the mean target axis and an external spatially fixed reference

direction, at time t_0 , and α_{b1} the corresponding angle at time t_1 , then the thermal expansion deflection is obtained from

$$b = \alpha_{b1} - \alpha_{b0}. \quad (62)$$

Here b is a function of time. Values for b obtained in the laboratory can only with reservation be assumed representative for field measurements.

3.4 Influence of Instrumental Errors on Direction Observations

Let the target axis fall on object direction \bar{P} (Fig. 26) for an error-free universal or transit instrument. Let P have the intended direction a determined by the circle, or the intended vertical a determined from the crosshair. Introducing in sequence the primary axis errors, the secondary axis errors and the stability errors, the target axis assumes the position \bar{P}' . The alidade is turned through Δa in targeting on P , so that the circle reading gives the error Δa . The intended direction is additionally affected by errors of measurement devices, reading errors, and the target error. The direction a_I observed with a universal instrument in telescope position I , must be corrected with respect to the intended direction a for the following error influences:*

a) Influence of Primary Axis Errors

The circle reading a_I is corrected for the primary target axis error c , the primary tilt axis error i and the primary vertical axis error (v, a_v) in accordance with Eq. (53a) as follows:

$$a = a_I + c/\sin z_I + i \cdot \cotan z_I + v \sin(a_v - a_I) \cdot \cotan z_I. \quad (63a)$$

where z_I is the zenith distance of the object for telescope position I .

b) Influence of Secondary Axis Errors

The secondary target axis error c_a and the vertical component of the secondary tilt axis error i_v affect the direction a_I in the same way as the primary errors c and i , respectively. The azimuthal component i_a of the secondary tilt axis error manifests itself in full magnitude on the direction. In place of the sum of primary and secondary vertical axis errors, the instantaneous vertical axis inclination (v_I, a_{vI}) is employed, which works analogously as the primary vertical axis inclination. Equation (63a) is to be expanded as follows:

*A summary of the notations for all instrumental and observational errors is found on page

$$a = a_I + i_{a(z_I)} + (c + c_{aI}) / \sin z_I + i + i_{v(z_I)} \cdot \cotan z_I + v_I \sin(a_{vI} - a_I) \cdot \cotan z_I. \quad (63b)$$

c) Influence of Errors of Measurement Devices

Diameter errors t and micrometer errors m affect the circle reading with their full amount. Equation (63b) becomes:

$$a = a_I + \left(t_{(a_I)} + m_{(a_I)} + i_{a(z_I)} \right) + (c + c_{aI}) / \sin z_I + \left(i + i_{v(z_I)} \right) \cdot \cotan z_I + v_I \sin(a_{vI} - a_I) \cdot \cotan z_I. \quad (63c)$$

d) Influence of Stability Errors

The azimuthal substructure rotation u_a and the azimuthal wobble error w_a affect fully the direction. The vertical wobble error w_i acts as a tilt axis error and the thermal expansion deflection b as a target axis error.

$$a = a_I + \left(u_{aI} + t_{(a_I)} + m_{(a_I)} + w_{aI} + i_{a(z_I)} \right) + (c + c_{aI} + b_I) / \sin z_I + \left(i + w_{iI} + i_{v(z_I)} \right) \cdot \cotan z_I + v_I \sin(a_{vI} - a_I) \cdot \cotan z_I. \quad (63d)$$

e) Influence of Observational Errors

Over and above the purely instrumental errors treated in the preceding, there arise observational errors, such as, reading and targeting errors. The sign of an observational error is such that a positive amplifies a positive error in the measuring devices or the target axis. The circle reading error z_a is manifested as a target axis error. The complete error formula then becomes:

$$a = a_I + \left(u_{aI} + a_{bI} + t_{(a_I)} + m_{(a_I)} + w_{aI} + i_{a(z_I)} \right) + (c + c_{aI} + b_I + z_{aI}) / \sin z_I + i + w_{iI} + i_{v(z_I)} \cotan z_I + v_I \sin(a_{vI} - a_I) \cotan z_I. \quad (64a)$$

Denoting O_I (orientation components) the group of errors with coefficient 1, C_I (target axis components) the group of secondary errors with the coefficient $1/\sin z_I$, and J_I (inclination components) the group of secondary errors with coefficient $\cotan z_I$, Eq. (64a) becomes

$$a = a_I + O_I + (c + C_I) / \sin z_I + \left(v_I \sin(a_{vI} - a_I) + i + J_I \right) \cotan z_I. \quad (64b)$$

Likewise, for telescope position II:

$$a = a_{\text{II}} + 180^\circ + \left(u_{a\text{II}} + a_{b\text{II}} + t(a_{\text{II}}) + m(a_{\text{II}}) + w_{a\text{II}} + i_a(z_{\text{II}}) \right) + (c + c_{a\text{II}} + b_{\text{II}} + z_{a\text{II}}) / \sin z_{\text{II}} + \left(i + w_{i\text{II}} + i_v(z_{\text{II}}) \right) \cotan z_{\text{II}} + v_{\text{II}} \sin(a_{v\text{II}} - a_{\text{II}}) \cotan z_{\text{II}}. \quad (65a)$$

If the target does not change position between the two observations (for example, a terrestrial target) or only slightly (for example, stellar target), then one may put $z_{\text{II}} = 360^\circ - z_{\text{I}}$ and $a_{\text{II}} = a_{\text{I}} + 180^\circ$. From Eq. (65a), one then obtains

$$a = a_{\text{I}} + 180^\circ + \left(u_{a\text{II}} + a_{b\text{II}} + t(a_{\text{I}} + 180^\circ) + m(a_{\text{I}}) + w_{a\text{II}} + i_a(360^\circ - z_{\text{I}}) \right) + (c + c_{a\text{II}} + b_{\text{II}} + z_{a\text{II}}) / \sin z_{\text{I}} - \left(i + w_{i\text{II}} + i_v(360^\circ - z_{\text{I}}) \right) \cotan z_{\text{I}} + v_{\text{II}} \sin(a_{v\text{II}} - a_{\text{I}}) \cotan z_{\text{I}}. \quad (65b)$$

With the abbreviations corresponding to Eq. (64b), Eq. (65b) then becomes:

$$a = a_{\text{I}} + 180^\circ + O_{\text{I}} - (c + C_{\text{I}}) / \sin z_{\text{I}} + \left(v_{\text{II}} \sin(a_{v\text{II}} - a_{\text{I}}) - i - J_{\text{II}} \right) \cotan z_{\text{I}}. \quad (65c)$$

On taking the average of telescope positions I and II, the influence of the primary target axis and tilt axis error drops out as is known. Equations (64a) and (65b) then become:

$$a = (a_{\text{I}} + a_{\text{II}} + 180^\circ) / 2 + \frac{1}{2} \left(u_{a\text{I}} + u_{a\text{II}} + a_{b\text{I}} + a_{b\text{II}} + t(a_{\text{I}}) + t(a_{\text{II}} + 180^\circ) + m(a_{\text{I}}) + m(a_{\text{II}}) + w_{a\text{I}} + w_{a\text{II}} + i_a(z_{\text{I}}) + i_a(360^\circ - z_{\text{I}}) \right) + \frac{c_{a\text{I}} - c_{a\text{II}} + b_{\text{I}} - b_{\text{II}} + z_{a\text{I}} - z_{a\text{II}}}{2 \sin z_{\text{I}}} + \frac{w_{i\text{II}} - w_{i\text{I}} + i_v(z_{\text{I}})}{2 \cotan z_{\text{I}}} - \frac{i_v(360^\circ - z_{\text{I}})}{2} + \frac{v_{\text{I}} \sin(a_{v\text{I}} - a_{\text{I}}) + v_{\text{II}} \sin(a_{v\text{II}} - a_{\text{I}})}{2}. \quad (66)$$

In a transit instrument, a_{I} and a_{II} correspond to the azimuth of the instrument verticals in telescope positions I and II. The errors associated with a circle reading drop out; the instantaneous vertical axis inclination must be replaced by the instantaneous tilt axis inclination $i_{p\text{I}}$ and $i_{p\text{II}}$; $i_{p\text{I}}$ and $i_{p\text{II}}$ differ by the influence of a vertical substructure tilt. Equation (66) must accordingly be altered as follows for the transit instrument.

$$a = \frac{1}{2} (a_{\text{I}} + a_{\text{II}} + 180^\circ) + \frac{1}{2} \left(u_{a\text{I}} + u_{a\text{II}} + w_{a\text{I}} + w_{a\text{II}} + i_a(z_{\text{I}}) + i_a(360^\circ - z_{\text{I}}) \right) + \frac{c_{a\text{I}} - c_{a\text{II}} + b_{\text{I}} - b_{\text{II}} + z_{a\text{I}} - z_{a\text{II}}}{2 \sin z_{\text{I}}} + \frac{i_{p\text{I}} + i_{p\text{II}} + w_{i\text{II}} - w_{i\text{I}} + i_v(z_{\text{I}}) - i_v(360^\circ - z_{\text{I}})}{2 \cotan z_{\text{I}}}. \quad (67)$$

Vertical axis inclination and tilt axis inclination are measured with bubble levels in astronomical observations. If n_{I} and n_{II} are the scale values for the bubble centers in telescope positions I and II, n_0 the scale value of the level point, and p the pars value, then, according to Mathias (1961), for components, of the instantaneous

vertical axis inclination in the direction of the tilt axis

$$v_I \sin(a_{vI} - a_I) = v_I^i = p \cdot (n_I - n_0); \quad v_{II} \sin(a_{vII} - a_{II}) = v_{II}^i = p \cdot (-n_{II} + n_0).$$

The mean of the instantaneous vertical axis components in telescope positions I and II is, therefore:

$$\frac{1}{2} (v_I^i + v_{II}^i) = \frac{1}{2} p \cdot (n_I - n_{II}). \quad (68)$$

Taking into account the bubble-level error l as well as the reading error l_a of the bubble center, then,

$$\frac{1}{2} (v_I^i + v_{II}^i) = \frac{p}{2} (n_I + l(n_I) + l_{aI} - (n_{II} + l(n_{II}) + l_{aII})) \quad (68a)$$

If the bubble level readings are given in angle units and the notations of Eqs. (64b) and (65c) employed, then for a universal instrument with an alidade bubble level (DKM 3A) the error-free azimuth a is obtained from

$$a = (a_I + a_{II} + 180^\circ) / 2 + (O_I + O_{II}) / 2 + (C_I - C_{II}) / 2 \sin z_I + (w_{II} - w_{I} + i_{v(z_I)} - i_{v(360^\circ - z_I)} + n_I + l(n_I) + l_{aI} - n_{II} - l(n_{II}) - l_{aII}) \frac{\cotan z_I}{2}. \quad (66a)$$

In a universal instrument with an axial bubble level (T4), the bubble level gives the actual inclination, which is composed of: the component v^i of the instantaneous vertical axis inclination, the primary and secondary tilt axis errors i and i_v as well as the vertical wobble error w_i . The vertical secondary tilt axis error i_v can be split up into a "position component" and an "axis component." The position component gives the error contribution of the axial position and the axis component gives the error contribution of the axis. The setting of the bubble center of an axial bubble level is in addition influenced by the axis errors, which become effective on suspension positions. This error contribution is termed the "bubble-level component" i_L of the stagger error of the tilt axis. Furthermore, the bubble position can be influenced by a vertical wobble error, effective on the suspension positions, the bubble-level wobble error w_{iL} . Turning the tilt axis of a universal or transit instrument causes a bubble position change i_N from the sum of the following errors:

$$i_N = i_v + w_i + i_L + w_{iL}. \quad (69)$$

Here i_N is called the "inclination component" of the stagger error of the tilt axis. Bubble level components and inclination components are not identical to the notations

employed in Eq. (69). If one neglects the contributions of wobble error in Eq. (69), then the bubble level components i_L , which are alone of interest, are obtained as follows:

$$i_L = i_N - i_V. \quad (69a)$$

Here i_L cannot be directly measured, but must be computed as a difference of the measurable quantities i_N and i_V . i_L is thus in principle less precisely determined than i_V for Eq. (66a). For a universal instrument with axial bubble level, therefore, Eq. (66) becomes

$$a = (a_I + a_{II} + 180^\circ) / 2 + (O_I + O_{II}) / 2 + (C_I - C_{II}) / 2 \sin z_I + (w_{iLI} - w_{iLII} + i_L(z_I) - i_L(360^\circ - z_I) + n_I + 1(n_I) + 1 a_I - n_{II} - 1(n_{II}) - 1 a_{II}) \frac{\cotan z_I}{2} \quad (66b)$$

For a transit instrument with axial bubble level, the considerations which led to Eqs. (69) and (69a) hold with equal force, so that Eq. (67) becomes

$$a = (a_I + a_{II} + 180^\circ) / 2 + \frac{1}{2} (u_{aI} + u_{aII} + w_{aI} + w_{aII} + i_a(z_I) + i_a(360^\circ - z_I)) + (c_{aI} - c_{aII} + b_I - b_{II} + z_{aI} - z_{aII}) / 2 \sin z_I + (w_{iLI} - w_{iLII} + i_L(z_I) - i_L(360^\circ - z_I) + n_I + 1(n_I) + 1 a_I - n_{II} - 1(n_{II}) - 1 a_{II}) \frac{\cotan z_I}{2}. \quad (67a)$$

Equations (66a), (66b), and (67a) form the basis for a comparison of accuracy of universal and transit instruments. Next is the task of reporting values of the individual error magnitudes for the different instruments. It is especially necessary to be careful in the separation of random and systematic error contributions, since the effect of systematic errors on a measurement depends strongly on the individual measurement procedure.

To facilitate an overview, the notations for the instrumental errors and observational errors are briefly summarized. In those error quantities which, by their definition, depend on a parameter, the parameter is given in brackets:

u_a	azimuthal component of substructure rotation
a_b	reading error in horizontal circle reading
$t(a)$	diameter error of the horizontal circle
$m(a)$	micrometer error of the horizontal circle micrometer
w_a	azimuthal component of wobble error of the tilt axis
w_i	vertical component of wobble error of the tilt axis
w_{iL}	vertical component of wobble error of the suspension bubble-level

w_e	azimuthal wobble effect
w_n	vertical wobble effect
c	primary target axis error
c_a	azimuthal component of secondary target axis error
b	azimuthal component of deflection of telescope by thermal expansion
z_a	azimuthal component of target error
i	primary tilt axis error
$i_a(z)$	azimuthal component of secondary tilt axis error (azimuthal component of stagger error of tilt axis)
$i_v(z)$	vertical component of secondary tilt axis error
i_n	primary tilt axis inclination
$i_L(z)$	bubble-level component of secondary tilt axis error
$i_N(z)$	inclination component of secondary tilt axis error
v	inclination component of primary vertical axis inclination
$v_i(a)$	inclination component of instantaneous vertical axis inclination
$v_{si}(a)$	inclination component of secondary vertical axis error
a_v	direction of primary vertical axis inclination
$a_{v_i}(a)$	direction of instantaneous vertical axis inclination
$a_{v_{si}}(a)$	direction of secondary vertical axis error
n	scale value of bubble center
n_o	scale value of level point
p	pars value of bubble level
$l(n)$	bubble level error
l_e	reading error of bubble center

4. PROCEDURES FOR THE DETERMINATION OF INSTRUMENTAL ERRORS

For the investigation of the instrumental errors defined in Section 3, we must now develop measurement procedures by means of which the individual errors can be determined independently of each other, with high accuracy ($\pm 0.05''$), and with justifiable expense. Measurement procedures based on the principle of autocollimation broadly fulfill the listed requirements (Section 2). Therefore, the investigations were carried out by means of autocollimation as much as possible and suitable. The applied methods are more closely discussed in Section 4.1. In addition, there is given an evaluation of the autocollimation measurements and their connection with the definition of each error. Several of the instrumental errors are determined by well-known and generally proven methods (Section 4.3). In instrumental investigations it is advisable to give not only the magnitude of errors, but also their origins. Therefore, in Section 4.4, the mathematical procedures for the analysis of measurement results are discussed briefly.

4.1 Measurement Procedures With Autocollimation

In procedures with autocollimation, the measurement mirror is fastened to the part of the instrument body that is to be investigated (Fig. 27). The mirror must be fastened carefully, to avoid falsification of results by motions of the mirror with respect to the body parts. In principle, the instrumental errors to be measured are influenced by the presence of the mirror in magnitude and characteristics. Since the weight of the mirror (150 g) is sufficiently small and possible inhomogeneous loadings of the body parts can be balanced out with care, one can assume that these influences are negligible.



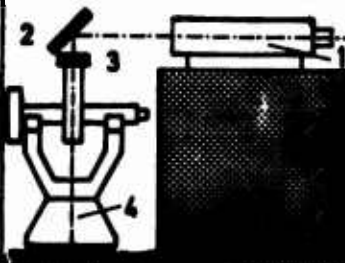
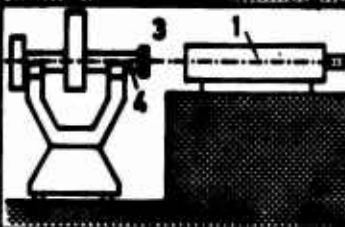
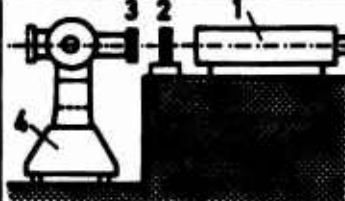
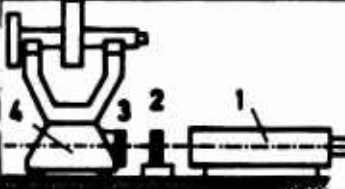
Figure 27. Mounting the Azimuth Component Measurement Mirror on Tilt Axis Investigation (Wild T4)

The mirrors are to be so set up that the crosshair image remains within the measurement range of the autocollimator during the whole measurement process. The necessary preparations, namely setting up and arranging the instruments, mirrors, and autocollimator, represent a substantial portion of the labor in the individual investigations. The investigations should, basically, be so arranged, according to Section 2.7.2.3, that measurement series for which constant external conditions are required, take no more than 30 min. In this time two people can take 60-80 coordinate measurements, including the manipulations of the investigation object.

After these general observations, the investigation of secondary vertical axis errors will be more closely described, as an example for measurement procedures with autocollimation (Table 8a). Measurement mirror 3 is fastened to the telescope of the universal instrument roughly perpendicularly, and arranged with respect to the vertical axis so that the mirror normals run roughly parallel to the rotation axis. The ray path is deflected by 90° at mirror 2. Turning the alidade, the mirror normal traverses the envelope of a cone if secondary vertical axis errors are disregarded, whose axis coincides with the mean vertical axis. If the deflection mirror is set up so that it is inclined to the horizontal by exactly 45° , then the crosshair image describes a circle in the micrometer plane. In multiple reflection (Section 2.3.3) and on deficient arrangement of the deflection mirror for the case of 90° deflection, the scale relationships for the longitudinal and transverse tilting of the azimuth component measurement mirror are different, according to Janich (1954) and Eq. (18). This causes a distortion of the circle into the corresponding affinitive image, that is, into an ellipse. The parameters of the ellipse depend on

the angle between the mirror normals and the mean verticals. The center point of the ellipse can be displaced by a change in the angle between the mean vertical axis and target axis of the autocollimator. If secondary vertical errors are present, the crosshair image describes a curve, whose deviations from the ellipse are a measure for the secondary axis errors.

Table 8. Measurement of Instrumental Errors - Procedures with Autocollimation

Nr	In-strument	Error	Measurement arrangement 1 autocollimator 2 U or T mirror* 3 Measure mirror 4 Object investigated	Autocollima- tion System	Rotation	Fitted Curves
a	T4 DKM3	Secondary vertical axis error v_s, a_{vs}		Simple auto- collimation with 90° deflection vertical axis. Measurement of 2 co- ordinates	Rotation alidade about	Closed ellipse
b	T4 DKM3 AP70	Secondary tilt axis error i_a, i_v		Simple auto- collimation. Measurement of 1 or 2 coordinates	Telescope about tilt axis	Sine curve closed to open circle
c	T4 DKM3	Micrometer error m , reading error a_b		Multiple auto- collimation 0th and 1st order image. Measurement of 1 co- ordinate	Rotation of alidade	Line
d	T4 DKM3 AP70	Underbody rotation u_a, u_i		Multiple auto- collimation 0th and 1st order image. Measurement of 1 co- ordinate	Rotation of alidade. Turning tilt axis	
e	T4 DKM3 AP70	Azimuthal wobble effect w_e	Same as No. b or No. c	Simple auto- col. or mul- tiple auto- collimation	Telescope about tilt axis	
f	T4 DKM3 AP70	Thermal deflection b	Same as No. c	Simple auto- col. or mul- tiple auto- collimation		

*Deflection mirror of semitransparent mirror

The actual measurement consists of a stepwise rotation (say by 20° intervals) of the alidade and the reading of the coordinates of the crosshair image in the fixed coordinate system of the micrometer. The curve given with points is approximated in the sense of Eq. (48) by a fitted ellipse, whose deviations from the individual points serve as a measure of the secondary axis errors. Specifics are given in Section 4.2. The investigation of the vertical axis must precede an investigation of the vertical substructure rotation, since the setting of the measurement mirror is influenced in the same way by axis errors and vertical substructure rotations. It is further to be noted that, according to Section 5.5.2, separate measurement series must be self-consistent without additional supplementary rotations of the alidade.

In a measurement of the secondary tilt axis error (Table 8b), the measurement mirror is fixed to the tilt axis (Fig. 27). The telescope is turned about the tilt axis and the azimuthal and vertical wobble errors must be eliminated as much as possible (see Section 5.2). Disregarding secondary axis errors, the crosshair image describes a circle, which is closed or open according to the range of the possible zenith distance change. On measurement of both coordinates, the data curve is to be fitted by a circle, and on measurement of one coordinate, by a sine curve (Section 4.2). It is advisable to rotate the autocollimator about the longitudinal axis in such a way that the micrometer plane stays vertical or horizontal. The x coordinate then gives the azimuthal or vertical, respectively, and the y coordinate the vertical or azimuthal, respectively, component of the secondary tilt axis error.

Micrometer errors as well as coincidence accuracy are determined by means of Table 8c. The measurement mirror is fastened to the telescope so that the angle α' in Eq. (57b) is formed by the mirror normal and the target axis of the autocollimator. The alidade is rotated by intervals through the measurement range of the micrometer. Each setting of the alidade α' is measured with the autocollimator and read off on the micrometer. a and o are computed by solving with Eq. (57b) as correction equation and m_g as correction in quantities of the observation, β . The deviation of the conversion factor from its normalization value consists of the run of the micrometer and of possibly occurring stability errors of the autocollimation system. The run must therefore be given separate from secondary micrometer errors, by two extreme micrometer settings. The coincidence accuracy is determined by using the fine setting screw of the alidade and measuring each setting of the alidade by means of the autocollimator. A comparison with results of customary determination methods is desirable.

The azimuthal and vertical substructure rotations are determined with measurement arrangement d (Table 8). Angle α_u in Eq. (60) is formed by the mirror normal and the target axis of the autocollimator. Since substructure rotations involve no length measurements, the 11nd-order image was used exclusively for

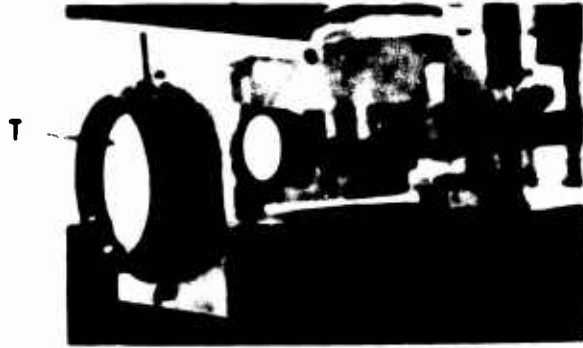


Figure 28. Measuring Substructure Rotation with Multiple Autocollimation (Wild T4)

measurement (Section 2.3.4). The stability of the autocollimator is controlled by the image of zero order. In the measurement arrangement for the Wild T4, the semitransparent mirror T is fastened to the intermediate plate P, in order to simultaneously control the motions of the plate (Fig. 28).

For measurement of azimuthal wobble effect, the measurement mirror can be fastened

either on the telescope (forward or back side) or on the tilt axis (see Table 8c or 8b, respectively). Angle α_w in Eq. (61a) is formed by the mirror normal and the target axis of the autocollimator. For various reasons, given in Section 5.2, the latter observation arrangement is preferable, where the telescope can be advantageously set at zenith distance 0° .

In the measurement of heat deflection of the telescope the measurement mirror is fastened to the objective end of the telescope in instruments with lens telescope (T4, AP70). In Eq. (62), the normal of the measurement mirror replaces the mean target distance. The telescope is set at zenith distance 90° , and the wobble error must be eliminated as much as possible. In instruments with mirror-lens systems (DKM3), the heat deflection is caused more by displacement of the mirror of the telescope system than by a deflection of the tube. Theodolite telescope and autocollimator [effective, according to Eq. (11), as collimator or as measurement telescope] must therefore be brought into reciprocal collimation, so that the mean target axis of the instrument may be observed directly.

Further specifics on the described measurement procedures are given in Section 5.

4.2 Evaluation of Measurements With Autocollimation

Measurements for the investigation of secondary axis errors require a specific evaluation, whose principle is determined by the measurement procedures and the definition of the secondary error. The result of the measurements is a curve of points which is to be approximated, in the sense of Eq. (48) by a definite equation of second degree. The individual points are given by their coordinates and ordered by the parameter u . u is the rotation angle of the axial portion with respect to the guide portion of the system (for example, in the vertical axis investigation, the rotation of the alidade with respect to the substructure). The principle

of the evaluation and corresponding adjustment will be discussed in more detail for the case of the vertical axis investigation.

The (x, y) coordinate system (App. B) determined by the micrometer of the autocollimator, is permitted to coincide with the (x, y) system of Figure 26 (Fig. 29). Let the origin O give the direction of zenith. The mean vertical axis is fixed by coordinates x_m, y_m of point M . The instantaneous vertical axis is given by P_1 for alidade setting u_1 and by P_2 for alidade setting u_2 . The corresponding secondary axis errors \vec{v}_{si} (v_{si}, a_{vsi}) are given by vectors \vec{MP}_i . Because of the divergence of mirror normal and mean vertical axis, disregarding secondary axis errors, the crosshair image describes an ellipse whose center coincides with the mean vertical axis M .

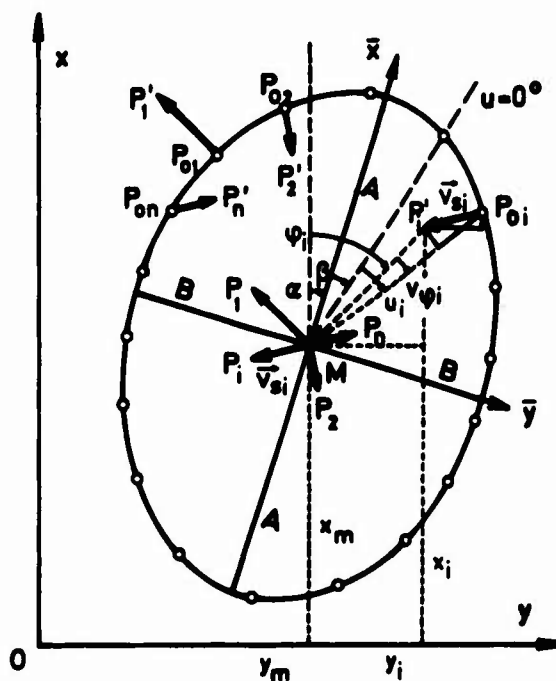


Figure 29. Vertical Axis Investigation - Fitted Ellipse

Let the crosshair image have intended setting P_{01} for alidade setting u_1 , intended setting P_{02} for alidade setting u_2 , etc. In consequence of the secondary vertical axis errors, the crosshair image has the positions P_1', P_2' , etc. $\vec{P}_{01}\vec{P}_1'$ is parallel to \vec{v}_{s1} and $|\vec{P}_{01}\vec{P}_1'|$ is equal to $|\vec{v}_{s1}|$. The fitted ellipse is to be fitted to the points P_i' in such a way as to satisfy the following condition for n alidade settings u_i :

$$\left[|\vec{P}_0\vec{P}_i'|^2 \right] = \left[|\vec{v}_s|^2 \right] = [v_s v_s] = [v_x v_x + v_y v_y] = [v_r v_r + v_t v_t] = \text{Minimum. (70)}$$

Here, v_{xi}, v_{yi} are the x, y components of the total wobble error, v_{ri} and v_{ti} the radial and tangential, respectively, components (see Fig. 29). Let it be pointed out that, in the fitting, the condition $[v_r v_r + v_t v_t] = \text{minimum}$ must not be erroneously replaced by the condition $[v_r v_r] = \text{minimum}$.

The geometric quantities x_m, y_m, A, B, α of the ellipse and the orientation unknown β are entered in the adjustment as unknowns. x_m, y_m are the coordinates of the center of the ellipse, A and B are the major and minor half-axes, and α is the angle of the major half-axis with respect to the x axis. β is the angle between

the major half-axis and the starting direction $u = 0^\circ$ of the alidade setting. In the (\bar{x}, \bar{y}) system, whose \bar{x} and \bar{y} axes coincide with the major and minor axes, respectively, the parametric ellipse equations are as follows:

$$\bar{x}_i = A \cos (u_i + \beta), \quad (71a)$$

$$\bar{y}_i = B \sin (u_i + \beta). \quad (71b)$$

With the measured coordinates x_i, y_i , Eqs. (71a, b) become, by linear transformation:

$$\bar{x}_i = x_i \cos \alpha + y_i \sin \alpha - x_m = A \cos (u_i + \beta), \quad (72a)$$

$$\bar{y}_i = -x_i \sin \alpha + y_i \cos \alpha - y_m = B \sin (u_i + \beta). \quad (72b)$$

Designating approximation values of the unknowns with index 0, and corrections in observations x_i and y_i with v_{xi} and v_{yi} , one obtains from Eqs. (72a, b):

$$\begin{aligned} (x_i + v_{xi}) \cos (\alpha_0 + d\alpha) + (y_i + v_{yi}) \sin (\alpha_0 + d\alpha) - (x_{m0} + dx_m) - (A_0 + dA) \cos (u_i + \beta_0 + d\beta) &= 0, \\ -(x_i + v_{xi}) \sin (\alpha_0 + d\alpha) + (y_i + v_{yi}) \cos (\alpha_0 + d\alpha) - (y_{m0} + dy_m) - (B_0 + dB) \sin (u_i + \beta_0 + d\beta) &= 0. \end{aligned} \quad (73a, b)$$

In the fitting, in accordance with Eq. (70), the square sum $[v_x v_x + v_y v_y]$ is minimized. Equations (73a, b) form the system of the original condition equations for a fitting of limited observations with unknowns. For n measurement settings there are n equation pairs, each with different corrections v_{xi} and v_{yi} . For measurement setting i , the linearized equation pair, with coefficients abbreviated by a and b becomes:

$$\left. \begin{aligned} a_{xi} v_{xi} + a_{yi} v_{yi} + a_{\alpha} d\alpha + a_{\beta} d\beta + a_{xmi} dx_m + a_{Ai} dA_i + w_{ai} &= 0, \\ b_{xi} v_{xi} + b_{yi} v_{yi} + b_{\alpha} d\alpha + b_{\beta} d\beta + b_{ymi} dy_m + b_{Bi} dB_i + w_{bi} &= 0. \end{aligned} \right\}^*_{i=1, 2, \dots, n} \quad (74a)$$

$$\left. \begin{aligned} a_{xi} v_{xi} + a_{yi} v_{yi} + a_{\alpha} d\alpha + a_{\beta} d\beta + a_{xmi} dx_m + a_{Ai} dA_i + w_{ai} &= 0, \\ b_{xi} v_{xi} + b_{yi} v_{yi} + b_{\alpha} d\alpha + b_{\beta} d\beta + b_{ymi} dy_m + b_{Bi} dB_i + w_{bi} &= 0. \end{aligned} \right\}^*_{i=1, 2, \dots, n} \quad (74b)$$

The solution of the homogeneous system of equations resulting from Eqs. (74a, b) gives values for the unknowns and the correlates from which the wanted corrections v_{xi} and v_{yi} are computed in the well-known way. Disregarding the errors of autocollimation, the corrections v_{xi} and v_{yi} can be set equal to v_{xi} and v_{yi} of the secondary vertical axis error:

$$v_{xi} = v_{xi}' \quad (75a)$$

$$v_{yi} = v_{yi}' \quad (75b)$$

* Coefficients a and b are not derived, since the evaluations were done by another method, to be described next.

The rigorous, but computationally burdensome solution from limited observations with unknowns can be replaced with a solution from adjusted observations if polar coordinates r_i and ϕ_i are used in place of the directly measured coordinates x_i and y_i . For a uniform distribution of measurement settings and for n even, the fitted coordinates x_m and y_m of the ellipse center are identical to the coordinates for the center of gravity of the data points. The polar coordinates, referred to the ellipse center, are then:

$$r_i = \sqrt{(x_i - x_m)^2 + (y_i - y_m)^2}, \quad (76a)$$

$$\phi_i = \arctan \frac{y_i - y_m}{x_i - x_m}. \quad (76b)$$

With the approximation values for the unknowns and the corrections v_{ri} and $v_{\phi i}$ of the imaginary observations r_i and ϕ_i , there is obtained from Eqs. (76a, b) and Eqs. (71a, b) the original correction-equation pair.

$$r_i + v_{ri} = \sqrt{(A_0 + dA)^2 \cos^2(u_i + \beta_0 + d\beta) + (\beta_0 + dB)^2 \sin^2(u_i + \beta_0 + d\beta)}, \quad (77a)$$

$$\phi_i + v_{\phi i} = \alpha_0 + d\alpha + \beta_0 + d\beta + u_i. \quad (77b)$$

The tangential components v_{ti} are computed from $v_{\phi i}$ and the associated ellipse half diameter r_{oi} :

$$v_{ti} = r_{oi} v_{\phi i} = \sqrt{(A_0 + dA)^2 \cos^2(u_i + \beta_0 + d\beta) + (\beta_0 + dB)^2 \sin^2(u_i + \beta_0 + d\beta)} \cdot (\alpha_0 + d\alpha + \beta_0 + d\beta + u_i - \phi_i). \quad (77c)$$

Equations (77a) and (77c) are to be linearized and are the basis of the solution by adjusted observations, in which, in accordance with Eq. (70) the square sum $[v_r v_r + v_t v_t]$ is minimized. The linearized correction equations are given in Appendix K. The radial and tangential components v_{ri} and v_{ti} of the stagger error are obtained, with the observations on Eqs. (75a, b) from:

$$v_{ri} = v_{ri}, \quad (78a)$$

$$v_{ti} = v_{ti}. \quad (78b)$$

The approximation values for the unknowns are computed from three coordinate pairs by means of the second-degree equation for the ellipse. Evaluation of means of adjusted observations has been used in the present investigations, and was programmed in the formula language ALGOL. The computations were carried out on the computer TR4 of the Recheninstitut der TH Stuttgart.

For analysis of wobble errors it is necessary to relate an arbitrary number of measurement settings (for example, two whole rotations), to be determined for the individual case, to an adjustment by the same number of unknowns (see Section 5.5.2). For the determination of unknowns, the measurement values are obtained that correspond to the same alidade setting. With the computed unknowns, the corrections of those observations are given which were not obtained directly. The wobble errors can be expressed in any of the forms given in Eq. (70). The program is set up so that vertical axis investigations by the principle of multiple reflection (Section 2.3.3) can also be evaluated with arbitrary values for δ_0 .

The evaluation of investigations of tilt axis by simultaneous measurements of x_i and y_i is done by means of a fitted circle. The formulas for the fitting by adjusted observations are derived in detail in Mathias (1961), so that an assessment is here given only for the sake of completeness. The fitted circle corresponds to the fitted ellipse treated above if the major and minor half axes A and B are replaced by the radius R; also the orientation α of the ellipse with respect to the coordinate system drops out. The remaining unknowns, x_m , y_m , R, and β and the observations x_i and y_i are related by the relationships:

$$x_i = x_m + R \cos(u_i + \beta), \quad (79a)$$

$$y_i = y_m + R \sin(u_i + \beta). \quad (79b)$$

Denoting again the approximation x values of the unknowns with the index 0 and the corrections of the observations with v_{xi} and v_{yi} , the original correction equations are:

$$x_i + v_{xi} = x_{m0} + dx_m + (R_0 + dR) \cos(u_i + \beta_0 + d\beta), \quad (80a)$$

$$y_i + v_{yi} = y_{m0} + dy_m + (R_0 + dR) \sin(u_i + \beta_0 + d\beta). \quad (80b)$$

The linearization of Eqs. (80a) and (80b) produces the transformed correction equations:

$$v_{xi} = dx_m - R_0 \sin(u_i + \beta_0) d\beta + \cos(u_i + \beta_0) dR + (x_{m0} + R_0 \cos(u_i + \beta_0) - x_i), \quad (81a)$$

$$v_{yi} = dy_m + R_0 \cos(u_i + \beta_0) d\beta + \sin(u_i + \beta_0) dR + (y_{m0} + R_0 \sin(u_i + \beta_0) - y_i). \quad (81b)$$

With uniform distribution of the test points over the whole circle, x_m and y_m are identical to the center-of-mass-coordinates of the aggregates of points. In this case, the correctional equations are considerably simplified if one introduces polar coordinates.

If in a horizontal axis study only one coordinate is measured, as is the case in most of the studies described here and in Section 5.4, then Eq. (81a) or Eq. (81b) is the correction of an equilibrant sine curve. R is the amplitude, β is the phase displacement, and x_m is an addition constant. The evaluation of horizontal axis studies with one coordinate has also been programmed for ALGOL. It should also be mentioned in this connection, that in horizontal axis studies that are based exclusively on one-coordinate measurements, elliptic deformation of the axis cannot be detected.

4.3 Measurement Methods Without Autocollimation

For the study of divided circle and level error, methods which have already been proved useful in practice were employed. The diameter errors were determined by the Heuvelink method, in which the rules and experience derived from Jochmann (1956, 1957), Wermann (1957), and Forstner (1964) were taken into consideration. Level error at present can best be determined by an attached level tester. In principle, this could have been done with autocollimation as in Section 4.1; however, the increased expenditure necessary in the level studies would not be profitable.

In the Heuvelink method, a constant test angle $\alpha_2 - \alpha_1$ serves as a standard for the angles $\beta_{2i} - \beta_{1i}$ observed at the β_{2i} and β_{1i} points on the divided circle. According to Eq. (56a), the difference corrections d_i turn out to be:

$$d_i = t_{2i} - t_{1i} = (\alpha_2 - \alpha_1) - (\beta_{2i} - \beta_{1i}) . \quad (82)$$

If one plots the d_i values as a function of the circle points β_{1i} , one obtains the difference curve. From the systematic part of the distribution curve, which is given according to Eq. (88) through a Fourier series, the function of the systematic diameter corrections t_{si} can be calculated according to the formulas given in Wermann (1957). Since the systematic divided circle error is due above all to the errors of the dividing machine (Jochmann, 1956, 1957), they occur with quite definite periods which depend on the division process. The widespread restriction of the Fourier series to the first three terms is therefore without reason. The accuracy of the amplitude and phase displacement of the systematic diameter corrections depends, according to Wermann (1957), on the size of the test angle. In preliminary tests the phases that occur must be determined by means of the difference curve, and the optimal test angle is determined according to Forstner (1964). In the divided circle experiments performed here for the Wild T4, the test angle determined in this way is 33° . The test angle is formed from two rigidly supported collimators.



Figure 30. Measurement of Level Error (Level in operation)

The level investigations are conducted with the fine level tester No. 39407 of the Freiberg Precision Mechanics firm; it is used according to Wanach's method and the reduced sum line method (Ramsayer, to be published). The level tester shows a maximum error of $0.08''$ according to the author's experiments in a $50''$ to $100''$ range, and this error is designated as errorless in relation to level error. The levels were tested with a special device in the operation (Fig. 30). The maximum bubble variation can be kept confined to under 0.5 pars for 2-3 hours by means of a special heat insulation. Further details are given in Section 5.7.

4.4 Analysis of Instrumental Error

The development of geodetic instruments in recent years has contributed greatly to the fact that random error in precision measurement is disappearing. Systematic measurement error which includes a large part of systematic instrument error has been dealt with in the same way in the foreground of theoretical error consideration (Bohm, 1967). Theoretical error considerations in which we shall include both random and systematic error, will be treated statistically. The requirement in instrumental investigations for wider application of statistical method has been properly stated in the International Conference on Geodetic Measuring Technique and Instrument Problems (Budapest, 1966). The use of statistics, on the other hand, should not lead to neglect of measurement methods which are used in instrumental error experiments. Specially adapted measurement procedures will always be more promising for experimental aims than procedures in which individual error influences first must be determined by extensive statistical experiments.

In the present study the use of statistics is confined above to analysis of systematic error. Some degree of error can be given by the type and extent of instrumental error.

4.4.1 EVIDENCE OF SYSTEMATIC ERROR

A true error ϵ_{ij} can be divided into random components Δ_{ij} and systematic components c_{ij} (Bohm, 1967).

$$\epsilon_{ij} = \Delta_{ij} + c_{ij} \quad (83)$$

c_{ij} can occur as a constant, unidirectional, or variable systematic error. For a constant systematic error (for example, primary axis error) the sign and the

magnitude are constant; unidirectional systematic error (for example, stability error) has the same sign, but varying magnitudes; in variable systematic error (for example, secondary axis error) both sign and magnitude change according to a fixed principle usually first determined by experiment.

Analysis of systematic error proceeds in the following way. For short series of unidirectional or variable systematic error variance analysis is used. The ϵ_{ij} error is determined n_i -times within a group, that is, under constant conditions. The mean value $\bar{\epsilon}_i$ of the i -group is, with sufficiently large n_i values, equal to the mean value \bar{c}_i of the group's systematic components:

$$\bar{\epsilon}_i = \frac{\sum_{j=1}^{n_i} \epsilon_{ij}}{n_i} = \frac{\sum_{j=1}^{n_i} \Delta_{ij}}{n_i} + \frac{\sum_{j=1}^{n_i} c_{ij}}{n_i} \approx \frac{\sum_{j=1}^{n_i} c_{ij}}{n_i} = \bar{c}_i \quad (84)$$

Conditions are now varied for the parameter in which a relationship with systematic error \bar{c}_i is supposed and the measured ϵ_{ij} is subdivided into corresponding groups; the group average $\bar{\epsilon}_i$ is further calculated according to Flugge (1962) and the distribution within the group is compared with the distribution of the group mean. Probability can be expressed by means of known student tests if the deviation of the mean from the theoretical value is random or is actually the systematic error $\bar{c}_i = \bar{\epsilon}_i$. The distribution within the group is used to calculate the reproducibility accuracy m_{Δ} :

$$m_{\Delta} = \pm \frac{\sqrt{[(\epsilon_{ij} - \bar{c}_i)^2]_{ij}}}{N-K} \quad \begin{array}{l} N = \text{total error} \\ K = \text{number of groups} \end{array} \quad (85)$$

The reproducibility accuracy indicates that a systematic error \bar{c}_i can be reproduced with constant proportions with some accuracy.

The group series, that is, the distribution of error is completely random in variance analysis or in tests of normal distribution (Van der Waerden, 1965). Thus, the systematic error is demonstrated not only by instrumental experiments, but also should be tested as to its functional dependence on the corresponding parameters; group or single error values are arranged according to increasing parametric values. The system should be arranged in a suitable manner for analysis. Group tests are used which do not demonstrate the systematic error as being reproducible. The group test operation is briefly illustrated by Helmert's criterion. In a series of K group means $\bar{\epsilon}_1, \bar{\epsilon}_2, \dots, \bar{\epsilon}_K$ or K single errors $\epsilon_{1j}, \epsilon_{2j}, \dots, \epsilon_{Kj}$ the number of sign series f and the number of sign changes w (2 ϵ values next to each other in series have equal or unequal signs) is determined and collated as follows:

$$f-w = 0 \pm \sqrt{K-1}. \quad (86a)$$

The f - w difference from the theoretical value 0 is exceeded by an amount which is larger than the mean error $\pm \sqrt{K-1}$; thus, the ϵ distribution is normal only with a probability of 31.7%. If the strength of the test evidence is increased by 5% or 1% according to the normal significance index α in statistics, then a corresponding r_s multiple must be determined as a permissible limit instead of the simple mean error in Eq. (86a)

Along with Helmert's criterion, the criteria of Gleisberg, Kermack-MacKendrick, and Goekmen and also Abbe's modified criterion (Wolf, 1952; Wermann, 1958) are discussed in the error analysis in Section 5. These criteria are introduced in a way similar to Eq. (86a): a_k is the actual criterion calculated on the basis of the error distribution that is present; b_k is the theoretical value for normal distribution; and s_k is the associated mean error. Thus:

$$a_k = b_k \pm r_s \cdot s_k \quad (86)$$

The r_k value

$$r_k = \frac{a_k - b_k}{s_k} \quad (87)$$

can be understood as a test quantity in a statistical sense which is equal to the r_s interval (Van der Waerden, 1965). r_k has a theoretical value of 0. The mean value r of the r_k test quantities determined for the known criteria is uncertain by about 15% according to present observation. Therefore, we have a term that acts differently in the individual tests of a given system. Thus, the uncertainty of the test is to be considered significant in the interval determination for the various statistical significances S ($S = 1 - \alpha$). In the experiments in Section 5, the following values for r_s were used for statistical certainties of 90%, 95%, and 99%.

Distribution	α	r_s	Test	Notation	Abb.*
			$0 < r < 1.5$	Not significant	NS
90%	10%	1.5	$1.5 < r < 1.8$	Sufficiently significant**	SS
95%	5%	1.8	$1.8 < r < 2.3$	Significant	S
99%	1%	2.3	$2.3 < r$	Highly significant	HS

For example, if an r -value lies in the interval between 1.8 and 2.3, then the probability that the distribution present is normal is less than 5%. Therefore, the system is calculated as significant (S).

*According to a proposition in Reissmann (1966).

**The abbreviations NS, SS, S, and HS are used here and later as symbols for statistical significance of the tests.

Array tests were used in Section 5 for testing sufficiently long ($K > 15$) error series which were parametrically systematic. As a rule, the reproducibility m_{Δ} is also compared to the mean group value, but the error is reproducible. The wobble error of the vertical axis is basically not reproducible in the Wild T4 so that the system can be tested only by means of array tests.

4.4.2 ANALYSIS OF SYSTEMATIC ERRORS

In an error series ϵ_i which shows sufficiently significant systematization according to the criteria of Section 4.4.1, the systematic components c_i must be further separated and analyzed. The mathematical function by which the systematic error series can be expressed is determined only according to pertinent physical data.

For this purpose, thorough theoretical studies are frequently necessary, by means of which the operation of the individual error sources on the systematic error can be explained and mathematically formulated. In the present studies, periodic systematic error is of primary interest; this can be determined with the following Fourier series expression:

$$\epsilon_i = \Delta_i + c_i = \Delta_i + a_0 + a_1 \sin(n_1 x_i + \phi_1) + a_2 \sin(n_2 x_i + \phi_2) + \dots + a_r \sin(n_r x_i + \phi_r) + \dots \quad (88)$$

where

a_0 is the addition constant, a_r is the amplitude, n_r is the period, x_i is a parameter, and ϕ_r is phase displacement.

Equation (88) is to be understood as an error equation in which ϵ_i is the observation, Δ_i the correction, and a_r and ϕ_r are unknowns. The periods n_r are assumed hypothetically as a rule on the basis of the above-mentioned theoretical studies. If the periods are numerically proportional to each other, the normal equation system breaks down and the unknowns can be calculated independently of each other. In the study of secondary vertical axis error of the Wild T4, this supposition holds true only approximately (Section 5.5.2). In this case, however, a strong equilibrium would be given up and the unknowns ascertained by an approximation process which relies on normal Fourier analysis. The separation of random and systematic error components is estimated:

(1) by the distribution of residual error λ_i on the basis of the random criteria cited in Section 4.4.1, and

(2) by the average unit of weight error m_0 , according to the observations of Wolf (1952),

$$m_0 = \pm \sqrt{\frac{[\lambda\lambda]}{n-u}}$$

n = number of support points
 u = number of unknowns

(3) by the particular relation of unknown values (amplitudes) to their mean error.

The hypothesis on which the advance of the periods depends is confirmed if the separation of the random and systematic error components according to the above points of view can be considered as effected. In this case the random components Δ_1 will be assumed equal to the corresponding residual error λ_1 . The approximation of the error series by the ascertained mathematical function is characterized by m_q , which according to Wermann (1957) can be calculated to:

$$m_q = \pm \sqrt{\frac{[\lambda\lambda]}{n}}. \quad (89)$$

In divided circle studies the periods are not at first certain. Therefore, the analysis is best carried out with a large number of terms, and one decides according to the above considerations which terms to take as real. It has been shown that because of the short-period divided circle error a satisfactory separation of random and systematic components is difficult.

Besides the periodic errors, there occur in the present studies partial systematic errors which are obtained by the addition of exponential series. The residual error will be studied again in regard to distribution. Fourier analysis, compensating polynomial,* and the array tests applied in Section 4.4.1 were programmed for ALGOL, as a result of which the array tests for any given point of time in the analysis can be called up as a subprogram.

4.4.3 CRITERIA FOR CHARACTERIZATION OF INSTRUMENTAL ERRORS

The adequate separation of random and systematic components of the individual instrumental error ϵ_1 is indispensable if the error is to be explained. In many cases, for example, in series studies, there exists only the problem of ascertaining the quantity of the various instrumental errors, in order to estimate the worth of the instrument. Then, splitting up the individual error can be eliminated, and Δ_1 , c_1 , and ϵ_1 , can be characterized by means of the following error quantities:

$$\bar{m} = \sqrt{\frac{[\epsilon\epsilon]}{n}} \quad \text{the root mean square of total error or mean total error,} \quad (90a)$$

$$\bar{m}_\Delta = \sqrt{\frac{[\Delta\Delta]}{n}} \quad \text{mean incidental error or reproducibility accuracy,} \quad (90b)$$

$$\bar{m}_c = \sqrt{\frac{[cc]}{n}} \quad \text{root mean square of the systematic error or mean systematic error.} \quad (90c)$$

According to Bohm (1967), the following applies:

$$\bar{m}^2 = \bar{m}_\Delta^2 + \bar{m}_c^2. \quad (91)$$

*The program for the compensating polynomial was gratefully obtained from Dr. W. Lorch.

\bar{m} is calculated directly from the individually measured errors ϵ_i ; \bar{m}_Δ is to be ascertained for reproducible instrumental errors from repeat measurements in the sense of Section 4.4.1; the mean systematic error can be estimated according to Eq. (91):

$$\bar{m}_c^2 = \bar{m}^2 - \bar{m}_\Delta^2 . \quad (91a)$$

\bar{m}_c is computed directly from the individual systematic components c_i when these - as is the case in the present studies - have been determined according to Section 4.4.2.

A definite instrumental error - apart from the mean total error (90a) or the average total error - is characterized by the extreme value ϵ_{\max} of ϵ_i and the "mean increase" m_δ . If $x_{i+1} - x_i$ is the difference between two consecutive parameter values and $\epsilon_{i+1} - \epsilon_i$ is the difference of the accompanying error values, then, with $\delta_i = (\epsilon_{i+1} - \epsilon_i) / (x_{i+1} - x_i)$ the mean increase \bar{m}_δ is characterized by:

$$m_\delta = \sqrt{\frac{[\delta_i^2]}{n}} . \quad i = 1, 2, \dots, n-1 \quad (92)$$

A comparison between \bar{m} and \bar{m}_δ points - as long as \bar{m} and \bar{m}_δ differ by more than 15 per cent - according to present experience toward an eventual systematization, without referring to (91a) or the criteria in Section 4.4.1. For

$$\bar{m}_\delta > \bar{m} \quad (93)$$

the distribution of ϵ_i is random; in other cases it is not random.

5. EXPERIMENTAL RESULTS FOR THE UNIVERSAL INSTRUMENTS WILD T4, KERN DKM3, AND THE TRANSIT INSTRUMENT ASKANIA AP70

From instruments used in precision astronomical measurements the following were selected:

- (1) the universal instrument Wild T4 No. 48978 (Appendix L).
- (2) the Kern theodolite DKM3 No. 78233 (Appendix L), and
- (3) the Askania transit AP70 No. 580644 (Appendix L).

Besides size and applicability, the Wild T4 and the Kern DKM3 differ essentially in their construction principles so that statements concerning the advantages and disadvantages of the different principles are to be expected. It can be inferred from Section 4 that the secondary target axis error c_a and the target sighting error z_a are not involved in the investigation; both error quantities must be considered in relation to the observation and recording method, for which reason they

will not be considered in the present work. Plausible values for c_a and z_a were taken from the literature. The series of individual tests were made in such a way that instrumental errors (for example, stability error), which basically influence the measurement of other instrumental errors (secondary errors) (for example, secondary axis error) were measured first. Basically, in the present section only those instrumental errors are dealt with in detail which, because of their magnitude, noticeably influence the instrument's accuracy. An exception to this is substructure rotation, since in the literature, while there is thorough discussion of the operation and elimination of substructure rotation, there is no detailed information concerning its cause and magnitude. The following data were gathered principally by the Wild T4 and partly by the transit instrument.

5.1 Azimuthal and Vertical Substructure Rotation

In determining - up to the present time - the accuracy of universal and transit instruments, rigidity of the substructure has played an essential role. In general, the transit instrument displays better rigidity than the universal instrument. Moreover, since the study of the other instrumental errors will be influenced by motion of the instrument substructure, it must next be established whether and to what extent substructure rotation occurs in the various instruments. With this aim, the following were measured:

- (1) azimuthal substructure rotation u_a during a large number of unidirected operations, and
- (2) azimuthal and vertical substructure rotation u_a and u_i between individual operations, and
- (3) azimuthal substructure rotation over long periods of observation time.

In addition to the operations indicated by the definition of u_a (rotation of the alidade, change in the horizontal axis) further operations were carried out on the instrument (rotation of the telescope, manipulation of the level and micrometer). In the Wild T4, the azimuthal substructure rotation resulting from such operations is under $0.02''$. The tests were carried out with the Wild T4 with high and low placement of mounting screws and with the transit, with and without the substructure for the divided circle.

Results:

for (1): The measurement of the substructure position α_u for each ten alidade revolutions produces the curve shown in Figure 31 in clockwise and counterclockwise directions. The dependence of the substructure rotation on the rotational direction of the alidade is, according to the random error criteria in Section 4.1, highly significant.

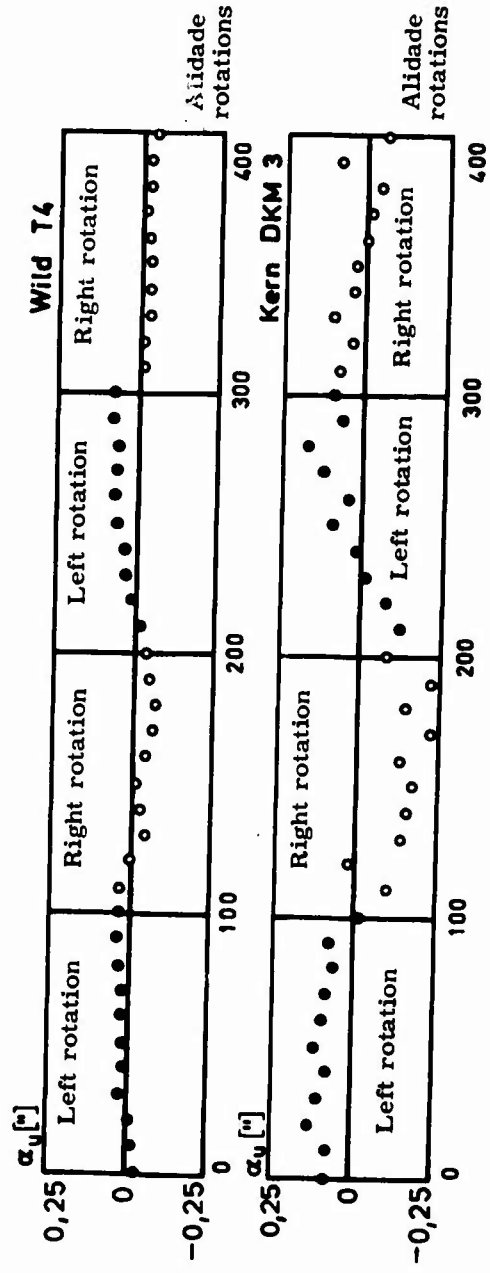


Figure 31. Azimuthal Substructure Rotation During a Large Number of Revolutions

As can be seen from Figure 31, the substructure rotation dies out from 30-40 unidirected alidade revolutions; this phenomenon is due, supposedly, to an elastic deformation of the mounting screw setup. The root mean square of u_a for the Wild T4 (high mounting screw placement) is $0.04''$ and for the DKM 3, $0.09''$; with low mounting screw placement, the maximum substructure rotation for the Wild T4 is under $0.03''$. The multiple rotation of the alidade recommended in Danilow (1957) and Bahnert (1963) before beginning measurements is only effective for a large number of revolutions.

for (2): The measurement of the substructure position α_u is produced with the universal instrument after each full revolution of the alidade with continuous alternation of the rotational direction as well as after a rotation of 30° with continuous identical direction of rotation. The substructure rotation u_a is calculated as the difference between the substructure position before and after a unidirected rotation. u_a for the transit instrument is found to be analogous to this for the five different operations given in Appendix M. Variance analysis of the data presented in Appendix M shows that for measurements without the substructure the variation within the groups is larger than the variance of the groups and that for measurements with the substructure, the systematization is quite significant. The groups, in regard to the small absolute values of u_a are taken together so that "level oscillation" or "pickup" is not involved. The total results are given in Table 9. The instruments display a highly significant substructure rotation of $0.03 - 0.05''$ per revolution or per turn of the telescope seat. The accuracy of reproducibility m_Δ is $\pm 0.02''$ (T4), $\pm 0.05''$ (AP70 without substructure) and ± 0.1 (DKM3 and AP70 with substructure). With a small angle of rotation no systematization is established. The cause of the observed substructure rotation must lie primarily in the free motion and in the elastic deformation of the mounting screw setup. The results confirm the rule that during a measuring process the rotational direction of the alidade should not change.

for (3): From the total change in substructure position which resulted from the tests for (1) and (2) above, the following statements concerning rigidity of the substructure are derived. The stability of the measurement system, including the stability of plate P (Fig. 28) can be estimated according to Eq. (21b) from the shift a_o of the zero-order image as follows: a tilt β_t of the semitransparent reflector falsifies the tilt of the measuring reflector β_a devised from the second-order image shift a_{II} by $\beta_t/2$. The image shift a_o can serve as true error (compared to the theoretical value 0), from which the mean error m_o of the autocollimation measurement (external accuracy) can be derived. m_o and the maximum true error of the measurement - related to the units of time 30 min - are given in Table 10. The root mean square error of m_o is $\pm 0.035''$ and is taken as the mean error of a single measurement of substructure rotation $u_a/30$ min; the mean $u_a/30$ min given in Table 10 vary, according to the student test, significantly from the theoretical value 0, that is, the measured substructure rotations are real.

Table 9. Azimuthal Substructure Rotation Per Alidade Revolution or Shift

Instrument	Notes on setup	Azimuthal Substructure Rotation u_a per Revolution												
		Alidade revolution 360°			Alidade revolution 30°			Shift at zenith distance						
		K*	Mean u_a	m Δ	K	Mean u_a	m Δ	K	Mean u_a	m Δ				
T4	Mounting screw height 25mm (h) 2mm (l)	180	-0.03"	±0.02"	120	0.00"	±0.02"	-	-	-	-	-	-	
DKM3	-	25	-0.05"	±0.10"	46	-0.01"	±0.05"	-	-	-	-	-	-	
AP70	Divided circle substructure with without	-	-	-	-	-	-	93	-0.03"	-	79	-0.01"	±0.09"	±0.05"

* Number of measurements

** Reproducibility

Table 10. Azimuthal Substructure Rotation Over a Long Observation Time

Instrument	Notes on setup	Total time of Observations	Autocollimation Measurement error/30 min.		Azimuthal Substructure Rotation/30 min.		Systematic test for u_a /30 min.
			Average mean m_o	Maxim. error	Mean	Maximum	
T4	Mounting screw h l	7.6 hr 1.8 hr	±0.029"	0.062"	0.031"	0.081"	HS
DKM3	-	2.0 hr	±0.015"	0.019"	0.031"	0.056"	S
AP70	Support with without	6.7 hr 5.5 hr	-	-	0.074"	0.13"	S
			±0.050"	0.060"	0.16"	0.47"	HS
			±0.039"	0.060"	0.088"	0.16"	HS

The best rigidity is displayed by the Wild T4 with a mean deviation of $0.03''/30$ min, while with the transit instrument with the substructure, mean deviations of $0.15''/30$ min were measured. This result - contradicted by the prevailing concept - can be accepted as plausible, since in modern vertical axis systems, the rotation of the alidade produces very little friction, although in the shift process mechanical vibrations are unavoidable. The azimuthal rigidity of the Wild T4 does not seem to be in need of any correction whatever.

The vertical substructure rotation u_1 is of interest only in connection with the study of secondary vertical axis error. The studies can be limited, therefore, to the behavior of the substructure during a single revolution of the alidade. With the Wild T4 motion of the substructure is dependent on the position of the alidade, which entails a vertical axis slope with constant inclination ν and a direction a_ν which varies continuously with the position of the alidade. By means of the measurement procedure the effective component in the direction of the mirror normals is found, which has a sinusoidal curve and is reproducible within $\pm 0.03''$. The mean of six measurement series (revolutions) can be approximated by means of a compensating sinusoidal curve with an amplitude of $0.16''$ and mean approximation of $\pm 0.014''$ (Fig. 32).

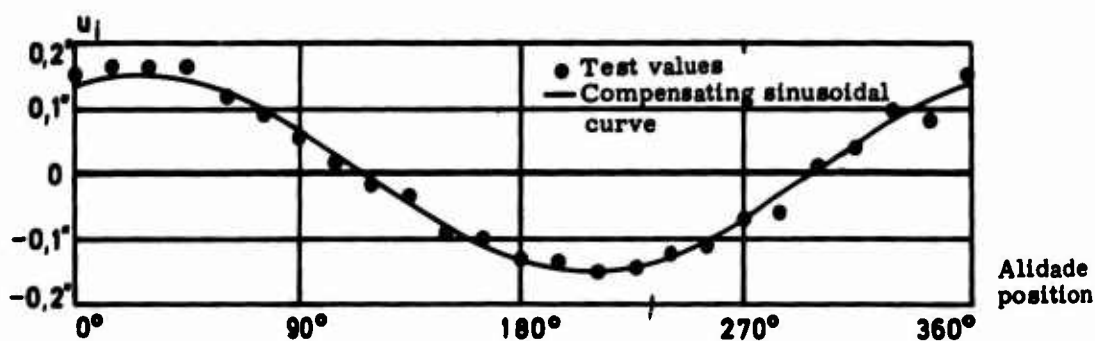


Figure 32. Vertical Substructure Rotation During a Full Revolution (Wild T4)

This phenomenon is limited by an eccentric position of the alidade center of mass and by the vertical play of the mounting screws; it is without effect in the study of secondary vertical axis error. With level "pickup", slope deviations from the stated amplitude can be observed.

The data presented in Figure 32 should at the same time be viewed as confirmation of the high degree of accuracy of the autocollimator indicated in Section 2.

With the DKM3 there occur random inclination variations of the substructure with a root mean square of $\pm 0.09''$.

5.2 Azimuthal and Vertical Roll Effect

In contrast to the secondary horizontal axis errors, the stability errors of the horizontal axis have, at times past, attracted the attention of users. According to Steinert (1964), an azimuthal "roll effect" in transits ΔK was defined as follows: if a_{IZ} and a_{IG} are azimuths of the target axis in telescope position I with clockwise and counterclockwise setting of the sight and a_{IIZ} and a_{IIG} the corresponding azimuth in telescope position II turns out to be:

$$\Delta K = \frac{a_{IZ} + a_{IIZ}}{2} - \frac{a_{IG} + a_{IIG}}{2}. \quad (94)$$

The roll effect of the transits under discussion was first studied by a method corresponding to Eq. (94) (Method 1).

To this end, the measuring mirror is attached to the objective end of the telescope and rotated clockwise and counterclockwise in positions I and II at the zenith distance of 90° and then the position obtained by the mirror normals a is measured by the autocollimator. The roll effect is then calculated according to Eq. (94). In further cases, if one departs from this method on the basis of considerations given below, the measurements are carried out according to definition 3 (Eq. 61a):

- (1) For determination of the roll effect defined according to Eq. (94), circle readings for a universal instrument must be consulted;
- (2) The magnitude of ΔK , according to Stephani (1965, unpublished), depends on the accurate series of sight corrections and shifts;
- (3) Causes of roll effect and heat deflection of the telescope are unavoidable.

For the measurement of roll effect according to Eq. (61a), the measuring mirror can be attached to the heavy end of the telescope (Method 2) or directly to the tilt axis (Method 3). Method 3 is preferred over Method 2 for the following theoretical and practical reasons:

- (1) The roll error or roll effect is a tilt axis system error and should therefore be measured to the extent possible against the tilt axis;
- (2) The zenith distance for which the telescope should be set can be chosen freely and adjusted roughly; the magnitude of zenith distance deviation is less limited;
- (3) The vertical roll effect defined below can be measured only with Method 3.

According to Steinert (1964), the azimuthal roll effect w_e depends on the axis balance setting with the very fine adjustment knobs and the magnitude of the zenith distance deviation. In the present studies, dependence of the roll effect of the axis balance cannot be demonstrated on the basis of a suitable variance analysis, inasmuch as the axis balance does not essentially exceed the limits stated by the manufacturer. The theoretical value of the axis balance can be set by means of balance springs to ± 50 g. A relationship between the setting of the very fine adjustment

knobs and w_e as well as between the measurement methods (2 and 3) and w_e is nevertheless not demonstrable. It is therefore permissible to gather together measurements according to the parameter "magnitude of zenith distance deviation" Δz in groups, by increasing values of Δz and carry out suitable variance analysis. Results are given in Table 11. Dependence of rolling effect on the magnitude of zenith deviation is highly significant in the Wild T4 and the transit instrument. For the Wild T4 the roll effect reaches values up to $0.75''$; even with zenith distance deviation of 10 to 20° values of $0.5''$ still occur. The Kern DKM3 exhibits an insignificant roll effect of $0.02''$ with a maximum value of $0.04''$. The roll effect of the transit, for a zenith distance deviation of more than 20° , is from $0.2''$ to $0.25''$. The reproducibility accuracy for roll effect is equal for all the instruments within $\pm 0.1''$. For a zenith distance deviation with the very fine adjustment knobs the indication of roll effect reverses and reaches values from $0.1''$ to $0.2''$ in the Wild T4 and the transit instrument.

It can be concluded from the dependence of roll effect on magnitude of zenith distance deviation and the relationship of roll effect and roll error that the roll error w_a depends on the zenith distance deviation in a similar manner (Fig. 34): With the start of rotation w_a grows strong; with continual rotation w_a increases slowly until the axis reaches an extreme position in which the forces working on the axis are in equilibrium. w_a declines sharply upon reversing direction of rotation, reaches a 0-value, and increases again with reverse sign in the continued reverse rotation.

A method for reducing the dependence of the roll defect on rotation direction and on the magnitude of zenith distance deviation was given by Steinert (1964) and used earlier with success (method a): Focusing the telescope to the desired zenith distance does not proceed at once, but oscillates at this zenith distance with decreasing amplitude; both of the above-mentioned reversals should proceed in the same direction on the basis of approximate and fine focusing of the telescope. The roll effect is almost completely eliminated by the preventive measures in Table 11. Elimination of roll is especially significant for the investigation of secondary tilt axis error, since the direction of the momentary axis is influenced in the same way by both the secondary axis error and the roll effect. This fact was not noted in the previously known tilt axis investigations (Mathias, 1961).

In the investigation the secondary tilt axis error of the transit instrument according to normal "focusing methods" (gradual deviation of the zenith distance; see Section 5.4.1) has shown that in less careful single oscillations the residual roll defect can be added on systematically. In Figure 33 half of the $\Delta a_1/2$ difference of the measured azimuth direction a_1 of the mirror normal (line) is shown between forward and reverse, and is indeed dependent on the zenith distance position of the telescope (transit instrument, mean from four series of measurements).

Table 11. Test Data for Roll Effect

Instrument	Graphs	Zenith Distance Deviation	Roll Effect w_e ["]	Mean Error w_e ["] (Mean)	Reproducibility Accuracy m_o ["]	No. of Observations	No. of Groups	Measurement Setup (main)		
Wild T4		5°	+0.13	±0.03	±0.09	83	6	2		
		10°	+0.43	±0.04	±0.11	85	6	2		
		15°	+0.59	±0.06	±0.12	62	5	3		
		30°	+0.75	±0.04	±0.10	31	2	2		
		45°	+0.51	±0.07	±0.13	77	5	2		
		90°	+0.76	±0.05	±0.20	15	1	3		
		135°	+0.69	±0.03	±0.13	15	1	3		
		Root mean square	+0.59	±0.05	±0.13	368				
		Fine adj. 1°	-0.19	±0.02	±0.06	44	2	2		
		Fine adj. 2°	-0.14	±0.02	±0.04	84	5	3		
Kern DKM 3		Single Variation	+0.01	±0.03	±0.15	27	2	2		
		1°	+0.02	±0.02	±0.09	20	1	2		
		5°	+0.04	±0.02	±0.09	20	1	2		
		15°	+0.02	±0.02	±0.06	20	1	2		
		30°	+0.01	±0.02	±0.10	20	1	2		
		360°	+0.02	±0.02	±0.10	30	1	3		
		Root mean square	+0.03	±0.02	±0.09					
		Fine adj.	+0.03	±0.02	±0.10	20	1	2		
		Askania AP70		5°	+0.04	±0.04	±0.10	10	1	3
				10°	+0.18*	±0.04	±0.08	9	1	1
15°	+0.09			±0.03	±0.12	10	1	3		
45°	+0.20*			±0.04	±0.10	34	2	3		
90°	+0.23			±0.03	±0.10	10	1	3		
135°	+0.25			±0.03	±0.09	10	1	3		
Root mean square	+0.18			±0.04	±0.10					
Fine adj. 1°	-0.11			±0.02	±0.06	10	1	3		
Single Variation	+0.04			±0.02	±0.11	40	2	3		

*Contains measurements according to Eq. (94).

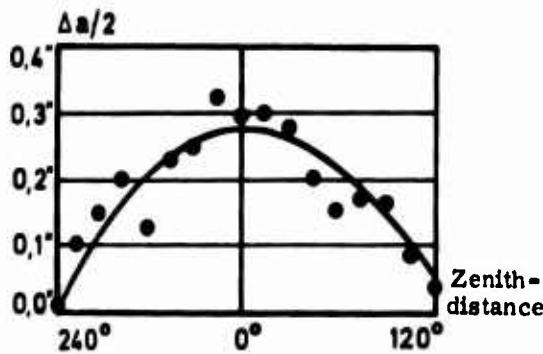


Figure 33. Addition of the Residual Roll Defect During a Tilt Axis Experiment

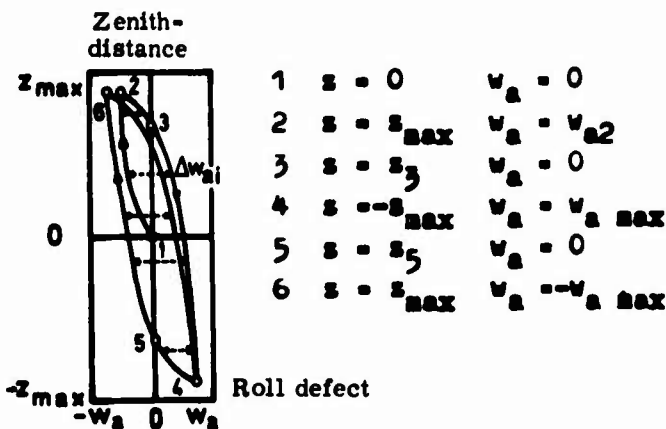


Figure 34. Theoretical Motion of the Mean Axis During a Tilt Axis Experiment

The systematic component can be comprehended by a second-order polynomial with a mean approximation of $\pm 0.12''$. This phenomenon as well as both of the described rolling defect dependencies on zenith distance deviation is suggested for motion of the mean axis in the known tilt axis experiment by the model which is presented in Fig. 34: At the starting position 1 ($z = 0^\circ$), the rolling defect w_a is set equal to 0; the roll defect increases to a w_{a2} value with gradual deviation of the zenith distance, attaining a 0 value in reversal of rotary direction in position 3; it then increases in the other extreme position to a $w_{a max}$ value and so forth. The noted differences Δw_{ai} of the main tilt axis position between forward and reverse measurement depends on the zenith distance position and corresponds to the measured

distances Δ_{ai} of Figure 33. No analogous system occurs in the "symmetrical focusing method" (Section 5.4).

A careful single oscillation of the telescope is difficult to obtain for practical measurements, especially for astronomical observations. Since each target will be observed in two telescope seats, the mean of telescopes seats I and II is freed from systematic roll defect if the target focusing in the telescope seats I and II proceeds from the zenith distance 0° (method b): The rolling effect is then for both telescope seats equal in magnitude even if the signs are different. The focusing of zenith direction should proceed in each case before the axis shift in the transit instrument and by an approximate single oscillation in the universal instrument. Methods a and b can also be combined.

Although the rolling defect can be reduced by the described method of observation, what is basically sought is the prevention of such an error at the outset by practical preventive measures. In the telescope rotation the mean axis makes a roll motion toward the axis seat. If this roll motion is unequal in both supports, then a roll defect occurs. The asymmetry of the roll motion is due to the unequal friction on the tilt axis on both sides of the telescope, the unequal seat pressure, and probably the unequal elastic deformation of the seat. None of these causes can be identified specifically as the main error source in spite of detailed experiments. The supposition expressed in Steinert (1964) that the roll defect is connected with the eccentric seat of the handwheel can be marked incorrect.

Some phenomena, for example, the sign reversal of the approximate and fine focusing indicate a great friction influence. The stability of the tilt axis should generally increase if there occurs as little friction as possible in the rotation between the axis and the clamp and release attachments. The most efficient practical preventive measure for roll defect consists of directing the tilt axis in a closed seat. Such a solution has been incorporated into the Kern DKM3 (Fig. 37). To be sure, this preventive measure has far-reaching conclusions for the practical total construction of an instrument and contradicts the principle of the transit instrument.

In addition to the roll defect, further azimuth stability errors of the tilt axis occur, which, however, are less significant in comparison to the roll error. Thus, for example, in the Wild T4, a systematic "clamp" error of 0.16" was found (reproducibility ± 0.04 "), which is schematically equal for each direction and falls off in reduction of directions. For the transit instrument, the tilt axis shifts act as a further source of error. The reproducibility of the azimuth axis seat was measured by the shift (without deviation in zenith distance) at ± 0.15 "; a systematic process is not determined. Stresses on the tilt axis or the telescope (to about 0.5 kg horizontal stress) influence the stability of the tilt axis only within the reproducibility of the roll effect. Upon intensive investigation the known phenomena were abandoned.

We are going to define and measure a "vertical roll effect" w_n in the seat on the basis of the present knowledge of tilt axis behavior in zenith distance deviation. Let β_{w0} be the vertical angle between an outer reference direction and a reference direction rigidly combined with the tilt axis in a zenith distance focusing without roll error; let β_{wz} be the corresponding angle according to such a zenith distance focusing in a clockwise direction. The vertical roll effect is defined by:

$$w_n = \beta_{wz} - \beta_{w0}.$$

The zenith distance focusing without roll error must proceed according to the known rules for elimination of azimuth roll effect. Since vertical roll error is not important in the Wild T4 and in the transit instrument according to Eqs. (66b) or (67a) and almost no roll error occurs in the DKM3, it was dropped in further experiments.

5.3 Thermal Deflection of the Telescope

A periodic deviation of the telescope azimuth according to zenith distance focusing z_1 ($z_1 \approx 90^\circ$) was determined in the transit instrument by the roll effect experiment according to method 1. The focusing of z_1 proceeds by rotation of the telescope with the handwheel and the attached operation of the altitude slow-motion screw. The azimuth direction of the mirror normal (line) is measured according to the actual focusing in brief time intervals (0.5-1 min) and is incorporated as dependent on time (Fig. 35). The observation takes place according to Eq. (94) in telescope seats I and II as well as by clockwise and counterclockwise focusing.

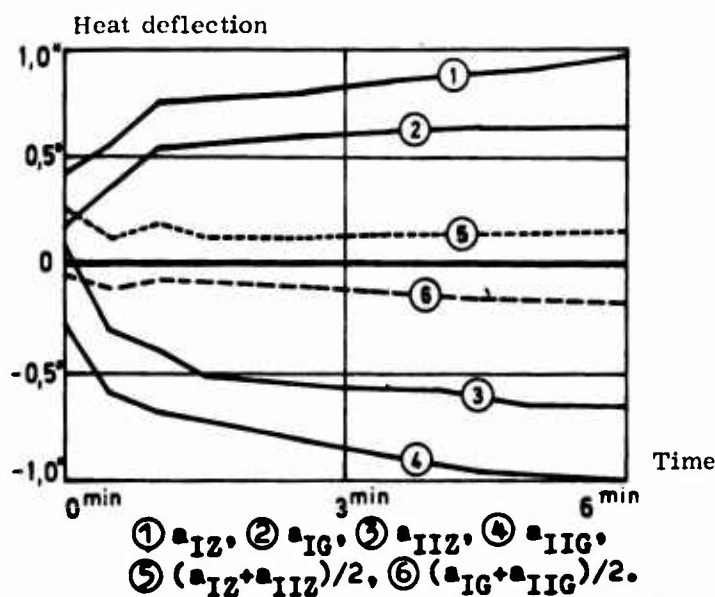


Figure 35. Effect of Heat Deflection of the Telescope in Telescope Seats I and II (Transit Instrument)

During the rough approximate focusing so much heat is brought to the telescope tube by the hand of the observer on the handwheel that a deflection of the tube occurs. According to the actual approximate focusing, that is, upon termination of the heat conductance, the deflection declines; this can be understood by the observations described.

In the rotation of the telescope seat the handwheel varies its seat toward the target so that the periodic deviation of the azimuth a_{IZ} and a_{IIZ} in the telescope seats I and II proceed symmetrically to the target axis and the mean $(a_{IZ} + a_{IIZ})/2$ [as well as $(a_{IG} + a_{IIG})/2$] is progressively independent of time (see Fig. 35).

From the 76 observations made in telescope seats I and II the mean error of the target axis is $\pm 0.2''$ in the telescope seat, inasmuch as the observations for both telescope seats proceed to an equal point in time after focusing and both telescope seats were averaged. The mean total deviation up to the fading of the phenomena (6-8 min) of the target axis amounts to $0.65''$ whereby the component of the first two minutes amounts to $0.45''$ (from 152 observations). A periodic difference of measurement for telescope seats I and II is assumed at about 0.5-1 min; thus, a further mean error of $0.15'' - 0.2''$ of the collimation axis must be calculated for a telescope seat. Consequently, on the basis of the heat deflection of the telescope, the mean error of the collimation axis of the transit instrument for a telescope seat amounts to $\pm 0.25'' - 0.3''$.

In the Wild T4 the heat deflection of the telescope is larger than that in the transit instrument since the telescope must be handled directly in order to vary the zenith distance. The average azimuth deviation during the first two minutes after zenith distance focusing amounts to $0.85''$; the deflection symmetry in telescope seats I and II is projected less, according to its nature, so that a mean error of the target axis in a telescope seat according to the present investigation must be calculated in total as $0.35'' - 0.4''$. The observation must therefore occur in two telescope seats in order that the systematic (symmetrical) component is eliminated. The strong susceptibility of the tube to heat is also shown in the experiment presented in Figure 36: Heat is manually introduced to the tube of the telescope and is distributed from the left and from the right for 10 sec (the distance between the tube and the hand is 1-2 cm). The deviations of the target axis azimuth that occurred after heat was terminated are given in Figure 36; the mean total deviation of the azimuth is $0.6''$. Since a great heat deflection can also be calculated at lower outside temperatures, an improved tube heat insulator is to be desired for both instruments (for example, an insulating collar).

In the DKM3 no corresponding heat deflection occurs because of the short telescope tube ($b < 0.05''$). The heat introduced by moving the telescope, however, results in motion of the optical component of the telescope system, and above all in mirror motion. Experiments according to the method described in Section 4.1 gave a mean target axis error of $0.15''$.

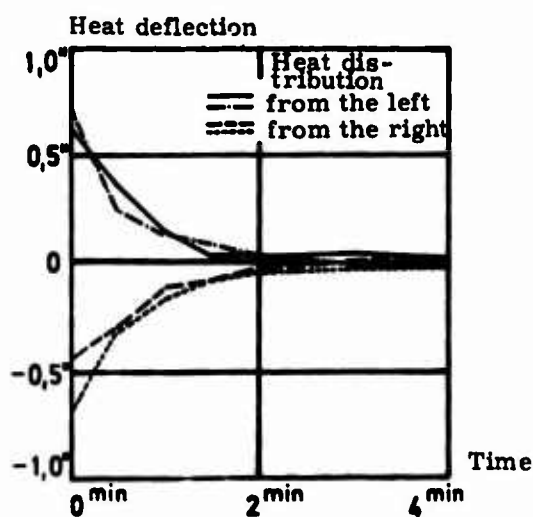


Figure 36. Effect of Heat Deflection of the Telescope on the Basis of Manual Heat Distribution

5.4 Secondary Tilt Axis Error

In astronomical observations one can bear in mind the secondary tilt axis error - inasmuch as it is not eliminated by the arrangement of observations - if its value is determined exactly and if it is introduced into the observation as a calibration correction. Since such measurements can never be more accurate than the calibration value itself, the tilt axis errors of the present instruments are particularly studied in detail (Stephani, 1965, unpublished; and Vogel, 1966). Therefore, the causes of error are essentially revealed.

5.4.1 MEASUREMENT PROGRAM FOR DETERMINING SECONDARY TILT AXIS ERRORS; RESULTS

In the measurement of the tilt axis wobble error according to Section 4.1, two different methods were used for focusing the zenith distance. In the "normal" focusing method (Index n) the telescope is rotated from an extreme position z_1 (for example, $z = +120^\circ$) in each case by an interval Δz (for example $\Delta z = 15^\circ$) in the zenith distances $z_1 + \Delta z$, $z_1 + 2 \Delta z$, $z_1 + 3 \Delta z \dots$ to another extreme position $z_1 + n \Delta z$ (for example, $z = -120^\circ$); each zenith distance is oscillated separately for elimination of the roll error. In the "symmetrical" focusing method (Index s) the telescope is focused from the zenith distance of 0° and proceeds according to zenith distances Δz , $-\Delta z$, $2 \Delta z$, $-2 \Delta z$, etc., following one right after another. The focusing of the actual zenith distance results also in oscillation. The danger of a summation of the residual roll error is not as great in symmetrical focusing, according to Section 5.2. The width of the interval Δz is small enough to be selected so that in a Fourier analysis, terms of short period can be comprehended corresponding to Eq. (88).

In present investigations the azimuthal and vertical components i_a and i_v are usually measured separately; the measurement series (the mean from forward and reverse measurement) is adjusted separately for each according to Eq. (81a) and the values for i_a or i_v determined for the same zenith distance position are grouped together for the mean. The reproducibility of wobble error can be calculated according to Eq. (85). Measurement series, in which the measuring points are taken together, can be joined together after adjustments are made separately. In the Wild T4 the outer rings of the four spherical seats (Fig. 37) can be shifted toward one another; according to Section 5.4.2, this results in the dependence of tilt axis wobble error on the actual position of the outer rings opposite each other and the spherical system. The present investigations were carried out with four different arbitrarily determined outer-ring positions (Roll positions I...IV).

For the autocollimation measurements which are at one's disposal in Section 2.4.2.2 described for the ocular measurement coordinates, 4 or 3 series were measured with simultaneous measurements of x and y in order to comprehend

the elliptical deformation of the axis in the Wild T4 and the transit instrument.

The results of the investigation are given in Table 12 and are presented graphically in Figure 39 and Appendix N. In the Wild T4 the secondary axis error occurs and influences the measurements: the azimuthal component i_a amounts to the root mean square value of $0.4''$ and the average extreme value is $0.7''$; the average mean increase - corresponding to the Δz interval - amounts to $0.35''/7.5^\circ$ (from 12 series of measurement); the corresponding values for the vertical components are $0.3''$, $0.5''$, and $0.2''/7.5^\circ$. The dependence of the wobble error on the zenith distance position is presented as an example of the azimuth component i_{anI} (normal focusing method, roll position I) in Figure 39 (the curve of the vertical component i_{vnI} is presented in Appendix N).

The Kern DKM3 shows a slight wobble error; the root mean square for the azimuthal and vertical components amounts to about $0.1''$; the extreme value is $0.3''$ or $0.2''$; and the mean increase $0.1''/12.5^\circ$ (see Appendix N).

The corresponding values for the transit instrument are $0.25''$, $0.4''$, $0.2''/15^\circ$ (i_a) and $0.2''$, $0.35''$, $0.2''/15^\circ$ (i_v); the graphical representation is given in Appendix N. Reproducibility for an individual measurement (forward and reverse measurement) for the Wild T4 is $0.25''(i_a)$ and $0.2''(i_v)$; for the DKM3 $0.1''(i_a)$ and $0.15''(i_v)$; and for the transit instrument $0.2''(i_a)$ and $0.25''(i_v)$.

Reproducibility depends significantly on the roll error. The measurement of an elliptical deformation of the tilt axis in the experiments can be treated in the following way:

- a) Evaluation with compensating disc [Eq. (81a, b)] and compensating ellipse [Eq. (77a, c)]. An elliptical axis deformation can be deduced from the differences of the wobble errors determined according to both methods as well as the difference between the radius and half-axis.
- b) Evaluation with compensating ellipse. The elliptical deformation is deduced only from the difference between the large and small half-axes of the ellipse.

Measurements used for the Wild T4 and the transit instrument were taken according to a) and for the DKM3 according to b) above. The root mean square of the difference amounts to $\pm 0.07''$ in the Wild T4 and $\pm 0.13''$ in the transit instrument. The mean difference between the radius and half-axis amounted to $0.09''$ in the Wild T4, $0.14''$ in the transit instrument, and is thus sufficiently significant or highly significant. In the Kern DKM3 one-half the distance of the half-axis is $0.05''$ and is viewed as significant. The elliptical deformation is therefore small in all the instruments.

5.4.2 ANALYSIS OF ERROR CAUSES

The measured tilt axis wobble error is (i_a and i_v) in the Wild T4, (i_a) in the DKM3, and (i_a) in the transit instrument; all of these are systematically highly

Table 12. Results of the Tilt Axis Experiments

Measurement n = normal s = symmetric method I, II... roll positions	No. of Measure- ment Series*	No. of Measure- ment Points	Inter- val Δz	(Total) Measured Secondary Axis Error				Systematic Secondary Axis Error									
				Maxi- mum [$^{\circ}$]	Mini- mum [$^{\circ}$]	Mean Quadr. [$^{\circ}$]	Mean Increase [$^{\circ}/\Delta z$]	Repro- ducibility [$^{\circ}$]	Mean Error of the Mean [$^{\circ}$]	System- atic Test Sig.	Series Period	Mean Variation [$^{\circ}$]	Highest Value [$^{\circ}$]	System Test Sig.			
Wild	Azimuth Component			7.5°	0.72	-0.87	0.39	±0.27	±0.23	±0.08	HS	180°, 45°	±0.15	0.60	NS		
	i_{an} (1 Coord.)	4	39		0.56	-0.55	0.27	±0.28	±0.23	±0.12	HS	180°, 45°	±0.22	0.55	CS		
	i_{vn} (1 Coord.)	2	39		0.60	-1.07	0.36	±0.34	±0.20	±0.14	HS	180°, 45°	±0.22	0.50	NS		
	i_{an} (1 Coord.)	1	39		0.66	-0.73	0.39	±0.32	±0.23	±0.16	HS	180°, 45°	±0.25	0.58	NS		
	i_{vn} (1 Coord.)	1	39		0.71	-0.69	0.40	±0.45	±0.35	±0.12	S	180°, 45°	±0.27	0.55	NS		
	i_{an} (2 Coord.)	4	19		0.67	-0.76	0.37	±0.36	±0.26	±0.13	HS	180°, 45°	±0.21	0.55	NS		
	Taken together				12	0.65	-0.62	0.30	±0.25	±0.16	±0.05	HS	180°, 45°	±0.17	0.61	CS	
	Vertical Component				7.5°	0.57	-0.44	0.32	±0.22	±0.14	±0.07	HS	180°, 45°	±0.20	0.37	NS	
	i_{vn} (1 Coord.)	4	39			0.47	-0.51	0.21	±0.16	±0.11	±0.11	HS	180°, 45°	±0.12	0.30	S	
	i_{an} (1 Coord.)	2	39			0.34	-0.45	0.21	±0.15	±0.09	±0.06	HS	180°, 45°	±0.15	0.31	NS	
	i_{vn} (1 Coord.)	1	39			0.52	-0.41	0.28	±0.20	±0.27	±0.09	HS	180°, 45°	±0.18	0.25	NS	
	i_{an} (2 Coord.)	4	19			0.55	-0.50	0.28	±0.21	±0.18	±0.08	HS	180°, 45°	±0.16	0.37	NS	
Taken together			12	0.30		-0.27	0.13	±0.13	±0.12	±0.03	HS	180°, 120°	±0.10	0.19	NS		
Azimuth Component			12.5°	0.18		-0.23	0.09	±0.11	±0.15	±0.04	NS	-	-	-	-	-	
i_{an} (2 Coord.)	5	32		0.34		-0.27	0.19	±0.14	±0.18	±0.04	S	180°	±0.12	0.27	NS		
i_{vn} (2 Coord.)	6	15		0.56		-0.41	0.33	±0.24	±0.23	±0.07	HS	180°	±0.16	0.47	NS		
Azimuth Component				15°		0.42	-0.32	0.25	±0.18	±0.20	±0.06	-	-	±0.14	0.35	-	
i_{an} (1,2 Coord.)	10	15				0.29	-0.27	0.14	±0.18	±0.23	-	NS	-	-	-	-	
i_{vn} (1 Coord.)	6	15				0.47	-0.36	0.23	±0.28	±0.25	-	NS	-	-	-	-	
Vertical Component					15°	0.36	-0.30	0.18	±0.22	±0.24	-	-	-	-	-	-	
i_{an} (1,2 Coord.)	8	15				0.47	-0.36	0.23	±0.28	±0.25	-	-	-	-	-	-	
i_{vn} (1 Coord.)	5	15				0.36	-0.30	0.18	±0.22	±0.24	-	-	-	-	-	-	
Taken together						13	0.36	-0.30	0.18	±0.22	±0.24	-	-	-	-	-	-

*A measurement series consists of a forward and reverse measurement.

significant. For analyzing the functional relationships between wobble error and zenith distance position, it is necessary to know the schematic and dimension of the tilt axis seat (Fig. 37).

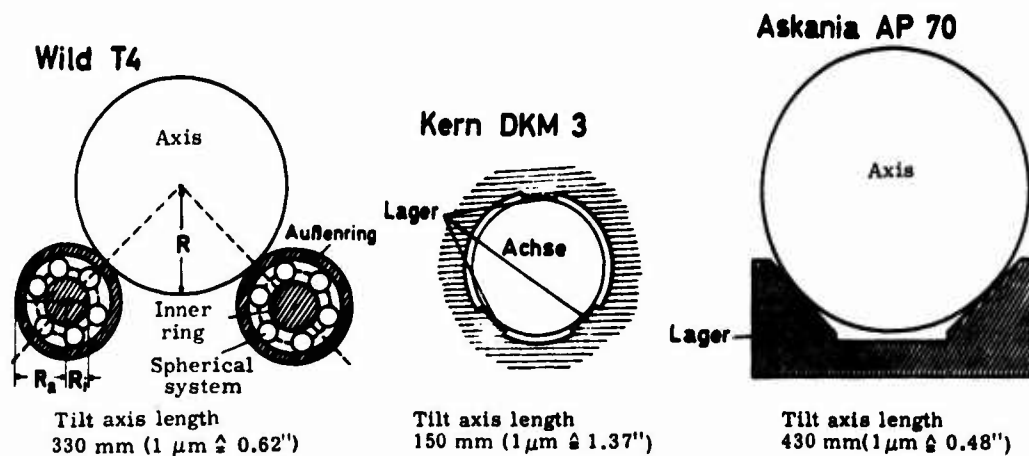


Figure 37. Practical Solutions for Tilt Axis Seating (scale: 1:1)

The tilt axis of the Wild T4 is conducted on both sides by two spherical seats whose outer ring radius R_a is equal to half the radius R of the tilt axis. A zenith distance deviation Δz and the rotation δ of the outer ring resulting from the deviation is proportional to the reciprocal value of the radius:

$$\frac{\Delta z}{\delta} = \frac{R_a}{R} = \frac{1}{2}. \quad (95)$$

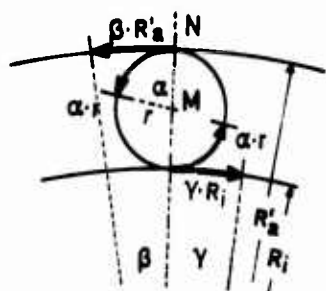
Error in the concentricity of the outer ring and eccentricity error of the spherical seat occurs therefore with a period p_1 of 180° . Furthermore, the motion of the outer ring and of the spherical system must be considered as going toward the inner ring.

By more complete static friction the spherical mean point can be set and the rotation can be associated with both rings according to Vogel (1966). According to Figure 38, the following relations are valid:

$$\alpha \cdot r = \beta \cdot R_a'; \quad \alpha \cdot r = \gamma \cdot R_i. \quad (96)$$

The angular rotation δ of the outer ring toward the inner ring results from:

$$\delta = \beta + \gamma = \alpha \cdot r \frac{R_a' + R_i}{R_a' \cdot R_i}. \quad (97)$$



- r = radius of the sphere
 Ra' = radius of the inner side of the outer ring
 Ri = radius of the inner ring
 α = angular rotation of the sphere at the horizontal axis by a mean spherical point M
 β = angular rotation of the outer ring with respect to the normal N through a mean spherical point
 γ = angular rotation of the spherical system toward the inner ring
 δ = angular rotation of the outer ring toward the inner ring

Figure 38. Motion Run-off in a Spherical Seat

The angular rotation γ of the spherical system with respect to the inner ring is:

$$\gamma = \alpha \frac{r}{Ri}. \quad (98)$$

For a complete revolution of the sphere, that is, $\alpha = 360^\circ$, the following values of δ and γ and β result in the present spherical seat.

$$\delta = 261^\circ = \Delta z = 130^\circ; \quad \gamma = 173^\circ \hat{=} \Delta z = 86^\circ; \quad \beta = 88^\circ \hat{=} \Delta z = 44^\circ. \quad (99)$$

By Eq. (99) the periods of the different error causes that operate in the secondary axis error can be determined. We limited ourselves to deducing only those error causes which are actually operating in the instrument under investigation. The outer ring of a spherical seat is deformed at the point of contact with the tilt axis if it is not stopped directly by a sphere (Fig. 37). The period of this phenomenon results from the angular distance a of the sphere ($a = 60^\circ$) and from the b ratio between a rotation Δz of the tilt axis and of the $\Delta \gamma$ rotation of the spherical system that corresponds to this. With Eq. (99) $b = 130^\circ/173^\circ = 0.751$, so that the period p_2 that is sought results from:

$$p_2 = a \cdot b = 60^\circ \cdot 0.751 = 45^\circ.$$

The remaining error causes, which result in the theoretical wobble error with periods of 272° , 90° , and 65° , are not obtained according to the above-mentioned Fourier analysis. (The magnitudes of the corresponding amplitudes are within the mean error.) The systematic secondary axis error can be given corresponding to Eq. (88) by the following Fourier series:

$$i_a = i_{a\Delta} + a_2 \sin(2z + \phi_2) + a_8 \sin(8z + \phi_8). \quad (100)$$

The Fourier series for the vertical components i_v are analogous to Eq. (100). Figure 39 shows as an example the results of Fourier analysis for the azimuthal components i_{anI} . In Figure 39a the measured wobble error i_a and the systematic component i_a' occurring with a 180° period are shown. If one reduces i_a by i_a' , then curve i_a'' of the residual error results (Fig. 39b). i_a'' is reduced by a systematic component i_a''' (45° period) so that the residual error $i_{a\Delta}$ (Fig. 39c) is now the remainder of this. The residual error $i_{a\Delta}$ is distributed accidentally in the arrangement test; thus the above theoretical statements can be considered valid.

The error component with the 180° period is due to the eccentricity of the spherical seat, since it results in a sinusoidal course of the error curve. The results of Fourier analysis for the remaining measurement series are taken from Table 12. The root mean square approximation for i_a and i_v amounts to $0.2''$ or $0.15''$ and the arrangement test as a rule shows a random distribution of the remaining error. Consequently, the systematic component of the wobble error can be clearly identified as the seat component [see notes to Eq. (69)]. The amplitudes of the terms in Eq. (100) show the following values for roll positions I to IV:

Roll Position	Azimuth Component		Vertical Component	
	a_2	a_8	a_2	a_8
I	0.33''	0.20''	0.36''	0.25''
II	0.22''	0.30''	0.18''	0.12''
III	0.43''	0.12''	0.28''	0.06''
IV	0.25''	0.30''	0.21''	0.11''

The variation among the amplitudes is significant. Since the phase shifts ϕ also depend on the roll position, a different curve (for example, i_{anI} and i_{anII} in Appendix N) is obtained for different roll positions. Calibration values for the Wild T4 are, therefore, significant only when the four outer rings as well as the four ball systems are always brought into the same relative position; this is practically, however, almost impossible.

In the Kern DKM3 a highly significant systematic curve in the azimuthal components i_a occurs which can be given by a Fourier series with periods of 120° and 180° (amplitudes of $0.12''$ or $0.09''$ root mean square approximation $\pm 0.10''$); see Appendix N. The error component with a 120° -period can proceed from a three-sided solid (equal diameter) axle-end pivot. In the transit instrument only the azimuthal component i_a shows a highly significant systematic curve which can be shown by a Fourier series with a 180° period (Appendix N). According to the remarks in Section 5.2 and Figure 33, a part of the measured systematic wobble error is due to a summation of the residual roll defect, and error curves i_{an} and i_{as} differ significantly in normal and symmetrical focusing methods (Appendix N) in the transit instrument; these cannot be completely excluded.

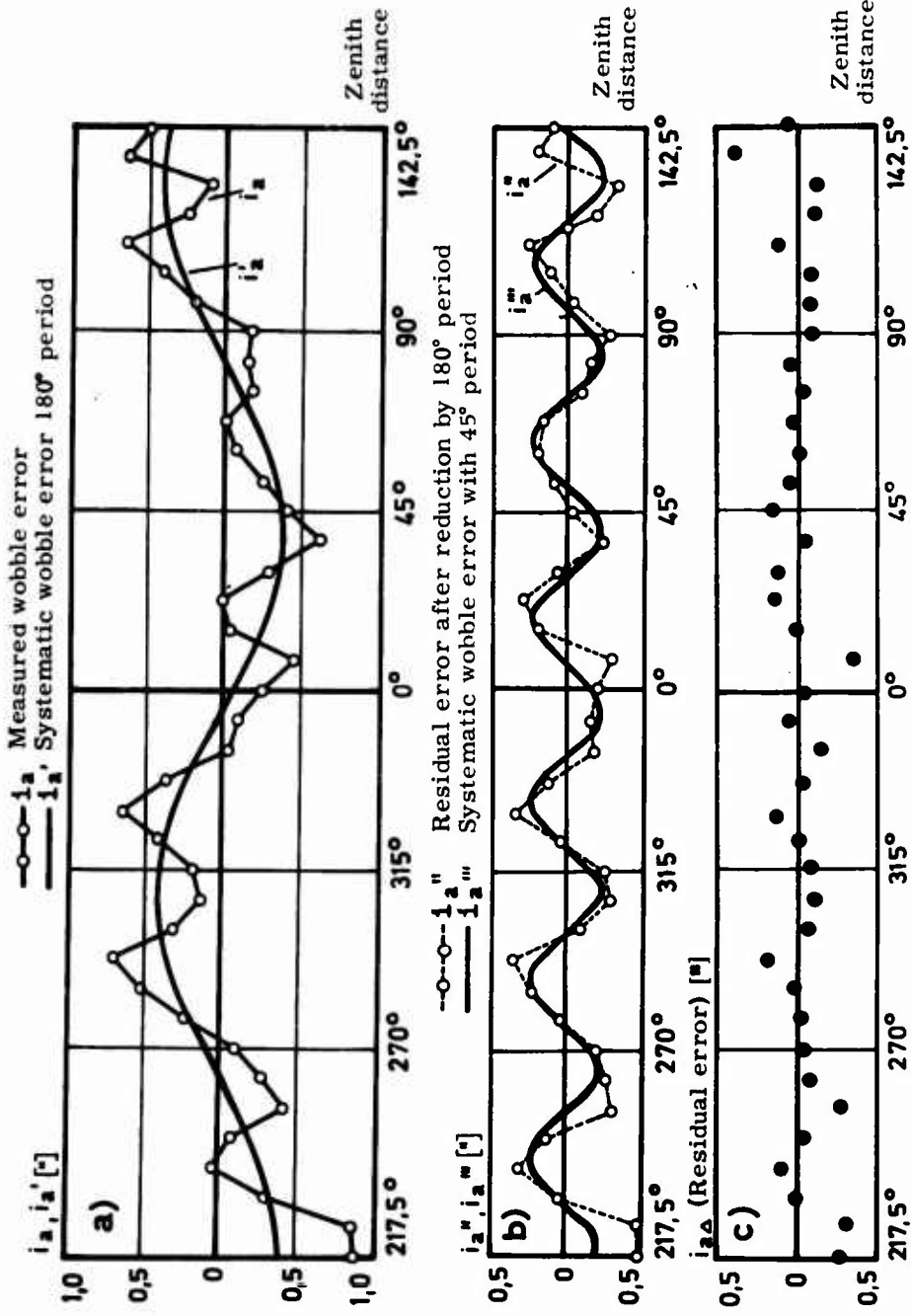


Figure 39. Azimuth Secondary Tilt Axis Error of the Wild T4. Analyses a, b, and c of Error Causes

5.5 Secondary Vertical Axis Error

The importance of the vertical axis for theodolite precision construction is shown historically by the plurality of practically-developed solutions. The variety of present vertical axis systems indicates the difficulty of finding practical solutions which can satisfy precision requirements as well as technical manufacturing considerations. The following investigation has a goal of determining the magnitude, type, and cause of wobble error for the semikinematic* (Wild T4) and the fully kinematic (Kern DKM3) vertical axis system. The first intensive investigations with such a goal were carried out by Janich (1954) and Alpar (1960).

5.5.1 MEASUREMENT PROGRAM

The basic measurement and evaluation methods are described in Sections 4.1 and 4.2. The measurement points - 20° interval range (T4) and 12.5° (DKM3) - were distributed uniformly on the circle. The measurements were taken at various slopes of the vertical axis ($v = 2''$ and $9''$), various rotation directions, and with and without alidade clamping. In the Wild T4 one must pay attention therefore to single measurement series so that they join without interruption (one measurement series comprises one alidade rotation), that is, without an additional complete revolution.

In addition to measurement method 1 - based on the theoretical considerations of Section 5.5.2 - another method was used which makes it possible to comprehend individual error causes with greater certainty. In method 2a the direction of the momentary vertical axis is measured by a determined alidade position in each case after two complete alidade rotations; for measurements after one rotation a method 2b is used. For the Kern DKM3 only the 2b method is applicable whereby the measurements are taken for the two least different alidade positions. Further explanations for the 2a, b method are given in the following section.

5.5.2 THEORETICAL CONSIDERATIONS OF ERROR CAUSES IN SEMIKINEMATIC AND FULLY KINEMATIC VERTICAL AXIS SYSTEMS

In the Wild semikinematic axis system the axle-end pivot is conducted to the upper end by a spherical system which operates in the conical enlargement of the case (Fig. 40a). It is conducted to the lower end by a sliding fit.

The motion of the axis and the spherical system opposite the case is derived analogously to Section 5.4.2. The fundamental theoretical investigations are considered in Vogel (1966).

The spheres rest on the axis in two points so that the spherical rotation must be divided by its mean point into two components. For the rotation at the vertical

*In a semikinematic system the axis is directed through the spherical seat and slide seat (Fig. 40a); in a fully kinematic system, through the spherical seat only.

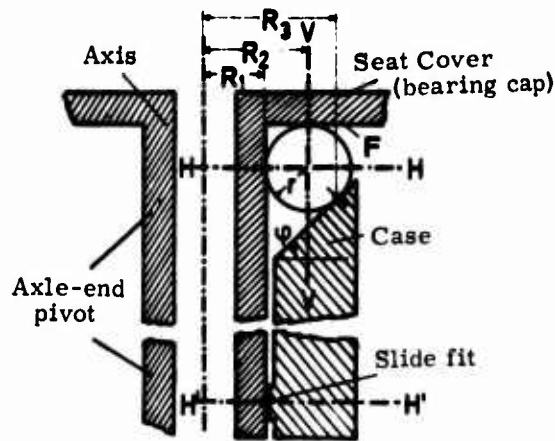


Figure 40a. Semikinematic Axis System of the Wild T4 (front sketch)

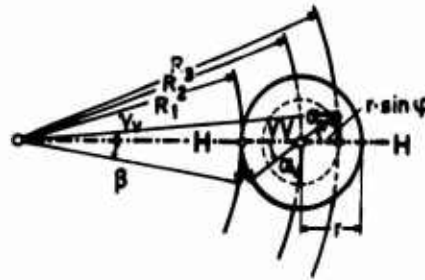


Figure 40b. Motion of a Sphere Opposite Axis and Case (cross section)

axis VV with the designations from Figure 40a, b analogous to Eq. (96), the following is valid:

$$r \cdot \alpha_V = R_1 \cdot \beta; \quad r \cdot \alpha_V \cdot \sin \phi = R_3 \cdot \gamma_V. \quad (101)$$

The motion β of the axis section produces a rotation α_H of the spheres at the horizontal axis HH by which means the spheres are "rolled off" onto the case part.

$$r \cdot \alpha_H = R_2 \cdot \beta; \quad r \cdot \alpha_H \cdot \cos \phi = R_3 \gamma_H. \quad (102)$$

If one eliminates α_V and α_H in Eqs. (101) and (102), then one obtains for γ_V and γ_H :

$$\gamma_V = \frac{R_1 \sin \phi}{R_3} \beta; \quad \gamma_H = \frac{R_2 \cos \phi}{R_3} \beta. \quad (103)$$

The rotations δ_a and δ_k of the alidade or spherical system in respect to the substratum are:

$$\delta_a = \beta + \gamma_V + \gamma_H; \quad \delta_k = \gamma_V + \gamma_H. \quad (104)$$

For a complete revolution of the spherical system ($\delta_k = 360^\circ$) the alidade must be rotated at $\delta_a = p_1$. p_1 is the period of a revolution of the spherical system opposite the case and is calculated from Eqs. (104) and (103) as follows:

$$p_1 = 360^\circ + \beta = 360^\circ \left(1 + \frac{R_3}{R_2 \cos \phi + R_1 \sin \phi} \right) \quad (105)$$

For a complete revolution of the spherical system with respect to the alidade, the alidade must be rotated at $\delta_a = p_2$. p_2 is the period of a spherical ring revolution opposite the alidade section and is calculated from Eqs. (104) and (103)

$$p_2 = \beta \left(1 + \frac{R_2}{R_3} \cos \phi + \frac{R_1}{R_3} \sin \phi \right) = 360^\circ \left(1 + \frac{R_2}{R_3} \cos \phi + \frac{R_1}{R_3} \sin \phi \right). \quad (106)$$

With the dimensions of the T4 axis system presently under investigation $p_1 = 665.8^\circ$ and $p_2 = 783.9^\circ$. The ratio of motion w_1 between the motion of the spherical system opposite the case and the motion of the alidade opposite the case results from

$$w_1 = \frac{360^\circ}{p_1} = 0.541. \quad (107a)$$

The motion ratio w_2 between the motion of the spherical system opposite the alidade and the motion of the alidade opposite the case is obtained from

$$w_2 = \frac{360^\circ}{p_2} = 0.459. \quad (107b)$$

The motion of the alidade and spherical system in reference to the case is estimated in Figure 41.

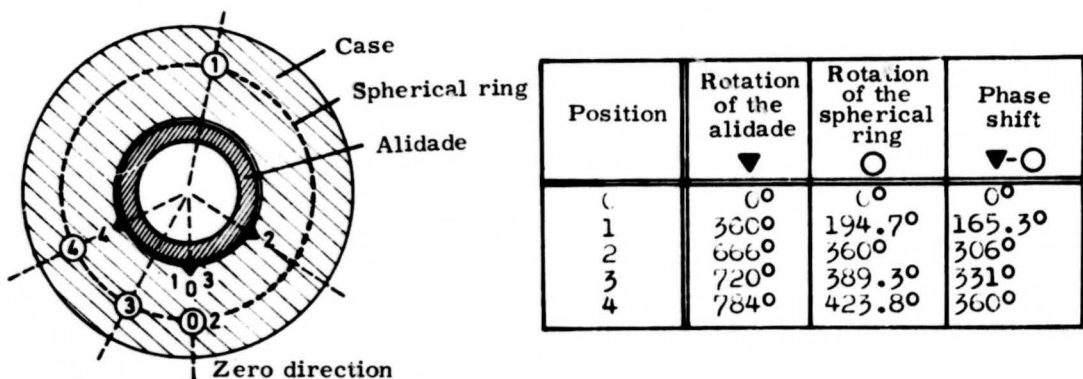


Figure 41. Motion of the Alidade and the Spherical System Opposite the Case (Wild T4)

Further basic differences between a stationary and movable measurement system must be considered. In the stationary system the direction of the momentary vertical axis is measured in a coordinate system which is stationary with respect to the substructure, for example, the x, y system of the autocollimator. In a

movable measurement system the measurements refer to a coordinate system in which the alidade is combined in a stationary way, but the system is movable with regard to the substructure. As an example, the polar coordinates given by Eq. (76a, b) or the right-angle coordinate system described by Alpar (1960) can be given; both of these are formed by a level cross rigidly joined to the alidade.

According to the above fundamental determinations on motion run-off in a semikinematic vertical axis system, we shall show on the basis of the following simple examples taken individually, how a determined error cause operates on the periodicity of the wobble error. In an error-free track, differing spherical diameters result in a secondary axis error, the slope component of which v_1 is constant and whose direction a_{v_1} varies with the rotation of the spherical system (Table 13, No. 1). In the measurements in a stationary system the motion ratio w_1 is valid and the period of wobble is 666° . The components v_{x1} and v_{y1} result from projection of v_1 onto the measurement directions are:

$$v_{x1} = v_1 \cos (0.541 \cdot \delta_a + \phi_1) , \quad (108a)$$

$$v_{y1} = v_1 \sin (0.541 \cdot \delta_a + \phi_1) . \quad (108b)$$

δ_a = Alidade position, that is, the angle between a direction fixed in space and one with a direction r_A joined rigidly to the alidade

ϕ_1 = Phase shift.

If the measurements are obtained for a system that is joined to the alidade, then the motion ratio w_2 is valid and the period of the radial component v_{r1} is 784° .

$$v_{r1} = v_1 \sin (0.459 \delta_a + \phi_1) . \quad (108c)$$

Equations (108a, b) both form the basis for the method 2a given in Section 5.5.1. In an alidade rotation of 720° , the spherical system moves 389.3° , that is, 29.3° out over its departure position (Fig. 41). The spherical system after 12.3 double rotations again reaches its departure position. Unequal spherical diameter produces a wobble error which shows a sinusoidal curve with a period of 24.6 rotations = 8860° in a component measurement (x or y) (Fig. 44). The curve course remains essentially uninfluenced by the track and slide error since the alidade and case always occupy together the same position.

In addition to spherical diameter inequality, the following further causes of error occur (Table 13, error causes 2-8):

- a) The spheres have an aspherical form (Table 13, No. 2).
- b) The axle-end pivot is deformed in cross section HH (Fig. 40a) (Table 13, No. 3); the deformation, that is, the radial deviation of the actual form of the circle results in a variable systematic wobble error, which can be shown by a Fourier

series F_3 as dependent on the alidade position δ_a . The elliptical deformation of the axis is designated (Fig. 42a; Table 14, No. 4) as the most important exception; this results from a wobble error of amplitude A_4 and a period which is half as large as the period of a rotation of the axis opposite the guide.

- c) The spherical tract F of the axis is not even, but shows a deformation which causes secondary axis error as in b) above. If the spherical tract is a saddle-like surface, for example a hyperbolic paraboloid (Fig. 42b), then the wobble error resulting from it shows the same period as the error from an elliptical deformation of the axle-end pivot. In a Fourier analysis influences from error causes corresponding to those of Section 4.4.2, cannot be separated under b) and c).
- d) The spherical tract of the case shows deformation opposite a conical surface; the axis error that results from this is described by the Fourier analysis F_3 (Table 13, No. 5). An elliptical deformation (Fig. 42c) results in a wobble error with amplitude A_8 and a period which is half as large as the period of a rotation of the spherical system opposite the case (Table 13, No. 6).
- e) A deformation of the axle-end pivot in cross section $H'H'$ (Fig. 40a) produces the wobble error F_7 (Fourier series), which shows a period of 360° ; an elliptical deformation produces a wobble error with the amplitude A_8 and a period of 180° .

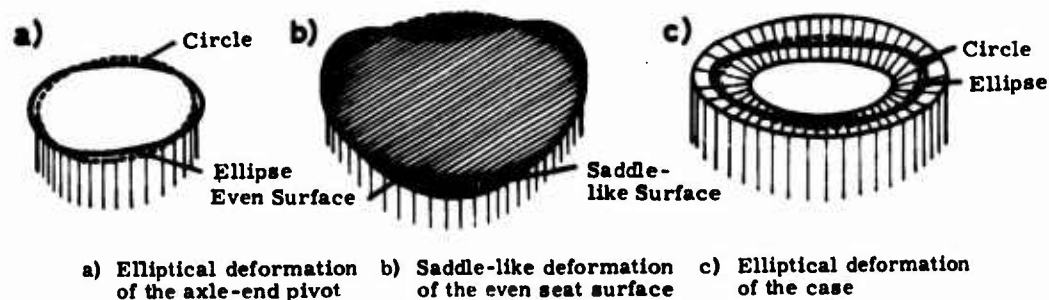


Figure 42. Error Causes in Semikinematic Axis Systems

It was further investigated which period in the wobble error under b) and d) occurred separately. By deformation of the axle-end pivot in cross section HH , the resulting F_3 error is repeated after a full revolution of the axis opposite the spherical system, that is, after one rotation of the alidade by $p_2 = 360^\circ/w_2 = 784^\circ$ [Eq. (107b)]. Further details can be established first of all if a special error form

is designated. The known elliptical deformation results in a wobble error v_4 with amplitude A_4 and a fundamental period $360^\circ/2$ in the r_K direction rigidly joined to the spherical system:

$$v_4 = A_4 \sin(2\alpha + \epsilon_4^i) . \quad \epsilon_4^i = \text{phase shift} \quad (109)$$

α is the angle between the r_K direction and a direction r_A rigidly joined to the alidade. Between α and the alidade position δ_a the relationship corresponding to Eq. (107b):

$$\alpha = w_2 \cdot \delta_a + \epsilon_4^n . \quad \epsilon_4^n = \text{phase shift} \quad (110a)$$

With (110a), (109) is transformed into:

$$v_4 = A_4 \sin\left(2\left(w_2 \cdot \delta_a + \epsilon_4^n\right) + \epsilon_4^i\right) = A_4 \sin\left(2w_2 \cdot \delta_a + \epsilon_4\right) . \quad (109a)$$

If the wobble error is measured in the stationary (x, y) coordinate system, then v_4 must be divided into the v_{x_4} and v_{y_4} components. If one denotes with β the angle between the x -direction and the direction r_K rigidly combined to the spherical system, then the result corresponding to Eq. (107a) is:

$$\beta = w_1 \cdot \delta_a + \epsilon_4^* . \quad \epsilon_4^* = \text{phase shift.} \quad (110b)$$

With (109a) and (110b) the components v_{x_4} and v_{y_4} proceed from:

$$v_{x_4} = A_4 \sin(2w_2 \cdot \delta_a + \epsilon_4) \cos \beta = A_4 \sin(2w_2 \cdot \delta_a + \epsilon_4) \cos(w_1 \cdot \delta_a + \epsilon_4^*) , \quad (111a)$$

$$v_{y_4} = A_4 \sin(2w_2 \cdot \delta_a + \epsilon_4) \sin \beta = A_4 \sin(2w_2 \cdot \delta_a + \epsilon_4) \sin(w_1 \cdot \delta_a + \epsilon_4^*) . \quad (111b)$$

Equations (111a) and (111b) can be trigonometrically transformed; with $\phi_4 = \epsilon_4 + \epsilon_4^*$ and $\phi_4^i = \epsilon_4 - \epsilon_4^*$ we have:

$$v_{x_4} = \frac{A_4}{2} \left(\sin\left((2w_2 + w_1) \cdot \delta_a + \phi_4\right) + \sin\left((2w_2 - w_1) \cdot \delta_a + \phi_4^i\right) \right) , \quad (112a)$$

$$v_{y_4} = -\frac{A_4}{2} \left(\cos\left((2w_2 + w_1) \cdot \delta_a + \phi_4\right) - \cos\left((2w_2 - w_1) \cdot \delta_a + \phi_4^i\right) \right) . \quad (112b)$$

If one inserts a numerical value for w_1 and w_2 , then according to Eqs. (112a, b) the wobble error results with the periods $p_4 = 360^\circ/(2w_2 + w_1) = 247^\circ$ and $p_4^i = 360^\circ/(2w_2 - w_1) = 953^\circ$.

In a movable coordinate system the measurement direction r_B rigidly joined to the alidade rotates with a motion ratio w_2 opposite the direction r_K joined to the spherical system. Between the angle γ formed from r_B and r_K and the alidade position δ_a , the relation corresponding to Eq. (110a) consists of:

$$\gamma = w_2 \cdot \delta_a + \epsilon_4^m.$$

With Eqs. (109a) and (110c) the radial component v_{r_4} results from:

$$v_{r_4} = A_4 \sin(2w_2 \cdot \delta_a + \epsilon_4) \cos \gamma = A_4 \sin(2w_2 \cdot \delta_a + \epsilon_4) \cos(w_2 \cdot \delta_a + \epsilon_4^m). \quad (111c)$$

If one denotes $\epsilon_4 + \epsilon_4^m$ by ψ_4 and $\epsilon_4 - \epsilon_4^m$ by ψ_4' , then, according to the trigonometric transformation of (111c) we have:

$$v_{r_4} = \frac{A_4}{2} \left(\sin(3w_2 \cdot \delta_a + \psi_4) + \sin(w_2 \cdot \delta_a + \psi_4') \right)$$

The periods 261° and 784° are taken with the numerical values of w_2 .

Table 13. Error Causes and Results of Error Analysis (Wild T4)

No.	Error Cause	Error Curve Course	Amp. of A Fourier Ser. F	Stationary Sys. v_x			Movable Sys. v_r		
				Period	Measured Amplitude	Phase Shift	Period	Measured Amplitude	Phase Shift
1	Uneven spher. dia.	Sinusoidal	A_1	666°	$0.52''$	ϕ_1	784°	$0.52''$	ψ_1
2	Aspherical sphere	Random	-	-	-	-	-	-	-
3	Spherical tract of Seat and pivot	Variable	F_3	784°			784°		
4	Irregular deformation	Sinusoidal	A_4	953°	$0.52''$	ϕ_4	784°	$0.80''^*$	ψ_4
		Sinusoidal	A_4	247°	$0.28''$	ϕ_4'	261°	$0.84''$	ψ_4'
5	Elliptical deformation	Variable	F_5	666°			666°		
6	Elliptical deformation	Sinusoidal	A_6	666°	$0.40''^*$	ϕ_6	579°	$0.44''$	ψ_6
		Sinusoidal	A_6	222°	$0.24''$	ϕ_6'	234°	$0.84''$	ψ_6'
7	Sliding seat	Variable	F_7	360°	$0.37''^{**}$	ϕ_7	360°	$0.92''^{**}$	ψ_7
8	Irregular deformation	Systematic	F_7	360°	$0.37''^{**}$	ϕ_7	360°	$0.92''^{**}$	ψ_7
8	Elliptical deformation	Sinusoidal	A_8	180°	-	ϕ_8	180°	-	ψ_8

*Error causes 1 and 4 and 1 and 6 are superimposed

**Maximum value

The effect of another form error that occurs can be deduced with a basic period of $360^\circ/K$ in the same way (for example, a three-sided equal thickness with the basic period $360^\circ/3=120^\circ$) if in Eq. (109) the value of 2α is replaced by $K \cdot \alpha$. Finally, the general case of a deformation given in Table 13, No. 3, can be treated, if one uses the above considerations, on the single sum terms of the F_k Fourier analysis. The present investigation is confined, however, to the elliptical deformation in the special case.

The effect of the error causes given under d), that is, in a general or elliptical deformation of the spherical tract of the case, can be treated in the same way as the error of the axis if one replaces the motion ratio w_2 by w_1 in Eq. (109a). The resulting periods are found in Table 13 under Nos. 5 and 6.

If one takes error causes 1, 4, 6, and 8 together, then with numerical values for the periods of x, y components v_x and v_y and for the radial component v_r , the total wobble error results as follows:

$$v_x = A_1 \cos(0.541 \delta_a + \phi_1) + A_4 \sin(0.378 \delta_a + \phi_4)/2 + A_4 \sin(1.459 \delta_a + \phi_4')/2 + A_8 \sin(0.541 \delta_a + \phi_8)/2 + A_8 \sin(1.622 \delta_a + \phi_8')/2 + A_8 \cos(0.500 \delta_a + \phi_8), \quad (113a)$$

$$v_y = A_1 \sin(0.541 \delta_a + \phi_1) + A_4 \cos(0.378 \delta_a + \phi_4)/2 - A_4 \cos(1.459 \delta_a + \phi_4')/2 + A_8 \cos(0.541 \delta_a + \phi_8)/2 - A_8 \cos(1.622 \delta_a + \phi_8')/2 + A_8 \sin(0.500 \delta_a + \phi_8), \quad (113b)$$

$$v_r = A_1 \sin(0.459 \delta_a + \psi_1) + A_4 \sin(0.459 \delta_a + \psi_4)/2 + A_4 \sin(1.378 \delta_a + \psi_4')/2 + A_8 \sin(0.622 \delta_a + \psi_8)/2 + A_8 \sin(1.541 \delta_a + \psi_8')/2 + A_8 \sin(0.500 \delta_a + \psi_8). \quad (113c)$$

The periods indicated in Eq. (113c) are given for the measurement of secondary vertical axis error in a system put in motion by the alidade; thus, it is also the measurement of the vertical axis slope using a level indicator.

Terms with equal periods are grouped together in a Fourier analysis. Thus, for example, in Eq. (113c) the terms A_1 and A_4 with a period of $360^\circ/0.459$ are grouped together to a term of A_1' amplitude and phase displacement ψ_1' . Equation (113c) proceeds also in:

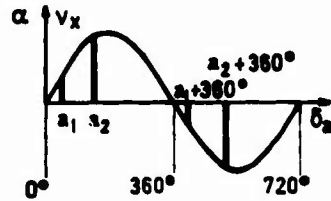
$$v_r = A_1' \sin(0.459 \delta_a + \psi_1') + A_4 \sin(1.378 \delta_a + \psi_4')/2 + A_8 \sin(0.622 \delta_a + \psi_8)/2 + A_8 \sin(1.541 \delta_a + \psi_8')/2 + A_8 \sin(0.500 \delta_a + \psi_8). \quad (114)$$

Equation (114) and the corresponding transformed equation [Eq. (113a)] are the basis for the Fourier analysis described in the next section.

In the DKM's the ratios are simpler due to the evenness of the spherical tract. We have for the periods p_1 and p_2 [Eqs. (105) and (106)]:

$$p_1 = p_2 = 720^\circ.$$

Both spherical tracts, the spherical system and the lower spherical tracts occupy exactly the same position with regard to each other after two complete revolutions. Unequal spherical diameter produces, as in the Wild T4, a relatively constant wobble error v_s direction a_{v_s} rotates with a 720° period; the x component v_x of this error displays theoretically a sinusoidal course shown in the sketch below. According to method 2b, the $\alpha_{(a_1)}$ direction of the mirror normal which corresponds to the momentary vertical axis slope, is measured at the a_1 point on the sphere after one rotation of the alidade. The difference between the two successive measurements is equal to the difference between the corresponding v_x components of the wobble error:



$$\alpha_{(a_1)} - \alpha_{(a_1 + 360^\circ)} = v_x(a_1) - v_x(a_1 + 360^\circ) \quad (115)$$

If one undertakes the measurements in Eq. (115) for an a_2 point, this should differ as much as possible from a_1 at 180° ; thus, v_s and the a_{v_s} direction of the wobble error can be calculated; with more than two measuring points, v_s and a_{v_s} can be ascertained by adjustment.

According to the experiments of Haller (1959), in a completely kinematic axis system the danger is that both spherical tracts are hidden by their attachment to the alidade or substructure. In the DKM3 the tracts are attached by screws in three places on the alidade or substructure. Therefore, the unavoidable distortion of the bearing (tract) surface results in a secondary vertical axis error which can show a period of 120° in a moving measurement system. Other essential causes of error could not be determined in this instrument.

5.5.3 RESULTS AND ANALYSIS OF ERROR CAUSES

The experimental results (Table 14, Figs. 43a, 46a) show that the secondary vertical axis error - as is to be expected - is assumed to be a higher value than the secondary tilt axis error, but that it can be disregarded, however, by measuring with a zenith distance $z > 60^\circ$, that is, with almost all practically used geodetic measuring distances. The root mean square of the total wobble error v_s [Eq. (70)] is $0.53''$ in the Wild T4 according to Table 14 and $0.60''$ in the Kern DKM3; the extreme value of v_s reaches $1.11''$ and $0.84''$, respectively.

The total wobble error v_s can be used only as a general measurement for the evaluation of a vertical axis system. For error analysis the components v_x, v_y (stationary system), the components v_r, v_t (movable system), or - as in the present case - a mixed pair of components v_x, v_r must be used. The latter combination generally allows for the most reliable statement in regard to the active error

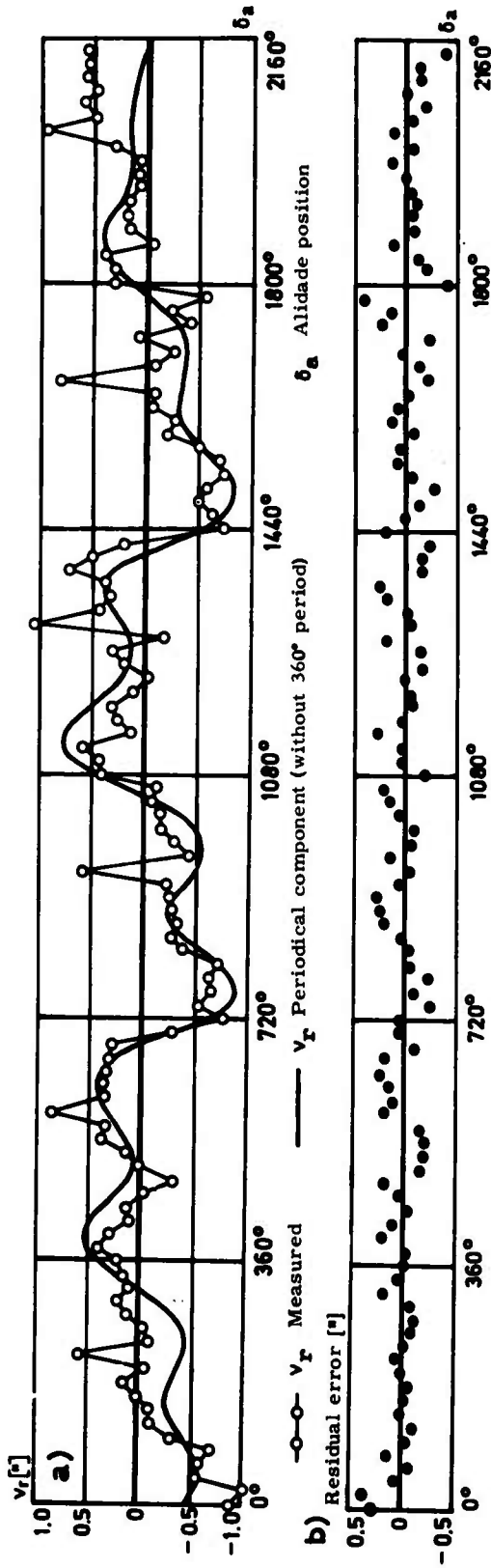


Figure 43a. Radial Component v_r of the Secondary Vertical Axis Error (Wild T4). 43b. Remaining Error According to Fourier Analysis

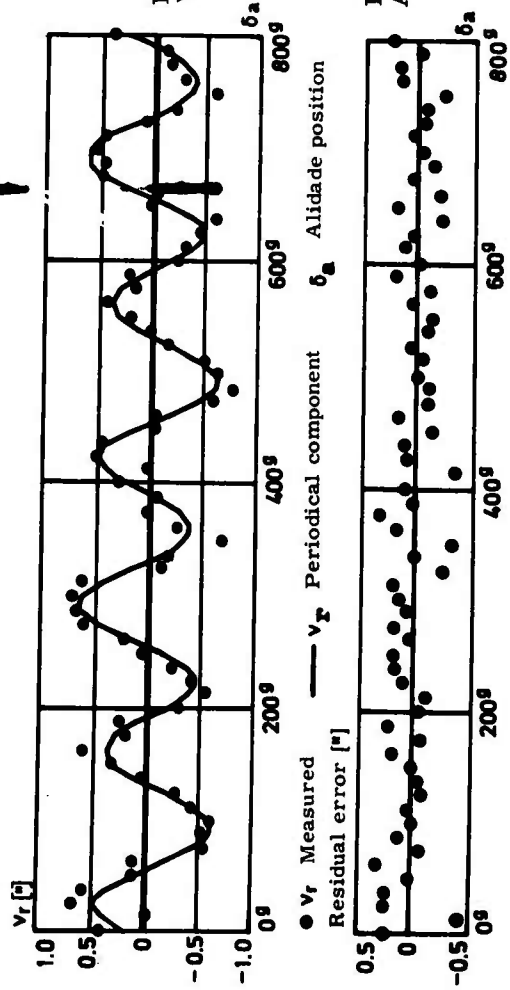


Figure 46a. Radial Component of the Secondary Vertical Axis Error of the Kern DKM3

Figure 46b. Residual Error According to Fourier Analysis

sources. Moreover, they should not be relinquished basically on the analysis of the v_r radial component which is the exclusive authority in slope measurements with the level.

Table 14. Summary of Results of Vertical Axis Investigations for the Wild T4 and the Kern DKM 3

Wobble Error	Error Type S-Systematic Z-Random	Extreme Values		Root Mean Square		Mean Rate of Increase		System Test	
		T4 ["]	DKM 3 ["]	T4 ["]	DKM 3 ["]	T4 ["/20"]	DKM 3 ["/25"]	T4	DKM 3
Total wobble error experimental	S+Z	1.11	0.84	0.53	0.60	-	-	-	-
Radial Component experimental theoretical residual	S+Z	1.06	0.76	0.43	0.40	0.35	0.32	HS	HS
	S	1.11	0.64	0.40	0.37	-	-	-	-
	Z	0.41	0.43	0.16	0.16	0.19	0.25	NS	NS
x-Component experimental theoretical random	S+Z	0.89	0.69	0.33	0.32	0.25	0.24	HS	HS
	S	0.65	0.42	0.29	0.29	-	-	-	-
	Z	0.45	0.34	0.17	0.13	0.19	0.21	NS	NS

As an example of error analysis the treatment of the v_r radial component of the Wild T4 (vertical axis slope $v \approx 2''$, counterclockwise rotation, alidade clamping) is more precisely illustrated. The component dependence on the alidade position is shown for six complete, unbroken, and successive alidade revolutions in Figure 43a. The errors are not reproducible according to Section 5.5.2, and show a highly significant system according to the arrangement test of Section 4.4.1. A Fourier analysis with the periods determined in Eq. (114) gives the amplitudes for individual error causes in Table 13.

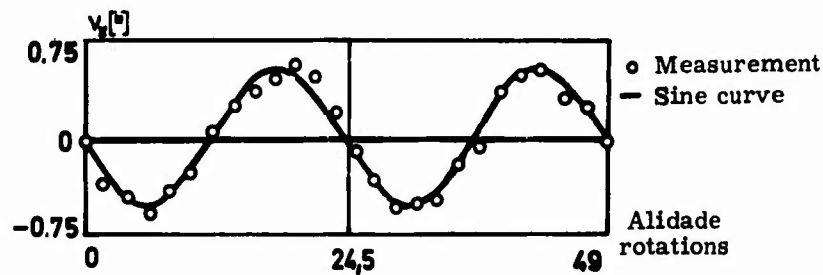


Figure 44. Wobble Error of the Vertical Axis (x-component) Because of the Inequality of Spherical Diameter (Wild T4)

In the Fourier term with the 784° period, the influence of the No. 4 error cause overlaps the influence of the unequal spherical diameter. This error cause can, however, be determined separately according to method 2a (Fig. 44); the amplitude A_1 determined by this method is $0.53''$, which is the period introduced as an unknown in agreement with the theoretical value of 24.5 revolutions. The result is confirmed by method 2b in which an amplitude of $0.51''$ is the result. The systematic error curve calculated on the basis of error causes 1, 4, 6, and 8 is also shown in Figure 43a. One reduces the measured radial component by this systematic influence.

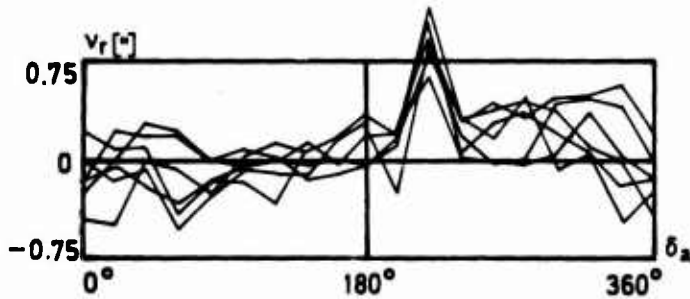


Figure 45. Error of Sliding Adjustment (360° period) After Reducing Residual Error (six revolutions)

There remains for each individual rotation the error of sliding adjustment with a period of 360° (Table 13, No. 7). The course of the error curve is evident from Figure 45 for six single revolutions; reproducibility is $0.19''$; the sharp wobble of $0.9''$ at the 220° point is noteworthy.

One reduces the mean wobble error further by eliminating the sliding adjustment error; thus in Figure 43b the remaining errors are shown (root mean square $0.16''$, extreme value $0.41''$); the distribution of the remaining error is incidental.

The analysis of the v_x x-component proceeds analogously to the described method. The results are from Appendix O, Tables 13 and 14.

If the results of all the analyses for single error causes are summarized, then the following is obtained: the wobble error (Table 13, No. 4) limited by an elliptical deformation of the axle-end pivot (cross section HH) or by a saddle-like deformation of the bearing (seat) cap amounts to $0.54'' \pm 0.12''$; the wobble error based on an elliptical deformation of the sleeve is about $0.50'' \pm 0.14''$; the mean error is calculated from the distribution of the results. Since in cross section H'H' no axle-end pivot elliptical deformation ($A_8 < 0.1''$) is observed, one can assume that the known wobble error under 4 is caused primarily by the saddle-like deformation of the bearing (seat) cap.

If one estimates the singly-ascertained error components in the corresponding linear quantity at about ($0.5'' \hat{=} 0.1 \mu\text{m}$), it is shown that no improvement in technical production is expected for error causes 1, 4, and 6. This was first produced by a particularly large axis diameter (up to 46mm).

In the Kern DKM3 the total wobble error of the vertical axis is about equal to that in the Wild T4. The component curve course (radial component v_r in Fig. 46a,

x-component v_x of App. Q) however, is significantly uniform and reproducible within $\pm 0.15''$. The curve of the radial component for the individual measurement series is given in Appendix P. The mean of all of the measurement series (Fig. 46a) is systematically highly significant and can be understood by the following Fourier series with a root mean square approximation of $\pm 0.18''$:

$$v_r = 0.14'' \sin(\delta_a + 169^\circ) + 0.51'' \sin(3\delta_a + 21^\circ).$$

δ_a = position of the alidade.

The distribution of the residual error is random (Fig. 46b). The Fourier term with the 720° period has an amplitude of $0.05''$ which is only slightly above the mean error of $\pm 0.03''$. An amplitude of $0.04''$ is given according to the 2b method so that, contrary to the Wild T4, no essential differences in the spherical diameter occur. The corresponding values for the x-components are presented in Appendix Q, in which the 120° period is converted into a 180° period on the basis of the relation between movable and stationary measuring systems. An essential correction of the Kern vertical axis system is therefore expected if the rings of the spherical tract that are without deformation are connected with the alidade or the substructure.

5.6 Horizontal Circle Reading Precision

Universal and transit instruments are distinguished primarily by the type and way by which a direction is fixed. In the transit instrument, precision of fixed direction depends entirely upon stability error, secondary axis error, and level error; while in the universal instrument, disc reading error is added to the other errors.* In the universal instrument, exclusively visual and photographic methods of disc reading become a problem today. Visual disc reading precision depends on the accuracy of coincidence, micrometer precision, and graduated disc precision.

a) Optical Micrometer Error

In comparison with the graduated disc of the geodetic instrument, the optical micrometer was previously assumed error-free, disregarding run. In Haller's work (1957) it is stated that the optical micrometer precision "can be almost randomly increased" by the designer. Later experiments have shown that micrometer of minute and second theodolites show considerable error (Dyer, 1958; Farkas, 1966). Therefore, since we are attempting to find the instrument producing the greatest accuracy, the micrometers of both universal instruments are integrated into the experiments.

The method for determining the mean coincidence error, the run, and the secondary micrometer error m_s are described in Section 4.1. The results of

*The error of "circle reading" is composed of the coincidence, the micrometer, and the graduated circle error.

Table 15. Results of the Micrometer Experiments

Instrument	Coincidence Precision		Run		Secondary Micrometer Error					System Test
	Disc Reading Measurement	Repetition Measurement*	Disc Reading Measurement	Normal Course	Number of Measurement Series	Points of Measurement	Root Mean Square	Maximum	Reproducibility	
T4	±0.22"	±0.16"	0.05"	0.19"	8	24	0.07"	0.16"	±0.1"	NS
DKM3	-	±0.21"	0.34"	-	4	30	0.13"	0.37"	±0.2"	SS

*From repeated measurements.

Table 16. Results of the Divided Circle Experiments (Wild T4)

	Fourier Terms	Extr. Value	Root Mean Square	Mean Increase	Systematic Test
Measured difference curve		0.61"	0.27"	0.13"/4.5°	HS
Residual error according to Fourier analysis	2, 4, 6	0.49"	0.18"	0.12"/4.5°	HS
	2, 4, 6, 8	0.38"	0.14"	0.12"/4.5°	HS
	2, 4, 6, 8, 18	0.29"	0.12"	0.11"/4.5°	S
Systematic diameter correction	2, 4, 6, 8, 18	0.39"	0.16"	-	-

Table 17. Results of the Level Experiments According to Wanach

Level No.	Calibration pars	Experiment Inter.	No. of Bubbles	Bubble Length		Specifications ["/pars] for		Mean Error F for			Maximum Level Error for 1 s. max			Quality Calculated by Wanach*
				b _{Min}	b _{Max}	b _{Min}	b _{Max}	b _{Min}	b _{Mean}	b _{Max}	b _{Min}	b _{Mean}	b _{Max}	
493 (T4)	10-90	1"	10	36.0	48.6	1.012	1.007	±0.29	±0.20	±0.05	1.44"	0.47"	0.15"	Poor (F > 0, 11)
693975 (DKM3)	3-38	2"	3	15.1	18.2	2.274	2.264	±0.30	±0.26	±0.14	0.95"	0.68"	0.43"	Poor (F > 0, 20)
202 (AP70)	0-70	2"	11	27.0	36.2	1.136	1.146	±0.19	±0.10	±0.10	0.47"	0.19"	0.24"	Sufficient

*For the mean bubble length

the experiments are given in Table 15 and Figure 47. A single determination of m_s to $\pm 0.15''$ resulted from the mean error of a double-coincidence of $\pm 0.2''$ and from the mean error of the autocollimation measurements of $\pm 0.05''$ by a 4-fold coincidence of the mean error m_o . In the Wild T4, the root mean square of the secondary micrometer error is $\pm 0.07''$; the distribution of error is random. The reproducibility m_Δ of the micrometer error can be concluded from reproducibility of the measurement series ($\pm 0.19''$) and the above-mentioned m_o at $0.1''$.

The micrometer error of the Kern DKM3 is at $\pm 0.13''$ greater than for the T4 and shows a sufficiently significant systematic distribution; the reproducibility of micrometer error corresponding to the above calculation is $\pm 0.2''$. The results raise the question of abandoning the application of calibration improvements in the DKM3 as well - especially since the distribution of reading points is, as a rule, appreciably random.

b) Divided Circle Error

Of the instruments discussed here, only the Wild T4 was previously studied (Schmidt, 1963) with reference to its divided circle error. Details on the divided circle precision of the DKM3 are given by Fondelli (1956). The results for the Wild T4 are presented in Table 16, Figure 48, and Appendix R.

The difference curve d [for definition, see Eq. (82)] is ascertained by a single experiment (using 40 measuring points) with an m_o accuracy of $\pm 0.11''$; m_o is calculated opposite the mean value from the distribution in four experiments (Appendix R). The new total calibration error is $\pm 0.27''$. The difference curve is considered systematically as highly significant and can be understood by the following Fourier series with a root mean square approximation m_q of $\pm 0.12''$:

$$d_s = 0.109'' \sin(2\delta_a + 217^\circ) + 0.157'' \sin(4\delta_a + 128^\circ) + 0.247'' \sin(6\delta_a + 270^\circ) + 0.131'' \sin(8\delta_a + 221^\circ) + 0.117'' \sin(10\delta_a + 315^\circ).$$

m_q gives the mean incidental calibration error. Because of error components with brief periods, the distribution of the residual error remains significantly systematic according to the arrangement test. Recalculation of the systematic components d_s of the difference curve gives the systematic diameter corrections $t_{s(H)}$ shown in Figure 48.

The mean error for $t_{s(H)}$ according to the formulas given by Wermann (1957) is $\pm 0.03''$; this value is viewed only as the internal precision of the Heuvelink method. The results of the Heuvelink method were confirmed by another author, Prof. Ramsayer, who developed a method based on the use of a polygon reflector. The systematic diameter corrections $t_{s(R)}$ ascertained according to this method of Kessler (1966) are shown in Figure 48. The root mean square of the difference $t_{s(H)} - t_{s(R)}$ is $0.09''$, the maximum deviation $0.19''$. The mean error for the

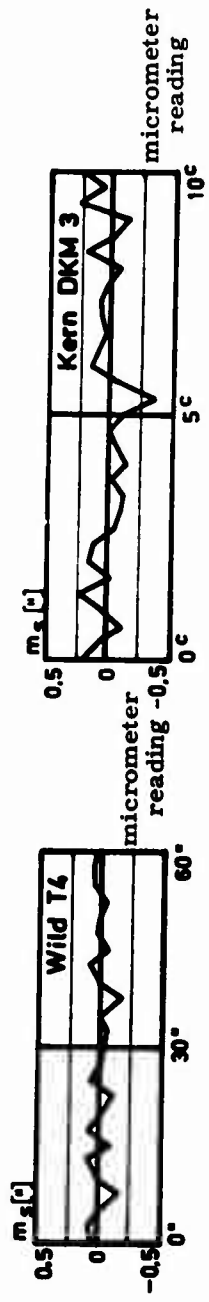


Figure 47. Secondary Micrometer Error for Wild T4 and Kern DKM3

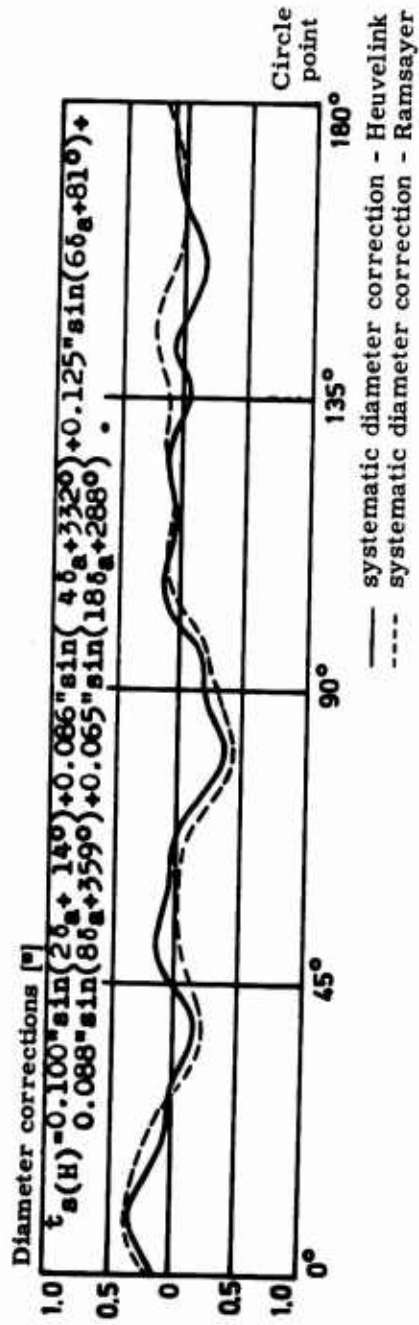


Figure 48. Diameter Corrections (Wild T4)

systematic diameter corrections according to Heuvelink lies below 0.1".

The investigation of Fondelli (1956), of three instruments of the DKM3 type, give a maximum total calibration error of 0.08". The systematic diameter corrections in no case exceeded 0.2". The precision experiments in Section 6 were based on a higher value.

5.7 Level Error

Accuracy experimentation for precision levels occupies a great deal of space in geodetic literature. First, if we go back to what was discussed earlier, the level error l [Eq. (58b)] determined as the calibration correction is brought into the measurements (Tarczy-Hornoch, 1961; Ramsayer, 1967). The aim of the present experiment is:

- a) to determine the dependency of the pars value on the bubble length and to obtain data on the accuracy of the three levels in question;
- b) to determine the size of the calibration correction dependent on position of the bubble center;
- c) and to determine the accuracy of the slope measurement in using the calibration correction.

For a) the measurements are evaluated best according to Wanach. The results are given in Table 17. The deviation of pars value with bubble length must be considered for all three levels, but above all in the DKM3 level, in cases of very different bubble lengths and in cases of large slope deviation. In the average bubble length the pars deviation per deviation for one pars of bubble length amounts to 0.0025"/pars for the Wild T4, 0.011"/pars for the DKM3, and 0.0010"/pars for the AP70 level. In the DKM3, in cases of large slope deviations, small deviations in bubble length must be considered for fixing the pars value.

The level precision is judged according to the "average focusing error" F defined by Wanach (1926) for a mean bubble length (average value of the secondary level error l_s corresponding to Equation (58b)). F is so great in the investigated levels that, according to the classification in Wanach (1926), only the level of the transit instrument can be given as "sufficient." A level calibration is somewhat awkward.

The determination and application of a calibration correction favorably proceeds according to the method of reduced cast lines (Ramsayer, 1967) which is based on Equation (58b). If the associated $p_0 \beta_0 - \alpha_0$ value of the C constant in Eq. (58b) is not given, but a random value is chosen favorable to the C_B value, which is estimated according to the bubble length B , then Equation (58b) can be given as:

$$l_r = \alpha - p_0 \beta + C_B. \quad (116)$$

i_r is different from the level error l only by a constant value $C_B - C$ for a determined bubble length. As an interpretative example, the level No. 493 of the Wild T4 is given in Figure 49.

The i_r values calculated according to Eq. (116) were plotted for the individual (as a rule, these are not concentric) bubble lengths dependent on the position of the bubble center and connected by an intervening curve E_{Bi} . E_{Bi} is the measured calibration curve. The determined spacing for the calibration values is thus to be selected by C_B , so that the two necessary interpolations can proceed easily and precisely. Between the measured calibration curves the E_{Bo} curves for concentric bubble lengths were interpolated. If one takes as a constant bubble length B the slope difference $\alpha_2 - \alpha_1$ measured at points β_2 and β_1 , then the result will proceed according to Eqs. (59) and (116):

$$\alpha_2 - \alpha_1 = p_0(\beta_2 - \beta_1) + l_2 - l_1 = p_0(\beta_2 - \beta_1) + l_{r_2} + C - C_B - l_{r_1} - C + C_B = p_0(\beta_2 - \beta_1) + l_{r_2} - l_{r_1} \quad (117)$$

Example (Fig. 49):

$$B = 38.6''; \alpha_2 - \alpha_1 = 12.0''; \beta_2 = 46.5''; \beta_1 = 34.0''; l_{r_2} = 1.0''; l_{r_1} = 1.5''; \\ 12.0'' = (46.5'' + 1.0'') - (34.0'' + 1.5'') = 12.0''.$$

The calibration curves clearly show that as the level error advances toward the end of the level, values greater than $1''$ are obtained.

In order to test the calibration and to study the precision of the calibration value, the following method was used: In a determined bubble length B a theoretical slope deviation $\alpha_2 - \alpha_1$ is set on the level tester, the displacement $\beta_2 - \beta_1$ of the level bubble is measured and corrected with the proper calibration values l_{r_2} and l_{r_1} , whereby l_{r_2} and l_{r_1} must be twice interpolated. The difference

$$\epsilon = (\alpha_2 - \alpha_1) - \left(\beta_2 + l_{r_2} - (\beta_1 + l_{r_1}) \right)$$

is perceived as a further slope measurement error; with its help the mean error m_0 under the application of calibration corrections can be calculated by a sufficient number of control tests. From 50 control tests, the distribution of which was presented earlier, m_0 amounts to $\pm 0.12''$. This result shows the usefulness of the method. It can be further stated that with "poor" levels at unfavorable ratios, that is, with small, varying bubble lengths and large slope deviation, good results can be obtained. The latter observation is valid for the DKM3 level and the transit instrument.

5.8 Inclination Components and Level Components of the Wobble Error in the Tilt Axis

In the instrument with a suspended level according to Eqs. (66b) and (67a) instead of the vertical components i_v of secondary tilt axis error, the level

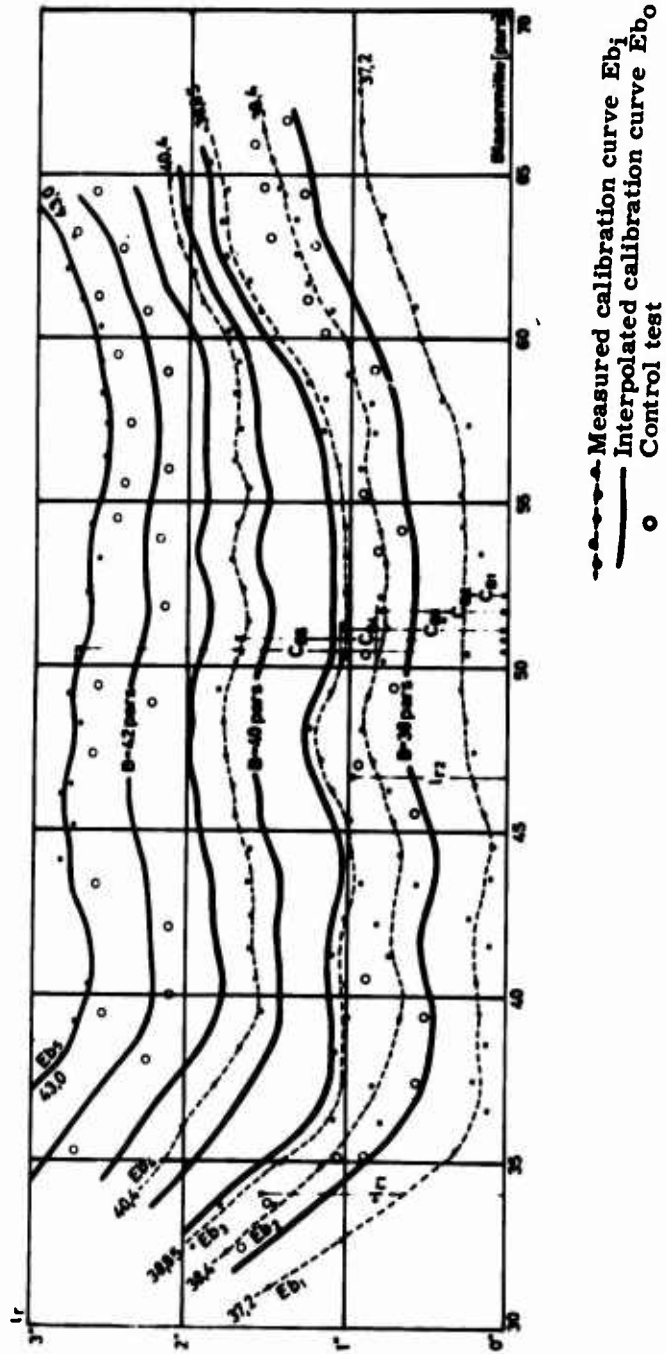


Figure 49. Level Error According to Reduced Cast Lines (Wild T4)

components i_L are calculated according to Eq. (69a). The slope components i_N are ascertained by successively varying the zenith distance of the telescope and reading the corresponding position of the level bubble (Mathias, 1961). On the basis of special experiments (simultaneous measurements of the slightest slope deviations with an autocollimator and level) it can be doubted that levels with slope deviation below $0.3''$ can be reliable. The determination of the systematic components of i_L is therefore demonstrated as being fundamentally difficult.

For both instruments with suspended levels the following can be stated: According to Section 5.4.2 in the Wild T4 the total systematic component of the vertical secondary tilt axis error i_V is caused by the seating of the tilt axis (seat component); therefore, no essential elliptical deformation of the tilt axis can be detected according to Section 5.4.1. The error of slope estimate which is based on the axis errors operating in the suspension position, is therefore to be viewed as random. In this way we can abandon the determination of i_N or i_L in the Wild T4. In the transit instrument the determined slope components i_N show a random distribution; the root mean square of i_N is $0.16''$ for the average of four measurement series (forward and reverse measurements). According to Section 5.4.2, the vertical secondary tilt axis error shows, nevertheless, no systematic component; so the calculation of level components in the transit instrument can also be abandoned.

5.9 Summary of Results and Conclusions

The results of Sections 5.1 through 5.7 are given together in Table 18. Generally corresponding to Eq. (90a, b, c) the mean total (\bar{m}) the mean systematic (\bar{m}_c) and the mean random (\bar{m}_Δ) instrument error are given. Therefore, it is only slightly significant that single values are to be given more precisely than $0.05''$. In heat deflection instead of the mean total error, the average heat deflection is quoted for both of the first two minutes after telescope focusing. The given level error is valid for a bubble length which is equal to half the calibration length.

The analysis is clearly expressed as: the systematic error component generally outweighs the random error component. It is shown that the three instruments presently under investigation differ from each other in a way which does not correspond to the previous conception.

The error that occurs can be avoided or reduced partly by means of practical, and partly by technically observed preventive measures. The following statements summarize the practical capabilities of the individual instruments:

Wild T4

The stability of the instrument is given by $\bar{m}_{ua} = \pm 0.05''$; the accuracy of the horizontal disc $\bar{m}_t = \pm 0.2''$ and the horizontal disc micrometer $\bar{m}_m = \pm 0.1''$ are demonstrated to be satisfactory.

Table 18. Summary of the Results of the Instrument Investigations

Instrument Error	Wild T 4			Kern DKM 3			Askania AP70			Technically Observed Preventive Measures For Eliminating Systematic Error
	Total Syst. ["]	Ran-dom ["]	Resid-ual ["]*	Total Syst. ["]	Ran-dom ["]	Resid-ual ["]	Total Syst. ["]	Ran-dom ["]	Resid-ual ["]	
Azimuthal substructure rotation v_a	0.05	-	0.05	0.15	-	0.1	0.15**	-	0.1	DKM 3: see Section 5.1 AP70: observation without support
Azimuth rolling defect w_e	0.6	0.6	0.2	0.1	0.05	0.1	0.25	0.2	0.1	Observation in 2 TP Focusing of $z = 0$ Single oscillation
Heat deflection b of the telescope	0.85	0.35		0.25	0.15		0.45	0.25		Observation in 2 TP Heat insulation
Divided circle error t	0.2	0.15	0.15	0.15	0.1	0.15	-	-	-	Observation method Correction intro-duction
Micrometer error m	0.1	0.05	0.1	0.25	0.15	0.2	-	-	-	
Level error l	0.2	-	0.1	0.25	-	0.15	0.15	-	0.1	Calibration of level modif. of meas. field
Secondary tilt axis err. Azimuth i_a Vertical i_v	0.45 0.35	0.4 0.3	0.45 0.35	0.2 0.2	0.15 0.1	0.15 0.15	0.3 0.3	0.25 0.2	0.2 0.3	Correction intro-duction Arrangement ob-servation
Secondary vertical axis error Radial component v_r	0.45	0.4	0.45	0.4	0.35	0.2	-	-	-	Level reading Correction intro-duction

*Error remaining after using the observed technical preventive measures

**With or without support

† For DKM 3 taken from Fondelli (1956)

The surprisingly large azimuth rolling defect ($\bar{m}_{we} = \pm 0.6''$) can be eliminated if the tilt axis is supported in a closed seat. The heat deflection of the telescope ($b = 0.85''$), which is of particular importance in steep reference points, demonstrates the need for a suitable tube heat insulation. In the tilt axis system the behavior of the (well-operating) tilt axis is found unfavorable in the spherical seat, with values of ($\bar{m}_{ia} = \pm 0.45''$, $\bar{m}_{iv} = \pm 0.35''$); the determination of azimuth wobble error for the purpose of employing the corresponding calibration corrections in the observations is not very significant, since the opposite position of the spherical seat is altered by each new position of the instrument. The semikinematic vertical axis system cannot be completely satisfactory ($\bar{m}_{vr} = \pm 0.45''$) because of the small spherical tract dimension; the wobble error is not reproducible. The suspended level shows a very large unsatisfactory error of ($\bar{m}_1 = \pm 0.2''$, $l_{max} = 0.5''$) in the marginal zones.

In all it can be stated that the great dimension of the instrument introduces disadvantages that hinder the increase in precision measurement expected by the designer.

Kern DKM 3:

Instrument stability is satisfactory ($\bar{m}_{ua} = \pm 0.15''$) and the tilt axis stability is calculated as ($\bar{m}_{we} = \pm 0.1''$); tilt axis precision is found to be entirely satisfactory ($\bar{m}_{ia} = m_{iv} = \pm 0.2''$) in spite of the comparatively small length of the tilt axis (150mm). The heat deflection of the telescope is insignificant ($b = 0.25''$).

The horizontal disc micrometer is in need of correction ($\bar{m}_m = \pm 0.25''$). The vertical axis system ($\bar{m}_{vr} = \pm 0.4''$) can be corrected if the spherical tract is combined without deflection to the supports above and below. A strong data dependency on bubble length (the deviation of the pars value per one bubble length deviation is equal to $0.11''$) is found in the level. The slide surface cannot satisfy the requirements of astronomical position finding ($\bar{m}_1 = \pm 0.25''$, $l_{max} = 0.7''$).

Askania AP70:

The support stability with the disc-support substratum is not altogether satisfactory ($\bar{m}_{ua} = \pm 0.15''$). The tilt axis stability ($\bar{m}_{we} = \pm 0.25''$) should be corrected as much as possible by a friction control. The heat deflection ($b = 0.45''$) of the telescope can be reduced by heat insulation as in the Wild T4. The tilt axis precision ($\bar{m}_{iu} = \bar{m}_{iv} = \pm 0.3''$) does not correspond to the expectations that were based on the large axis dimension (430mm). The level precision is satisfactory ($\bar{m}_1 = \pm 0.15''$, $l_{max} = 0.2''$).

In Table 18 technical preventive measures are given by which the user can essentially reduce the determined error. To be sure, each user does not have at his disposal the appropriate equipment to determine, for example, the secondary tilt axis error. In the column "residual" error, every error is shown that remains after the preventive measures were taken. A comparison between the residual and the total error shows that these preventive measures operate very effectively.

6. THE INFLUENCE OF INSTRUMENTAL ERRORS ON THE ACCURACY OF HORIZONTAL ANGLE MEASUREMENTS AND DETERMINATIONS OF ASTRONOMICAL POSITIONS

Based on the results of Section 5, the influence of instrumental errors on geodetical horizontal angle measurements and on selected methods of astronomical position determinations will be discussed in the following. Particularly interesting is the question of whether the accuracy of modern universal instruments can meet the requirements of exact determinations of astronomical positions or if instruments and methods without divided circles can be used for such purposes in the future - as mentioned in Niethammer's work (1947).

The instrumental errors introduced in Section 3 can be classified into two groups according to their effects and characteristics. The first group consists of those errors which can be eliminated completely by making the observation with two telescope positions. To this group belong the primary target error C and the error of the tilt axis i as well as the symmetric part of the thermal deflection b . c and i will not be mentioned in the following derivations any longer since the observations will always be performed for two telescope positions. The second group contains the secondary instrumental errors which have mainly a systematic character generally, as shown in Section 5. The systematic part of the error can vary and depends both in sign and magnitude on a definite parameter. The individual instrumental errors listed on pages 79 and 80 depend on the following parameters:

<u>Error</u>	<u>Parameter</u>
Substructure rotation u_a	amount and direction of alidade rotation
Roll error w_a , w_l , and w_{iL}	amount and direction of telescope rotation
Diameter error t	position of reading on divided circle (target azimuth)
Micrometer error m	position of reading on micrometer (target azimuth)
Level error l	leveling and azimuth of target
Primary horizontal axis inclination v' in the direction of the tilt axis	leveling and azimuth of target
Secondary tilt axis errors i_a , i_v , and level component i_L	zenith-distance of target
Secondary horizontal axis errors v_s in the direction of tilt axis	azimuth of target

Principally, the measurements have to be arranged in a way, that is, the parameters have to be chosen in such a way, that the systematic errors are completely or partly eliminated or - if this is not possible - that they lose their systematic character by a proper variation of the parameter. This precaution causes a reduction of the systematic error by repeated measurements, analogous to precautions for the random error.

Among the above mentioned parameters the positions of the readings on the divided circle and on the micrometer as well as the leveling can be changed independent of the target distribution. The zenith-distance and the azimuth of the target can be chosen freely in astronomical observations except in a few cases (for example, polar azimuth). This is not possible in terrestrial measurements which means that the possibilities of reducing the systematic errors are restricted. The alidade and telescope notations depend on the distribution of the targets as well as on the method of observation so that the corresponding systematic errors can be eliminated or reduced even in terrestrial measurements.

Besides the purely instrumental errors, the errors of reading off the circular and level positions a_b and l_a , the aiming error z_a and the secondary target axis error c_a have to be mentioned. These errors are going to be considered as random in the following examples which is generally true for a_b , l_a , and z_a .

Because of the mainly systematic character of the instrumental errors, their influence on the quantities to be observed and their functions cannot be calculated using merely the classical law of error propagation. Rather, an equation valid for the simultaneous propagation of incidental and systematic errors has to be derived from each individual case (Bohm, 1967). For this it is necessary to know the observation procedure, the effect of the errors, and the magnitude of the random and systematic error. The treatment of complicated functions is so involved, however, that only simple cases will be considered in the following sections. First, of all, the principle of the calculation, taking into account random and systematic errors simultaneously, will be shown in its general formulation in Section 6.1. It is recommended to follow the simple example given in Section 6.2.1 together with the individual steps of the derivation to get a better understanding of the procedure.

6.1 Simultaneous Propagation of Random and Systematic Errors

A function f of n observables l_i

$$f = g(l_1, l_2, \dots, l_1, \dots, l_n) \quad (118)$$

changes by df if the observables are changed by dl_i :

$$df = \frac{\partial g}{\partial l_1} dl_1 + \frac{\partial g}{\partial l_2} dl_2 + \dots + \frac{\partial g}{\partial l_1} dl_1 + \dots + \frac{\partial g}{\partial l_n} dl_n = g_1 dl_1 + g_2 dl_2 + \dots + g_1 dl_1 + \dots + g_n dl_n. \quad (119)$$

Let quantity dl_i be connected with the k instrumental errors ϵ_{ij} by the function h_{ij} in the following way:

$$dl_i = h_{i1} \epsilon_{i1} + h_{i2} \epsilon_{i2} + \dots + h_{ij} \epsilon_{ij} + \dots + h_{ik} \epsilon_{ik}. \quad (120)$$

The index i signifies the observable and the index j the instrumental error. ϵ_{ij} will be split up in the following into a random and systematic part, Δ_{ij} and c_{ij} , respectively, according to Eq. (83). If we put Eq. (120) into Eq. (119) and call f the product of the coefficients g and h

$$f_{ij} = g_i h_{ij}, \quad (121)$$

we get:

$$\begin{aligned} df = & f_{11} (\Delta_{11} + c_{11}) + f_{12} (\Delta_{12} + c_{12}) + \dots + f_{1k} (\Delta_{1k} + c_{1k}) + \\ & f_{21} (\Delta_{21} + c_{21}) + f_{22} (\Delta_{22} + c_{22}) + \dots + f_{2k} (\Delta_{2k} + c_{2k}) + \\ & \vdots \\ & f_{n1} (\Delta_{n1} + c_{n1}) + f_{n2} (\Delta_{n2} + c_{n2}) + \dots + f_{nk} (\Delta_{nk} + c_{nk}). \end{aligned} \quad (122)$$

In all of the following examples f_{ij} is either a constant or a function of the zenith-distance. Considering the random error contribution in Eq. (122) and ordering the terms for $j = \text{const}$ we get:

$$\begin{aligned} df_{\Delta} = & f_{11} \Delta_{11} + f_{21} \Delta_{21} + \dots + f_{n1} \Delta_{n1} + f_{12} \Delta_{12} + f_{22} \Delta_{22} + \dots + f_{n2} \Delta_{n2} + \dots + \\ & f_{1j} \Delta_{1j} + f_{2j} \Delta_{2j} + \dots + f_{nj} \Delta_{nj} + \dots + f_{1k} \Delta_{1k} + f_{2k} \Delta_{2k} + \dots + f_{nk} \Delta_{nk}. \end{aligned} \quad (122a)$$

The error propagation law can be applied to Eq. (122a) so that the mean random error $m_{f_{\Delta}}$ can be calculated:

$$m_{f_{\Delta}}^2 = \left[f_{11}^2 \right]_{i=1}^n \bar{m}_{\Delta 1}^2 + \left[f_{12}^2 \right]_{i=1}^n \bar{m}_{\Delta 2}^2 + \dots + \left[f_{1j}^2 \right]_{i=1}^n \bar{m}_{\Delta j}^2 + \dots + \left[f_{1k}^2 \right]_{i=1}^n \bar{m}_{\Delta k}^2. \quad (123)$$

$\bar{m}_{\Delta j}$ is calculated according to Section 4.4.

In some of the following examples the coefficients f_{ij} differ only in sign for $j = \text{const}$, that is, for the same instrumental error.

$$|f_{ij}| = |f_{i+1,j}| = |f_j|. \quad (121a)$$

Equation (123) becomes then

$$m_{f_{\Delta}}^2 = n f_1^2 \cdot \bar{m}_{\Delta 1}^2 + n f_2^2 \cdot \bar{m}_{\Delta 2}^2 + \dots + n f_j^2 \cdot \bar{m}_{\Delta j}^2 + \dots + n f_k^2 \cdot \bar{m}_{\Delta k}^2 = n \left[f_j^2 \cdot \bar{m}_{\Delta j}^2 \right]_{j=1}^k. \quad (123a)$$

For the systematic part in Eq. (122) we have analogous to Eq. (122a)

$$df_c = (f_{11} c_{11} + f_{21} c_{21} + \dots + f_{n1} c_{n1}) + (f_{12} c_{12} + f_{22} c_{22} + \dots + f_{n2} c_{n2}) + \dots + f_{1j} c_{1j} + f_{2j} c_{2j} + \dots + f_{nj} c_{nj} + (f_{1k} c_{1k} + f_{2k} c_{2k} + \dots + f_{nk} c_{nk}). \quad (122b)$$

For the special case according to Eq. (121a) holds

$$df_c = f_1 (c_{11} + c_{21} + \dots + c_{n1}) + f_2 (c_{12} + c_{22} + \dots + c_{n2}) + \dots + f_j (c_{1j} + c_{2j} + \dots + c_{nj}) + \dots + f_k (c_{1k} + c_{2k} + \dots + c_{nk}). \quad (122c)$$

In Eqs. (122b) and (122c) it has to be investigated in detail how the individual errors c_{ij} and the corresponding coefficients f_{ij} within the error group j are influenced by the experimental setup. With a given experimental setup p_j error groups can be formed for a certain instrumental error j . Within these error groups there are always some errors c_{ij} equal:

$$c_{ij} = c_{i+1,j} = c_{i+2,j} \dots = C_{ij}, \quad (124a)$$

for example, $c_{11} = c_{21} = C_{11}$. Therefore, the coefficients f_{ij} within the groups can be combined:

$$f_{ij} + f_{i+1,j} + \dots = F_{ij}, \quad (124b)$$

for example, $f_{11} + f_{12} = F_{11}$. In the case when several errors c_{ij} are eliminated by the experimental setup $F_{ij} = 0$. With Eqs. (124a) and (124b) we obtain for Eq. (122b):

$$df_c = (F_{11} C_{11} + F_{21} C_{21} + \dots + F_{p_1,1} C_{p_1,1}) + (F_{12} C_{12} + F_{22} C_{22} + \dots + F_{p_2,2} C_{p_2,2}) + \dots + (F_{1j} C_{1j} + F_{2j} C_{2j} + \dots + F_{p_j,j} C_{p_j,j}) + \dots + (F_{1k} C_{1k} + F_{2k} C_{2k} + \dots + F_{p_k,k} C_{p_k,k}). \quad (125)$$

Equation (125) represents the actual influence of the systematic errors on the function f for a certain experimental setup. Furthermore, there exists the possibility of varying parameters of the systematic errors, that is, the experimental setup, in such a way that the remaining systematic errors have a quasi-random distribution. The error propagation law can be applied to Eq. (125) according to Eq. (123):

$$m_{fc}^2 = [F_{11}^2]_{i=1}^{p_1} \bar{m}_{C_1}^2 + [F_{12}^2]_{i=1}^{p_2} \bar{m}_{C_2}^2 + \dots + [F_{1j}^2]_{i=1}^{p_j} \bar{m}_{C_j}^2 + \dots + [F_{1k}^2]_{i=1}^{p_k} \bar{m}_{C_k}^2. \quad (123b)$$

\bar{m}_{C_j} is calculated according to Section 4.4. By means of the experimental setup and certain observation procedures listed in Table 18, one can usually achieve that the systematic errors C_{ij} are not fully effective. Therefore, the mean systematic

error \bar{m}_{Cj} in Eq. (123b) has to be reduced. The degree of reduction will be expressed by the reduction factor r_j . r_j gives the ratio by which the individual mean systematic errors \bar{m}_{Cj} in Eq. (123b) actually occur. r_j has to be estimated in the individual cases according to the special setup and method of observation. Equation (123b) can be written, therefore:

$$m_{fc}^2 = \left[F_{i1}^2 \right]_{i=1}^{p1} (r_1 \bar{m}_{C1})^2 + \left[F_{i2}^2 \right]_{i=1}^{p2} (r_2 \bar{m}_{C2})^2 + \dots + \left[F_{ij}^2 \right]_{i=1}^{pj} (r_j \bar{m}_{Cj})^2 + \dots + \left[F_{ik}^2 \right]_{i=1}^{pk} (r_k \bar{m}_{Ck})^2. \quad (123c)$$

The main systematic error m_{fc} can be reduced in the same way as the mean random error by repeated measurements if the assumption of a quasi-random distribution of parameters is justified. If this assumption does not hold Eq. (123a) can be used according to Bohm (1967) to estimate the influence of the systematic errors on the function. In this case the mean systematic error cannot be reduced, of course, by repeated measurements.

The described procedure will be illustrated by a simple example in the next section, the measurements of horizontal angles by horizontal aiming.

6.2 Accuracy of the Measurement of a Horizontal Angle

6.2.1 HORIZONTAL ANGLE MEASUREMENTS BY HORIZONTAL AIMING

In triangulations of high accuracy the inclination of the rays to the object is so small usually that horizontal rays can be assumed for the theoretical investigation of the errors. The angle α between two objects can be calculated according to

$$\alpha = \frac{1}{2} (a_1 + a_2) - \frac{1}{2} (a_3 + a_4). \quad (126)$$

a_1 = direction at telescope position (TP) I for target 1,

a_2 = direction at TP II for target 1

a_3 = direction at TP I for target 2

a_4 = direction at TP II for target 2.

The influence of a change of direction da_1 on the angle α is given by

$$d\alpha = \frac{1}{2} da_1 + \frac{1}{2} da_2 - \frac{1}{2} da_3 - \frac{1}{2} da_4. \quad (127)$$

Equation (127) corresponds to Eq. (119) with $n = 4$. da_1 is connected with the individual instrumental errors according to Eq. (64a) in the following way:

$$da_i = \left(u_{ai} + a_{bi} + t_i + m_i + i_{ai} + w_{ai} \right) + \left(c_{ai} + b_i + z_{ai} \right) / \sin z_i + \left(i_{vi} + w_{i i} + v_i \sin (a_{vi} - a_i) \right) \cdot \cotan z_i. \quad (128)$$

According to the remarks to Section 6 the primary target and tilt axis errors are not contained in Eq. (128) because they can be eliminated completely by observations with two telescope positions. Equation (128) corresponds to Eq. (120) with $k = 12$. If the random error contribution in Eq. (128) is denoted by a single primed quantity and the systematic one by a double primed quantity we get for the random part according to Eq. (122a).

$$d\alpha' = \frac{1}{2} \left(\left[u_{ai}' \right]_{i=1}^4 + \left[a_{bi}' \right]_{i=1}^4 + \left[t_i' \right]_{i=1}^4 + \left[m_i' \right]_{i=1}^4 + \left[i_{ai}' \right]_{i=1}^4 + \left[w_{ai}' \right]_{i=1}^4 + \left[c_{ai}' \right]_{i=1}^4 + \left[b_i' \right]_{i=1}^4 + \left[z_{ai}' \right]_{i=1}^4 \right). \quad (129)$$

Because of $z = 90^\circ$, that is, $\cotan z = 0$, the last term representing the influence of the inclination does not appear in Eq. (129) anymore. The coefficients f_{ij} have the value $\pm 1/2$. The mean accidental error of α is obtained according to Eq. (123a):

$$m_\alpha'^2 = m_{ua}'^2 + m_{ab}'^2 + m_t'^2 + m_m'^2 + m_{ia}'^2 + m_{wa}'^2 + m_{ca}'^2 + m_b'^2 + m_{za}'^2. \quad (130)$$

In the treatment of the systematic errors one has to realize that the rotation of the substructure u_a and the micrometer error m do not have a systematic part. If one further assumes - as already mentioned - that the error of reading off from the divided circle a_b , the aiming error z_a and the secondary target axis error c_a have a random nature, the systematic part $d\alpha''$ can be obtained from Eqs. (127) and (128):

$$d\alpha'' = \frac{1}{2} \left(t_1'' + t_2'' - t_3'' - t_4'' + i_{a1}'' + i_{a2}'' - i_{a3}'' - i_{a4}'' + w_{a1}'' + w_{a2}'' - w_{a3}'' - w_{a4}'' + b_1'' - b_2'' - b_3'' + b_4'' \right). \quad (131)$$

The following remark has to be made concerning the individual errors in Eq. (131): The diameter errors t_1'' and t_2'' are the same for the Wild T4, as well as t_3'' and t_4'' . The azimuthal secondary error of the tilt axis i_{a1}'' is a function of the zenith-distance, that is, $i_{a1}''(z = 90^\circ) = i_{a3}''(z = 90^\circ)$ and so on; the roll error w_a is a function of the change of the zenith distance and of the direction of rotation, that is, $w_{a1}'' = w_{a3}'' \dots$; the thermal deflection b_1 is the same if the observation is performed for two telescope positions, that is, $b_1'' = b_2'' \dots$. Only the diameter error $t''(a)$ remains in the systematic error contribution in Eq. (131). It is for

$$\text{the Wild T4: } d\alpha'' = \frac{1}{2} \left(2t_1''(a_1) - 2t_2''(a_3) \right), \quad (132a)$$

$$\text{the DKM3: } d\alpha'' = \frac{1}{2} \left(t_1''(a_1) + t_2''(a_1 + 180^\circ) - t_3''(a_3) - t_4''(a_3 + 180^\circ) \right). \quad (132b)$$

Equations (132a, b) correspond to Eq. (125). If the places where the readings are taken would be varied so that the variable systematic errors i^n obtain random character, the following mean systematic error m_α^n would have to be used in the calculation according to Eq. (123b):

$$\text{Wild T4: } m_\alpha^n = 2m_t^n; \quad \text{DKM3: } m_\alpha^n = m_t^n. \quad (130a)$$

m_α^n would be reduced by $1/s$ by the averaging corresponding to m_α' if s is the number of sets of angle measurements. In reality, the circle is shifted by $180^\circ/s$, or $360^\circ/s$, respectively, so that the $(s-1)$ first terms of the series [Eq. (88)] are eliminated. The reduction of the systematic diameter error is expressed corresponding to Eq. (123c) by the reduction factor r_t which depends on s in this case. Therefore, we get for Eq. (130a)

$$\text{Wild T4: } m_\alpha^n = 2(r_t m_t^n)^2; \quad \text{DKM3: } m_\alpha^n = (r_t m_t^n)^2. \quad (130b)$$

Only the random errors are, therefore, significant for the accuracy of horizontal angle measurement with horizontal aiming. With Eq. (130) and the numerical values in Appendix S we get for the mean error of a single measurement of the angle α for the Wild T4 $\pm 0.61''$ and for the DKM3 $\pm 0.57''$. Those numbers agree with the values which were obtained in actual measurements (Weigand, 1964).

6.2.2 HORIZONTAL ANGLE MEASUREMENTS WITH INCLINED AIMING

Contrary to the above treated problem, the systematic errors in horizontal angle measurements where the rays are inclined very much appear markedly. This case cannot be treated as exactly as the previous angle measurements with horizontal aiming.

The target 1 may be observed under a zenith-distance z_1 , the target 2 with z_2 . Starting with Eqs. (127) and (128), the inclination of the horizontal axis effective momentarily in the direction of the tilt axis $\nu_i \sin(a_{\nu i} - a_i)$ is replaced in Eq. (128) by the radial component ν_{pr} and ν_r of the primary or secondary, respectively, error of the horizontal axis. Then the mean random error m_α' of a single measurement of α can be obtained according to Eq. (123) from the expression:

$$m_\alpha'^2 = (m_{ua}^2 + m_{ab}^2 + m_t^2 + m_m^2 + m_{ia}^2 + m_{wa}^2) + (m_{ca}^2 + m_b^2 + m_{za}^2) \left(\frac{1}{2 \sin^2 z_1} + \frac{1}{2 \sin^2 z_2} \right) + (m_{iv}^2 + m_{wi}^2 + m_{vr}^2) \cdot (\cotan^2 z_1 + \cotan^2 z_2) / 2. \quad (133a)$$

With regard to the systematic errors two groups have to be distinguished: In the first group the systematic errors are included which can be converted into quasi-random

errors by variation of the parameters (shifting of the divided circle, change of the sequence in the aiming and change of the leveling between the individual sets of measurements). For this group Eq. (123c) is valid without limitations.

$$m_{\alpha}^{\prime\prime 2} = 2(r_t m_t^{\prime\prime})^2 + (r_{wa} m_{wa}^{\prime\prime})^2 + \left((r_{wi} m_{wi}^{\prime\prime})^2 + (r_{vpr} m_{vpr}^{\prime\prime})^2 \right) (\cotan^2 z_1 + \cotan^2 z_2) / 2. \quad (133b)$$

In the second group (secondary axis errors exclusively) the parameters (azimuth and zenith-distance of the targets) cannot be varied so that Eq. (123c) can only be used to estimate the influence of the secondary axis errors on α according to the remarks of Section 6.1:

$$m_{\alpha}^{\prime\prime 2} = (r_{ia} m_{ia}^{\prime\prime})^2 + \left((r_{iv} m_{iv}^{\prime\prime})^2 + (r_{vr} m_{vr}^{\prime\prime})^2 \right) \cdot (\cotan^2 z_1 + \cotan^2 z_2) / 2. \quad (133c)$$

Equations (133a, b, c) are used in the following to calculate the mean total error of the angle α between the targets 1 and 2. Let the zenith-distance of target 1 be 75° and the zenith-distance of target 2 vary between 90° and 30° . With the numerical values for the individual mean systematic errors and the estimated reduction factors in Appendix S we obtain the mean errors for the instruments T4 and DKM3 as shown in Figure 50.

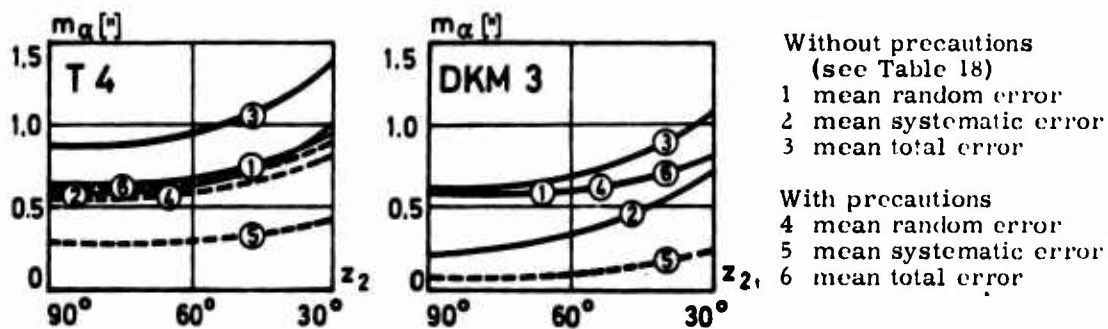


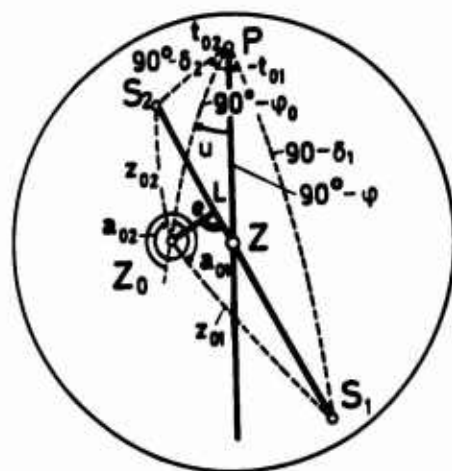
Figure 50. Mean Error of an Angle α at Very Different Zenith-Distances of the Aims

It is obvious from the figure that the systematic errors at very different zenith-distance of the targets have a great influence on the accuracy of the angular measurement.

6.3 The Influence of Instrumental Errors on the Accuracy of Determinations of Astronomical Positions

6.3.1 POSITION DETERMINATION FROM VERTICAL PASSAGES WITH A TRANSIT INSTRUMENT

The geographical longitude and latitude of a position can be determined by observing the time of passage of stars through an instrument vertical. If both coordinates should be determined by this method, the passage of the stars through two or more different verticals must be observed. For the error calculation the method of the so-called vertical base lines is used, according to Ramsayer (1967). In this method a base line is derived from the passage of a pair of stars through an instrument vertical and the zenith is defined by the intersection of two base lines. The base line S_1ZS_2 of the pair S_1 and S_2 is determined as follows (Fig. 51): Close to the zenith Z , a reference point Z_0 is chosen with the latitude φ_0 and the time angle u where u corresponds to the clock time. From the observations of the time of passage the time angles t_{01} and t_{02} relative to the meridian of Z_0 the zenith-distance z_{01} and z_{02} and the azimuths a_{01} and a_{02} can be calculated.



Legend

- a = azimuth
- z = zenith-distance
- t = time angle
- φ = geographical latitude
- δ = declination

Figure 51. Determination of Position with Vertical Base Lines

The distance e of the reference point Z_0 from the vertical S_1Z can be obtained from:

$$e = - \frac{\sin z_{01} \cdot \sin z_{02}}{\sin (z_{01} - z_{02})} (a_{02} - a_{01}) \quad (134)$$

The sign of z_{01} shall always be positive; the sign of z_{02} shall be positive if S_1 and

S_1 are at the same side of the zenith and negative if S_1 and S_2 are on different sides of the zenith. With the azimuth $a_{O_2} + 90^\circ$ and e the pole L and $-$ vertical to Z_0L through L - the base line S_1ZS_2 can be constructed. The zenith Z is obtained as the intersection of two base lines which are as vertical as possible to each other. If longitude and latitude are given, Z is obtained as the intersection of the base line with the known circle of latitude or meridian, respectively. The pair of stars is placed best on the meridian (meridian time) or in the first vertical (determination of latitude by observation of the passage through the 1. vertical). For an estimate of the errors it is sufficient to determine the influence of the different errors on the quantity e . In Eq. (134) it is assumed that:

- 1) the verticals through S_1 and S_2 make an angle of 180°
- 2) the inclination of the tilt axis is zero, and
- 3) there are no aiming or target axis errors.

Since there exist primary as well as secondary instrumental errors the calculated azimuths a_{O_1} and a_{O_2} have to be corrected according to Eq. (67a). In Eq. (67a), as well as in Eq. (64b), the error group with the factor 1 will be denoted by O (orientation component), the group of secondary errors with the factor $1/\sin z$ by C (target axis component), and the group of secondary errors with the factor $\cotan z$ by J (inclination component). Further, the first index in the instrumental errors refers to the star, the second to the telescope position. Then Eq. (134) can be written in the following way, taking into account Eq. (67a) and using the notation O , C , and J :

$$e = -\frac{\sin z_{O_1} \cdot \sin z_{O_2}}{\sin(z_{O_1} - z_{O_2})} \left(a_{O_2} + \frac{1}{2} (O_{21} + O_{22}) + \frac{1}{2} (C_{21} + C_{21} - C_{22} - C_{22}) / \sin z_{O_2} \right. \\ \left. + \frac{1}{2} (n_{21} + J_{21} - n_{22} - J_{22}) \cdot \cotan z_{O_2} - a_{O_1} - \frac{1}{2} (O_{11} + O_{12}) - \frac{1}{2} (C_{11} + C_{11} - C_{12} - C_{12}) / \sin z_{O_1} \right. \\ \left. - \frac{1}{2} (n_{11} + J_{11} - n_{12} - J_{12}) \cdot \cotan z_{O_1} \right). \quad (135)$$

Considering the influence of the primary errors on e , one obtains from Eq. (135) after transforming the coefficients:

$$e_p = -\frac{\sin z_{O_1} \sin z_{O_2}}{\sin(z_{O_1} - z_{O_2})} (a_{O_2} - a_{O_1}) + \frac{1}{2} \frac{\sin z_{O_2}}{\sin(z_{O_1} - z_{O_2})} (C_{11} - C_{12}) - \frac{1}{2} \frac{\sin z_{O_1}}{\sin(z_{O_1} - z_{O_2})} (C_{21} - C_{22}) \\ - \frac{1}{2} \left(\frac{1}{2} + \frac{1}{2} \frac{\sin(z_{O_1} + z_{O_2})}{\sin(z_{O_1} - z_{O_2})} \right) \cdot (n_{21} - n_{22}) - \frac{1}{2} \left(\frac{1}{2} - \frac{1}{2} \frac{\sin(z_{O_1} + z_{O_2})}{\sin(z_{O_1} - z_{O_2})} \right) \cdot (n_{11} - n_{12}). \quad (135a)$$

Equation (135a) agrees with the corresponding equation in Ramsayer's work (1967) if $-(n_{11} - n_{12})/2$ is denoted by i_1 and $-(n_{21} - n_{22})/2$ by i_2 and if one considers that $c_{ij} = c = \text{const}$. The influence d_e of the secondary instrumental errors can be obtained from Eq. (135) in an analogous way:

$$\begin{aligned}
d_e = & -\frac{1}{2} \frac{\sin z_{O_1} \sin z_{O_2}}{\sin(z_{O_1} - z_{O_2})} (O_{21} + O_{22} - O_{11} - O_{12}) + \frac{1}{2} \frac{\sin z_{O_2}}{\sin(z_{O_1} - z_{O_2})} (C_{11} - C_{12}) \\
& - \frac{1}{2} \frac{\sin z_{O_1}}{\sin(z_{O_1} - z_{O_2})} (C_{21} - C_{22}) - \frac{1}{2} \left(\frac{1}{2} + \frac{1}{2} \frac{\sin(z_{O_1} + z_{O_2})}{\sin(z_{O_1} - z_{O_2})} \right) (J_{21} - J_{22}) \\
& - \frac{1}{2} \left(\frac{1}{2} - \frac{1}{2} \frac{\sin(z_{O_1} + z_{O_2})}{\sin(z_{O_1} - z_{O_2})} \right) (J_{11} - J_{12}). \tag{136}
\end{aligned}$$

Equation (136) corresponds to Eq. (122).

Besides the instrumental errors, the errors of recording the time of passage and of the coordinates of the stars influence e . If m_u' is the mean error of the average of the passage recordings reduced to the corresponding vertical, m^* the mean error of the declination δ and $m^*/\sin(90-\delta)$ the mean error of the right ascension; we obtain for the mean error m_e^{*2} of the base line according to Niethammer (1947) and Ramsayer (1967):

$$m_e^{*2} = \frac{\sin^2 z_{O_1} + \sin^2 z_{O_2}}{\sin^2(z_{O_1} - z_{O_2})} (m_u'^2 + m^{*2}). \tag{137}$$

This equation is usually used as a criterion for the selection of the stars. The coefficient which depends on the zenith-distances of the two stars should be kept as small as possible. According to the discussion in Niethammer (1947) and Ramsayer (1967), it is best for a pure position determination to observe the pairs as close to the zenith and as symmetric to the zenith ($z_{O_2} = -z_{O_1}$) as possible (case a = symmetric arrangement of stars). If, in addition the azimuth of terrestrial points has to be determined, the zenith-distances of a pair of stars has to be chosen so that $z_{O_1} - z_{O_2} = 90^\circ$ according to Figure 52, that is, that the vertical directions to stars 1 and 2 are normal to each other (case b = vertical arrangement). For the cases a) and b) Eq. (136) takes the form:

$$\begin{aligned}
\text{a) } de'_a = & \frac{1}{2} \frac{\sin^2 z_{O_1}}{\sin 2z_{O_1}} (O_{21} + O_{22} - O_{11} - O_{12}) - \frac{1}{2} \frac{\sin z_{O_1}}{\sin 2z_{O_1}} (C_{21} - C_{22} + C_{11} - C_{12}) \\
& - \frac{1}{2} (J_{21} - J_{22} + J_{11} - J_{12}), \tag{136a}
\end{aligned}$$

$$\begin{aligned}
\text{b) } de'_b = & \frac{1}{2} \sin z_{O_1} \cos z_{O_1} (O_{21} + O_{22} - O_{11} - O_{12}) - \frac{1}{2} \sin z_{O_1} (C_{21} - C_{22}) \\
& - \frac{1}{2} \cos z_{O_1} (C_{11} - C_{12}) - \frac{1}{2} \left(\frac{1}{2} - \frac{1}{2} \cos 2z_{O_1} \right) (J_{21} - J_{22}) - \frac{1}{2} \left(\frac{1}{2} + \frac{1}{2} \cos 2z_{O_1} \right) (J_{11} - J_{12}). \tag{136b}
\end{aligned}$$

The error propagation law can be applied to the random error part of Eq. (136a, b) according to Eq. (123). If again the individual instrumental errors are introduced instead of the abbreviations O, C, and J, the mean error m_e' of e can be calculated by:

$$a) \quad m_{ca}^{\prime 2} = \frac{\sin^4 z_{O1}}{\sin^2 2z_{O1}} (m_{ua}^{\prime 2} + m_{ia}^{\prime 2} + m_{wa}^{\prime 2}) + \frac{\sin^2 z_{O1}}{\sin^2 2z_{O1}} (m_{ca}^{\prime 2} + m_{lb}^{\prime 2}) + \frac{1}{2} (m_{wl}^{\prime 2} + m_{ll}^{\prime 2} + m_l^{\prime 2} + m_{la}^{\prime 2}), \quad (138a)$$

$$b) \quad m_{cb}^{\prime 2} = \sin^2 z_{O1} \cos^2 z_{O1} (m_{ua}^{\prime 2} + m_{ia}^{\prime 2} + m_{wa}^{\prime 2}) + \frac{1}{2} (m_{ca}^{\prime 2} + m_{lb}^{\prime 2}) + \left(\frac{1}{2} + \frac{1}{2} \cos^2 2z_{O1}\right) (m_{wl}^{\prime 2} + m_{ll}^{\prime 2} + m_l^{\prime 2} + m_{la}^{\prime 2}). \quad (138b)$$

The coefficients of Eqs. (138a, b) and (137) have the values listed in Appendix T for different zenith distances, z_{O1} .

The effect of the systematic errors is to be investigated closer using Eqs. (136a, b). The errors u_a , c_a , and l_a do not have to be taken into account according to the remarks in Section 6.2.1. According to Eq. (136a) the following holds for the case a:

$$de_a^{\prime 2} = \frac{1}{2} \frac{\sin^2 z_{O1}}{\sin^2 2z_{O1}} (i_{a21}^{\prime 2} + i_{a22}^{\prime 2} - i_{a11}^{\prime 2} - i_{a12}^{\prime 2} + w_{a21}^{\prime 2} + w_{a22}^{\prime 2} - w_{a11}^{\prime 2} - w_{a12}^{\prime 2}) - \frac{1}{2} \frac{\sin z_{O1}}{\sin 2z_{O1}} (b_{21}^{\prime 2} - b_{22}^{\prime 2} + b_{11}^{\prime 2} - b_{12}^{\prime 2}) - \frac{1}{2} (i_{L21}^{\prime 2} - i_{L22}^{\prime 2} + i_{L11}^{\prime 2} - i_{L12}^{\prime 2} + l_{21}^{\prime 2} - l_{22}^{\prime 2} + l_{11}^{\prime 2} - l_{12}^{\prime 2}). \quad (139)$$

If the stars have a symmetric arrangement around the zenith it is $z_{O1} = 360^\circ - z_{O2}$ and $z_{O2} = 360^\circ - z_{O1}$. For the azimuthal component $i_a^{\prime 2}$ of the secondary tilt axis error we obtain, if the pair of stars is observed with both telescope positions,

$$i_{a11}^{\prime 2} = i_a^{\prime 2}(z_{O1}) = i_a^{\prime 2}(360^\circ - z_{O2}) = i_{a22}^{\prime 2}; \quad i_{a12}^{\prime 2} = i_a^{\prime 2}(360^\circ - z_{O1}) = i_a^{\prime 2}(z_{O2}) = i_{a21}^{\prime 2},$$

that is, the azimuthal wobble error cancels in Eq. (139); also the influence of the error of the level $i_L^{\prime 2}$ is eliminated. The roll error $w_a^{\prime 2}$ drops out because of the positioning to the stars with the zenith distance 0° . The symmetrical deflection of the telescope is eliminated by performing the observation with two telescope positions. Since the position of the bubble of the level at one telescope position can only be changed because of wobbling of the tilt axis and of errors in the stability, it is $l_{11}^{\prime 2} = l_{21}^{\prime 2}$ and $l_{12}^{\prime 2} = l_{22}^{\prime 2}$. Therefore, we get for Eq. (139):

$$de_a^{\prime 2} = -\frac{1}{2} (l_{11}^{\prime 2} - l_{12}^{\prime 2}). \quad (139a)$$

The error of the level can be reduced markedly by a good adjustment of the horizontal line ($l_{11}^{\prime 2} = l_{12}^{\prime 2}$). If this adjustment, finally, is changed so that $l^{\prime 2}$ exhibits a quasi-random distribution, the mean systematic error $m_{ca}^{\prime 2}$ can be obtained according to Eq. (123c):

$$m_{ca}^{\prime 2} = \frac{1}{2} (r_1 m_l^{\prime 2})^2. \quad (139b)$$

The reduction factor r_1 depends on how well the horizontal adjustments are performed. m_{ca}^n is reduced if it is averaged over several pairs of stars as the mean random error given in Eq. (138a) is averaged. In Eqs. (139a) and (139b) it is expressed that the accuracy of an astronomical determination of positions depends essentially on the accuracy of the level as far as systematic instrumental errors are concerned. This is true only if the random error contribution is disregarded and if the discussed arrangement of the observation and the recommended method of observation are applied.

For an unsymmetrical star arrangement (case b) the situation for a single pair of stars is not so favorable. Taking into consideration the rules to eliminate the roll error w_a^n and the heat deflection b^n , the following systematic errors remain according to Eq. (136b)

$$dc_b^n = \frac{1}{2} \sin z_{01} \cos z_{01} \left(i_{a21}^n + i_{a22}^n - i_{a11}^n - i_{a12}^n \right) - \frac{1}{2} \left(i_{L21}^n - i_{L22}^n + i_{L11}^n - i_{L12}^n + i_{21}^n - i_{22}^n + i_{11}^n - i_{12}^n \right) + \frac{1}{2} \cos 2z_{01} \left(i_{L21}^n - i_{L22}^n - i_{L11}^n + i_{L12}^n + i_{21}^n - i_{22}^n - i_{11}^n + i_{12}^n \right). \quad (140)$$

Since $i_{11}^i = i_{21}^n$ and $i_{12}^i = i_{22}^n$ according to the remark above, Eq. (140) can be simplified in the following way:

$$dc_b^n = \frac{1}{2} \sin z_{01} \cos z_{01} \left(i_{a21}^n + i_{a22}^n - i_{a11}^n - i_{a12}^n \right) - \frac{1}{2} \left(2i_{11}^n - 2i_{12}^n + i_{L21}^n - i_{L22}^n + i_{L11}^n - i_{L12}^n \right) + \frac{1}{2} \cos 2z_{01} \left(i_{L21}^n - i_{L22}^n - i_{L11}^n + i_{L12}^n \right). \quad (140a)$$

Concerning the azimuthal wobbling error of the tilt axis, the following holds:

$$i_{a11}^n = i_a^n(z_{01}); \quad i_{a12}^n = i_a^n(360^\circ - z_{01}); \quad i_{a21}^n = i_a^n(270^\circ + z_{01}); \quad i_{a22}^n = i_a^n(90^\circ - z_{01}).$$

Aside from the special case $z_1 = 45^\circ$ three cases can be distinguished according to the choice of the stars:

- 1) The individual pairs of stars are arranged symmetrical to $z = 45^\circ$ (Fig. 52a): the average value of e calculated from all pairs (even number of pairs of stars) does not contain the wobbling error of the tilt axis, as is easily shown.
- 2) The pairs of stars are distributed randomly around the vertical (Fig. 52b): i_a^n loses its systematic character and is reduced by forming the average like i_a^i . Considering the remarks to Eq. (139b) for the calculation of the level error the mean "systematic" error m_{cb}^n for one pair of stars is obtained as:

$$me_b^{n2} = \sin^2 z_{01} \cos^2 z_{01} \left(r_{ia} m_{ia}^n \right)^2 + \frac{1}{2} \left(r_1 m_1^n \right)^2 + \left(\frac{1}{2} + \frac{1}{2} \cos^2 2z_{01} \right) \left(r_{iL} m_{iL}^n \right)^2. \quad (140b)$$

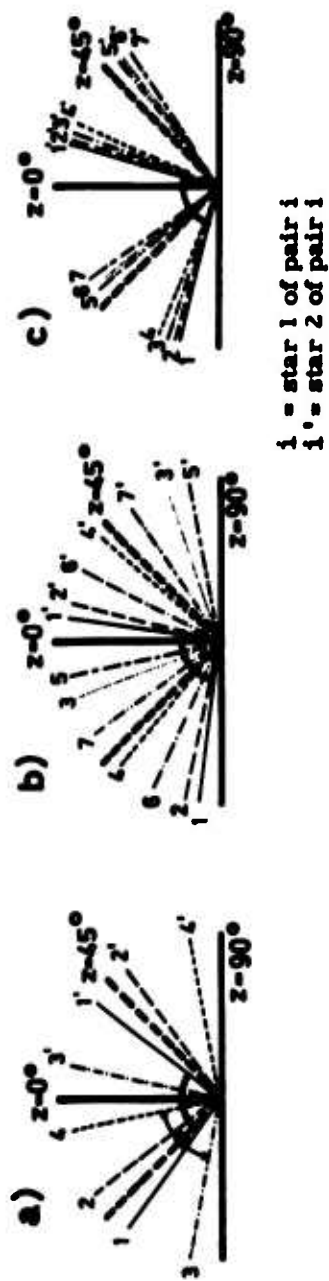


Figure 52. Possibilities of Arranging the Pairs of Stars

r_{1a} and r_{iL} must be estimated with regard to the number and distribution of the pairs.

- 3) The pairs of stars are arranged unbalanced as in Figure 52c: The systematic errors appear with their full weight according to Eq. (140a) and are not reduced by repeated measurements. Arrangements of stars like c) should therefore be avoided.

In Section 6.3.3 further details are given about the accuracy of the base line distance e .

6.3.2 POSITION DETERMINATION FROM MEASUREMENTS OF AZIMUTHAL DIFFERENCE WITH A UNIVERSAL INSTRUMENT

The position determination from passages through the vertical using a transit instrument corresponds to the position determination from measurements of azimuthal differences using a universal. For a comparison of the instrumental accuracies the same observation arrangement has to be assumed for the universal instrument as for the transit instrument. That means that both stars have an azimuthal difference of about 180° and zenith-distances are arranged symmetrically and close to the zenith in case a and vertical to each other in case b. The vertical base line corresponds to the base line of the azimuthal differences according to Ramsayer (unpublished). This base line has the distance e from the zenith-point analogous to Eq. (134):

$$e = - \frac{\sin z_{O1} \sin z_{O2}}{\sin(z_{O1} - z_{O2})} (L_2 - L_1 - (a_{O2} - a_{O1})) \quad (141)$$

with

$L_2 - L_1$: measured azimuthal difference

$a_{O2} - a_{O1}$: azimuthal difference calculated from approximated values.

The influence of the instrumental error on the base line distance e is investigated analogous to the treatment in Section 6.3.1. In the derivation of the formulas the orientation component has to be expanded only by the errors made by reading the divided circle.

For the Wild T4 we get for the random error contribution according to Eqs. (138a, b):

$$a) \quad m'_{ea}{}^2 = \frac{\sin^4 z_{O1}}{\sin^2 2z_{O1}} (m'_{ua}{}^2 + m'_{ab}{}^2 + m'_t{}^2 + m'_m{}^2 + m'_{ia}{}^2 + m'_{wa}{}^2) + \frac{\sin^2 z_{O1}}{\sin^2 2z_{O1}} (m'_{ca}{}^2 + m'_b{}^2) + \frac{1}{4} (m'_{wiL}{}^2 + m'_{iL}{}^2 + m'_1{}^2 + m'_{ia}{}^2), \quad (142a)$$

$$b) m'_{eb}{}^2 = \sin^2 z_{o1} \cos^2 z_{o1} (m'_{ua}{}^2 + m'_{ab}{}^2 + m'_t{}^2 + m'_m{}^2 + m'_{ia}{}^2 + m'_{wa}{}^2) + \frac{1}{2} (m'_{ca}{}^2 + m'_{cb}{}^2) + \left(\frac{1}{4} + \frac{1}{4} \cos^2 2z_{o1} \right) (m'_{iL}{}^2 + m'_{wiL}{}^2 + m'_1{}^2 + m'_{1a}{}^2) \quad (142b)$$

The mean random error given by Eqs. (142a, b) is increased, compared to the mean error obtained for the transit instrument [Eqs. (138a, b)], by the influence of the mean error of the reading m'_{ab} and the mean diameter and micrometer errors, m'_t and m'_m . In regard to the systematic error contribution, only the errors of the divided circle have to be taken into account. Since the diameter errors have a period of 180° in the Wild T4, they are eliminated completely for an azimuthal difference of 180° . Therefore, Eqs. (139a, b) and (140a, b) are valid for the Wild T4 without limitations.

For the Kern DKM3 the vertical component i_v of the secondary tilt axis error has to be taken instead of the level component i_L in Eq. (68a) and the error due to vertical roll w_i instead of the level roll error w_{iL} . The mean random error of the base line m'_e is given, therefore, by Eqs. (142a, b) if m'_{iL} is replaced by m'_{iv} and m'_{wiL} by m'_{wi} . In calculating the systematic error contribution it has to be considered that the diameter errors appear with a period 360° , that is, that they are not eliminated directly by the observation of a pair of stars. According to Eqs. (139b) and (140b) the mean systematic error m_e'' of the base line is obtained:

$$a) m''_{ea}{}^2 = \frac{\sin^4 z_{o1}}{\sin^2 2z_{o1}} (r_t m_t'')^2 + \frac{1}{2} (r_1 m_1'')^2, \quad (143a)$$

$$b) m''_{eb}{}^2 = \sin^2 z_{o1} \cos^2 z_{o1} \left((r_t m_t'')^2 + (r_{ia} m_{ia}'')^2 \right) + \frac{1}{2} (r_1 m_1'')^2 + \left(\frac{1}{4} + \frac{1}{4} \cos^2 2z_{o1} \right) (r_{iv} m_{iv}'')^2. \quad (143b)$$

In the following section a numerical comparison of the two instruments will be performed.

6.3.3 NUMERICAL VALUES FOR THE ACCURACY AND CONSEQUENCES FOR ASTRONOMICAL POSITION DETERMINATIONS

The mean accidental error m_e' of the base line distance can be given in the following general form according to Eqs. (137), (138a, b) and (142a, b):

$$m_e'^2 = U_o'^2 + U_c'^2 + U_i'^2 + U_u'^2 + U^{*2}. \quad (144)$$

U_o' , U_c' , U_i' , U_u' , and U^* represent the influence of the incidental error contribution of the orientation component O, of the target axis component C, of the inclination component J, and of the errors of the passage times and the star coordinates.

If the position determination is performed with a vertical star arrangement (case b) the influence U_i^1 of the inclination component J , for example, is given for the transit instrument according to Eq. (138b) by:

$$U_i^1 = \left(\frac{1}{4} + \frac{1}{4} \cos 2z_{o1} \right) (m_{wiL}^1 + m_{iL}^1 + m_1^1 + m_{1a}^1).$$

In the following examples the coefficients for the individual errors corresponding to the quantities f_j in Eq. (123a) are equal within the same group of errors. Denoting these coefficients by K' and the corresponding sum of the squares of the individual mean errors m' by M' Eq. (144) takes the form:

$$m_e'^2 = K_o' M_o'^2 + K_c' M_c'^2 + K_i' M_i'^2 + K_u' M_u'^2 + K^{*'} M^{*'}^2. \quad (144a)$$

In the example given for Eq. (144) it is:

$$K_i^1 = \frac{1}{4} + \frac{1}{4} \cos^2 2z_{o1} \quad \text{and} \quad M_i'^2 = m_{wiL}^1{}^2 + m_1^1{}^2 + m_{1a}^1{}^2 + m_{iL}^1{}^2.$$

The equations for the coefficients K' for the discussed cases of symmetrical and vertical star arrangement are listed in Appendix U. Generally, they depend on the procedure of the determination of the position and the choice of the stars. In our cases the coefficients are either constant or a function of the zenith-distance and have values as given in Appendix T. The quantities M' depend principally on the individual instruments and are tabulated in Appendix U for the investigated instruments.

The mean systematic error m_e^n can be written using Eqs. (139b), (140b), and (143a, b) according to Eq. (144) in the following way:

$$m_e^{n2} = U_o^{n2} + U_c^{n2} + U_i^{n2}. \quad (145)$$

U_o^n , U_c^n , and U_i^n give the influence of the systematic part of the orientation component, the target axis component, and the inclination component. For the above mentioned example is

$$U_i^{n2} = \frac{1}{2} (r_1 m_1^n)^2 + \left(\frac{1}{4} + \frac{1}{4} \cos^2 2z_{o1} \right) (r_{iL} m_{iL}^n)^2.$$

In a symmetrical star arrangement (case a) the coefficients of the individual errors of one error group are equal again, so that Eq. (145) can be expressed in a form analogous to (144a):

$$m_e^{n2} = K_o^n M_o^{n2} + K_c^n M_c^{n2} + K_i^n M_i^{n2}. \quad (145a)$$

K'' and M'' are listed in Appendix U for the individual procedures and instruments. K'' depends on the procedure and choice of stars, generally, and M'' on the procedure, the choice of stars and the instrument used for the specific measurement.

The total error m_e of the base line distance is obtained from Eqs. (144) and (145):

$$m_e^2 = m_e'^2 + m_e''^2 = U_o'^2 + U_o''^2 + U_c'^2 + U_c''^2 + U_i'^2 + U_i''^2 + U_u'^2 + U_u''^2. \quad (146)$$

Equation (146) is the basis for the following numerical comparison of the accuracy of an astronomical position determination which can be obtained with various instruments. In Appendix S the mean random and systematic errors are listed for the individual instruments and procedures using the results of Section 5. The mean errors m_e of a base line determination (using one pair of stars) shown in Figure 53 as a function of the zenith-distance z_{o1} of star 1 can be found from the numerical values of the coefficients K (App. T).

The values for the mean error M_u' of the mean of the reproduced passage times and the mean error M^{*1} of the star coordinates are taken from the literature. According to Niethammer (1947), the mean error of entrance m_u' dependent on the telescope magnification of the investigated instruments is given for an observation with the impersonal micrometer and a declination of 45° by:

Instrument	AP70	Wild T4	Kern DKM 3
Telescope magnification	80x	65x	45x
Error entrance m_u'	0.6"	0.7"	0.9"
Number of contacts	15	15	15
M_u'	0.15"	0.2"	0.25"

The listed values of M_u' were obtained by averaging over fifteen contact points. The systematic errors of the passage times (personal equation) are not included here. m^{*1} is taken according to Blaser (1959) as $\pm 0.2''$. In Figure 53 the contribution of $M_o 1$, $M_c 2$, $M_i 3$, the combined contribution of M_o , M_c , and $M_i 4$, the combined contribution of M_u' and $M^{*1} 5$ and the mean total error of $e 6$ are plotted. The following general statements can be made about the mean error of e (e derived from one pair of stars) from the figures.

Procedure	Star Arrangement	AP70	T4	DKM 3
a	symmetric, close to zenith $z (\leq 30^\circ)$	$\pm 0.3''$	$\pm 0.35''$	$\pm 0.35''$
b	vertical, $z_{o1} - z_{o2} = 90^\circ$	$\pm 0.4''$	$\pm 0.5''$	$\pm 0.45''$

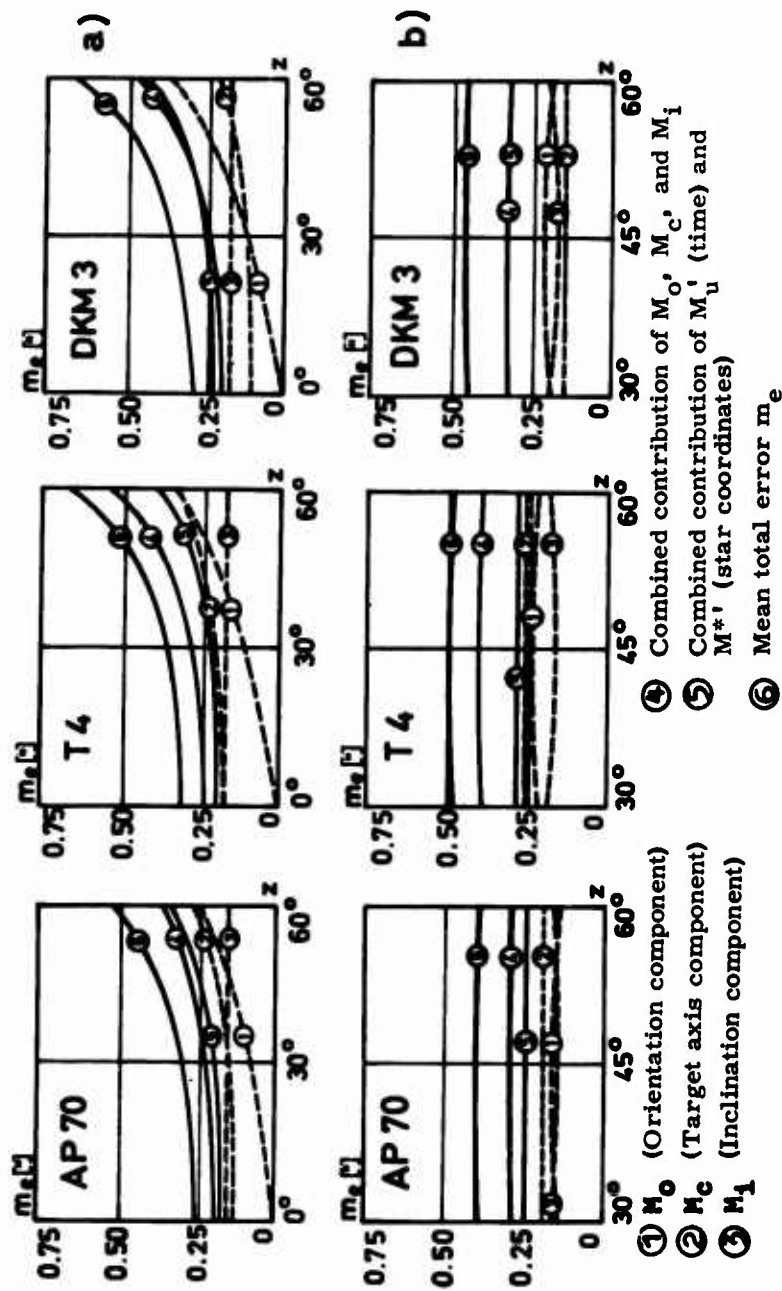


Figure 53. Mean Error m_e of the Base Line Distance e Dependent on the Zenith Distance of Star I
 Upper Figure: Procedure a, Symmetric Star Arrangement
 Lower Figure: Procedure b, Vertical Star Arrangement

The listed values have to be increased by 15 to 20 percent according to an estimate of the author if the mentioned conditions for the choice of the stars are fulfilled only within 3° to 5° .

An error of the base line distance e of $0.35''$ causes an error of the time correction of $0.35'' \sec \phi$ in a meridian time determination, for example, for $\phi = 45^\circ$ an error of $0.5''$ results. This corresponds approximately to the accuracies of actual measurements [for example: mean error of time correction $\pm 0.48''$ in Schrick's work (1963)].

The following statements can be made on the basis of the previous results:

- 1) The mean errors of positional determinations from one pair of stars differ only by less than $0.1''$ for the (examined) transit instrument and the (examined) universal instruments. The increase of accuracy with the transit instrument is between 10 percent and 15 percent.
- 2) The universal instrument Kern DKM3 A can be considered as equivalent to the Wild T4 for astronomical observations.
- 3) As a comparison of the curves 4 and 5 in Figure 53 shows, the instrumental errors have generally as strong an influence as do the errors of passage times and star coordinates.
- 4) The influence of the orientation component O , the target axis component C and inclination component J on the accuracy of position determinations is about the same for the individual instruments. For symmetrical star arrangement and small zenith distance, the contribution of O is insignificant so that the errors of the readings from the divided circle do not have an effect.
- 5) The systematic instrumental errors can be eliminated to a great extent by the discussed observation technique and arrangement. The observation with two telescope positions proves to be particularly useful.
- 6) Those variable systematic errors which cannot be eliminated can be transformed into quasi-random errors by a proper choice of the zenith-distance and the azimuth of the stars. The influence of these errors is reduced as well as the random error by the described procedure.

From 3) and 5) it follows that, in principle, the instrumental errors have to be taken into account for an optimum choice of stars, which is contrary to the usual procedure. In general, symmetric observation arrangements must be considered particularly useful. The results of an observation deteriorate considerably if the stars are chosen unbalanced. If 5) and 6) are not taken into account, an appreciable discrepancy between internal and external accuracy appears generally. Therefore, the usual procedures of astronomical position and azimuth determinations would have to be checked in order to find out if the rules used for an optimum choice of stars until now can be retained or if they must be changed. To obtain a general judgment of the capacity of the individual instruments one has to consider also

their efficiency, as for example, the fast sequence of observations with the transit instrument in addition to their accuracy.

7. SUMMARY

In this paper all instrumental errors of universal and transit instruments which are of importance for the definition of a horizontal direction are discussed, except the errors of aiming. The investigations concerning size, nature, cause and effect of the individual instrumental errors are the basis of a comparison of the accuracies which can be obtained by the universal and transit instrument for astronomical position determinations. The investigations include the following instruments: a universal instrument Wild T4, a universal instrument Kern DKM3, and a transit instrument Askania AP70.

First it was necessary to define the individual instrumental errors exactly and deal with their general influence on the direction measurement (Section 3). With regard to their nature and cause the group's secondary axis errors (horizontal, tilt, and target axis), errors of the instrument (divided circle, micrometer, level) and error in the stability (substructure, roll error, heat deflection of telescope) are distinguished.

Since the attempt was made to determine the individual instrumental errors with a mean error of $\leq \pm 0.05''$ an autocollimation setup with a large focal length ($f = 1500\text{mm}$) was built and its accuracy checked thoroughly (Section 2). The results of these investigations can be summarized as follows: For a simple autocollimation the mean error of a single measurement for the direction of the mirror normal lies - depending on the size of the scale - between $\pm 0.02''$ ($1''$ scale) and $\pm 0.05''$ ($5''$ scale). The average change of the position of mirror and autocollimator due to outside influences (mainly temperature) can be kept under $0.1''/30$ min. A further improvement of the accuracy is possible by multiple reflection and multiple autocollimation. With a multiple autocollimation an accuracy of $\pm 0.02''$ to $\pm 0.03''$ can be obtained for the 11th-order image. The zero-order image allows control of the stability of autocollimator and mirror systems. In addition, the multiple autocollimation makes it possible to check the accuracy of autocollimation measurements itself, that is, without given reference. Furthermore, the influence of the adjustment of the autocollimator, the residual deflection of the mirrors, and the distance mirror-autocollimator on focusing and on the scale factor of the autocollimation system is discussed according to the principles of geometrical optics (autocollimation with non-parallel rays). The results of these theoretical investigations are confirmed by experiments, especially by the direct determination of the scale factor. The investigations are of interest also for electro-optical autocollimators.

With the autocollimation technique, the secondary tilt and horizontal axis errors, the substructure rotation, the roll effect, the heat deflection, and the micrometer errors are determined (Section 4). Generally, the test mirror is attached to the part of the instrument whose behavior is to be checked. In investigations of axes the motion of the autocollimation image due to the rotation of the axis has to be measured point by point and approximated by an ellipse (horizontal axis) or a circle (tilt axis) because of the divergence of mean axis and mirror normal. The secondary axis errors can be found from the deviation of the measured position of the autocollimation image from the position given by the curve.

Statistical methods are used for the analysis of the instrumental errors where special arrangements were set up to separate the random and the systematic error contribution. The systematic part is represented by mathematical functions which can be derived from theoretical considerations concerning the effect of the individual sources of errors.

Partly, the results are very different from the individual instrument (Section 5): The present Wild T4 shows intolerably high values for the roll error ($0.6''$)*, the heat deflection of the telescope ($0.8''$), secondary tilt axis errors ($0.4''$), and the level error ($0.2''$). The stability of the instrument is excellent (azimuthal substructure rotations of $0.05''$); the accuracy of the horizontal divided circle ($0.2''$), of the horizontal scale micrometer ($0.1''$) and the horizontal axis ($0.55''$) is sufficient.

For the examined Kern DKM3 the accuracy of the micrometer ($0.25''$) and the level ($0.25''$) does not meet the required accuracy. The azimuthal stability ($0.15''$), the thermal constancy of the aiming axis ($0.25''$), and the accuracy of the horizontal axis ($0.6''$) are sufficient; the stability of the tilt axis ($0.1''$) and the accuracy of the tilt axis ($0.2''$) are excellent. For the transit instrument used in these investigations the values for the substructure rotation ($0.1'' - 0.15''$), the roll error ($0.25''$), the heat deflection ($0.45''$), and the secondary tilt axis error ($0.3''$) are between those of the Kern DKM3 and the Wild T4. The accuracy of the level $0.15''$ is sufficient.

If the root mean square error of an individual instrumental error is above $0.1'' - 0.2''$ there are generally systematic errors responsible for it. The reproducibility of systematic errors is between $\pm 0.1''$ and $\pm 0.25''$ in general. The causes of instrumental errors can be identified by means of Fourier analysis with periods which are determined theoretically so that measures for design and observation can be worked out to reduce or eliminate them. With regard to the individual instrumental errors the following details can be given:

The secondary tilt axis errors (T4) are caused exclusively by faults in the bearing tract; the roll error (T4, AP70) can be avoided in the construction by a

*The numerical value gives the root mean square error of the individual measured total instrumental error.

closed support of the axis and in the observations by adjusting the telescope while it is oscillating. The causes for secondary errors of the horizontal axis can be found with Fourier-analysis whose periods are derived from the equations of motion of the alidade and the bearing system and the theoretical specification of five different causes of errors. The most important causes were found to be the unevenness of the bearing-surface (T4, DKM3) and the difference of the diameters of the balls. The wobbling errors resulting from the last mentioned cause can be determined if the position of the axis is determined after every one or two revolutions of the alidade. The heat deflection of the telescope (T4, AP70) can be reduced by thermal insulation of the telescope tube.

In general, the investigations showed that an increase of the dimensions of an instrument causes difficulties in the construction and fabrication which affects the increase of accuracy expected from the designer.

The final investigations about the influence of instrumental errors on the accuracy of astronomical position determinations show that systematic errors except the systematic level error can be eliminated with a proper choice of the stars (especially an arrangement symmetrical to the zenith). Even under such favorable conditions the contribution of the instrumental errors exceeds that of the error of the star coordinates and the determination of the passage time, if the personal equation is not considered. Therefore, it is recommended to take the instrumental errors into account correspondingly, in addition to the till now generally used procedure for the choice of the stars. A comparison of the instruments shows that the mean error of a position determination with one pair of stars is $\pm 0.35''$ with the transit instrument, $\pm 0.45''$ with the Wild T4, and $\pm 0.4''$ with the Kern DKM3 in the discussed examples. The accuracy of the transit instrument is only by $0.1''$ better than the accuracy of the two examined universal instruments. An essential advantage of the transit instrument, however, is the fast change of the telescope position. Further, the comparison shows that the Kern DKM3 can be considered completely equivalent to the Wild T4.

The development of the Theo 002 of the optical company JENA with an automatically-stabilized target axis introduces a new period of design of universal instruments. With regard to accuracy, one has to caution against too large expectations; for example, such a device in one of the examined instruments would increase the total accuracy by $0.15''$ at the most. Besides the stabilization of the target axis, universal instruments should be equipped with a device which allows a fast and accurate change of the telescope axis. At the present state of the art it would be possible to perform the turning of the tilt axis by 180° which is done mechanically on the transit instrument and photoelectrically on the universal instruments with sufficient precision (Hock, 1966). The use of such an instrument for observations of vertical passages without scale readings or for measurements of azimuthal differences would introduce certain advantages in the observations.

References

- Alpar, Gy., Somogyi, I. (1960) Teodolitok allotengelyingadozasanak vizsgalata. (Examination of Wobbling of the Support Axis of Theodolites) *Geodezia es Kartografia* 1960/2.
- Alpar, Gy. (1963) Von der Komparierung (About Comparison). Lecture held at the geodetical conference in 1963 at Budapest.
- Bahnert, G. (1963) Zur Messung Parallaxischer Winkel (Measurement of parallactic angles) *Vermessungstechnik* 1963, p. 53.
- Blaser, I., P/Cavedon, M. (1959) La détermination d'erreurs de catalogue avec l'astrolabe a prisme (Error determination with the prism astrolabe) *Publications de l'observatoire de Neuchatel* No. 9.
- Bohm, I. (1967) Theorie der gesamten Fehler. (Theory of the Total Fields) *Z.f. Vermessungswesen*, p. 81.
- Danilow, W. (1957) *Prazisionspolygonometrie. (Precision polygonometry)* VEB Verlag Technik, Berlin.
- Danjon, M.A. (1955) L'Astrolabe impersonnel de l'Observatoire de Paris. (The Impersonal Astrolabe of the Paris Observatory) *Bulletin Astronomique*, Vol. XVIII, Paris.
- Duhmke, M. (1964) Interferenzanordnung für Winkelstücke (Interference Arrangement for Angular Sections). *Z.f. Instrumentenkunde*, p. 368.
- Dyer, D.A. (1958) An Error in the Optical Micrometer of a Theodolite. *Empire Survey Review*, p. 213.
- Farkas, T. (1966) Intervallvergleich von Planplattenmikrometern. (Comparison of the Intervals of Plane Plate Micrometers) *Allgemeine Vermessungsnachrichten*, p. 153.
- Flugge, I. (1954) Einführung in die Messung der optischen Grundgrößen. (Introduction to the Measurement of the Fundamental Quantities of Optics). Verlag G. Braun, Karlsruhe.

References

- Flügge, I. (1956) *Leitfaden der geometrischen Optik und des Optikkrechnens (Guidelines of geometrical Optics and Calculations in Optics)* Vandenhoeck & Ruprecht, Göttingen.
- Flügge, I. (1962) *Praxis der geometrischen Optik (Practical Geometrical Optics)* Vandenhoeck & Ruprecht, Göttingen.
- Fondelli, M. (1956) *Ricerche sulla precisione dei teodoliti Kern DKM 3 (Investigations of the Accuracy of the Theodolite Kern DKM 3)* Bolletino di Geodesia, p. 485.
- Forstner, G. (1964) *Zur Wahl des Prüfwinkels bei dem Kreisteilungsprüfverfahren nach Heuvelink (About the Choice of the Test Angle for Heuvelink's Method for Checking a Circular Scale)* Z.f. Instrumentenkunde, p. 265.
- Graul, F. (1952) *Die Mehrfachautokollimation, eine neue Methode für optische Prüf- und Messverfahren (Multiple Autocollimation; a New Method for Optical Test and Measuring Procedures)* Feingeratetechnik, p. 397.
- Grossmann, W. (1961) *Grundzüge der Ausgleichsrechnung (Principles of Balancing Calculations)* Springer Verlag, Berlin.
- Haller, R. (1957) *Einige konstruktive Möglichkeiten bei der Kreisablesung von Theodoliten und Tachymetern (Some Possibilities of Designing Circular Scales of Theodolites and Tachymeters)* Z.f. Vermessungswesen, p. 12.
- Haller, R. (1959) *Theodolitachsen, ihre Konstruktion, Herstellung und Herstellungsgenauigkeit (Theodolite Axes, Their Construction, Production, and Production Precision)* Vermessungstechnische Rundschau, p. 109.
- Hock, F. (1966) *Ein photoelektrischer Messtubus als Mikroskop, Automikroskop, Autokollimator und Refraktometer (A Photoelectrical Test Tube as Microscope, Automicroscope, Autocollimator and Refractometer)* Microtechnic No. 5/1966, Vol. XX.
- Hoffmann, H.E. (1965) *Beitrag zur Ermittlung der dynamischen Drehachsenfehler eines Kinotheodolits (About the Determination of the Dynamical Errors of the Rotation Axis of a Kinotheodolite)*. Deutsche Luft- und Raumfahrt, Forschungsbericht 65-68.
- Hopcke, W. (1953) *Die Hannoverschen Libellenprüfer (The Level Tests of Hannover)* Niedersächsisches Landesvermessungsamt, Hannover.
- Hume, K.L. (1964) *Metrology with Autocollimators*, Hilger & Watts LTD, London.
- Janich, E. (1954) *Über eine Methode und ein Gerät zur Messung des Taumelfehlers von Vertikalachsen geodätischer Instrumente (A Method and an Instrument for Measuring the Wobble Error of Vertical Axes of Geodetical Instruments)* Jenaer Jahrbuch.
- Jochmann, H. (1956/57) *Die Kreisteilfehler der Horizontalkreise neuer Gradteilung von Präzisionstheodoliten moderner Bauart (Errors in the Graduation of Horizontal Scales with a New Angular Graduation of Theodolites of Modern Design)* Wissenschaftliche Zeitschrift der Technischen Hochschule Dresden 5 (1955/56) H. 5 and 6 (1956/57) H. 1.
- Jochmann, H. (1964) *Die Eliminierung des Einflusses von Neigungs- und Richtungsänderungen der Ziellinie an Instrumenten für geodätisch-astronomische Ortsbestimmungen mit Hilfe mechanischer Neigungskompensatoren (The Elimination of the Tipping and Direction Changes of the Optical Axis of Instruments for Geodetical-Astronomical Position Determinations)* Deutsche Geodätische Kommission, Series B, No. 95 III, p. 81, München.

References

- Kessler, R. (1966) Horizontalkreisuntersuchung des Wild T4 mit einem Spiegel-polygon (Investigations of the Horizontal Scale of a Wild T4 with a Mirror Polygon) (thesis), Geodatisches Institut Stuttgart (unpublished).
- Kong, A., Kohler, H. (1959) Die Fernrohre und Entfernungsmesser (Telescopes and Rangefinders) Springer Verlag, Berlin.
- Mathias, H. (1964) Umfassende Behandlung der Theodolitachsenfehler auf vektor-ieller Grundlage unter spezieller Berücksichtigung der Taumelfehler der Klippachse (Detailed Treatment of Theodolite Axis Errors in Vector Description with Special Consideration of the Wobble Errors of the Tipping Axis) Verlag Leeman, Zurich.
- Michalek, S. (1966) Der Zielfehler vom Standpunkt der derzeitigen Theodolit-prüfung (The Aiming Error from the Point of View of Modern Test Methods for Theodolites) Vermessungstechnik, p. 418.
- Mugica-Buhigas, F. (1960) Neue Ideen über die Anwendung des Theodolits in der geodatischen Astronomie (New Ideas About Using a Theodolite in Geodetical Astronomy) Deutsche Geodatische Kommission, Series C No. 38, München.
- Niethammer, Th. (1947) Die genauen Methoden der astronomisch-geodatischen Ortsbestimmung (The Methods of Exact Position Determinations in Astronomical-Geodetical Measurements) Verlag Birkhäuser, Basel.
- Ochsenhirt, H. (1962) Prüfen und Justieren moderner geodatischer Instrumente und Geräte mit Hilfe von Kollimatoren im Laboratorium (Testing and Adjustment of Modern Geodetical Instruments with Collimators in the Laboratory). Nieder-sächsisches Landesvermessungsamt, Hannover.
- Peglow, M. (1963) Anleitung und Messmethoden zum Autokollimationsfernrohr (The Autocollimation Telescope; Guide Lines and Methods) Ernst Leitz GmbH, Wetzlar.
- Ramsayer, K. (1967) Astronomische Orts- und Zeitbestimmung mit Hilfe von Vertikalstandlinien (Astronomical Position and Time Measurements with Vertical Reference Lines). Festschrift, Aus der geodatischen Lehre und Forschung, for 70th birthday of Prof. Walter Grossmann, Wittwer-Verlag, Stuttgart.
- Ramsayer, K. Handbuch der Vermessungskunde (Handbook of Geodesy) Vol. IIa, Geodatische Astronomie (to be published).
- Reissmann, G. (1966) Die Festlegung der statistischen Sicherheit bei der Anwendung der mathematischen Statistik auf geodatische Probleme (Definition of Statistical Accuracy for Application of Mathematical Statistics to Geodetical Problems). International Conference on Geodetic Measuring Technique and Instrument Problems, Budapest.
- Rothe, R. (1956) Höhere Mathematik Teil II. (Advanced Mathematics, Part II) B.G. Teubner Verlagsgesellschaft, Stuttgart.
- Schmidt, E. (1963) Teilkreisuntersuchung des Wild T4 nach einem modifizierten Verfahren nach Heuvelink (Investigation of the Scale of the Wild T4 with a Modified Method of Heuvelink) thesis, Geodatisches Institut, Stuttgart (unpublished).
- Schrick, K.-W. (1963) Längen und Breitenbestimmungen auf den Stationen I. Ordnung Brillit (1958) (Longitude and Latitude Determination on the Stations of I. Order Brillit (1958), Sievern and Wingat (1959)). Deutsche Geodatische Kommission, Series B, No. 101, München.
- Steinert, K.-G. (1961) Die persönlichen Fehler der Zeitbestimmungen mit dem Passageinstrument (The Personal Errors of Time Determinations with the Passage Instrument). Wissenschaftliche Zeitschrift der Technischen Universität, Dresden, pamphlet.

References

- Steinert, K.-G (1964) Die Achsstabilität bei Passageinstrumenten (The Axis Stability of Passage Instruments) *Vermessungstechnik*, p. 129.
- Stephani, M. (1965) Untersuchung der Stabilität und der Genauigkeit der Achse eines Passageinstrumentes (Investigation of the Stability and Accuracy of the Axis of a Passage Instrument), thesis, Geodatisches Institut Stuttgart (unpublished).
- Straubel, R. (1894) Die Justierung und Prüfung von Fernrohrobjectiven (Adjustment and Test of Telescope Objectives) *Z.f. Instrumentenkunde*, p. 113.
- Tarczy-Hornoch, A. (1961) Über die Messung mit Sekundenlibellen (Measurements with Second-Levels), *Vermessungstechnik*, p. 363.
- Van der Waerden, B.L. (1965) *Mathematische Statistik (Mathematical Statistics)*, Springer Verlag, Berlin.
- Vogel, P. (1966) Untersuchung der Stabilität und der Genauigkeit der Achsen des Universalinstrumentes Wild T4 (Investigations of the Stability and Accuracy of the Axis of the Universal Instruments Wild T4), thesis, Geodatisches Institut Stuttgart, (unpublished).
- Waimer, H. (1965) Genauigkeitsuntersuchung einer 1500 mm-Kollimatoranlage, (Investigations of the Accuracy of 1500 mm-Collimator), thesis, Geodatisches Institut Stuttgart (unpublished).
- Wanach, B. (1926) Untersuchungen von Sekundenlibellen (Investigations on Second-Levels), *Z.f. Instrumentenkunde*, p. 221.
- Weigand, A. (1964) Winkel- und Richtungsmessungen im Basisvergrößerungsnetz München-Ebersberg. Bericht und kritische Untersuchung (Angular and Direction Measurements in the Magnification Net Munich-Ebersberg. Report and Critical Investigation). Deutsche Geodatische Kommission, Series B, No. 97, München.
- Wermann, G. (1957) Kreisteilungsuntersuchungen (Kritische Betrachtung des Heuvelink-Verfahrens). (Investigations on Circular Scales; critical Inspection of the Heuvelink's Method), Deutsche Geodatische Kommission, Series C, No. 18, München.
- Wermann, G. (1958) Zur Berechnung systematischer Fehler aus Beobachtungsreihen. (About the Calculation of Systematic Errors from Series of Observations), *Z.f. Vermessungswesen*, p. 348.
- Wiemerslage, H. (1962) Entwicklung von Instrumenten und Verfahren für die Bestimmung der nivellitischen Refraktion. (Design of Instruments and Methods of Determination of Level Refraction). Wissenschaftliche Arbeiten der Institute für Geodäsie und Photogrammetrie der Technischen Hochschule Hannover, Hannover.
- Wolf, H. (1952) Nachweis und Analyse systematischer Fehler (Demonstration and Analysis of Systematic Errors). *Bolletino di Geodesia*, p. 125.
- International Conference on Geodetic Measuring Technique and Instrument Problems. Budapest, 1966.

CURRICULUM VITAE

I was born in Wolfach (Baden) as the son of Konrad Schwebel and his wife, Elli, n. Muller, on March 13, 1938. After four years of elementary school in Wolfach and nine years of high school in Hausach, I graduated there in the Spring of 1957. After working in the Staatliche Vermessungsamt Wolfach for half a year, I enrolled at the University of Bonn in the Fall of 1957 to study geodesy. After I received the bachelor's diploma, I enrolled in the Technical University of Karlsruhe and passed the examinations for the diploma in the Summer of 1962. My academic teachers were Prof. Dr. Draheim, Prof. Dr. Lichte, and Prof. Dr. Schwidefski in Karlsruhe. In a three-month training program at the International Training Center for Aerial Survey, Delft (Netherlands), I intensified my knowledge in photogrammetry. From January 1963 to January 1967 I was research assistant at the Geodetical Institute of the Technical University Stuttgart, with Prof. Dr. K. Ramsayer. During this time I was able to perform the present measurements. In February 1967 I began the training for the advanced Geodetical Administration Bureau of Baden-Wurttemberg. Since April 1968, I have been working for Carl Zeiss Company, Oberkochen, in the Department for Geodesy and Photogrammetry.

Appendix A

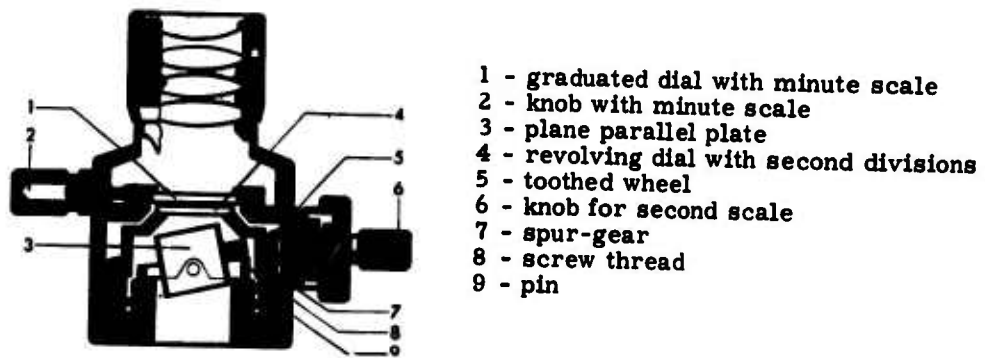


Figure A1. Optical Micrometer of the Leitz Autocollimation Telescope

Appendix B

Coordinate ocular; scale
range 16 min, scale
value 0.1 sec, indicated
value 8 min 6 sec

Cross image

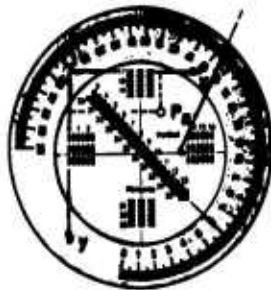


Figure B1. Field of View of the Coordinate Ocular (Leitz)

Appendix C

Table C1. Series Fabricated Electro-optical Autocollimators

No.	Producer	Name	Focal Length [mm]	Optical System	Obj. [mm]	Coord. Direction	Range [']	Smallest Div. ["]	Measuring Device	Position Scale-micr.	Length [mm]	Weight kg	Notes
1	Davidson USA	Two axis autocol. D656	508	Objective plane mir. oc.	64	2	20'	0.5"	Screw micro. diameter		320	9.5	
2	Davidson USA	Compar autocol. D600	508	Objective micro-scope 40x	60	1	2'	0.1"	Plane plates between obj. and scale	Scale on side micro. in center	590	4.5	Simultaneous mes. with 2 mirrors tipping
3	Hensoldt Wetzlar	autocol. telescope 500	500	Objective ocular	60	1	30'	1"	1' scale opt. micrometer	Scale on side micro. in center	590	4.5	
4	Hilger & Watt Eng.	Micro-opt. auto TAI (274)**	840*	Objective micro-scope 39x	35	1	10'	0.1"	Screw micrometer	Scale in center - micro. in center	480	5.5	
5	Keuffel & Esser USA	Visual autocol. 7142	900 (300)	Objective micro-scope 45x	50	1	10'	0.2"	Screw micrometer	Scale in center - micro. in center	500		
6	Leitz Wetzlar	autocol. telescope	500	Objective plane mir. oc. 20x	58	1.2	16' 30'	0.1" 0.5"	0.5' & 0.1' scale optical micrometer	Scale on side micro. in center	330	10	
7	Moller Wedel	autocol. telescope AK500	500	Objective ocular 10x	50	1.2	14'	2"	1 and 2 screw micro.	Scale in center - micro. in center	570	3.5	Micro. without angular div.
8	Wild Switzerland	Test inst. for plates	400	Objective plane mir. oc. 15x	40	1	24'	1"	Screw micrometer	Scale in center - micro. on side	220	3.5	Micro. without angular div.

*Equivalent focal length

**Focal length of objective

D1

Appendix D

Table D1. Series Fabricated Electro-optical Autocollimation

No.	Producer	Name	Maxim. Range [°]	Max. Accur. of Pos. ["]	Acc. over Max. Range ["]	Relat. Accur. [e/sec]	Zero Const. [°/time]	Posit. Veloc. [°/sec]	Coord. Direc.	Max. Mirror Diam. [mm]	(Obj.) Diameter [mm]	Focal Length [mm]	Length of AC Telescope	Weight of AC Telescope [kg]	Measuring Method
1	Barnes Eng., USA	PEAC-1, 2	2'	0.1"	1"	0.3	0.5°/24h	20°/sec	1, 2	50	76	100	300	0	Optical micro. with servomotor photo multiplier
2	Controls Comp. USA	R-300-50	12'	0.1"			0.1°/4h	100°/sec	1	1.5	76	100	400	2.5	Revolving plane mirror reflecting plate lamp prism and photo multiplier
3	Davidson Optronics USA	D665-187 D787-281	2'	0.1"	0.5"	4.2		15°/sec	1	40	60		640	1.2	Plane plate opt. servomotor 2 phase discharge tube photo multiplier
4	Hilger & Watts Eng.	TA3	10'	0.1"	±2"	2.0	0.4°/12h	30°/sec	1	0	35	0.60	400	0	Servo micro. (telescope and photo multiplier), manual adjustment, screw micrometer
5	Kreidler & Esser USA	TAS8 EACP1 P2	5' 0.8'	0.1" 0.02"	0.5"	2.0 10	0.4°/12h 0.5°/24h	30°/sec	1, 2	10 5	46 70	0.6 4.50	430 450	0.5 4	Light intensity measurement opt. photo-cells
6	Kollmorgen R 342 USA	R 342	6'	±0.1"	±0.5"	1.7	0.2°/24h	200°/sec	2	150	50	0.70	520	1.5	Micrometer lens and light photo multiplier
7	Leritz Wetzlar	Photoel. test tube	15'	0.05"	±0.1"	0.1	0.05°/24h	200°/sec	1	50	50	500	400	4	Meas. grid photo. balancing multiplier
8	Raschow	Midsram	2.5'	0.02"	±0.05"	0.005	0.05°/4h	20°/sec	2	0.3	51	500	500	6	Collimation grid and measure-ment grid with photo-cells

E1

Appendix E

Vector	Optical action	Vector Components		
		x	y	z
Single autocollimation				
\vec{s}		+1	$-y_a$	$+z_a$
\vec{i}_0	reflect.	+1	$-y_a$	$+z_a$
\vec{s}'		-1	$-y_a + 2y_a$	$+z_a - 2z_a$
ang. rot.			$-y_a + 2y_a$	$-z_a + 2z_a$
Single AC with 90° deflection with deflecting mirror				
\vec{s}		+1	$-y_a$	$+z_a$
\vec{i}_0	reflect.	$0 + cy_u$ 1)	$0 - cy_u$	$0 \beta_u - 0 \alpha_u$
\vec{s}'	reflect.	-1	$-y_a + y_u - 2y_a$	$+z_a - 2z_a + 2\alpha_u - 2\alpha_u$
ang. rot.			$-y_a + y_u - 2y_a$	$-z_a + 2z_a - 2\alpha_u + 2\alpha_u$
Single AC with 90° deflection with pentagon prism				
\vec{s}		+1	$-y_a$	$+z_a$
\vec{i}_0	refract.	+1	$-y_a$	$+z_a$
\vec{i}_1	reflect.	$u - vy_p$ 2)	$-y_a - vy_p$	$+z_a + vy_p$
\vec{i}_2	reflect.	$-v + uy_p$	$+u + vy_p$	$-z_a - uy_p$
\vec{i}_3	refract.	-1	$-y_a$	$+z_a$
\vec{s}'	reflect.	-1	$-y_a + 2y_a$	$+z_a - 2z_a + 2\alpha_p - 2\alpha_p$
ang. rot.			$-y_a + 2y_a$	$-z_a + 2z_a - 2\alpha_p + 2\alpha_p$

1) $c = \cos 45^\circ = \sin 45^\circ$
 2) $u = \cos 22.5^\circ$; $v = \sin 22.5^\circ$.

Figure E1. Image Path for Single Autocollimation

Appendix F

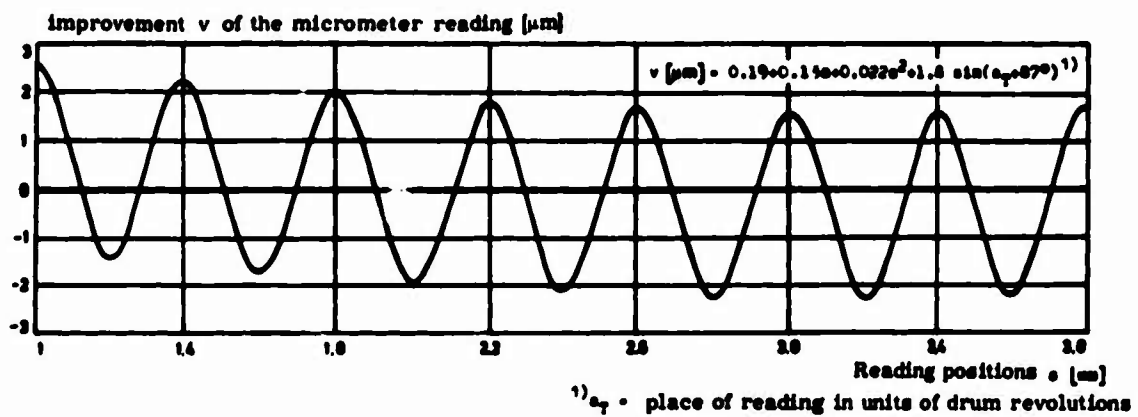


Figure F1. Curve for Improvement of the Micrometer Readings on the Autocollimator (Wild-Micrometer)

Appendix G

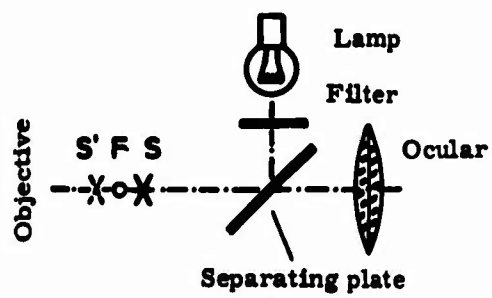


Figure G1. Principle of Gauss-ocular

Appendix H

Table H1. Results of Focusing (22 Mirror Combinations)

Experimental Setup	Optically Active Area*	$c_1 - c_0$ [mm]**	Notes
Single autoc.	As	0.00	
Single autoc.	Am	0.62	
Single AC 90° defl.	U-Am-U	0.76	Mirror dis † 0.2-0.4m
"	U-Am-U	0.76	" 0.7-1.2m
"	U-Am-U	0.78	" 1.1-2.0m
"	U-Am-U	0.76-0.78-0.77	AC mirror turned by 120° each
"	U-Am-U	0.89-1.03-1.00	the same AC mirror shifted
"	U-Am-U	0.76	
"	U-As-U	0.20	
Multiple AC O.Ord.	S	-0.07	} mirror Moller } mirror layer
" I. Ord.	P-Am-P	+0.84	
" II. Ord.	P-Am-P-S-P-Am-P	+1.64	} away from
" I. Ord.	P-As-P	+0.37	} mirror away } from As
" II. Ord.	P-As-P-S-P-As-P	+0.84	
Multiple AC O.Ord.	P-S-P	+1.23	} mirror towards Moller } mirror layer towards
" I. Ord.	P-Am-P	+0.82	
" II. Ord.	P-Am-S-Am-P	+0.54	} AC mirror
" I. Ord.	P-As-P	+0.44	} mirror towards As
" II. Ord.	P-As-S-As-P	-0.21	
Multiple AC defl. O.	U-P-S-P-U	+1.14	} mirror towards Moller
" I.	U-P-Am-P-U	+0.80	
" II.	U-P-Am-S-Am-P-U	+0.80	
" I.	U-P-As-P-U	+0.37	} mirror towards As
" II.	U-P-As-S-As-P-U	-0.67	
Multiple AC defl. O.	P-S-P	+1.10	} mirror towards Moller } other mirror sequence
" I.	P-U-Am-U-P	+0.78	
" II.	P-U-Am-U-S-U-Am-U-P	+0.70	
Multiple AC defl. O.	S	-0.18	} mirror away from } Moller
" I.	P-U-Am-U-P	+0.82	
" II.	P-U-Am-U-P-S-P-U-Am-U-P	+1.60	
" I.	P-U-As-U-P	-0.08	} mirror away from } Askania
" II.	P-U-As-U-P-S-P-U-As-U-P	+0.02	

*Following the incident light

**Difference of focusing position c_1 and focusing position c_0 of As

† Mirror distance

Appendix I

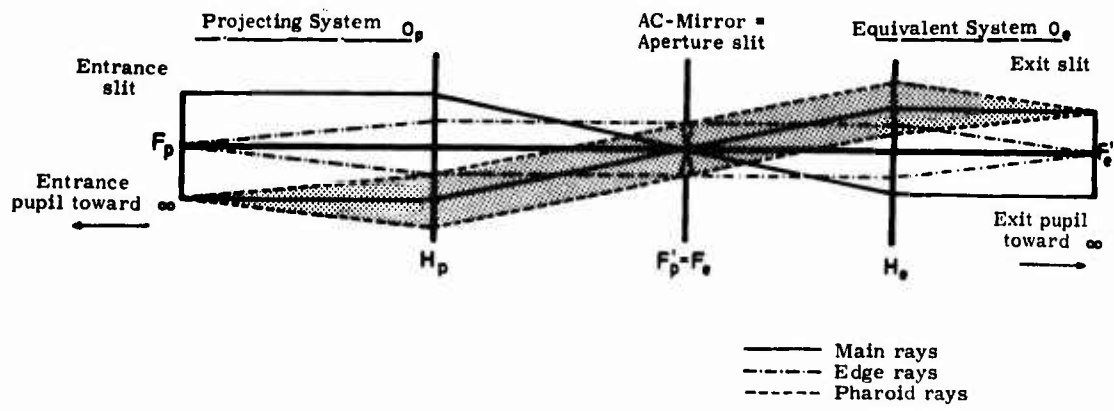


Figure II. Determination of Scale Factor with Telecentric Beam Path

Appendix J

Axis	General	Target Axis	Tilt Axis	Horizontal Axis
<ul style="list-style-type: none"> ● Theoretical dir. \vec{w}_0 ● Mean direction \vec{w}_m ○ Instantaneous dir. \vec{w}_1 				
Theoretical Axis Mean Axis Instantaneous Axis	ψ_0, ψ_0 ψ_m, ψ_m ψ_1, ψ_1	$z_0, 0, z_0$ $z_m, c/\sin z_m$ $z_1, (c+c_a)/\sin z$	$0, 270$ (y-Axis) $i, 270^\circ$ $i+i_v, 270^\circ+i_m$	$90^\circ, u^1$ (z-Axis) $90^\circ-v, a_v$ $90^\circ-i, a_i$
Primary Axis error in spherical coord. in cartes. coord.	\vec{w}_p τ_p, ψ_p, ψ_p x_p, y_p, z_p	\vec{c} τ_c, ψ_c, ψ_c $x_c, -c, z_c$	\vec{i} $i, 90^\circ, u^1$ $0, 0, i$	\vec{v} $v, 0, a_v$ $v \cos a_v, -v \sin a_v, 0$
Secondary Axis error spherical coord. cartes. coord.	\vec{w}_{s1} τ_s, ψ_s, ψ_s x_s, y_s, z_s	\vec{c}_{s1} $\tau_{cs}, \psi_{cs}, \psi_{cs}$ $x_{cs}, -c_a, z_{cs}$	\vec{i}_{s1} $\sqrt{\frac{z_a^2 + i_a^2}{i_a^2}}, \arctan \frac{i_a}{z_a}, 0$ $i_a, 0, -i_a$	\vec{v}_{s1} $v_{s1}, 0, a_{v_{s1}}$ $v_{s1} \cos a_{v_{s1}}, -v_{s1} \sin a_{v_{s1}}, 0$

1) u--undetermined
2) z--zenith-distance

Figure J1. Primary and Secondary Axis Errors, Comparison of the General Case and the Theodolite Axis Errors

Appendix K

Linearized Improved Equation for the Fitted Ellipse

$$v_{ri} = a_{i1} dA + a_{i2} dB + a_{i3} d\beta + a_{i4} d\alpha - l_{ai}$$

$$v_{ti} = b_{i1} dA + b_{i2} dB + b_{i3} d\beta + b_{i4} d\alpha - l_{bi}$$

$$a_{i1} = A_0 \cos^2(u_i + \beta_0) / r_{oi}$$

$$a_{i2} = B_0 \sin^2(u_i + \beta_0) / r_{oi}$$

$$a_{i3} = \frac{(A_0^2 - B_0^2) \cdot \sin(u_i + \beta_0) \cdot \cos(u_i + \beta_0)}{r_{oi}}$$

$$a_{i4} = 0$$

$$-l_{ai} = r_{oi} - r_i$$

$$b_{i1} = A_0 \cos^2(u_i + \beta_0) (\phi_{oi} - \phi_i) / r_{oi}$$

$$b_{i2} = B_0 \sin^2(u_i + \beta_0) (\phi_{oi} - \phi_i) / r_{oi}$$

$$b_{i3} = \frac{(A_0^2 - B_0^2) \sin(u_i + \beta_0) \cos(u_i + \beta_0) (\phi_{oi} - \phi_i)}{r_{oi} + r_{oi}}$$

$$b_{i4} = r_{oi}$$

$$-l_{bi} = (\phi_{oi} - \phi_i) r_{oi}$$

Appendix L



Figure. L1. Examined Instruments: Wild T4, Kern DKM3, and Askania AP70

Appendix M

No.	Operation	With Circular Base			Without Circular Base				
		No. of Measurements	Mean of u_a	Reproducibility m_{Δ}	Systematics Test*	No. of Measurements	Mean of u_a	Reproducibility m_{Δ}	Systematics Test
1	Lay down	24	-0.031"	±0.113"	NS	23	-0.019"	±0.052"	SS
2	Zenith-distance change 180°	22	-0.047"	±0.053"	HS	20	+0.001"	±0.044"	NS
3	Lay down and z. dis. change 90°	24	-0.031"	±0.080"	SS	16	-0.028"	±0.055"	S
4	Lay down and 3x set in	23	-0.018"	±0.090"	NS	20	-0.006"	±0.052"	NS
5	Level of mounting	22	-0.081"	±0.114"	HS	16	-0.005"	±0.060"	NS
	Total 1-4	93	-0.032"	±0.087"	HS	79	-0.013"	±0.051"	S

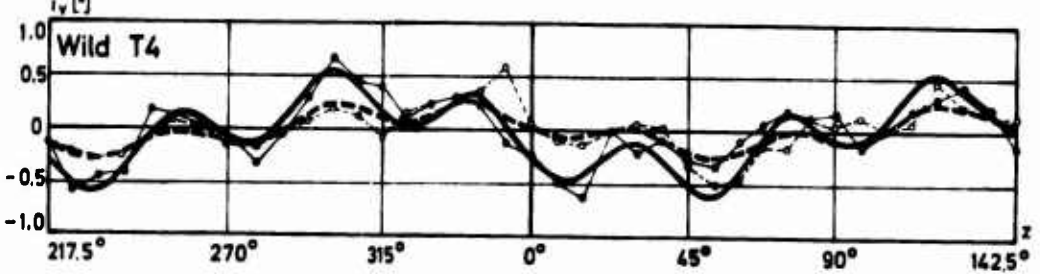
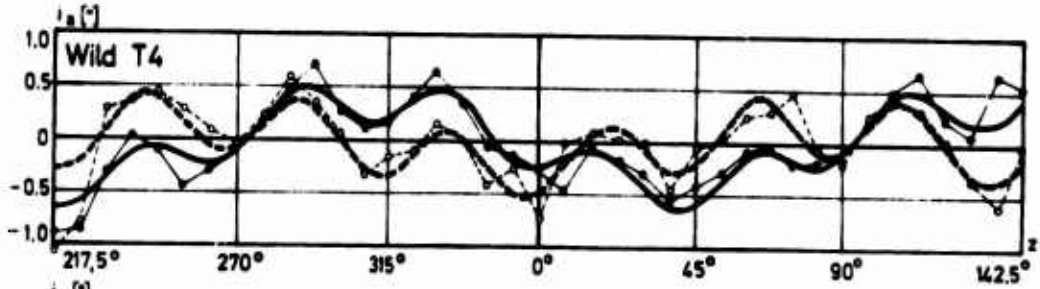
*The systematics test shows if the deviation of the mean of u_a from the theoretical value 0 is significant or random.

Figure M1. Azimuthal Substructure Rotation of Transit Instrument at Different Operations

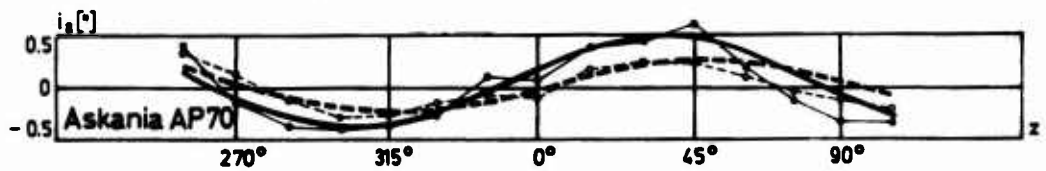
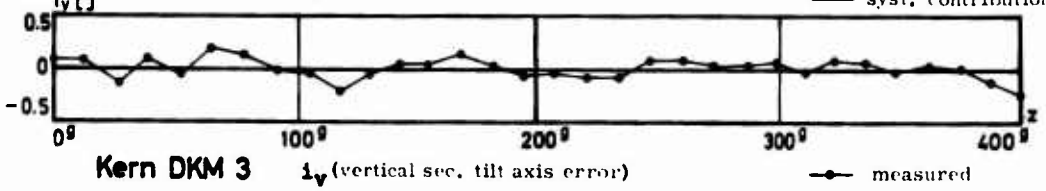
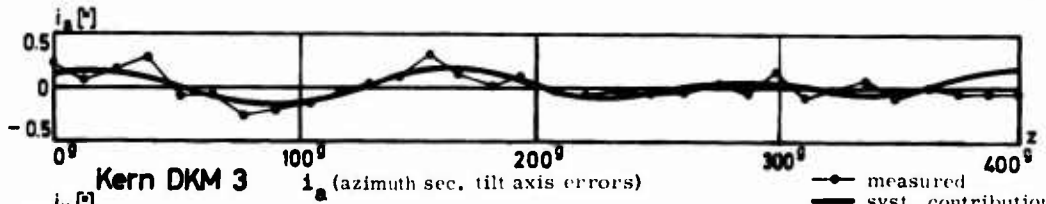
N1

Appendix N

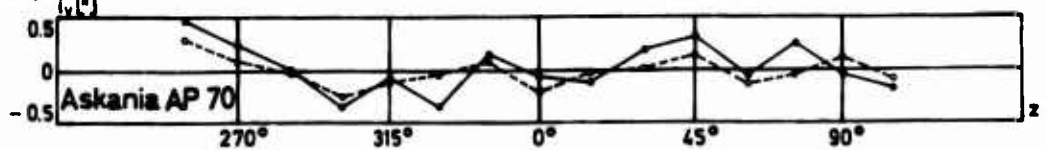
N2



i_{anI} } (azimuthal and vertical tilt axis error normal adjustment procedure, bearing position I) —●— measured, ——— syst. contribution
 i_{vnI} }
 i_{anII} } (azimuthal and vertical tilt axis error, normal adjustment procedure, bearing position II) -●- measured, - - - syst. contribution
 i_{vnII} }



i_{as} } (azimuth sec. tilt axis error symm. and normal adjustment procedure) —●— measured, ——— syst. contribution
 i_{an} } -●- measured, - - - syst. contribution



i_{vs} } (vertical sec. tilt axis error) —●— measured, symm. adj., pro.
 i_{vn} } -●- measured, normal adj. pro.

Figure N1. Results of the Tilt Axis Investigation

Appendix O

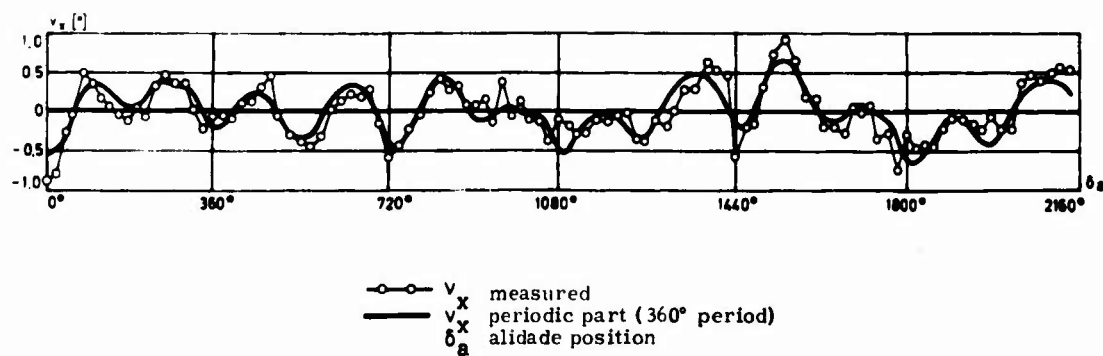
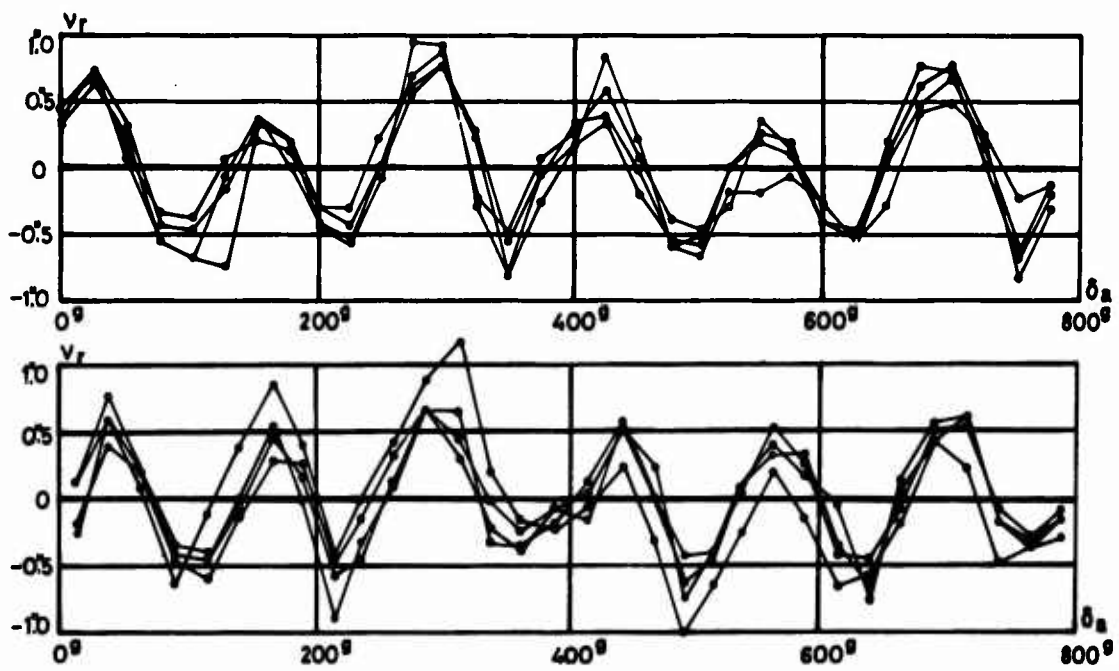


Figure O1. x-Component of Secondary Error of Support Axis (Wild T4)

Appendix P



Above: 4 series of measurements at $0^\circ, 25^\circ, \dots$
Below: 4 series of measurements at $12.5^\circ, 37.5^\circ, \dots$

Figure P1. Radial Component of Secondary Error of Horizontal Axis (Kern DKM3)

Appendix Q

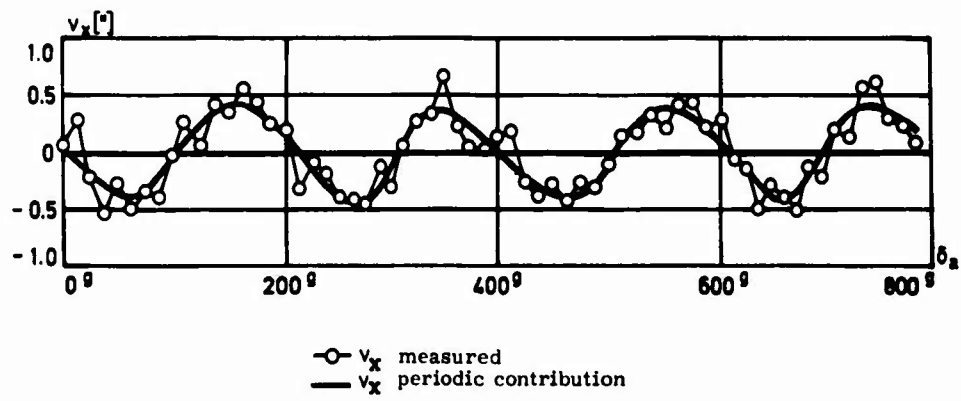


Figure Q1. x-Component of Secondary Horizontal Axis Error (Kern DKM3)

Appendix R

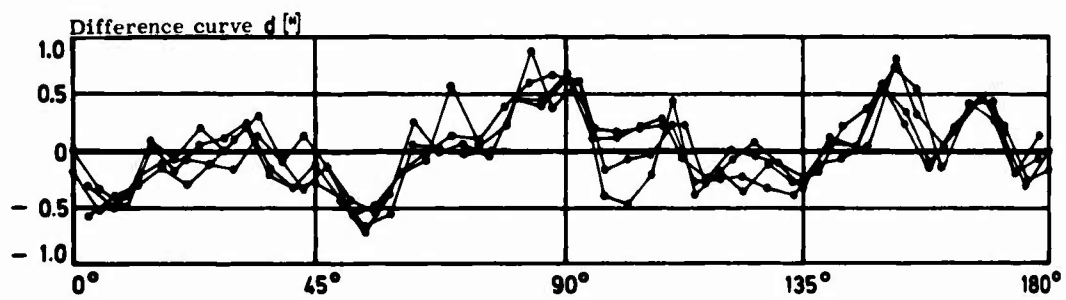


Figure R1. Scale Examination Wild T4 - Difference Curve Measured (4 Experiments)

Appendix S

Table S1. Numerical Values (") of Instrument Error for the Examples in Section 6

No.	Example	Instru- ment	Err. Com.	m _{ua}	m _{ab}	m _t	m _m	m _{la}	m _{wa}	m _{ca}	m _b	m _{za}	m _{iv}	m _{wi}	m _{vr}	m _{vp}	m _{la}	m _l	m _{lL}	m _{wlL}	m _u	m [*] _o	M _c	M _j		
1	Angle mea- sure with horizontal sighting	T4	random systematic	0.05 ②	0.2 ②	0.2 ②	0.1 ②	0.25 ④	0.15 ④	0.1 ③	0.3 ⑤	0.3 ⑤	①	①	①	①	-	-	-	-	-	-	-	0.42 0.14	0.43 -	
		DKM3	random systematic	0.15 ②	0.2 ②	0.2 ②	0.25 ②	0.1 ②	0.1 ②	0.15 ①	0.15 ①	0.3 ⑤	0.3 ⑤	①	①	①	①	-	-	-	-	-	-	-	0.43 0.05	0.38 -
2	Angle measure- ment with sharply inclined target sighting	T4	without preventive measures	0.05 ②	0.2 ②	0.2 ②	0.1 ②	0.25 ④	0.15 ④	0.1 ③	0.35 ⑤	0.3 ⑤	0.2 ③	0.1 ③	0.2 ③	0.2 ③	-	-	-	-	-	-	-	-	0.42 0.56	0.47 0.67
		DKM3	random systematic	0.15 ②	0.2 ②	0.2 ②	0.25 ②	0.1 ②	0.1 ②	0.15 ②	0.15 ②	0.3 ⑤	0.3 ⑤	0.1 ②	0.05 ②	0.2 ③	-	-	-	-	-	-	-	-	0.43 0.18	0.37 0.60
		T4	with preventive measures	0.05 ②	0.2 ②	0.2 ②	0.1 ②	0.25 ④	0.15 ④	0.1 ③	0.15 ③	0.2 ③	0.3 ⑤	0.3 ⑤	-	-	-	-	-	-	-	-	-	-	0.42 0.28	0.37 0.18
		DKM3	random systematic	0.15 ②	0.2 ②	0.2 ②	0.25 ②	0.1 ②	0.1 ②	0.15 ②	0.15 ②	0.2 ③	0.3 ⑤	0.3 ⑤	0.1 ②	0.05 ②	0.2 ③	-	-	-	-	-	-	-	-	0.43 0.06
3	Point deter. from verti- cal passages	AP70	random systematic systematic	0.15 ②	-	-	-	0.2 ④	0.15 ③	0.1 ③	0.25 ③	-	-	-	-	-	-	-	-	-	-	0.15 ⑤	0.29 -	0.27 0.15		
		T4	random systematic systematic	0.05 ②	0.2 ②	0.2 ②	0.1 ②	0.25 ④	0.15 ④	0.1 ③	0.35 ⑤	-	-	-	-	-	-	-	-	-	-	0.2 ⑤	0.3 ⑤	0.42 -	0.36 0.20	
4	Point deter. from azimuth difference measure method a method b	T4	random systematic systematic	0.05 ②	0.2 ②	0.2 ②	0.1 ②	0.25 ④	0.15 ④	0.1 ③	0.35 ⑤	-	-	-	-	-	-	-	-	-	-	0.2 ⑤	0.3 ⑤	0.42 -	0.27 0.20	
		DKM3	random systematic systematic	0.15 ②	0.2 ②	0.2 ②	0.25 ②	0.1 ②	0.1 ②	0.15 ②	0.15 ②	0.3 ⑤	0.3 ⑤	0.1 ②	0.05 ②	0.2 ③	-	-	-	-	-	-	0.25 ⑤	0.3 ⑤	0.43 0.07	0.21 0.25

- Error which concerns an instrument or example that is basically dropped
 ① Error concerning an example that is not operating
 ② Error which is slight or can be neglected by the manufacturer or observer
 ③ Error which can be eliminated by the observed technique
 ④ Error which can be eliminated by arrangement observation
 ⑤ Error whose type and magnitude is unknown.

Appendix T

Table T1. Numerical Values of Coefficient K' [†]

Case a	Pure Position Determination $z_{02} = -z_{01}$					Case b	Position and Azimuth Determination $z_{01} - z_{02} = 90^\circ$				
z_{01}	K'_O	K'_C	K'_I	K'_U	K'^*	z_{01}	K'_O	K'_C	K'_I	K'_U	K'^*
0°	0.000	0.250	0.250	0.500	0.500	30°	0.187	0.500	0.312	1.000	1.000
1°	0.000	0.250	0.250	0.500	0.500	35°	0.221	0.500	0.279	1.000	1.000
5°	0.002	0.252	0.250	0.505	0.505	40°	0.242	0.500	0.258	1.000	1.000
10°	0.008	0.258	0.250	0.515	0.515	45°	0.250	0.500	0.250	1.000	1.000
15°	0.018	0.268	0.250	0.536	0.536	50°	0.242	0.500	0.258	1.000	1.000
30°	0.083	0.333	0.250	0.666	0.666	55°	0.221	0.500	0.279	1.000	1.000
45°	0.250	0.500	0.250	1.000	1.000	60°	0.187	0.500	0.312	1.000	1.000
60°	0.750	1.000	0.250	2.000	2.000						

[†]The formulas for the coefficient K' are listed in Appendix U.

U1

Appendix U

Table U1. Tabulation of the Formulas of the Random and Systematic Errors at Astronomical Position Determinations

Error Group	Random Error Part - Methods a and b (Symmetrical and Vertical Star Arrangement)			
	Coefficients K' (AP70, T4, DKM3)		Sums of Squares M ² of Individual Error Groups (Methods a and b)	
	Method a	Method b	AP70	T4
Orientation comp. K' _O	$\sin^2 z_{O1} / \sin^2 2z_{O1}$	$\sin^2 z_{O1} \cos^2 z_{O1}$	$M_O^2 m_{ua}^2 + m_{ia}^2 + m_{wa}^2$	$m_{ua}^2 + m_{ab}^2 + m_t^2 + m_m^2 + m_{ia}^2 + m_{wa}^2$
Target axis comp. K' _C	$\sin^2 z_{O1} / \sin^2 2z_{O1}$	1/2	$M_C^2 m_{ca}^2 + m_b^2$	$m_{ca}^2 + m_b^2$
Tilt component K' _I	1/4	$\frac{1}{4} + \frac{1}{4} \cos^2 2z_{O1}$	$M_I^2 m_{wi}^2 + m_{iL}^2 + m_l^2 + m_{ia}^2$	$m_{wi}^2 + m_{iv}^2 + m_l^2 + m_{ia}^2$
Passage time K' _u	$2\sin^2 z_{O1} / \sin^2 2z_{O1}$	1	$M_u^2 M_u^2$	M_u^2
Star coordinates K ^{*1}	$2\sin^2 z_{O1} / \sin^2 2z_{O1}$	1	$M^{*1} m^{*1}$	m^{*1}

Error Group	Systematic Error Contribution - Method a (Symmetric Star Arrangement)			
	Askania K ⁿ	AP70 M ⁿ	Wild T4 K ⁿ	M ⁿ
Orientation component O	-	0	-	0
Target axis component C	-	0	-	0
Tilt component J	1/2	$(r_1 m_l^2)^2$	1/2	$(r_1 m_l^2)^2$

Error Group	Systematic Error Contribution - Method b (Vertical Star Arrangement)	
	Askania AP70 and Wild T4	DKM3
Orientation component U ⁿ²	$\sin^2 z_{O1} \cos^2 z_{O1} (r_{ia} m_{ia}^2)^2$	$\sin^2 z_{O1} \cos^2 z_{O1} (r_t m_t^2)^2 + \sin^2 z_{O1} \cos^2 z_{O1} (r_{ia} m_{ia}^2)^2$
Target axis component U ⁿ²	0	0
Tilt component U ⁿ²	$\frac{1}{2} (r_1 m_l^2)^2 + (\frac{1}{4} + \frac{1}{4} \cos^2 2z_{O1}) (r_{iL} m_{iL}^2)^2$	$\frac{1}{2} (r_1 m_l^2)^2 + (\frac{1}{4} + \frac{1}{4} \cos^2 2z_{O1}) (r_{iv} m_{iv}^2)^2$

Unclassified
Security Classification

DOCUMENT CONTROL DATA - R&D		
<i>(Security classification of title, body of abstract and indexing annotation must be entered when the overall report is classified)</i>		
1. ORIGINATING ACTIVITY (Corporate author) Air Force Cambridge Research Laboratories (CRJ) L. G. Hanscom Field Bedford, Massachusetts 01730		2a. REPORT SECURITY CLASSIFICATION Unclassified
		2b. GROUP
3. REPORT TITLE ON THE INVESTIGATION OF INSTRUMENTAL ERRORS OF UNIVERSAL AND TRANSIT INSTRUMENTS BY MEANS OF AUTOCOLLIMATION		
4. DESCRIPTIVE NOTES (Type of report and inclusive dates) Scientific. Special.		
5. AUTHOR(S) (First name, middle initial, last name) Reiner Schwebel		
6. REPORT DATE February 1970	7a. TOTAL NO. OF PAGES 191	7b. NO. OF REFS 55
8a. CONTRACT OR GRANT NO.	9a. ORIGINATOR'S REPORT NUMBER(S) AFCRL-70-0097	
b. PROJECT, TASK, WORK UNIT NOS. N/A		
c. DOD ELEMENT N/A		
d. DOD SUBELEMENT N/A	9b. OTHER REPORT NO(S) (Any other numbers that may be assigned this report) Translations, No. 49	
10. DISTRIBUTION STATEMENT 1—This document has been approved for public release and sale; its distribution is unlimited.		
11. SUPPLEMENTARY NOTES Translation: from German Geodetic Commission at the Bavarian Acad. of Sciences Series C: Dissertations - Vol. 117, 1968.	12. SPONSORING MILITARY ACTIVITY Air Force Cambridge Research Laboratories (CRJ) L. G. Hanscom Field Bedford, Massachusetts 01730	
13. ABSTRACT Geodetic astronomy depends to a certain degree on the precision of available instruments. This investigation covers the instrument errors that effect the determination of a horizontal direction and the effect of these errors on position accuracy determination by horizontal angle measurements and vertical transits. The following errors were investigated: 1) axis errors; that is, horizontal, tilt and target axis 2) instrument errors; that is, divided circle, micrometer, and level bubble and heat deflection of the telescope. These errors seldom exceed + 1". Three common first order instruments, the Wild T-4, Kern DKM-3, and the Askania AP70 were investigated. The direct investigation of the instrumental errors was conducted utilizing very precise autocollimation methods, and statistical methods for defining the type and magnitude of the errors. Instrument errors cannot be ignored but they can be significantly reduced through the use of an adequate observation program.		

DD FORM 1473
1 NOV 65

Unclassified
Security Classification

Unclassified
Security Classification

14. KEY WORDS	LINK A		LINK B		LINK C	
	ROLE	WT	ROLE	WT	ROLE	WT
Geodesy Astronomy Instrumentation Precision						

Unclassified
Security Classification